

AN ABSTRACT OF A DISSERTATION

DEVELOPMENT OF SKEW CORRECTION FACTORS FOR LIVE LOAD SHEAR AND REACTION DISTRIBUTION IN HIGHWAY BRIDGE DESIGN

Qinghe Zhang

Doctor of Philosophy in Engineering

Live Load Distribution Factors have been used in bridge design for many decades as a relatively simple method to estimate live load effects on bridge members for the design and evaluation of bridges. Skew correction factors (SCF) are applied to the live load distribution factors for the corresponding non-skewed bridges to account for the effect of skew in skewed bridges. The distribution factor and SCF equations specified in the current AASHTO LRFD Specifications include limited ranges of applicability, and when these limitations are not met, the specifications mandate a refined analysis. In NCHRP Project 12-62, the SCF were kept fundamentally the same as the current LRFD. Therefore, the range of applicability for the SCF introduces an inconsistency between the almost unlimited newly developed distribution factor equations and the skew correction equations. Currently, no simplified methods can predict live load distribution factors for the bridges with structural parameters exceeding the range of applicability. In addition, the skew effect on reactions at piers of skewed continuous bridges are determined either by using the SCF for shear or by using no SCF, even though a difference between SCF for reaction and shear were found in skewed bridges.

The research described herein is intended to develop SCF equations for shear and reaction distributions without limitations on their range of applicability. In order to develop new equations, an automated analysis program with APDL (ANSYS Parametric Design Language) in ANSYS, a commercial finite element method code, was created so that the maximum responses for various types of bridges under live loads could be obtained. The analyzed bridges, developed with the α - θ method, covered all the possible ranges of applicability for the structural parameters in current practice. Distribution factors for reaction forces were compared to those for shear to verify the necessity to develop the specific skew correction factors for reactions. A parametric study on the effect of span length, girder spacing, and skew angle was conducted for various types of bridges. Two sets of simplified equations were developed for SCFs for both shear and reaction distributions for the LRFD types a, k, b, d, and f. One set was based on the AASHTO LRFD Specifications and the other was based on NCHRP project 12-62. The slightly-greater-than unity average, low standard deviation, and coefficient of variation for each proposed SCF equation indicate high reliabilities of these proposed equations in predicting the SCFs for shear and reaction distributions for various types of bridges without limitations on the range of applicability.

**DEVELOPMENT OF SKEW CORRECTION FACTORS FOR LIVE LOAD
SHEAR AND REACTION DISTRIBUTION IN HIGHWAY BRIDGE DESIGN**

A Dissertation

Presented to

The Faculty of the Graduate School

Tennessee Technological University

by

Qinghe Zhang

In Partial Fulfillment

of the Requirements for the Degree

DOCTOR OF PHILOSOPHY

Engineering

December 2008

UMI Number: 3339061

INFORMATION TO USERS

The quality of this reproduction is dependent upon the quality of the copy submitted. Broken or indistinct print, colored or poor quality illustrations and photographs, print bleed-through, substandard margins, and improper alignment can adversely affect reproduction.

In the unlikely event that the author did not send a complete manuscript and there are missing pages, these will be noted. Also, if unauthorized copyright material had to be removed, a note will indicate the deletion.

UMI[®]

UMI Microform 3339061
Copyright 2009 by ProQuest LLC
All rights reserved. This microform edition is protected against
unauthorized copying under Title 17, United States Code.

ProQuest LLC
789 East Eisenhower Parkway
P.O. Box 1346
Ann Arbor, MI 48106-1346

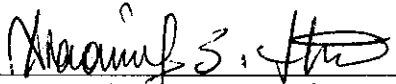
CERTIFICATE OF APPROVAL OF DISSERTATION

**DEVELOPMENT OF SKEW CORRECTION FACTORS FOR LIVELOAD
SHEAR AND REACTION DISTRIBUTION IN HIGHWAY BRIDGE DESIGN**


by


Qinghe Zhang


Graduate Advisory Committee:

 11/24/2008
Dr. X. Sharon Huo, Chairperson date


 11/24/2008
Dr. George R. Buchanan date

 11-24-08
Dr. R. Craig Henderson date

 11/24/08
Dr. L. K. Crouch date

 11/24/08
Dr. Yung-Way Liu date

Approved for the Faculty:


Francis Otuohye
Associate Vice President for Research
and Graduate Studies

12/8/08
Date

ACKNOWLEDGEMENTS

I would like to sincerely thank my major professor, Dr. X. Sharon Huo, for her guidance, support, and patience since we have known each other. I would also like to thank the other members of my committee, Dr. George R. Buchanan, Dr. L.K. Crouch, Dr. R. Craig Henderson, and Dr. Yung-Way Liu for the assistance and support they provided. I also acknowledge the support of the Center for Energy Systems Research and the Department of Civil and Environmental Engineering at Tennessee Technological University for the financial support provided during my study.

I would also like to thank my parents and parents-in-law for their unconditional love and support during this dissertation. A special thanks to my wife, Ying Peng, for her love, support, encouragement, and patience. This dissertation is dedicated to my baby girl, Jennifer J. Zhang.

TABLE OF CONTENTS

	Page
LIST OF TABLES	x
LIST OF FIGURES	xii
CHAPTER 1 INTRODUCTION	1
CHAPTER 2 BACKGROUND AND MOTIVATION	5
2.1 Review of Various LDF Procedures Used in North America.....	7
2.1.1 AASHTO Standard Specification	8
2.1.2 AASHTO LRFD Specification	9
2.1.3 Ontario Highway Bridge Design Code (OHBDC)	11
2.1.4 Canadian Highway Bridge Design Code (CHBDC).....	14
2.1.5 Equal Distribution Factor (EDF) Method	16
2.1.6 Lever Rule Method	17
2.1.7 NCHRP12-62.....	19
2.2 Review of Research on Skew Correction Factors.....	22
2.2.1 Skew Correction Factor in AASHTO LRFD Specifications	22
2.2.2 Other Research on Effect of Skew Angle	23
2.2.3 Possibility of Bridges That Have Parameters Exceeding Applicable Range...	26
2.3 Review of Research on LDF for Shear and Reactions	28
2.4 Potential Problems in Current Procedures	31
2.5 Objectives	33
2.6 Methodology	35
CHAPTER 3 FINITE ELEMENT MODELING OF GIRDER BRIDGES.....	38

	Page
3.1 General Introduction	38
3.2 Literature Review on Finite Element Modeling	39
3.2.1 Model A: Concentric Beam Model.....	39
3.2.2 Model B: Eccentric Beam Model	40
3.2.3 Model C: Detailed Beam Model.....	41
3.2.4 Model D: Solid Decks + Shell Beam Model	41
3.2.5 Model E: Solid Deck + Frame Beam Model	42
3.2.6 Model F: Solid Deck + Solid Beam Model	42
3.2.7 Model G: Shell Deck + Shell Beam Model	43
3.3 Comparison of Modeling Techniques.....	46
3.4 Improved Concentric Beam Model in ANSYS	47
3.4.1 Selected Elements in ANSYS.....	48
3.4.2 Boundary Conditions	50
3.4.3 Loading Applied to the Selected Model	51
3.5 Modeling Verification.....	52
3.5.1 Comparison of 2-D FEM to 3-D FEM.....	53
3.5.1.1 Steel girder bridge (068-0046).....	54
3.5.1.2 Concrete girder bridge (060-0319).....	56
3.5.2 Comparison of 2-D FEM to Experimental Results.....	57
3.6 Element Meshing Size Study	60
3.7 APDL and Macros	61
CHAPTER 4 CONSTRUCTION OF BRIDGE DATABASE.....	69

	Page
4.1 Method to Construct Bridge Database	69
4.3 Selection of Bridges	73
4.4 Loading Conditions.....	80
4.4.1 Transverse Positions where Maximum Responses Occur	81
4.4.2 Verification of Estimated Transverse Positions for Maximum Responses	82
CHAPTER 5 COMPARISON OF DISTRIBUTION FACTOR OF LIVE LOAD REACTION WITH SHEAR AT PIERS OF CONTINUOUS SKEWED BRIDGES.....	86
5.1 Bridges Analysis for Live Load Reaction Distribution	87
5.2 Results of Analysis and Comparison	90
5.2.1 Variation of Distribution Factor of Live Load Reaction at Supports	90
5.2.2 Comparison of the Distribution Factors of Live Load Reaction and Shear.....	92
5.2.3 Comparison to the Current Procedures	94
CHAPTER 6 PARAMETRIC STUDY ON SKEW CORRECTION FACTORS FOR SHEAR AND REACTION DISTRIBUTIONS	100
6.1 Steel I-girder Bridges	101
6.1.1 Effect of Span Length on SCF	101
6.1.2 Effect of Girder Spacing on SCF.....	103
6.1.3 Effect of Skew Angle on SCF.....	104
6.1.4 Comparison of SCF from AASHTO LRFD to FEM SCF.....	106
6.2 Precast Concrete I-girder Bridges	108
6.2.1 Effect of Span Length on SCF	108
6.2.2 Effect of Girder Spacing on SCF.....	109

	Page
6.2.3 Effect of Skew Angle on SCF.....	110
6.2.4 Comparison of SCF from AASHTO LRFD to FEM SCF.....	111
6.3 Precast Concrete Spread Box Girder Bridges.....	113
6.3.1 Effect of Span Length on SCF.....	113
6.3.2 Effect of Girder Spacing on SCF.....	115
6.3.3 Effect of Skew Angle on SCF.....	116
6.3.4 Comparison of SCF from AASHTO LRFD to FEM SCF.....	117
6.4 CIP Multi-cell Box Girder Bridges.....	119
6.4.1 Effect of Span Length on SCF.....	119
6.4.2 Effect of Girder Spacing on SCF.....	120
6.4.3 Effect of Skew Angle on SCF.....	122
6.4.4 Comparison of SCF from AASHTO LRFD to FEM SCF.....	123
6.5 Precast Cellular Concrete Box Bridges.....	125
6.5.1 Effect of Span Length vs. Girder Height on SCF.....	125
6.5.2 Effect of Skew Angle on SCF.....	126
6.5.3 Comparison of SCF from AASHTO LRFD to FEM SCF.....	127
CHAPTER 7 EQUATION DEVELOPMENT.....	129
7.1 Introduction.....	129
7.2 Methodology.....	131
7.3 Proposed Formulas for Skew Correction Factors.....	132
7.3.1 Steel I Girder Bridges.....	135
7.3.1.1 NCHRP 12-62 based equations.....	135

	Page
7.3.1.2 AASHTO LRFD based equations	137
7.3.1.3 Proposed equations validation	139
7.3.2 Precast Concrete I Girder Bridges	141
7.3.2.1 NCHRP 12-62 based equations	141
7.3.2.2 AASHTO LRFD based equations	142
7.3.2.3 Proposed equations validation	144
7.3.3 Precast Concrete Box Girder Bridges	146
7.3.3.1 NCHRP 12-62 based equations	146
7.3.3.2 AASHTO LRFD based equations	147
7.3.3.3 Proposed equations validation	149
7.3.4 CIP Concrete Multicell Box Girder Bridges.....	151
7.3.4.1 NCHRP 12-62 based equations	151
7.3.4.2 AASHTO LRFD based equations	152
7.3.4.3 Proposed equations validation	154
7.3.5 Precast Cellular Concrete Box Girder Bridges	156
7.3.5.1 NCHRP 12-62 based equations	156
7.3.5.2 AASHTO LRFD based equations	157
7.3.5.3 Proposed equations validation	160
CHAPTER 8 SUMMARY, CONCLUSIONS, AND RECOMMENDATIONS	161
8.1 Summary	161
8.2 Conclusions.....	163
8.3 Recommendations.....	166

	Page
DEFINITION	168
NOTATION	169
REFERENCES	170
APPENDICES	
Appendix A APDL for Slab-on-girder Bridges	176
Appendix B Example of calculation of α and θ	193
Appendix C LDF for Straight Bridges in NCHRP12-62	195
Vita.....	199

LIST OF TABLES

	Page
Table 2.1 SCFs for Shear Distribution in NCHRP12-62.....	21
Table 2.2 Correction Factors for LDFs for Support Shear of the Obtuse Corner.....	24
Table 3.1 Survey of Bridge Analysis Studies on LDF.....	45
Table 3.2 Truck Loads and Wheel Spacing (Cross et al., 2006)	54
Table 3.3 Coordinates for X and Y Positions for 068-0046 (Cross et al., 2006).....	55
Table 3.4 Comparison of 2-D FEM to 3-D FEM (068-0046).....	55
Table 3.5 Coordinates for X and Y Positions for 060-0319 (Cross et al., 2006).....	56
Table 3.6 Comparison of 2-D FEM to 3-D FEM (060-0319).....	57
Table 3.7 Comparison of Test Results to FEM for Simply Supported Bridges	59
Table 3.8 Comparison of Experimental Test Results to FEM for Continuous Bridges ...	60
Table 3.9 Element Meshing Study.....	61
Table 4.1 Practical Limits of Structural Parameters for Slab-on-girder Bridges.....	73
Table 4.2 Material Properties for Slab-on-girder Bridges Studied.....	73
Table 4.3 Database for Steel I-girder Bridges Studied	74
Table 4.4 Database for Precast Concrete I-girder Bridges Studied	76
Table 4.5 Database for Precast Concrete Box-girder Bridges Studied.....	77
Table 4.6 Database for Precast Cellular Concrete Box-bridges Studied	78
Table 4.7 Database for CIP Concrete Multi-cell Box-girder Bridges	79
Table 4.8 Transverse Positions for Maximum Responses	82
Table 4.9 Maximum Responses from Estimated Transverse Positions for A-15	84

	Page
Table 4.10 Comparison of Detail Analysis Results to Those from Estimated Transverse Positions for A-15	84
Table 4.11 Maximum Responses from Estimated Transverse Position for A-19.....	85
Table 4.12 Comparison of Detail Analysis Results to That from Estimated Transverse Positions for A-19	85
Table 5.1 Distribution Factors of Reaction and Shear at Support – Bridge #1	91
Table 5.2 Distribution Factors of Reaction and Shear at Support – Bridge #2	92
Table 5.3 Distribution Factors of Reaction and Shear at Support – Bridge #3	92
Table 5.4 Comparison of Distribution Factor of Reaction and Shear at Support with Different Methods– Bridge #3	98
Table 7.1 Comparative Statistics of SCFs for Steel I-girder Bridges	139
Table 7.2 Comparative Statistics of SCFs for Precast Concrete I-girder Bridges	144
Table 7.3 Comparative Statistics of SCFs for Precast Concrete Box-girder Bridges.....	149
Table 7.4 Comparative Statistics of SCFs for CIP Concrete Multi-Cell Box Girder Bridges	154
Table 7.5 Comparative Statistics of SCFs for Precast Concrete Cellular Box Girder Bridges	159

LIST OF FIGURES

	Page
Figure 2.1 Distribution Factor Illustrations	7
Figure 2.2 AASHTO Standard vs. AASHTO LRFD Moment Distribution Factors	9
Figure 2.3 AASHTO Standard vs. AASHTO LRFD Shear Distribution Factors	9
Figure 2.4 the α - θ Space (Reproduced from Bakht et al.).....	12
Figure 2.5 Charts for D and C_f from α - θ Space (Reproduce from OHBDC)	14
Figure 2.6 Loading Diagram for Exterior Girder with Two Lanes Loaded and Two Wheels to Beam	18
Figure 2.7 Bridge S.R. 0031 over PA Turnpike (Reproduced from Internet)	28
Figure 2.8 Bridge I-87 NB Connectors over I-287 EB (Reproduced from Internet).....	28
Figure 2.9 Distribution factors of reaction and shear at piers.....	30
Figure 3.1 Concentric Beam Model (Mabsout, 1997)	40
Figure 3.2 Eccentric Beam Model (Sotelino, 2004)	40
Figure 3.3 Detailed Beam Model (Brockenbrough 1986)	41
Figure 3.4 Solid Deck + Shell Beam Model (Tarhini and Frederick 1992)	42
Figure 3.5 Solid Deck + Frame Beam Model (Barr and Amin 2006)	42
Figure 3.6 Solid Deck + Solid Beam Model (Abendroth et al. 2004)	43
Figure 3.7 Shell Deck + Shell Beam Model (Choo et al. 2004)	44
Figure 3.8 Improved Concentric Beam Model	49
Figure 3.9 Improved Concentric Beam Model with Boundary Conditions.....	50
Figure 3.10 AASHTO HL-93 Truck.....	51

	Page
Figure 3.11 Beam Line Analyses.....	52
Figure 3.12 Loading Positions for Two Lanes Loaded.....	52
Figure 3.13 Truck Configurations (Cross et al., 2006).....	54
Figure 3.14 Bridge No 068-0046 plan (Cross et al., 2006).....	55
Figure 3.15 Bridge No 060-0319 plan (Cross et al., 2006).....	56
Figure 3.16 Details for Simply Supported Bridge Tested (Ebeido et al. 1995).....	58
Figure 3.17 Details for Continuous Bridges Tested (Ebeido et al. 1996).....	58
Figure 3.18 Main Flowchart	63
Figure 3.19 Input of General Information with the Dialog Box	65
Figure 3.20 Distributions of Concentrated Loads to Adjacent Nodes	66
Figure 3.21 Flowchart-Distribute Concentrated Loads	67
Figure 3.22 Flowchart-Obtain Element Position Based on Given Locations.....	68
Figure 4.1 Typical Cross Section Studied.....	72
Figure 4.2 Truck Arrangements in the Transverse Direction	81
Figure 4.3 Maximum Responses from Detailed Analysis for A-15	83
Figure 4.4 Maximum Responses from Detailed Analysis for A-19	85
Figure 5.1 Typical Cross Sections of Selected Bridges	88
Figure 5.2 Plan View of Skewed Bridges Studied.....	88
Figure 5.3 Support Designations of Selected Bridges	89
Figure 5.4 Sample Loading Positions for Two-lane Loads on Bridge #1	90
Figure 5.5 Ratio of LDF for Reaction to Shear– Bridge #1.....	93
Figure 5.6 Ratio of LDF for Reaction to Shear– Bridge #2.....	94

	Page
Figure 5.7 Ratio of LDF for Reaction to Shear– Bridge #3.....	94
Figure 5.8 Comparisons to the Current Procedures – Bridge #1	95
Figure 5.9 Comparisons to the Current Procedures – Bridge #2	96
Figure 5.10 Comparisons to the Current Procedures – Bridge #3	97
Figure 6.1 SCF on Exterior Girders with Spacing of 20ft	101
Figure 6.2 SCF on Interior Girders with Spacing of 20ft	102
Figure 6.3 SCF on Exterior Girders with Span Length of 400ft.....	103
Figure 6.4 SCF on Interior Girders with Span Length of 150ft.....	103
Figure 6.5 Effect of Skew Angle on SCF	105
Figure 6.6 Comparison of AASHTO LRFD Based SCF to FEM SCF- θ	106
Figure 6.7 Comparison of AASHTO LRFD Based SCF to FEM SCF-L.....	106
Figure 6.8 Comparison of AASHTO LRFD Based SCF to FEM SCF-S.....	107
Figure 6.9 SCF on Exterior Girders with Spacing of 18ft	108
Figure 6.10 SCF on Interior Girders with Spacing of 18ft	108
Figure 6.11 SCF on Exterior Girders with Span Length of 100ft.....	109
Figure 6.12 SCF on Interior Girders with Span Length of 100ft.....	110
Figure 6.13 Effect of Skew Angle on SCF	111
Figure 6.14 Comparison of AASHTO LRFD Based SCF to FEM SCF- θ	112
Figure 6.15 Comparison of AASHTO LRFD Based SCF to FEM SCF-L.....	112
Figure 6.16 Comparison of AASHTO LRFD Based SCF to FEM SCF-S.....	112
Figure 6.17 SCF on Exterior Girders with Spacing of 12ft	114
Figure 6.18 SCF on Interior Girders with Spacing of 12ft	114

	Page
Figure 6.19 SCF on Exterior Girders with Span Length of 150 ft.....	115
Figure 6.20 SCF on Interior Girders with Span Length of 150 ft.....	115
Figure 6.21 Effect of Skew Angle on SCF	117
Figure 6.22 Comparison of AASHTO LRFD Based SCF to FEM SCF- θ	118
Figure 6.23 Comparison of AASHTO LRFD Based SCF to FEM SCF-L.....	118
Figure 6.24 Comparison of AASHTO LRFD Based SCF to FEM SCF-S.....	118
Figure 6.25 SCF on Exterior Girders with Spacing of 14 ft.....	119
Figure 6.26 SCF on Interior Girders with Spacing of 14 ft	120
Figure 6.27 SCF on Exterior Girders with Span Length of 300 ft.....	121
Figure 6.28 SCF on Interior Girders with Span Length of 300 ft.....	121
Figure 6.29 Precast Cellular Box Girder Bridges	122
Figure 6.30 Comparison of AASHTO LRFD Based SCF to FEM SCF- θ	123
Figure 6.31 Comparison of AASHTO LRFD Based SCF to FEM SCF-L.....	123
Figure 6.32 Comparison of AASHTO LRFD Based SCF to FEM SCF-S.....	124
Figure 6.33 SCF on Exterior Girders with Spacing of 3 ft.....	126
Figure 6.34 SCF on Interior Girders with Spacing of 3 ft	126
Figure 6.35 Effect of Skew Angle	127
Figure 6.36 Comparison of AASHTO LRFD Based SCF to FEM SCF- θ	127
Figure 6.37 Comparison of AASHTO LRFD Based SCF to FEM SCF-L.....	128
Figure 7.1 Proposed NCHRP 12-62 based SCF vs. Rigorous SCF for Shear in Steel I-girder Bridges.....	136

	Page
Figure 7.2 Proposed NCHRP 12-62 based SCF vs. Rigorous SCF for Reaction in Steel I-girder Bridges.....	136
Figure 7.3 Proposed AASHTO LRFD Based SCF vs. Rigorous SCF for Shear in Steel I-girder Bridges.....	137
Figure 7.4 Proposed AASHTO LRFD Based SCF vs. Rigorous SCF for Reaction in Steel I-girder Bridges	138
Figure 7.5 Proposed SCF vs. FEM SCF for Shear in Steel I-girder Bridges.....	140
Figure 7.6 Proposed SCF vs. FEM SCF for Reaction in Steel I-girder Bridges.....	140
Figure 7.7 Proposed NCHRP 12-62 based SCF vs. Rigorous SCF for Shear in Precast Concrete I-girder Bridges	141
Figure 7.8 Proposed NCHRP 12-62 based SCF vs. Rigorous SCF for Reaction in Precast Concrete I-girder Bridges	142
Figure 7.9 Proposed AASHTO LRFD SCF vs. Rigorous SCF for Shear in Precast Concrete I-girder Bridges	143
Figure 7.10 Proposed AASHTO LRFD SCF vs. Rigorous SCF for Reaction in Precast Concrete I-girder Bridges	143
Figure 7.11 Proposed SCF vs. FEM SCF for Shear in Precast Concrete I-girder Bridges	145
Figure 7.12 Proposed SCF vs. FEM SCF for Reaction in Precast Concrete I-girder Bridges	145
Figure 7.13 Proposed NCHRP 12-62 based SCF vs. Rigorous SCF for Shear in Precast Concrete Box-girder Bridges	146

	Page
Figure 7.14 Proposed NCHRP 12-62 based SCF vs. Rigorous SCF for Reaction in Precast Concrete Box-girder Bridges.....	147
Figure 7.15 Proposed AASHTO LRFD SCF vs. Rigorous SCF for Shear in Precast Concrete Box-girder Bridges	148
Figure 7.16 Proposed AASHTO LRFD SCF vs. Rigorous SCF for Reaction in Precast Concrete Box-girder Bridges	148
Figure 7.17 Proposed SCF vs. FEM SCF for Shear in Precast Concrete Box-girder Bridges	150
Figure 7.18 Proposed SCF vs. FEM SCF for Shear in Precast Concrete Box-girder Bridges	150
Figure 7.19 Proposed NCHRP 12-62 based SCF vs. Rigorous SCF for Shear in CIP Concrete Multi-cell Box-girder Bridges	151
Figure 7.20 Proposed NCHRP 12-62 based SCF vs. Rigorous SCF for Reaction in CIP Concrete Multi-cell Box-girder Bridges	152
Figure 7.21 Proposed AASHTO LRFD SCF vs. Rigorous SCF for Shear in CIP Concrete Multi-cell Box-girder Bridges.....	153
Figure 7.22 Proposed AASHTO LRFD SCF vs. Rigorous SCF for Reaction in CIP Concrete Multi-cell Box-girder Bridges	153
Figure 7.23 Proposed SCF vs. FEM SCF for Shear in CIP Concrete Multi-cell Box-girder Bridges	155
Figure 7.24 Proposed SCF vs. FEM SCF for Reaction in CIP Concrete Multi-cell Box-girder Bridges.....	155

	Page
Figure 7.25 Proposed NCHRP 12-62 based SCF vs. Rigorous SCF for Shear in Precast Cellular Concrete Box-girder Bridges	156
Figure 7.26 Proposed NCHRP 12-62 based SCF vs. Rigorous SCF for Reaction in Precast Cellular Concrete Box-girder Bridges.....	157
Figure 7.27 Proposed AASHTO LRFD SCF vs. Rigorous SCF for Shear in Precast Cellular Concrete Box-girder Bridges	158
Figure 7.28 Proposed AASHTO LRFD SCF vs. Rigorous SCF for Reaction in Precast Cellular Concrete Box-girder Bridges	158
Figure 7.29 Proposed SCF vs. FEM SCF for Shear in Precast Cellular Concrete Box-girder Bridges.....	160
Figure 7.30 Proposed SCF vs. FEM SCF for Reaction in Precast Cellular Concrete Box-girder Bridges.....	160
Figure 8.1 Flowchart to obtain distribution factors in skewed bridges.....	166

CHAPTER 1

INTRODUCTION

Live load distribution factors have been used in bridge design for many decades as a relatively simple method to estimate live load effects on bridge members. Live load distribution is important for the design of new bridges as well as for the evaluation of the load carrying-capacity of existing bridges. With the specified formulas for distribution factors and simplified beam line analyses, the live load on each girder can be calculated for the purpose of design or evaluation. The original “s-over” equations in the AASHTO Standard Specifications, used for bridge design since the 1930s, are simple to calculate and yield acceptable results for the bridges with the structural parameters in some ranges. The current AASHTO LRFD Specifications were developed from the work done under NCHRP Project 12-26, which can predict the distribution factors of slab-on-girder bridges very well. However, since the adoption into the LRFD Specifications, many engineers have indicated that the complexity of the new equations is troubling. The new equations include limited ranges of applicability. The LRFD Specifications mandate that when these ranges of applicability are exceeded, a rigorous analysis is required. But the rigorous analysis usually requires special skill and software, which is time-consuming, costly, and inconvenient in most cases.

NCHRP Project 12-62 (2003-2006) was initiated to develop a new method for the calculation of distribution factors, based on fundamental engineering principles that reflected the wide variations in modern bridge design. In NCHRP 12-62, the distribution factors for straight bridges were calculated from the lever rule method and the modified

Henry's method without any significant limitations. However, for the skewed bridge, the skew correction factors were kept fundamentally the same as the current LRFD Specifications, which include limited ranges of applicability. To keep the consistency of the distribution factor and the skew correction factor in the range of applicability, it is important to develop new skew correction factor equations that have no limitations on the range of applicability. Thus the distribution factors for skewed bridges can be calculated without any limitations.

One of the objectives of the research presented in this dissertation was to eliminate the limitations on the range of applicability for skew correction factors. The following types of slab-on-girder bridges were investigated:

- Steel I girder bridge (LRFD Type A)
- Precast concrete I girder bridge (LRFD Type K)
- Precast concrete box girder bridge (LRFD Type B)
- Cast-in-place (CIP) concrete multicell box girder (LRFD Type D)
- Precast cellular concrete box girder bridge (LRFD Type F)

Live load reaction at piers is an important design value for substructure design. Most modern bridges are continuous, skewed bridges, so use of an inaccurate estimation of live load reactions would lead to a somewhat incorrect design for bridge substructures, such as pier caps and piers. Although extensive studies have been conducted for the skew effect on live load shear distribution, very little research has been done on the effect of bridge skewness on live load reactions of continuous bridges. In the current methods, distribution factors for reactions are predicted by shear distribution equations and corresponding skew correction factors. In other words, there are no specific equations for

reaction distribution factors in the current LRFD specifications. In some states, the lever rule method is used to calculate live load distribution for reactions without considering the effect of skew angle on the reactions. Based on a limited number of research studies, by Modjeski and Masters (2002), Ebeido and Kennedy (1996), and Huo and Zhang (2006, 2008), live load distribution for reactions is different from that for shear in skewed bridges. Another objective of this research was to develop the skew correction factors for reaction distributions.

This dissertation consists of eight chapters. Chapter 2 investigates the available literature regarding current design practices, simplified methods of live load distribution factor calculation, and effects of parameters on live load distribution, superstructure modeling, and field testing. Chapter 3 focuses on modeling and loading techniques of the slab-on-girder bridges. In addition, the improved modeling techniques used in this research are validated with the 3-D detailed FEM or experimental test results. Finally the APDL programs are developed in ANSYS to implement the finite element analyses of slab-on-girder bridges. Chapter 4 constructs the bridge database which is investigated in this dissertation. To obtain the maximum responses under live loads, the methods for arranging the trucks in the transverse direction are explored. Chapter 5 details the comparison study to show the difference between reactions and shear distribution factors in the skewed bridges. Chapter 6 explores the effects of various structural parameters on skew correction factors in detail so as to identify the parameters sensitive to the load distribution factors under live loads. Chapter 7 presents the newly recommended skew correction factor equations for shear and reaction distributions for various types of bridges. Statistical analyses and comparisons of the proposed equations to finite element

results are used to validate the proposed equations. Finally, the conclusions are drawn, and recommendations are made in Chapter 8.

CHAPTER 2

BACKGROUND AND MOTIVATION

The value of the maximum response, such as moment, shear, or reaction, in bridge girders is very critical in bridge design. Bridge engineers have to know the maximum response values of bridge members in order to design or rate the members. The maximum response for a particular girder depends on the magnitude and location of the imposed loads and on the properties of the bridge. The design moment and shear in the girder vary with girder spacing, span, flexural stiffness, torsional stiffness, and the properties of the deck and diaphragms. Computing the maximum response of a bridge to live loads is a complex task. The presence of skew further complicates this task.

To obtain the maximum response to live loads, three levels of analysis methods are suggested in the AASHTO LRFD Specification. Level One analysis methods use simplified formulas to predict the live load distribution factors. Level Two analysis methods involve graphical methods, influence surfaces, and plane grillage analyses. Finally, Level Three analysis methods are the most accurate and involve the detailed finite element modeling of bridge superstructures. The designer should select the appropriate level of analysis so as to obtain the maximum responses for bridge design by balancing the simplicity and accuracy of these three methods. Higher level methods produce more accurate results; however, the analysis process will be more complex.

Finite element analysis (FEA) is considered to be an accurate method and is commonly used by researchers, but it requires much effort in data preparation, bridge modeling, analysis, and interpretation of results. For Level Two methods, such as grillage

analysis, it is impossible to model important physical phenomena, such as the interactions between girders and deck slab and supports, even though it is relatively easy to implement. Level Two and Level Three methods require special skills and analysis tools. For finite element analysis, the commonly used general-purpose software are ANSYS, SAP2000, ABAQUS, etc. Modern computer technology makes it possible to analyze bridge superstructures directly, using finite element techniques. However, simplified methods of load distribution are still needed for routine design and rating of bridges.

Live load distribution factors have been used to facilitate the determination of maximum responses in bridge design for decades, as a simple method by which live load effects are estimated. Using the live load distribution factor equations, the maximum response in the girders is obtained by multiplying the response from a one-dimensional bridge analysis by the value obtained from the live load distribution factor equation. The live load distribution factor (LDF) is commonly defined as

$$LDF = \frac{F_{distributed}}{F_{beamline}} \quad (2-1)$$

$F_{distributed}$ corresponds to the largest bending moment or shear force distributed to the girder for all of the load combinations from the refined analysis. $F_{beamline}$ corresponds to the maximum bending moment or shear force determined from a simple beam-line analysis of one lane of traffic, assuming that the bridge superstructure can be idealized as a single beam line. For routine design of bridges, the LDF is used in conjunction with results from simple beam-line analysis to estimate the design bending moment or shear force in the girder (i.e., the maximum response in the girder = $F_{beamline} \times LDF$, as illustrated in Figure 2.1).

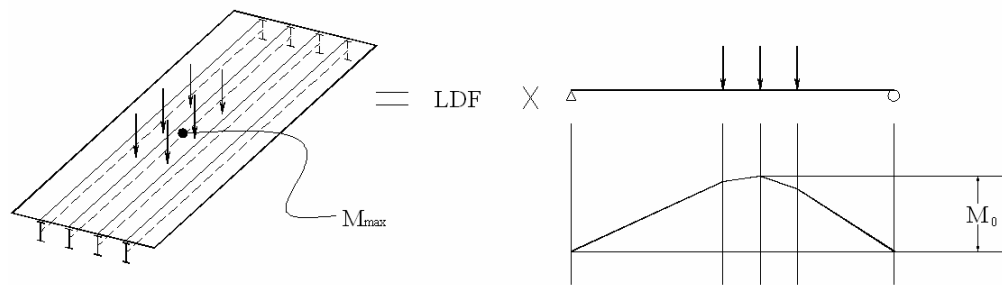


Figure 2.1 Distribution Factor Illustrations

The concept of live load distribution factors allows design engineers to predict bridge responses by treating the longitudinal and transverse effects of truck loads as uncoupled phenomena. Another advantage of live load distribution factors is that designers can predict the maximum responses without special skills and analysis tools. The following sections introduce the current procedures used in North America to obtain LDF.

2.1 Review of Various LDF Procedures Used in North America

In the United States, live load distribution factors are typically determined by using the procedures in the American Association of State Highway and Transportation Officials (AASHTO), Standard Specifications for Highway Bridges, the AASHTO Load Resistance and Factor Design (LRFD), Bridge Design Specifications, or a state-specified method such as Equal Distribution Factor (EDF) method and Lever Rule method. In Canada, the specifications used to determine load distribution factors include the Ontario Highway Bridge Design Code (OHBDC) or the Canadian Highway Bridge Design Code.

There are usually two ways of developing a simplified method. In one approach, a large number of realistic structures are analyzed, and the simplified method is derived

from a curve-fitting process of the numerical data obtained from the rigorous analyses. The AASHTO LRFD specifications were developed through this approach. In the second approach, the behavior of the structure is characterized by a minimum number of dimensionless parameters, and the method is directly based on fundamental engineering principles. For example, OHBDC was developed based on the second approach.

2.1.1 AASHTO Standard Specification

The wheel load distribution factor from the “S-over” equation, (i.e. the AASHTO standard equation – AASHTO 1996), for slab-on-girder bridges is

$$DF= S/D \qquad \qquad \qquad \text{(US customary unit)} \qquad \qquad \qquad (2-2)$$

S is girder spacing (ft), and D is a constant based on the bridge type. The S-over equation, first introduced in the 1930s, involves only one parameter, girder spacing. These formulas were developed for straight and right-angled bridges without considering the effect of skew supports. Such a high degree of simplification necessarily leads to rather large errors. The S-over equations result in values that are too conservative for long span bridges. In short span bridges with small girder spacing, however, they lead to underestimated results. Figures 2.2 (Sotelino et al., 2004.) and 2.3 (Cross et al., 2006) compared the distribution factors from AASHTO Standard Specifications to those from the current AASHTO LRFD specifications. The AASHTO Standard Specifications do not distinguish between exterior and interior girders, nor do they account for the effect of skew. The AASHTO Standard Specifications have not been used since 2007 in the bridge design community.

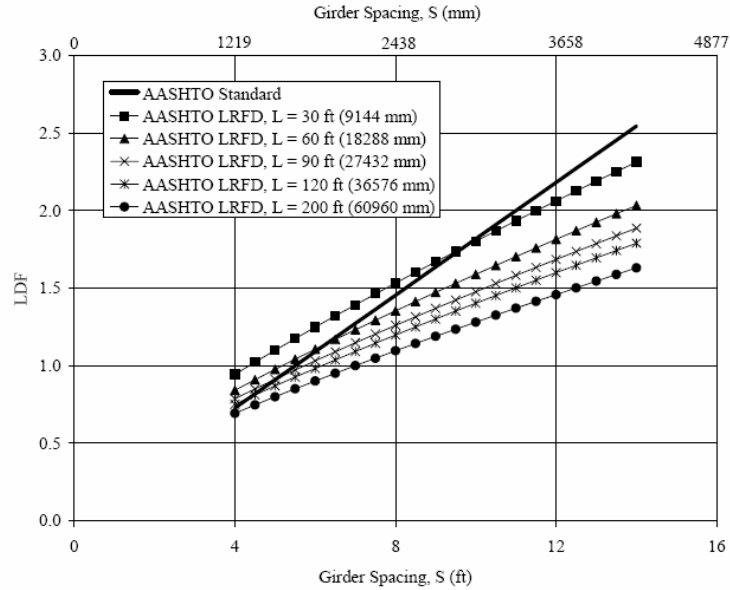


Figure 2.2 AASHTO Standard vs. AASHTO LRFD Moment Distribution Factors
(Reproduced from Sotelino et al. 2004)

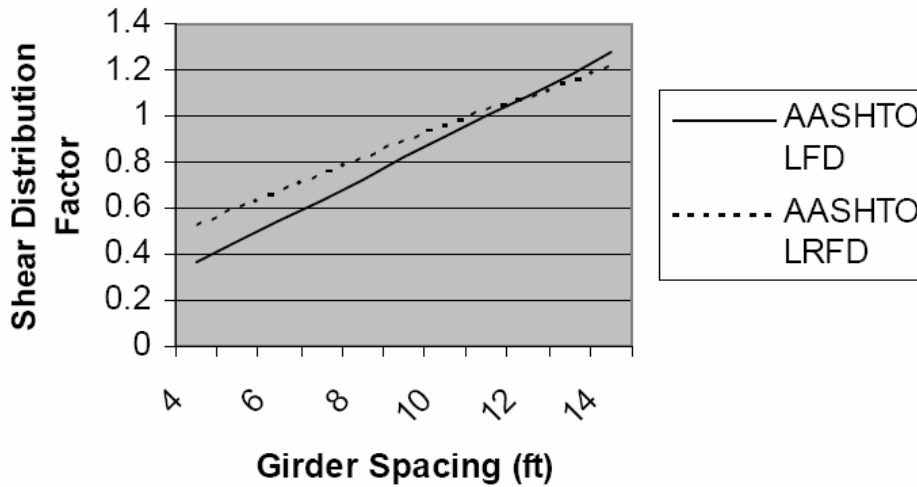


Figure 2.3 AASHTO Standard vs. AASHTO LRFD Shear Distribution Factors
(Reproduced from Cross et al. 2006)

2.1.2 AASHTO LRFD Specification

The derivation of the new AASHTO-LRFD formulas was based on the NCHRP (National Cooperative Highway Research Program) 12-26 project (Zokaie et al. 1993).

Finite element (Level Three) or grillage analysis (Level Two) methods were used to determine the simplified load distribution formulas (Level One) through parametric studies. The parameters sensitive to the lateral load distribution under AASHTO HL-93 design truck vehicles were identified. This specification gives the various simplified equations for moment and shear for various types of bridges. For example, the moment distribution factor (MDF) for interior beams for steel I-girder bridges is given by

$$MDF = 0.075 + \left(\frac{S}{14}\right)^{0.4} \left(\frac{S}{L}\right)^{0.3} \left(\frac{K_g}{12.0L t_s^3}\right)^{0.1} \quad \text{Two or more design lanes loaded} \quad (2-3)$$

S is the girder spacing in feet, L is the span length in feet, t_s is the concrete slab thickness in inches, and K_g is the longitudinal stiffness parameter = $n(I + Ae_g^2)$. In this formula, n is the material modular ratio between the beam and the deck, I is the moment of inertia of the girder in inches⁴, A is the area of girder, and e_g is the distance between the neutral axis of the girder and the slab in inches.

AASHTO-LRFD also includes several extensions to the basic distribution factor such as continuity and skew effect. According to the summary of NCHRP research by Zokaie(2000), the wheel load distribution factors in continuous bridges are slightly higher than simply supported bridges, and the average value of the adjacent spans are appropriate for use as a parameter. For skewed bridges, it was found that the moment in the middle span is smaller and the shear in the girder at obtuse corners of the bridge is larger when compared to those in the girder of straight bridges. In the AASHTO LRFD specifications, the skew correction factor (SCF) of the shear distribution factor for steel I-girder bridges, is given by

$$SCF = 1.0 + 0.20 \left(\frac{12.0 L t_s^3}{K_g} \right)^{0.3} \tan \theta \quad \text{Range of applicability} \quad \begin{cases} 0^\circ \leq \theta \leq 60^\circ \\ 3.5 \text{ ft} \leq S \leq 16.0 \text{ ft} \\ 20 \text{ ft} \leq L \leq 240 \text{ ft} \\ N_b \geq 4 \end{cases} \quad (2-4)$$

However, the AASHTO-LRFD wheel load distribution factors were developed under certain assumptions, namely: (1) the girder spacing is evenly distributed and all girder properties are the same; (2) the design vehicle for developing the formulas are assumed to be the HL-93 design truck; and (3) the thickness and width of the slab are not varied. In addition, the significant limitations on the range of applicability are imposed on live load distribution factor equations and skew correction factor equations.

2.1.3 Ontario Highway Bridge Design Code (OHBDC)

In 1979, the OHBDC introduced simplified methods of analysis which were similar in concept to the AASHTO standard “S-over” equations but in which the value of D depended upon the load distribution characteristics of the particular bridge under consideration, expressed in terms of two dimensionless characterizing parameters, α and θ . The Ontario method is based upon the fact that the load distribution in an orthotropic plate that is simply supported on two opposite edges can be described by the two characterizing parameters, α and θ . The use of the α - θ method retains the simplicity of the AASHTO standard method yet provides solutions that are comparable to computer based orthotropic plate theory and grillage analogy methods. The α - θ space, shown in Figure 2.4, covers the range of values for these parameters usually found in practice. The

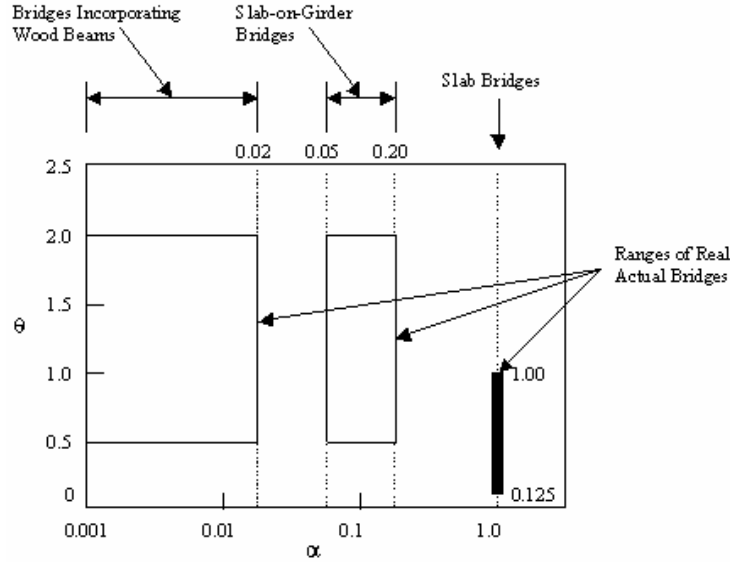


Figure 2.4 the α - θ Space (Reproduced from Bakht et al.)

larger values of α correspond to increasing amounts of torsional stiffness and larger values of θ correspond to wider and softer bridges. It has been shown by Bakht et al.

(1985) that two orthotropic plates having the same value of α and θ display the same transverse distribution of longitudinal responses under identical loads even with different aspect ratios.

As outlined by Bakht et al. (1985), for shallow superstructures, such as slab-on-girder bridges and concrete slab bridges, the desired longitudinal moments are calculated as follows:

(a) Calculate α, θ and μ from

$$\alpha = \frac{D_{xy} + D_{yx} + D_1 + D_2}{2(D_x D_y)^{0.5}}$$

$$\theta = \frac{W}{2L} \left(\frac{D_x}{D_y} \right)^{0.25} \tag{2-5}$$

$$\mu = \left(\frac{\text{lane width} - 11}{2} \right) \leq 1.0$$

where W = bridge width; L = span length; D_x = longitudinal flexural rigidity (corresponding to EI in a longitudinal beam) per unit width; D_y = transverse flexural rigidity (corresponding to EI in a transverse beam) per unit length; D_{xy} = longitudinal torsional rigidity (corresponding to GJ in a longitudinal beam) per unit width; D_{yx} = transverse torsional rigidity (corresponding to GJ in a transverse beam) per unit length; D_1 = longitudinal coupling rigidity (contribution of transverse flexural rigidity to longitudinal torsional rigidity through Poisson's ratio) per unit width; and D_2 = transverse coupling rigidity per unit length. For multi-span bridges, when considering positive moments, L shall be the length of the positive moment region, which is obtained by considering the bridge as a continuous beam and by subjecting the span under consideration to the dead load of the span. Likewise, for negative moments, L shall be equal to the length of the negative moment region corresponding to dead loads on the two adjacent spans. The values of stiffness D_x , D_y , D_{xy} , D_{yx} , D_1 , and D_2 are calculated from the actual bridge details using any well established method.

(b) Based on the calculated values of α and θ in the last step, determine the values of D and C_f for each loading case from relevant graphs for two-lane, three-lane, and four-lane bridges, noting that C_f is the correction factor that accounts for the design lane width being different from 3.3 m. Figure 2.5 presents an example of how to obtain D and C_f . The final value of distribution factor, D_d , for internal and external portions shall be obtained from the following equation:

$$D_d = D \left(1 + \frac{\mu C_f}{100} \right) \quad (2-6)$$

(c) Calculate the fraction (S/D_d) for each loading case, where S is the spacing of beams or webs in meters, or S is 1 m for slab bridges.

bridges as an example, the longitudinal moment per girder, M_g , is determined by using the following equations in the Canadian code:

$$M_{g \text{ avg}} = \frac{nM_T R_L}{N} \quad (2-7)$$

$$F_m = \frac{SN}{F \left(1 + \frac{\mu C_f}{100} \right)} \geq 1.05 \quad (2-8)$$

$$M_g = F_m M_{g \text{ avg}} \quad (2-9)$$

where

$M_{g \text{ avg}}$ = the average moment per girder determined by equally distributing the total moment on the bridge cross-section among all girders in the cross-section;

M_T = the maximum moment per design lane at the point of the span under consideration;

n = the number of design lanes;

R_L = the modification factor for multilane loading, which is equal to 1.0 for 1 lane loaded, 0.90 for two lanes loaded, 0.80 for three lanes loaded, 0.70 for four lanes loaded, 0.60 for five lanes loaded, and 0.55 for six or more lanes loaded;

N = the number of girders;

F_m = an amplification factor to account for the transverse variation in maximum longitudinal moment intensity, as compared to the average longitudinal moment intensity;

$$\mu = \frac{W_e - 3.3}{0.6} \leq 1.0;$$

W_e = the width of a design lane (m);

- S = the center-to-center girder spacing (m);
- C_f = a correction factor (%);
- F = a width dimension that characterizes load distribution for a bridge (m).

2.1.5 Equal Distribution Factor (EDF) Method

The EDF method is a simplified method for calculating the distribution factors of live load moment and shear. The method was originally developed by Henry Derthick, a former Bridge Engineer in the Tennessee Department of Transportation, and has been in use in Tennessee since 1963. In this method, it is assumed that all beams, including interior and exterior beams, have equal distribution of live load effects. Because the EDF method requires only the width of the roadway, number of traffic lanes, number of beam lines, and the multiple-presence factor of the bridge, it can be applied without difficulty to different types of superstructures and beam arrangements.

A comparison study was conducted by Huo et al. (2003) to investigate the differences between distribution factors calculated from the EDF method, finite element analysis (FEA), the AASHTO Standard, and the AASHTO LRFD. To examine the EDF method, 24 actual bridges of six different types of superstructures were selected for the study. The distribution factors from the EDF method for these actual bridges were compared with those from FEA, the AASHTO Standard, and the AASHTO LRFD. The comparison study investigated the effects of the type of superstructure and other key parameters that significantly affected the calculation of distribution factors. The key

parameters considered included span length, beam spacing, beam stiffness, skew angle, and slab thickness.

In general, the EDF method accurately predicted live load moment distribution factors for most bridge types. The distribution factors calculated from the EDF method were slightly greater than the results from the finite element analysis and stayed within a reasonable range of the values from both AASHTO methods. However, based on the comparison and evaluation, it was found that the distribution factors from the EDF method were not conservative for most bridge types for live load shear. In order to make the results from the EDF method more comparable to finite element analysis, modification factors for both moment and shear were introduced. The modified Henry's EDF method offers obvious advantages in calculation of moment and shear distribution factors because of its simplicity, reliability, and feasibility. This simple and reliable method enables bridge engineers to avoid the use of rigorous methods of analysis when the parameters of the bridges are in excess of the ranges of applicability set in the AASHTO LRFD. In addition, the modified Henry's EDF method is less conservative than the AASHTO methods, making it effective at cost reduction. The EDF method is modified by NCHRP12-62 to be a reliable and simple method to predict LDF.

2.1.6 Lever Rule Method

The lever rule method is defined as an approximate distribution factor method that assumes no transverse deck moment continuity at interior beams. This renders the transverse deck cross section statically determinate. The method uses direct equilibrium

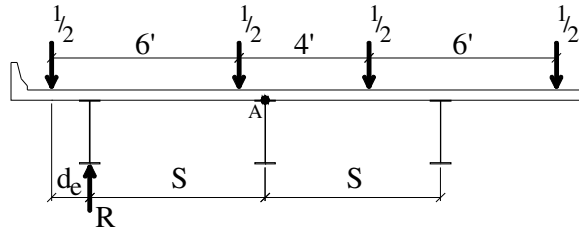


Figure 2.6 Loading Diagram for Exterior Girder with Two Lanes Loaded and Two Wheels to Beam

to determine the load distribution to a beam of interest. The Lever Rule formulas specified in the current LRFD Specifications were derived under the following assumptions:

- two-foot spacing between the outer wheel centroid and the curb/barrier
- six-foot axle gage
- four feet between vehicles.

There are limitations on the range of applicability for the specified Lever Rule equations. Where the limitations are not met, conventional lever rule computations apply. Figure 2.6 presents the equation for an exterior girder with two or more lanes loaded and two wheels to the beam:

$$\sum M_A : \frac{1}{2}(d_e + S) + \frac{1}{2}(d_e + S - 6) - RS = 0 \quad (2-10)$$

$$R = \frac{\frac{1}{2}d_e + \frac{1}{2}S + \frac{1}{2}d_e + \frac{1}{2}S - 3}{S} \quad (2-11)$$

$$R = 1 + \frac{d_e}{S} - \frac{3}{S} = LDF \quad (2-12)$$

Calibration of the codified lever rule equations was conducted in NCHRP 12-62 as a more simple method than the current LRFD equations to calculate the distribution factors. The calibration was performed so that the method would closely approximate the

mean of the rigorous values. This adjustment to the codified lever rule results was based on statistical analysis and is represented by the adjustment factor a . Another adjustment applied to the codified lever rule method was an upward shift in the results in order to account for the variability. This adjustment factor is represented by b .

2.1.7 NCHRP12-62

The NCHRP Project 12-62 (2003-2006) was initiated to determine a new method for calculating distribution factors that reflected the wide variations in modern bridge design. The objective of the NCHRP 12-62 project was to develop new live-load distribution equations to replace those found in the current AASHTO LRFD Bridge Design Specification. These new equations emphasized ease of application while resulting in accurate bridge analysis. Actually, the researchers in NCHRP12-62 had investigated the lever rule method and the Henry's method to develop the simplified live load distribution factor equations. A combination of the Henry's method and the calibrated lever rule was recommended. This combination predicts both moment and shear distribution factors more accurately than the current LRFD equations, without the restrictions on ranges of applicability set in those equations.

For one lane loaded and multiple lanes loaded, the live load distributions for shear and reaction are determined using distribution factor based upon the Lever Rule adjusted Equation 2-13 (NCHRP12-62). This equation is also used to predict the live load distribution for one lane moment.

$$mg = \gamma_s m[a(g_{leverrule}) + b] \geq m\left[\frac{N_{lanes}}{N_g}\right] \quad (2-13)$$

where

m_g = distribution factor including multiple presence

$g_{\text{leverrule}}$ = distribution factor based upon the lever rule

a, b = calibration constants for shear, reaction and moment (one lane loaded)

m = multiple presence factor

γ_s = live load distribution simplification factor

N_{lanes} = number of design lanes considered in the lever rule analysis

N_g = number of girders in the cross section

A modified Equal Distribution Factor (EDF) method is used for multiple loaded

lanes for moment:

$$mg = \gamma_s m \left[a_m \left(\frac{W_c}{10N_g} \right) + b_m \right] \geq m \left[\frac{N_L}{N_g} \right] \quad (2-14)$$

where

a_m, b_m = calibration constants for moment

W_c = the curb-to-curb distance, ft.

N_g = the number of girders.

N_L = the maximum number of design lanes

The calibration factors, multiple presence factors, simplification factors in Equations 2-13 and 2-14 are specified in NCHRP12-62. Since the Lever Rule method and EDF method are unlimited, equations for both moment and shear distributions for straight bridges specified in NCHRP12-62 are unlimited on the range of applicability. However, the skew correction factors were kept fundamentally the same as the current LRFD shown in Table 2.1. Therefore, in the proposed AASHTO distribution factor equations developed through NCHRP 12-62, the range of applicability for the skew correction

factors introduces an inconsistency in applicability between the almost unlimited newly developed distribution factor equations and the skew correction equations. This causes confusion when using the new distribution factor equations for skewed bridges. Consequently, the newly developed equations from NCHRP 12-62 are not applicable for bridges with structural parameters outside of the range of applicability. A rigorous analysis shall be performed for skews exceeding 60 degrees. The maximum bending moment in the beams of a skewed bridge is less than in a similar straight bridge. A reduction for such may be ignored.

Table 2.1 SCFs for Shear Distribution in NCHRP12-62

Type of Superstructure	Applicable Cross-Section from Table 4.6.2.2.1-1	Correction Factor	Range of Applicability
Concrete Deck, Filled Grid, Partially Filled Grid, or Unfilled Grid Deck Composite with Reinforced Concrete Slab on Steel or Concrete Beams; Concrete T-Beams, T- and Double T-Section	a, e and also h, i, j if sufficiently connected to act as a unit	$1.0 + 0.20 \tan \theta$	$0^\circ \leq \theta \leq 60^\circ$ $3.5 \leq S \leq 16.0$ $20 \leq L \leq 240$ $N_b \geq 4$
Precast concrete I and bulb tee beams	k	$1.0 + 0.09 \tan \theta$	$0^\circ \leq \theta \leq 60^\circ$ $3.5 \leq S \leq 16.0$ $20 \leq L \leq 240$ $N_b \geq 4$
Cast-in-Place Concrete Multicell Box	d	$1.0 + \left(0.25 + \frac{12.0L}{70d}\right) \tan \theta$	$0^\circ < \theta \leq 60^\circ$ $6.0 < S \leq 13.0$ $20 \leq L \leq 240$ $35 \leq d \leq 110$ $N_c \geq 3$
Concrete Deck on Spread Concrete Box Beams	b, c	$1.0 + \frac{\sqrt{Ld}}{6S} \tan \theta$	$0^\circ < \theta \leq 60^\circ$ $6.0 \leq S \leq 11.5$ $20 \leq L \leq 140$ $18 \leq d \leq 65$ $N_b \geq 3$
Concrete Box Beams Used in Multibeam Decks	f, g	$1.0 + \frac{12.0L}{90d} \sqrt{\tan \theta}$	$0^\circ < \theta \leq 60^\circ$ $20 \leq L \leq 120$ $17 \leq d \leq 60$ $35 \leq b \leq 60$ $5 \leq N_b \leq 20$

2.2 Review of Research on Skew Correction Factors

The skew angle is taken as the angle between the supporting abutment or pier and a line perpendicular to the roadway. It was found that the skewed supports change the load path. The load is transferred to the supports in their shortest path (i.e., towards the obtuse corners). Therefore, the moments in the middle span are smaller, and the shear in the girder at the obtuse corner is larger when compared to those obtained in a non-skewed bridge of the same length and size. This effect is dependent on the amount of skew. Skew correction factors for distribution factors account for this effect. Therefore, for skewed bridges, the distribution factors calculated from the specified equations for straight bridges should be adjusted by skew correction factors (SCFs), as shown below:

$$LDF_{skew} = LDF_{str} \times SCF.$$

LDF_{skew} is the live load distribution factor for shear or reaction in skewed bridges. LDF_{str} is the live load distribution factor for shear or reaction in straight bridges. LDF_{str} can be obtained with the methods mentioned in the previous sections, namely OHBDC, CHBDC, AASHTO LRFD, EDF or the lever rule method. Finally, SCF is the skew correction factor to account for the effect of skew. The related specification and research on skew correction factors are introduced in the following sections.

2.2.1 Skew Correction Factor in AASHTO LRFD Specifications

The AASHTO LRFD specifications (2005) contain skew reduction factors for moment and skew correction factors for shear for various bridge types. For example, for

steel I-girder bridges, the reduction factor is based on the angle of skew (θ), beam spacing (S), span length (L), beam stiffness (K_g), slab thickness (t_s), and the number of beams (N_b). The moment correction factor (MCF) in Table 4.6.2.2.2e-1 from the AASHTO LRFD Specifications is given by

$$MCF = 1 - c_1 (\tan \theta)^{1.5}$$

$$c_1 = 0.25 \left(\frac{K_g}{12L t_s^3} \right)^{0.25} \left(\frac{S}{L} \right)^{0.5} \quad (2-15)$$

If $\theta < 30^\circ$, then $c_1 = 0.0$. If $\theta > 60^\circ$, then use $\theta = 60^\circ$.

$$\text{Range of Applicability: } \begin{cases} 30^\circ \leq \theta \leq 60^\circ \\ 3.5 \text{ ft} \leq S \leq 16.0 \text{ ft} \\ 20 \text{ ft} \leq L \leq 240 \text{ ft} \\ N_b \geq 4 \end{cases}$$

As specified in the AASHTO LRFD (2005) article 4.6.2.2.3c, the shear in the beam ends at the obtuse corner of the bridge shall be adjusted when the line of support is skewed at an angle with the vertical. The skew correction factors set in the current LRFD specifications are shown in Table 2.2.

2.2.2 Other Research on Effect of Skew Angle

The effect of skewed supports on the wheel load distribution factor was studied by a number of investigators.

In a study of prestressed concrete girder bridges conducted by Barr et al. (2001), it was stated that, in general, the interior girders were more affected by skew than were the exterior girders. It was shown that skew had little effect for skew angles less than 20° .

Table 2.2 Correction Factors for LDFs for Support Shear of the Obtuse Corner
(Reproduced from the AASHTO LRFD Specifications)

Type of Superstructure	Applicable Cross-Section from [Table 4.6.2.2.1-1]	Correction Factor	Range of Applicability
Concrete Deck, Filled Grid, Partially Filled Grid, or Unfilled Grid Deck Composite with Reinforced Concrete Slab on Steel or Concrete Beams; Concrete T-Beams, T- and Double T-Section	a, e, k and also i, j if sufficiently connected to act as a unit	$1.0 + 0.20 \left(\frac{12.0Lt^3}{K_g} \right)^{0.3} \tan \theta$	$0^\circ \leq \theta \leq 60^\circ$ $3.5 \leq S \leq 16.0$ $20 \leq L \leq 240$ $N_b \geq 4$
Cast-in-Place Concrete Multicell Box	d	$1.0 + \left(0.25 + \frac{12.0L}{70d} \right) \tan \theta$	$0^\circ < \theta \leq 60^\circ$ $6.0 < S \leq 13.0$ $20 \leq L \leq 240$ $35 \leq d \leq 110$ $N_c \geq 3$
Concrete Deck on Spread Concrete Box Beams	b, c	$1.0 + \frac{\sqrt{Ld}}{6S} \tan \theta$	$0^\circ < \theta \leq 60^\circ$ $6.0 \leq S \leq 11.5$ $20 \leq L \leq 140$ $18 \leq d \leq 65$ $N_b \geq 3$
Concrete Box Beams Used in Multibeam Decks	f, g	$1.0 + \frac{12.0L}{90d} \sqrt{\tan \theta}$	$0^\circ < \theta \leq 60^\circ$ $20 \leq L \leq 120$ $17 \leq d \leq 60$ $35 \leq b \leq 60$ $5 \leq N_b \leq 20$

This finding is consistent with previous research (Bishara et al. 1993). Bishara et al. (1993) observed that, for concrete or multisteel beam composite bridges of medium span length with a skew angle not exceeding 30° , the reduction in the distribution factor for interior girders was less than 5%. For skew angles between 30° and 60° , the reduction was 28%. For exterior girders, the skew effect behaves differently. In the study, the load distribution factor for a 20° skewed bridge was 10% higher than that for a straight bridge. For a 40° skewed bridge, the increase in the distribution factor was only 5%. For a 60° skewed bridge, the distribution factor was reduced by 25%. A set of equations were developed from this study for the calculation of live load moment distribution factors.

Ebeido and Kennedy (1996) observed that skew had only a small effect on the moment distribution factor for skews less than 30° for continuous composite steel-

concrete bridges. It was also noted that there is no significant interaction between aspect ratio and skew on the moment distribution factor for skew angles between 0° and 30° . Skew was said to have a greater influence on the design of interior girders than exterior girders. In the study, empirical formulas for moment distribution were developed for two ranges of skew angles, namely, $\theta < 30^\circ$ and $30^\circ < \theta \leq 60^\circ$. Ebeido and Kennedy also developed similar empirical formulas for reaction and shear distribution factors at the pier support for exterior and interior girders of continuous skew composite bridges having two unequal spans.

Tobias et al. (2004) concluded that the skew correction/amplification for end shear in primary beams in the LRFD Specifications is reasonable for typical Illinois bridges given the uncertainty surrounding the phenomenon in the field. However, Illinois has set the longitudinal stiffness term in the amplification equation to unity in order to simplify the specification equations.

Huang et al. (2004) presented a study aimed at developing a better understanding of the transverse load distribution for highly skewed slab-on-steel girder bridges. However, only LDF for moment was discussed in this research. The LDFs for shear and reaction were not mentioned.

The NCHRP Project 12-62, "Simplified Live-Load Distribution Factor Equations," was to examine the distribution factors in detail, and recommend revisions to the LRFD Specifications. Revisions under consideration are primarily concerned with establishing simpler load distribution equations. In this research, the calibrated Lever Rule method and the Henry's method were investigated in detail to develop the recommended specification-based methods. With these methods, distribution factors for

bridge moment and shear can be calculated without significant limitations on the range of applicability. The effect of the skew angle was also considered in NCHRP12-62. The simplified LRFD skew correction factors for shear are listed in Table 2.1. The iterative term K_g was eliminated from the LRFD specification to simplify the design process. The parameters used to calculate the distribution factors are girder spacing, span length, and girder depth, which are readily available or easily estimated. As mentioned earlier, the range of applicability for the skew correction factors introduces an inconsistency in applicability between the almost unlimited newly developed distribution factor equations and the skew correction equations.

2.2.3 Possibility of Bridges That Have Parameters Exceeding Applicable Range

The objective for employing the concept of distribution factors is to simplify the design process. However, fairly strict restrictions are imposed by the LRFD Specifications on the use of these formulas. As shown in equations 2-4 and 2-13, in current specifications, limits are set on skew angle, span length, number of girders, beam depth, etc. On the other hand, bridges outside of these limits are frequently constructed. Consequently, these restraints place severe restrictions on the routine design of bridges. When engineers design a bridge with structural parameters in excess of the range of applicability, the simplified equations for shear and skew correction factors in LRFD specifications are not applicable, and rigorous analyses are required. Although still relatively rare, long-span girder bridges, especially steel plate girder bridges, are increasingly being selected by owners over more established long-span structural types,

such as arches and trusses. Developments in fabrication capabilities in the United States, coupled with the economics of bridge construction, the desire for structural redundancy, and a greater focus on bridge aesthetics for long-span structures, have resulted in an increased number of long-span girder bridges being constructed. For example, the new James Rumsey Bridge is a three-span, 1085-foot long, steel I-girder bridge, with a span length of 425 feet, crossing the Potomac River at Shepherdstown, Virginia.

The skew angle of the bridges is the most critical parameter that affects the wheel-load distribution factor, and was studied in this research. Skew in a bridge can result from many factors, including natural or manmade obstacles, complex intersections, space limitations, or mountainous terrain. Figures 2.7 and 2.8 show highly skewed bridges as examples of bridges outside the applicable limits. The skew angle of the first bridge in Figure 2.7 is 70° , which is outside the applicable range. For the second bridge in Figure 2.8, both the skew angle of 65° and the span length of 265 feet are outside the applicable ranges. In summary, in practice it is possible to build bridges with parameters outside of the applicable range set in the current LRFD specifications. However, no research has been performed to investigate the SCFs for these bridges.



Figure 2.7 Bridge S.R. 0031 over PA Turnpike (Reproduced from Internet)
(Spans: 161 ft each span, Skew: 70 degrees)



Figure 2.8 Bridge I-87 NB Connectors over I-287 EB (Reproduced from Internet)
(Span: 265 ft, Skew: 65 degrees)

2.3 Review of Research on LDF for Shear and Reactions

To design a continuous composite bridge properly, it is important to determine the maximum reactions and shears. When the bridge is skewed, the distribution factors for reactions and shears become more complicated. The AASHTO LRFD Bridge Design

Specifications require that shear in the beam at the obtuse corner of the bridge shall be adjusted when the line of support is skewed. The specifications provide correction factors for this adjustment and require that the correction factors be applied to all beams in the cross-section. Live load reaction at piers is also an important design term for substructure design, and is also affected by the skewness of the bridge. The current AASHTO Specifications do not address any specific modification for the distribution factor of live load reactions in skewed continuous bridges. As a result, the skew effect on reactions at piers of skewed continuous bridges is determined either by using the skew correction factor for shear or by using no skew correction factor.

It has been observed in previous studies that the reactions at piers in a skewed continuous bridge are amplified, and the skew correction factors for reactions are unique from those for beam shear (Modjeski and Masters 2002). The researchers, at Modjeski and Masters Inc., conducted research on shear in skewed multi-beam bridges in the NCHRP Project 20-7/Task 107. They found that the skew correction factor for reactions at piers in continuous bridges were different from those calculated from shear at the piers. The effects of the obtuse and acute corners on the girder shear on opposite sides of the bearings do not eliminate a correction factor for the reaction. It is recommended in the study that further research be performed to investigate the skew correction factors for reactions at the piers of continuous bridges.

Ebeido and Kennedy (1996) investigated the influence of skew on the shear and reaction distribution factors of continuous two-span composite steel-concrete bridges. The difference between the LDF for shear and that for reaction can be seen in the

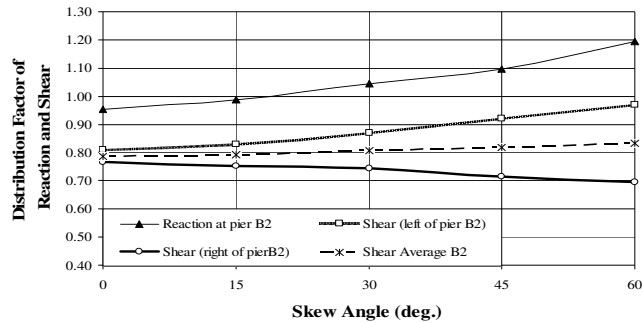


Figure 2.9 Distribution factors of reaction and shear at piers

expressions which were derived for both shear and reaction distribution factors for AASHTO truck loading, as well as for dead load from the parametric study.

For skewed bridges, the reaction distribution factors at abutments follow the same trend as the shear distribution factors at beam ends at the beginning and end of a bridge. However, the LDF for reaction can be very different from that for shear at piers of skewed continuous bridges (Huo and Zhang, 2006-2008). Figure 2.9 is reproduced from a paper by Huo and Zhang in 2008, which illustrates the difference of reaction distribution factors from those for shear in a four-span precast concrete bridge. Huo and Zhang (2008) observed that the distribution factors of reactions at piers were higher than those of shear near the piers. The reaction distribution factors increased faster than the shear distribution factors at piers as the skew angle increased. The increase in the reaction distribution factor on the interior beam line was more significant than that in the shear distribution factor when the skew angle was greater than 30° . The LRFD shear equations and the Lever Rule method could conservatively predict live load reaction distribution for piers on exterior beam lines but clearly underestimates live load reaction distribution on interior beam lines. It is recommended that more research be performed on the

distribution factor of live load reaction and that accurate and simple distribution factor equations for reactions be developed.

2.4 Potential Problems in Current Procedures

The AASHTO LRFD method is generally considered to be the most accurate among all the simplified methods. However, in order to use the AASHTO LRFD equations, several bridge parameters must be limited in the specified range of applicability. There are significant restraints on the range of applicability for the AASHTO LRFD skew correction factor equations. Table 2.2 lists the limitations on the range of applicability for skew correction factors of shear distributions. The bridges that have structural parameters outside the range of applicability cannot be designed with the simplified live load distribution equations specified in the current LRFD Specifications. As specified in section 4.6.3 of the AASHTO LRFD Specifications, refined methods of analysis are required when the ranges of applicability are exceeded. However, this rigorous analysis often requires special skills and analysis tools. In addition, it is time-consuming, costly, and inconvenient in most cases.

Even in the range of the limitations set in the AASHTO LRFD Specifications, the live load distribution factors calculated from the codified formulas are not always the same as the finite element analysis results. The AASHTO LRFD seems to give very comparable results to the finite element analysis results for bridges with parameters within the intermediate ranges and tends to deviate within the extreme ranges of these limitations. The AASHTO LRFD limitations on the LDFs need to be re-evaluated to

reduce the deviation from the finite element analysis results, because this deviation could significantly increase the cost in some cases or jeopardize the safety in others (Yousif and Hindi, 2007).

As far as the other state-specified methods are concerned, the effect of skew angle is not considered in the lever rule method and the Henry's method. Therefore, as mentioned earlier, moment distribution factors are too conservative and shear distribution factors are too risky without considering the effect of skew angle.

In NCHRP12-62, the moment and shear distribution factors for straight bridges can be calculated with the proposed methods without the restrictions on ranges of applicability, but the limitations on the range of applicability for the skew adjust factors were kept fundamentally the same as the current LRFD Specifications.

In summary, no simplified methods can predict the live load distribution for skewed bridges with structural parameters in excess of the applicable range set in the AASHTO LRFD specifications.

Most modern bridges are continuous and skewed, so use of inaccurate estimation of live load reactions would lead to somewhat incorrect design for bridge substructures, such as pier caps and piers. Underestimating the live load reactions could cause a design to be unsafe and would directly affect the performance and service life of bridge substructures. On the other hand, overestimating the live load reactions would increase the cost of bridge substructure unnecessarily. Although extensive studies have been conducted on the skew effect on live load shear distribution, very little research has been done on the effect of bridge skewness on live load reactions of continuous bridges. In current methods, distribution factors for reaction are predicted by shear distribution

equations and corresponding skew correction factors. In other words, there are no specific equations for reaction distribution factors in the current LRFD Specifications. In some states, the lever rule method is used to calculate LDF for reactions without considering the effect of the skew angle on reaction. Based on a limited number of research studies by Modjeski and Masters (2002) and Huo and Zhang (2006, 2008), LDF for reaction is different from that for shear in skewed bridges. Live load reaction at piers is an important design value for substructure design. Few studies have been done on LDF for reaction distribution.

2.5 Objectives

Less limiting ranges of applicability for skew correction factors would result in increased economy in the design process and less potential error from refined analysis. But in the current procedures, no simplified methods except rigorous analyses can be used to predict the maximum responses of the superstructures of bridges with parameters exceeding the range of applicability. Therefore, one of the objectives of this dissertation is to eliminate the restrictions on the range of applicability for skew correction factors set in the current LRFD Specifications. Then, the bridge engineers can easily predict the maximum responses for the skewed bridges without any restrictions on the applicable ranges.

The current AASHTO LRFD Specifications do not address any specific modification for the distribution factor of live load reactions in skewed continuous bridges. Few studies on distribution factors for live load reactions have been done,

especially for highly skewed bridges. The bridge design community is interested in learning how the live load reactions are being affected by the skewness of bridges and in understanding the difference between skew corrections for shear and reactions. Accordingly, the second objective of this dissertation is to study the distribution factors for live load reaction in skewed bridges.

The expected contributions of this research to the bridge design community are listed below:

- This research eliminates the restrictions on the range of applicability for the skew correction factor equations set in current procedures, such as the AASHTO LRFD Specifications and NCHRP12-62. Thus, bridge engineers can use the simplified SCF formulas instead of rigorous analyses to predict maximum responses, in order to design skewed bridges with structural parameters in excess of the limitations on the applicable ranges.
- The newly developed SCF formulas for shear and reaction can reduce the deviation from the finite element analysis results, because Yousif and Hindi (2007) revealed that the current AASHTO-LRFD Specifications tend to deviate within the extreme ranges of limitations.
- The newly developed SCF formulas for reaction can be used to accurately predict live load reactions in skewed bridges, which will lead to accurate design for bridge substructures, such as pier caps and piers.

2.6 Methodology

This research was based on NCHRP12-62, in which the calibrated lever rule and the Henry's method were presented to estimate live load effect with the unlimited equations for straight bridges. In NCHRP12-62, the shear distribution factors are calculated with the calibrated lever rule method. The skew correction factors for shear distributions are kept fundamentally the same as the current LRFD specifications. The process for the research is straightforward:

1. Investigate the finite element modeling techniques, present the improved finite-element models for slab-on-girder bridges in ANSYS, and verify the improved models with the 3-D detailed FEM and experimental test results.
2. Develop various types of hypothetical bridges with structural parameters exceeding the applicable ranges set in the current LRFD Specifications using the α - θ method (i.e. OHBDC). In addition, develop a certain number of regular bridges with parameters within the applicable ranges in order to study live load distribution factors for reaction.
3. Obtain the maximum shear and reaction for the developed bridges in the database with the proposed improved models. ANSYS is used to generate the finite element models and output the maximum responses. The corresponding beam line actions, including shear and reaction, are obtained by one-dimensional analyses. The rigorous actions are divided by the beam line actions to determine the distribution factors for shear and reaction. The

distribution factors for skewed bridges from finite element analyses are obtained in this step, named FEM-LDF-SKEW.

4. Compute the distribution factors for shear and reaction for the bridges defined in the database, using the simplified methods specified in the AASHTO LRFD specifications and NCHRP12-62, without considering the effect of skew. The distribution factors for straight bridges from the simplified methods are obtained in this step, named LRFD-LDF-STR or 12-62-LDF-STR.
5. For each bridge, the rigorous (FEM-LDF-SKEW) and simplified (LRFD-LDF-STR or 12-62-LDF-STR) results are available in a database. Obtain the skew correction factors by dividing the FEM-LDF-SKEW by the corresponding LRFD-LDF-STR or 12-62-LDF-STR.
6. Conduct parametric studies to identify the parameters sensitive to the skew correction factors.
7. Based on the skew correction factors that were calculated and the parametric studies, develop two sets of skew correction factor formulas. One will be based on the AASHTO LRFD Specifications, and the other will be based on NCHRP12-62. These proposed SCF formulas will be unlimited, since they are derived from bridges with parameters outside the applicable ranges.
8. The LDF for reaction and that for shear are considered equal in the straight bridges. In other words, the difference between the LDF for reaction and that for shear in skewed bridges is taken into account by the different skew correction factors. Therefore, for each bridge type, SCF formulas for reaction and shear are proposed, respectively.

9. Obtain the statistical results, such as average, coefficient of variants, etc., in order to evaluate the proposed equations. Finally, compare the skew correction factors obtained from the proposed formulas to the finite element analysis results in order to validate the proposed formulas.

CHAPTER 3

FINITE ELEMENT MODELING OF GIRDER BRIDGES

3.1 General Introduction

The responses of a bridge under live load are important for both design and evaluation purposes, because they enable the engineer to find the strength and serviceability of a given superstructure. However, determining the accurate maximum responses and load distributions is difficult because of the complexity of bridge structures. Because of the advances in computer technology and modern finite element (FE) programs with user-friendly graphical interfaces, the finite element method (FEM) is replacing other methods, such as grillage analysis, even for more straightforward bridge analyses.

First, in this chapter, FE modeling techniques are thoroughly investigated in order to select the most accurate and simple modeling for this research. Secondly, the improved modeling technique selected for this research is introduced in detail and verified by the 3-D detailed FEM and experimental test results. Thirdly, the flowchart is presented to show the process of the construction of finite element models, solution, and output of results with APDL (ANSYS Parametric Design Language).

3.2 Literature Review on Finite Element Modeling

Finite element analyses (FEA) enables bridge engineers to determine the distribution of wheel loads more accurately than empirical or restricted code formulas. More and more researchers have used FEA to model bridge superstructures. The following assumptions/conditions pertain to the FEA of bridge superstructures (Chen, 1996):

1. A small-deflection theory was used
2. Linearly elastic behavior of materials was assumed
3. All loading conditions were static
4. The deck slab was assumed to have a constant thickness

With FEA, a bridge superstructure can be idealized in the following 7 ways, which have been used and verified by previous researchers.

3.2.1 Model A: Concentric Beam Model

The first modeling technique (Model A) was based on studies conducted by Hays et al. (1986) and Mabsout et al. (1997). The concrete slab was idealized as quadrilateral shell elements with six degrees-of-freedom (DOF), and the girders were idealized as two-node space frame elements with six DOF at each node. The centroid of each girder coincided with the centroid of the concrete slab as shown in Figure 3.1. External supports were assumed to be located along the centroidal axes of the beam elements. Hinges and rollers were assigned at abutments and piers, respectively.

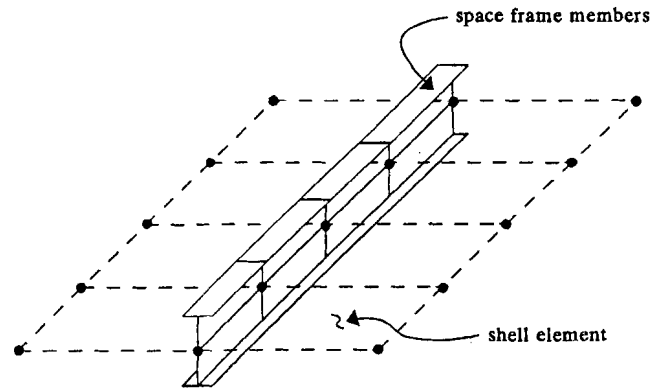


Figure 3.1 Concentric Beam Model (Mabsout, 1997)

3.2.2 Model B: Eccentric Beam Model

The second modeling technique (Model B) was studied by Imbsen and Nutt (1978) and Sotelino et al. (2004). As shown in Figure 3.2, the concrete slab was modeled as quadrilateral shell elements that incorporate both membrane and bending actions. Steel girders were modeled using eccentrically connected two-node beam elements. The eccentricity of the girders was taken into account through the use of rigid links between the centroid of the concrete slab and the centroid of the steel girders.

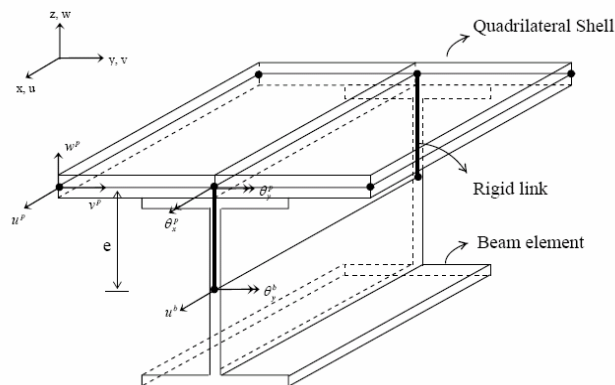


Figure 3.2 Eccentric Beam Model (Sotelino, 2004)

3.2.3 Model C: Detailed Beam Model

As shown in Figure 3.3, the third modeling technique (Model C), which is based on a study conducted by Brockenbrough (1986), modeled the girder flanges as space frame elements and the deck slab and girder webs as shell elements. The eccentricity between the concrete deck and the steel girder flange was idealized by a rigid link.

3.2.4 Model D: Solid Decks + Shell Beam Model

Model D, as suggested by Tarhini and Frederick (1992), idealized the bridge deck as three dimensional solid elements, with three DOFs at each node, and the girders as shell elements. Figure 3.4 shows the details of Model D, which is reproduced from Tarhini and Frederick.

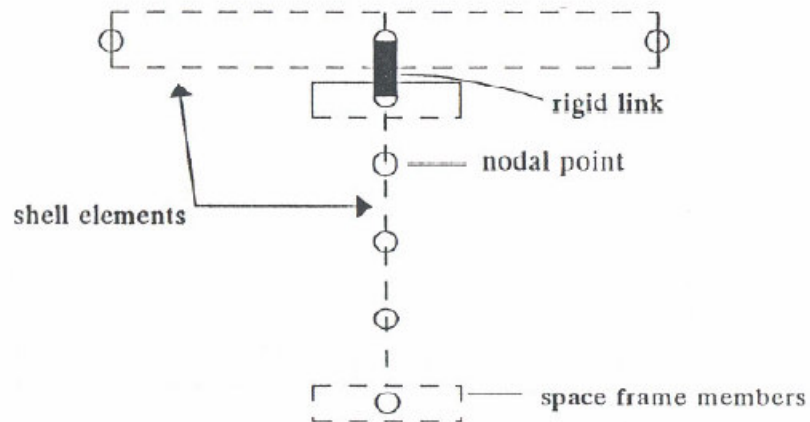


Figure 3.3 Detailed Beam Model (Brockenbrough 1986)

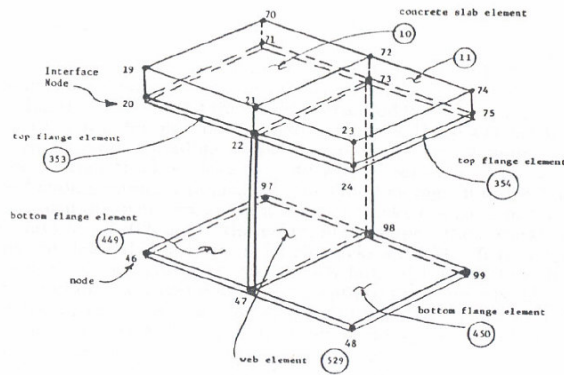


Figure 3.4 Solid Deck + Shell Beam Model (Tarhini and Frederick 1992)

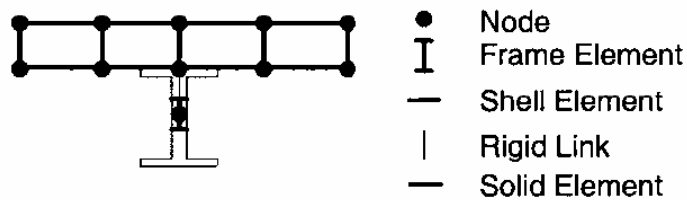


Figure 3.5 Solid Deck + Frame Beam Model (Barr and Amin 2006)

3.2.5 Model E: Solid Deck + Frame Beam Model

Model E, used by Barr and Amin (2006), is shown in Figure 3.5. The concrete decks were modeled with solid elements, and the girders were modeled with frame elements. The rigid body constraints were placed vertically at the centroid of the members and connected to achieve composite action.

3.2.6 Model F: Solid Deck + Solid Beam Model

In Model F (Abendroth et al. 2004), the girders and decks were modeled using solid elements (brick elements) with eight nodes (SOLID45 in the ANSYS element

library). This element has three translational DOFs at each node. Figure 3.6 shows the side view of this bridge model.

3.2.7 Model G: Shell Deck + Shell Beam Model

Choo et al. (2004) utilized Model G to model bridge superstructures. The model consists of girders and concrete decks represented by either three or four-node shell elements. All the girder shell elements have four nodes, while the concrete elements consist of both three- and four-node shells. The deck shell elements were connected to the girders using rigid links (frame elements) to transfer the concrete loads and to maintain compatibility between the deck and the girders. A detailed model and the boundary conditions are shown in Figure 3.7.

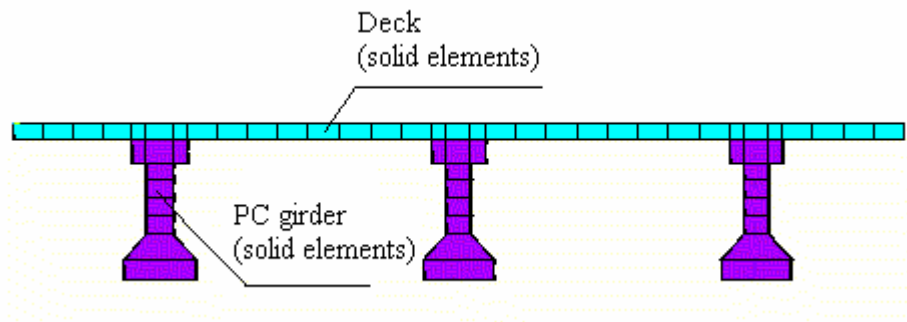


Figure 3.6 Solid Deck + Solid Beam Model (Abendroth et al. 2004)

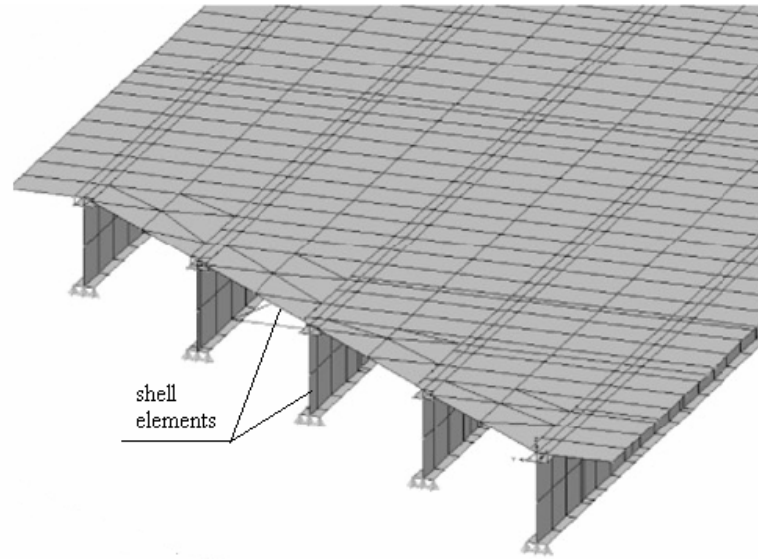


Figure 3.7 Shell Deck + Shell Beam Model (Choo et al. 2004)

Fifteen papers on distribution factors published from 1985 to 2001 were reviewed by Sotelino et al. (2004) to investigate the modeling techniques used in previous research. Similarly, another 18 papers published from 2002 to 2007 on distribution factors on slab-on-girder bridges were examined in this research. As shown in Table 3.1, these papers were categorized according to the analytical methods, finite element modeling techniques, and girder materials. The calculation of ratio in the table was based on the total 33 papers. For example, 4-node shell elements were used to model bridge decks in 23 papers among the total papers investigated (i.e., 69.7% shown in Table 3.1). The literature survey indicated that more previous researchers utilized the FEM (finite element method) as an analysis tool over the grillage analysis or other simplified methods. Based on the ratios shown in this table, the 4-node shell elements, 2-node beam element were most commonly used by previous researchers to model bridge deck and girders, respectively. The discussion about this survey is presented in the following sections in detail.

Table 3.1 Survey of Bridge Analysis Studies on LDF

Analytical method	Finite element analysis: 1-14,16-33 Grillage analysis: 15, 5	
Finite Element Model	Category	Ratio
	Concentric beam model: 3,8,9,18,24,26,32,33	24.2%
	Eccentric beam model:1,4,5,9,10,11,13,16,19,22,24,25,27,29,30	45.5%
	Detailed beam model: 2,7, 9,17,28	15.1%
	Solid deck+ Shell beam model: 6,9,12,14,20,31	18.2%
	Shell deck+ Shell beam model:23,27	6.0%
	Solid deck+ frame beam model: 27	3.0%
	Solid deck +solid beam model: 21,27	6.0%
	Deck FE element	
	Solid (8 node):6,9,14,20,21,29	18.2%
	Shell (3 node): 7,23,33	9.0%
	Shell (4 node): 2,3,5,8,9,11,12,13,15,16,17,18,19,22,23,24,26,27,28,30,31,32,33	69.7%
	Shell (8 node): 4, 10,25	9.0%
	Shell (9 node): 1	3.0%
	Girder FE element	
Beam (2 node): 3,5,8,9,10,11,13,16,18,19,22,24,26,27,30,32,33	51.5%	
Beam (3 node): 1,4,25,29	12.1%	
Flange (2 node beam) + Web (4 node shell): 2,7,9,17,28	15.1%	
Flange, Web (4 node shell): 6,9,12,14,20,23,31	21.2%	
Solid:21	3.0%	
Secondary member considered (diaphragms, cross bracings, stiffeners, curb, parapets)		
Yes: 7,8,12,13,14,16,17,19,20,21,22, 25,28,29,30,31	48.4%	
No: 1,2,3,4,5,6,9,11,18,23,24,26,27,32,33	45.2%	
Composite action		
Full: 1-25,27-30,32,33	93.9%	
None: 9,26,31	9.0%	
Proof of FE model		
Experiment: 3,5,7,8,12,13,14,20,21,22,23,24,25,27,29,30,31,32	54.5%	
N/A: 1,2,4,6,9,11,17,18,19,27,28,33	36.4%	
Material		
Steel: 2,3,6,7,8,9,10,12,14,15,17,18,19,20,21,22,23,25,27,28,29,33	66.7%	
Concrete: 1,4,5,11,13,16,25,26,30,31,32,33	36.4%	

Notes:

- | | | |
|-------------------------|----------------------|---------------------|
| 1. Marx (1985) | 12. Nicola (2000) | 23. Choo (2004) |
| 2. Brockenbrough (1986) | 13. Barr (2001) | 24. Patrick (2004) |
| 3. Hays (1986) | 14. Eom (2001) | 25. Sotelino (2004) |
| 4. Khaleel (1990) | 15. Schwarz (2001) | 26. Yousif (2005) |
| 5. Zokaie (1991) | 16. Shahawy (2001) | 27. Barr (2006) |
| 6. Tarhini (1992) | 17. Tabsh (2001) | 28. Berglund (2006) |
| 7. Bishara(1993) | 18. Mabsout (2002) | 29. Chung (2006) |
| 8. Ebeido (1996) | 19. Khaloo (2003) | 30. Corner (2006) |
| 9. Mabsout (1997) | 20. Nowak (2003) | 31. Cross (2006) |
| 10. Chan (1999) | 21. Abendroth (2004) | 32. Yousif (2007) |
| 11. Chen (1999) | 22. Cai (2004) | 33. Huo (2008) |

3.3 Comparison of Modeling Techniques

Models D, E, and F utilized three-dimensional solid elements with three DOFs at each node, having linear shape functions, to model the bridge decks. The main drawback in these three models was the use of only one linear solid brick element (8 nodes) throughout the thickness direction. To accurately simulate the flexural behavior of the deck, many solid elements were required throughout the thickness direction, since the solid elements have a linear variation. However, solid elements require more computation time and larger computer memory, even with a very simple bridge model.

All seven models, except A, B, and E, could be adopted to accurately idealize the actual boundary conditions with the application of the detail beam model. However, these models are time-consuming, requiring more time to prepare the input due to the increase in the number of nodes and elements and more computation time, as well as requiring larger computer memory, even with a very simple bridge model. Moreover, these modeling techniques require calculation of bending moments and shear forces for the composite section based on stress values, which increase the complexity of procuring results from FEA modeling. It is not practical to select these modeling techniques for this research, considering the number of bridges to be analyzed.

After reviewing the published papers about FE modeling techniques in Table 3.1, it was concluded that beam models, including the concentric beam model (Model A) and the eccentric beam model (Model B), were the most frequently used in the past 20 years. In Models A and B, shell elements were used to model the bridge deck, and beam elements were used to model the girders. The beam models, including Models A and B,

provide a realistic idealization of bridge behavior while retaining simplicity, which is essential for a great number of bridge analyses.

The modeling techniques selected should be capable of including physical behavior, such as composite action and the eccentricity effect between the slab deck and the girder. Obviously, Model A cannot incorporate the eccentricity effect. That is why, based on the survey, the eccentric modeling technique is more popular than concentric modeling. However, as suggested by Hays et al. (1986), Mabsout et al. (1997), and Yousif et al. (2007), the concentric beam model (Model A) gives as sufficiently accurate results as the other complicated modeling. This model is also easier to implement and makes it easier to avoid the possible errors in modeling preprocessing (i.e. data input) and post-processing (i.e. result extraction) compared to the other modeling techniques. Furthermore, this model is practical for this research, considering the hundreds of bridge models and thousands of loading cases required. Therefore, Model A was chosen to be the foundation for the modeling technique used in this research. It was improved in ANSYS to eliminate the model's shortcoming of being unable to incorporate the eccentricity between the decks and the girders of bridge superstructures. The following sections introduce and verify this model in detail.

3.4 Improved Concentric Beam Model in ANSYS

The ANSYS (2005) is a large-scale, user-oriented, general-purpose finite-element program for linear and nonlinear systems with analysis capabilities including static, dynamics, creep, buckling, etc. One of the main advantages of ANSYS is the integration

of the three phases of finite-element analysis: preprocessing, solution, and post-processing. Preprocessing defines the model, boundary conditions, and loadings. Post-processing may be used to retrieve analysis results in a variety of ways. The ANSYS finite-element program was selected to analyze the work, primarily because the preprocessing and post-processing of bridge superstructures can be accomplished with APDL conveniently and automatically. APDL is introduced in section 3.7.

ANSYS has the capability of offsetting the beam element from a reference node location in order to define the centroid location of the section relative to the node location. The reference nodes lie in the same plane as the deck slab centroid. The offset is equal to the distance between the slab centroid and the beam centroid. This capability was incorporated into the concentric beam model (Model A) to consider the eccentricity between decks and girders so that the improved concentric beam model can account for the eccentricity of the beam to the deck slabs.

3.4.1 Selected Elements in ANSYS

Since Models A and B are most commonly used in the past 20 years, and can also provide the accurate results compared to the other models, the improved finite element model in ANSYS was presented based on these two models for this research, named improved concentric beam model. Element of BEAM188 was chosen to idealize the girders, and Shell181 was chosen to idealize the deck slabs in the bridge superstructure, as shown in Figure 3.8. To account for the effect of eccentricity between decks and girders, the offset function in ANSYS was used to offset the girder from the bridge deck.

Through the validation of the improved FE model used in this research with the detailed 3-D FEM and test results, it was concluded that the improved FE model are accurate enough to obtain maximum responses for skewed bridges. Therefore, with the simplification and accuracy, the improved FE model was suitable for this research considering the number of the bridge to be analyzed.

BEAM188 is suitable for analyzing slender to moderately stubby/thick beam structures. This element is based on the Timoshenko beam theory. Shear deformation effects are included. BEAM188 has six DOFs at each node. These DOFs include translations in the x-, y-, and z-directions and rotations about the x-, y-, and z-axes. BEAM188 is based on linear polynomials, unlike other Hermitian polynomial-based elements (for example, BEAM4), which can maintain compatibility with a first order shell element (ANSYS, 2005).

SHELL181 is suitable for analyzing thin to moderately-thick shell structures. It is a 4-node element with six degrees of freedom at each node, which include translations in the x-, y-, and z-directions and rotations about the x-, y-, and z-axes. The degenerate triangular option should only be used as filler elements in mesh generation. (ANSYS, 2005)

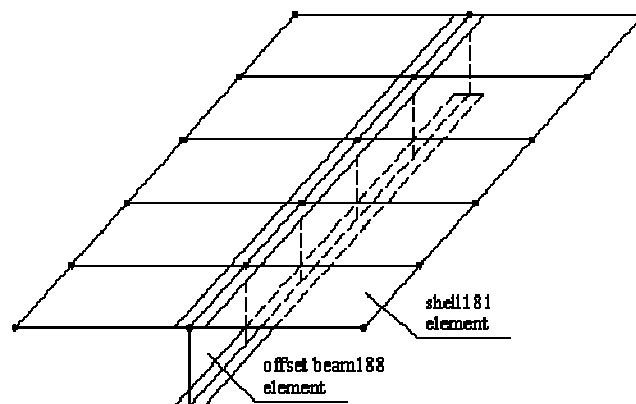


Figure 3.8 Improved Concentric Beam Model

3.4.2 Boundary Conditions

The slab-on-girder bridge in this study was modeled such that the longitudinal axis was along the global X direction, the transverse axis was along the global Y direction, and the vertical axis was along the global Z direction. The support at one abutment was assumed to be pinned, and roller supports were assumed for the other pier. At the pinned abutment, the girders of the bridge were restrained from translation in the global X, Y and Z directions. At the roller supports, the girder was restrained against translation in the global Y and Z directions.

Figure 3.9 shows the example of the improved concentric beam model with boundary conditions. Actually, this model is a 2-D model because the beam element and the shell elements share the same nodes in the deck plane. The amplified details in Figure 3.9 are used only for visualization purposes.

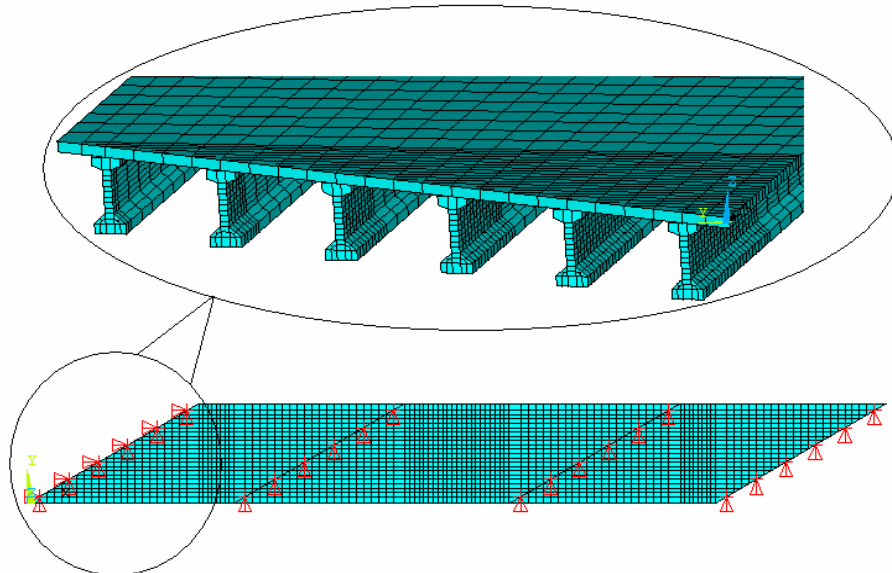


Figure 3.9 Improved Concentric Beam Model with Boundary Conditions

3.4.3 Loading Applied to the Selected Model

The live load applied to the bridges under consideration was an AASHTO HL-93 truck in the AASHTO LRFD Specifications. This vehicle is shown in Figure 3.10. For a beam line analysis, which consists of one longitudinal beam line from the bridge superstructure, a single truck was positioned so that the maximum responses of shear and reaction could be obtained, as shown in Figure 3.11. These values were later used to determine the live load distribution factor associated with the response in question.

The bridge was loaded with a series of moving loads, including one truck, two trucks, three trucks, and four or more trucks in order to search for the maximum responses. The trucks were placed at various locations in the longitudinal and transverse directions until the maximum response was obtained. An example of the transverse vehicle spacing is shown in Figure 3.12.

Due to the fact that, in ANSYS, concentrated loads cannot be directly applied to the shell elements, the concentrated load was linearly distributed to the adjacent nodes based on the location of the load after determining the truck position on the bridge. The detailed descriptions of this distribution are explained later in section 3.7.

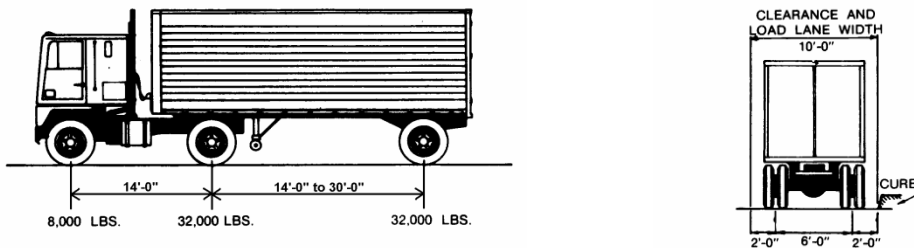


Figure 3.10 AASHTO HL-93 Truck

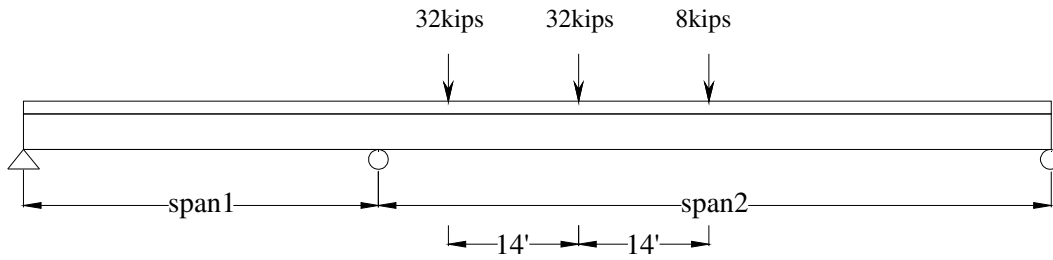


Figure 3.11 Beam Line Analyses

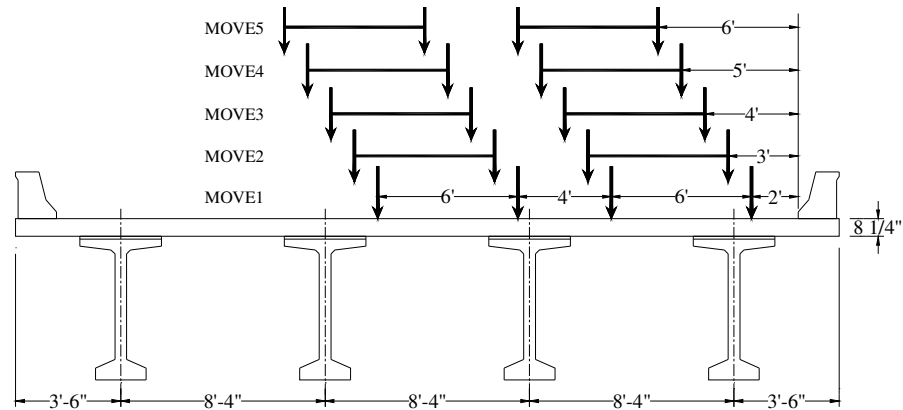


Figure 3.12 Loading Positions for Two Lanes Loaded

3.5 Modeling Verification

To verify that the selected 2-D finite element model (i.e., the improved concentric beam model) is capable of correctly simulating the real behavior of the bridge, the results from the improved concentric beam model were compared to those from the detailed three-dimensional FE analyses and experimental tests. After the verification, the improved concentric beam model was used in this research to search for the maximum responses for slab-on-girder bridges. Hereafter, the 2-D FEM model represents the improved two dimensional concentric beam model used in this research.

The first two bridges were analyzed with the detailed 3-D finite element analyses by Cross et al. (2006) at Southern Illinois University, Edwardsville. The 3-D finite element analyses were conducted in SAP2000. For further verification of the selected bridge models, the results from the selected, improved concentric beam models for the other two bridges were compared to those from experimental tests conducted by the University of Windsor, Canada (1995, 1996), on simply supported and continuous skew composite bridges. The main objective of this section was to validate the selected model used in the finite element analysis.

3.5.1 Comparison of 2-D FEM to 3-D FEM

One of the steel girder bridges investigated by Cross is Bridge 068-0046. This bridge is three-span skewed bridge. The span lengths are 84.5 ft, 113 ft, and 84.5 ft. The skew angle is 59.12° . There are six girders with girder spacing of 7.25 ft and an overhang width of 2.875 ft. The slab thickness is 8 in. The top and bottom flanges are 14 by 0.875 in. and 12 by 0.75 in, respectively. The web is 54 by 0.625 in. The modulus of elasticity for deck and beam is 2900 ksi and 29000 ksi, respectively.

The other bridge mentioned is a precast, prestressed concrete girder bridge named 060-0319. This bridge is a four-span skewed bridge with 43.2° skew angle. The span lengths are 69.885 ft, 100 ft, 100 ft, and 69.885 ft. There are six girders with a girder spacing of 7.417 ft and an overhang width of 3.042 ft. The slab thickness is 7.5 in. The beam is a 54" prestressed concrete girder. The modulus of elasticity for the deck and beam is 3372 ksi and 4415 ksi, respectively. The information about the applied trucks on the above bridges is shown in Figure 3.13 and Table 3.2, respectively.

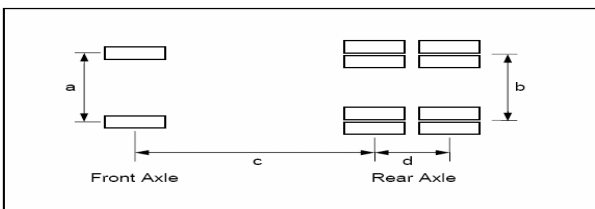


Figure 3.13 Truck Configurations (Cross et al., 2006)

Table 3.2 Truck Loads and Wheel Spacing (Cross et al., 2006)

Structure number	Axle Weight (lbs)		Wheel Spacing (in)		Axle Spacing (in)	
	Front	Rear (Combined)	a	b	c	d
068-0046	12,900	33,460	78	78	144	52
060-0319	11,740	35,980	79	72	145	54

3.5.1.1 Steel girder bridge (068-0046). Figure 3.14 shows the plan of the steel bridge NO. 068-0046. The structural reference point ($x=0$, $y=0$) is at the intersection of the north edge of the deck and east face of the parapet. The transverse truck position (Y) and longitudinal truck position (X) refer to the distance between driver side front wheel and the reference point. Table 3.3 shows coordinates for the X and Y positions for the bridge 068-0046. As shown in Table 3.4, the shears at the beam ends obtained with 2-D finite element models were compared to the corresponding 3-D finite element results for bridge 068-0046. The first and second columns show the load position and beam number, respectively. The remaining columns show the shear forces at D away from the supports with 2-D FEM, 3-D FEM, and the error between two models. In this table, the 2-D FEM represent the results from ANSYS with the proposed improved concentric beam models. The 3-D FEM are the results from SAP2000 with three-dimensional bridge models conducted at Southern Illinois University, Edwardsville.

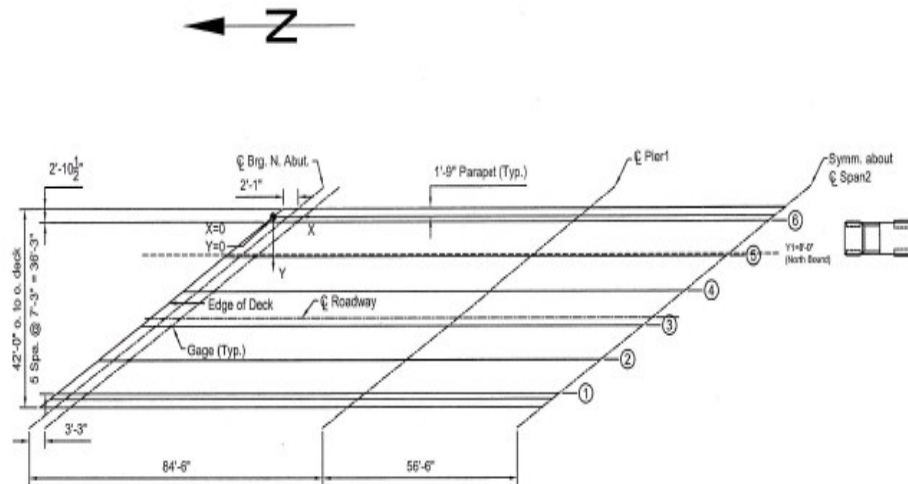


Figure 3.14 Bridge No 068-0046 plan (Cross et al., 2006)

Table 3.3 Coordinates for X and Y Positions for 068-0046 (Cross et al., 2006)

	Y1=8'	Y2=14.375'	Y3=18.25'
X1	40.5'	29.5'	17'
X2	30.5'	19.5'	7'
X3	20.5'	9.5'	-3'
X4	10.5'	-0.5'	-13'
X5	0.5'	-12.5'	-25'

Table 3.4 Comparison of 2-D FEM to 3-D FEM (068-0046)

Load Position	Beam	Shear Force D Away from Support (Kips)		
		2-D FEM ANSYS (Zhang Q.)	3-D FEM SAP (Cross et al.)	2-D vs. 3-D Error (%)
Y1X1	Beam6	5.563	5.968	-6.79
Y1X2	Beam6	8.45	8.7	-2.87
Y1X3	Beam6	11.602	11.407	1.71
Y1X4	Beam6	14.82	14.003	5.83
Y1X5	Beam6	12.75	11.757	8.45
Y2X1	Beam6	3.83	3.965	-3.40
Y2X2	Beam6	4.836	4.91	-1.51
Y2X3	Beam5	6.79	6.331	7.25
Y2X4	Beam5	10.929	11.103	-1.57
Y2X5	Beam5	11.414	12.25	-6.82
Y3X1	Beam5	4.745	4.716	0.61
Y3X2	Beam5	7.277	7.68	-5.25
Y3X3	Beam5	9.903	10.84	-8.64
Y3X4	Beam5	9.43	10.79	-12.60
Y3X5	Beam4	10.528	10.766	-2.21

3.5.1.2 Concrete girder bridge (060-0319). Figure 3.15 shows the plan of the concrete girder bridge. The structural reference point ($x=0$, $y=0$) is at the intersection of the east edge of the deck and south face of the parapet. The transverse truck position (Y) and the longitudinal truck position (X) refer to the distance between the driver side front wheel and the reference point. Table 3.5 shows the coordinates for the X and Y position for bridge 060-0319. The comparisons of 2-D FEM results to those from the 3-D FEM for bridge 060-0319 are shown in Table 3.6. The first and second columns show the load position and beam number, respectively. The remaining columns show the shear forces at D away from the supports with 2-D FEM, 3-D FEM, and the errors between two models. In this table, 2-D FEM and 3-D FEM are the same as mentioned in the previous section.

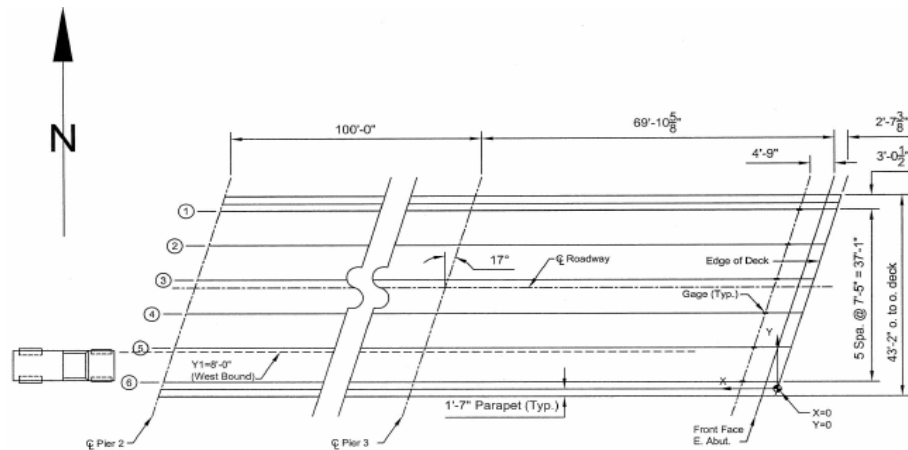


Figure 3.15 Bridge No 060-0319 plan (Cross et al., 2006)

Table 3.5 Coordinates for X and Y Positions for 060-0319 (Cross et al., 2006)

	Y1=8'	Y2=16.292'	Y3=19'
X1	29.5'	27'	26'
X2	19.5'	17'	16'
X3	14.5'	12'	11'
X4	9.5'	7'	6'

Table 3.6 Comparison of 2-D FEM to 3-D FEM (060-0319)

Load Position	Beam	Shear Force D Away from Support (Kips)		
		2-D FEM ANSYS	3-D FEM SAP	2-D vs. 3-D Error (%)
		(Zhang Q.)	(Cross et al.)	
Y1X1	Beam6	7.554	7.149	5.67
Y1X2	Beam6	10.908	10.77	1.28
Y1X3	Beam6	12.667	12.751	-0.66
Y1X4	Beam6	14.462	14.83	-2.48
Y2X1	Beam5	4.939	4.945	-0.12
Y2X2	Beam5	7.678	7.958	-3.52
Y2X3	Beam5	9.26	9.78	-5.32
Y2X4	Beam5	10.994	11.887	-7.51
Y3X1	Beam5	4.511	4.48	0.69
Y3X2	Beam5	6.393	6.524	-2.01
Y3X3	Beam4	9.313	10.062	-7.44

As shown in Tables 3.4 and 3.6, for both bridges, the shear forces from the improved concentric beam model in ANSYS are very close to those from the three dimensional finite element analyses with SAP2000. The maximum errors between the two models in shear are 12.6% and 7.51% for 068-0046 and 060-0319, respectively. However, the error of the maximum shear forces for the two bridges between the 2-D FEM and the 3-D FEM are down to 5.83% and 2.48%, respectively. The deviations between the two finite element methods remain within reasonable ranges. Thus, the improved concentric beam model can produce results that are comparable to the detailed 3-D FEM. This model was further verified by the experimental results obtained in the lab.

3.5.2 Comparison of 2-D FEM to Experimental Results

To verify the program and selected bridge model, the finite element analyses were compared to experimental tests conducted by Ebeido et al. (1995, 1996). One tested

bridge is simply supported with a 45° skew angle. The longitudinal steel beams, end diaphragms, and intermediate cross-beam were S3X5.7. The concrete in the deck slab was designed for a 7-day compressive strength of 6 ksi. The details of the simply supported bridge are shown in Figure 3.16. The other tested bridge was a two-span skewed bridge with a skew angle of 45°. The longitudinal steel beam was S4x7.7. The details of the continuous bridge are shown in Figure 3.17. The comparisons of finite element analysis to experimental results for simply supported and continuous skewed bridges are shown in Table 3.7 and Table 3.8, respectively. The FEM-ABAQUS are the analysis results from Ebeido et al. (1995, 1996) and FEM-ANSYS are the results with the improved concentric beam models employed in this research. The errors were calculated on experimental test results and FEM-ANSYS to verify the selected modeling used in the finite element analysis.

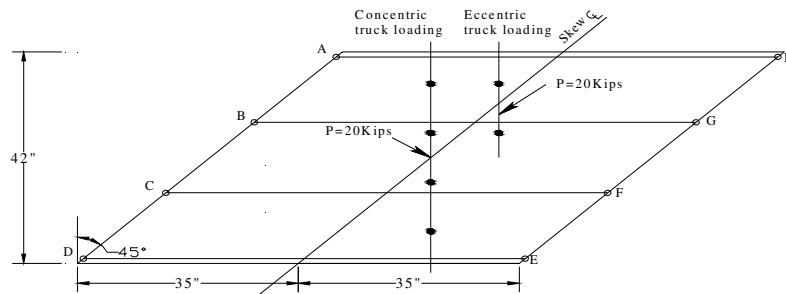


Figure 3.16 Details for Simply Supported Bridge Tested (Ebeido et al. 1995)

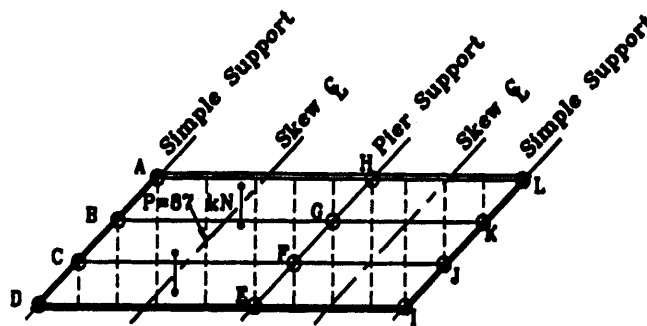


Figure 3.17 Details for Continuous Bridges Tested (Ebeido et al. 1996)

Table 3.7 Comparison of Test Results to FEM for Simply Supported Bridges

Model	Supp.	Reaction (k)							
		Under eccentric truck loading				Under concentric truck loading			
		Exp. Test	FEM-ABAQUS	FEM-ANSYS (Zhang Q.)	ANSYS vs. Exp. Error (%)	Exp. Test	FEM-ABAQUS	FEM-ANSYS (Zhang Q.)	ANSYS vs. Exp. Error (%)
		(Ebeido et al.)				(Ebeido et al.)			
#6	A	6.86	7.08	6.40	-6.71	4.09	4.00	3.82	-6.63
	B	2.68	2.61	2.63	-1.87	3.80	3.91	4.12	8.45
	C	0.92	0.88	1.01	9.78	1.51	1.55	1.42	-5.72
	D	0.20	0.20	0.18	-10.00	0.58	0.54	0.63	7.10
	E	0.09	0.02	0.10	5.56	3.98	4.00	3.73	-6.26
	F	3.28	3.30	3.60	9.76	3.96	3.91	4.13	4.39
	G	3.84	3.82	3.81	-0.78	1.53	1.55	1.46	-4.49
	H	2.14	2.09	2.14	0.00	0.56	0.54	0.61	8.54

As shown in Table 3.7, the maximum error for the finite element results compared to experimental test results are 10% and 8.54% for simply supported bridges under eccentric truck loading and concentric truck loading, respectively. For the continuous skew bridge shown in Table 3.8, the maximum difference between FEM and experimental test results is 14.98%. Because the maximum responses are what we care about in this research, the corresponding error in the maximum reactions of FEM to test results for simply supported bridges and continuous bridges are 6.71% at support A and 2.32% at support E, respectively. Thereafter, the conclusion can be drawn that the selected improved beam models were in fair to good agreement for all experimental test results with a reasonably small percentage of errors. The selected 2-D finite element model in this research can accurately predict the responses of slab-on-girder bridges and easy to implement, which is suitable for analyzing a huge number of bridges.

Table 3.8 Comparison of Experimental Test Results to FEM for Continuous Bridges

Model	Supp.	Reaction (k)			
		Under two lane loaded			
		Exp. Test	FEM-ABAQUS	FEM-ANSYS	ANSYS Vs. Exp. Error (%)
		(Ebeido et al.)		(Zhang Q.)	
Model #2	A	3.17	3.06	2.74	-13.46
	B	2.45	2.29	2.14	-12.87
	C	2.00	1.96	1.79	-10.63
	D	0.47	0.52	0.54	13.50
	E	5.37	5.24	5.25	-2.32
	F	4.09	4.32	4.42	8.13
	G	3.73	3.96	4.10	9.93
	H	1.06	0.94	1.21	14.88
	I	-1.42	-1.44	-1.30	-8.36
	J	-0.72	-0.61	-0.69	-4.22
	K	-0.52	-0.52	-0.50	-2.69
	L	-0.13	-0.16	-0.16	14.98

3.6 Element Meshing Size Study

The mesh density is directly related to computational time and also related to modeling accuracy. These two concerns must be balanced in order to achieve accurate results without consuming an impractical amount of computation time. The finer the mesh, the more accurate are the results obtained from the finite element model. But a finer mesh also takes up large quantities of disk space and requires a longer analysis time. So, an optimum mesh size which yields a desired accuracy should be known. A convergence study was performed to identify the optimum mesh size. The sizes of the elements were increased by one foot at a time from the original element mesh of one ft by one ft. The support reactions were investigated to show the sensitivity of the finite

Table 3.9 Element Meshing Study

Mesh Size (ft.)	load applied (kips)	Support Reactions (kips)		Variation (%)	
		Int. support	Ext. support	Int. support	Ext. support
3'x3'	72	39.17	4.85	-2.72	1.97
2'x2'	72	39.99	4.78	-0.69	0.49
1'x1'	72	40.26	4.76	/	/

element results to the element sizes. The variation was calculated as the difference between the maximum support reactions obtained from the current mesh size and the previous mesh size. As shown in Table 3.9, the mesh size of 2 ft by 2 ft was considered to be the optimum size used in the finite element analyses.

3.7 APDL and Macros

APDL stands for ANSYS Parametric Design Language, a scripting language used to automate common tasks or even build models in terms of parameters (variables). ANSYS offers many conveniences that we can use in day-to-day analyses (ANSYS 2005).

A frequently used sequence of APDL commands were recorded as a macro file (which is sometimes called a command file). Creating a macro enables us to create our own custom ANSYS command. By recording this set of commands in a macro, we can have a new, single command that executes all of the commands required for that calculation.

The magnitude of bridges and load cases to be analyzed is tremendous. For each bridge to be analyzed, there are hundreds of load positions that must be tested to obtain the maximum responses. So, it would be tedious, time-consuming, and even impractical to use the GUI (Graphical User Interface) path to create bridge models, apply truck loads, analyze the bridges, and obtain the results for thousands of bridges.

APDL was used to carry out the whole analysis process automatically, including preprocessing and post-processing, which expedited the analysis and avoided the possible mistakes made through the GUI path.

Figure 3.18 shows the main flowcharts which were used to obtain the maximum responses. The largest responses were selected as the governing design values due to live loads. In this research, the largest responses were used to calculate the distribution factors. The flowcharts were implemented by the program contained in Appendix A. The flowcharts and programs in Appendix A took steel girder bridges as an example, which are applicable to the other types of girder bridges such as precast concrete box girder, precast concrete I or Bulb-Tee girder bridges. Chart 1 in Figure 3.18 can also be realized by the dialogue boxes. One of examples is shown in Figure 3.19. This method of inputting general information can expedite the input and avoid the possible mistakes.

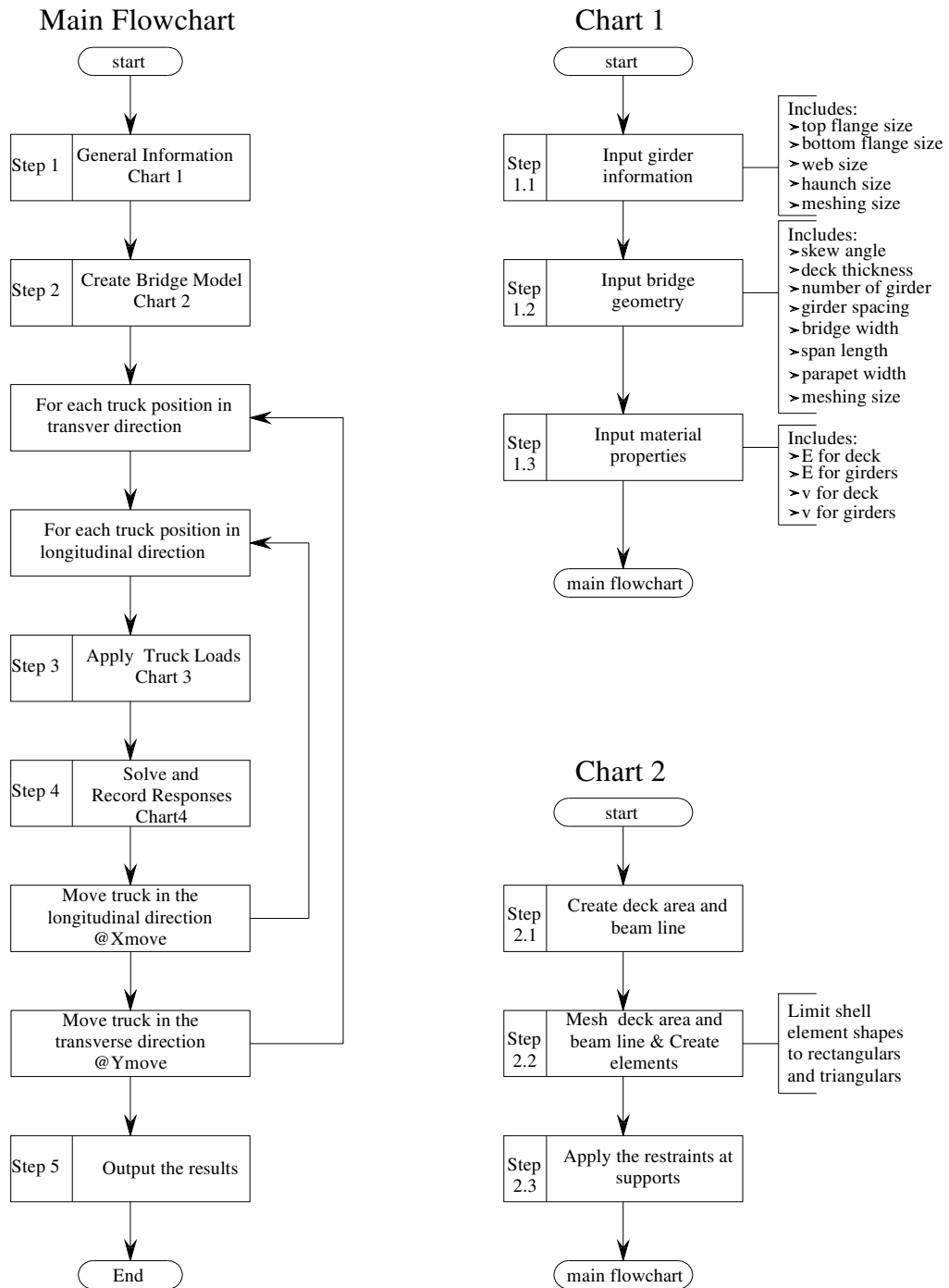


Figure 3.18 Main Flowchart

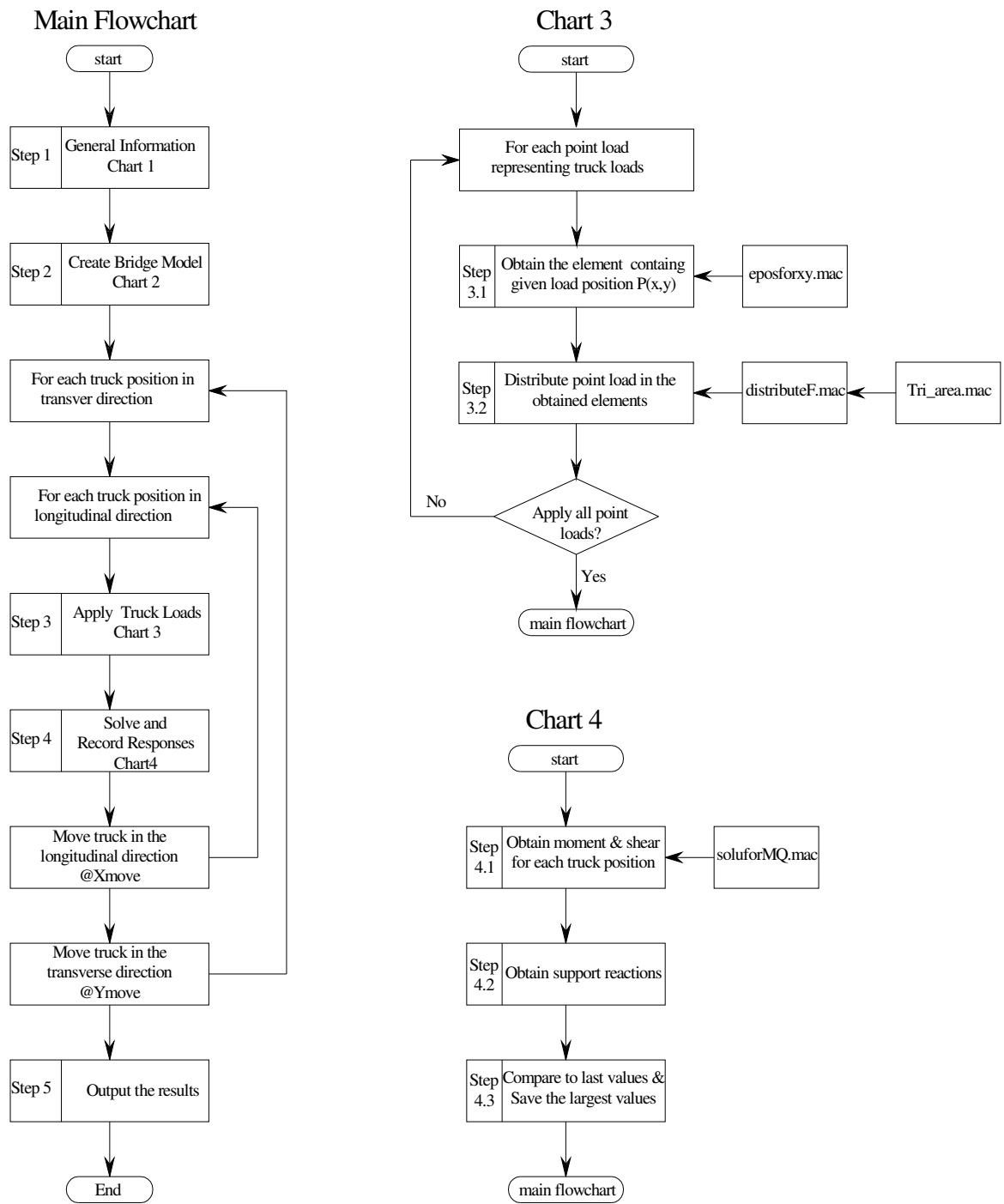


Figure 3.18 Continued

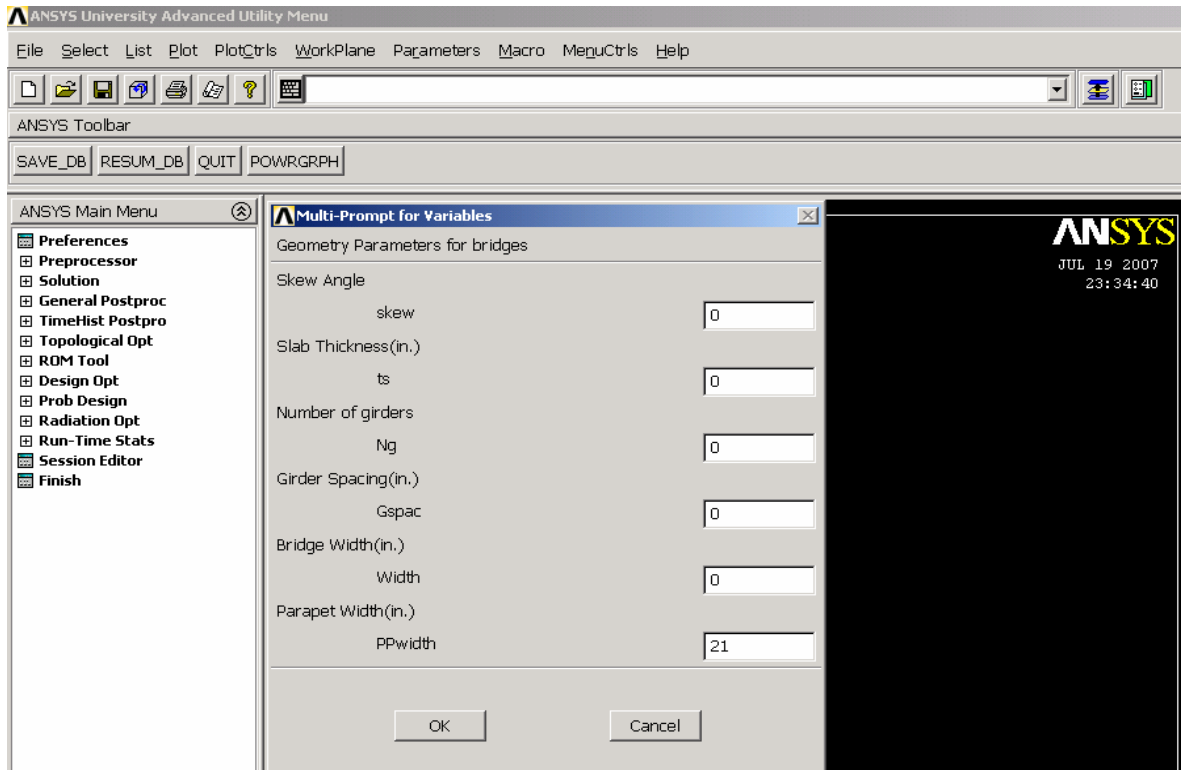
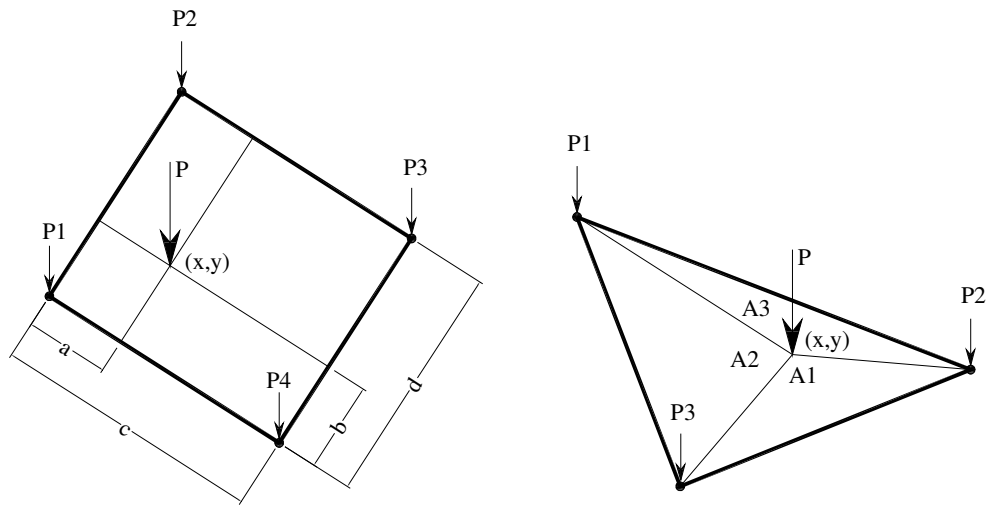


Figure 3.19 Input of General Information with the Dialog Box

As mentioned earlier, it is required that a number of load cases be tested to determine the maximum effect to the specific girder. For general ANSYS program, a new finite element mesh must be created accordingly whenever new load cases need to be placed. The ANSYS macro named “distributeF.mac” was developed to uncouple the FE mesh from the load position by introducing the work equivalent nodal force concepts. The goal of this macro was to calculate the work equivalent nodal forces (ENF) and to place these loads at the proper nodal points. The concentrated point loads cannot be applied directly within the shell elements that were selected for the deck. However, point loads can be applied to any of the nodes in shell elements. Therefore, once the location of the wheel load was determined, the load was statically distributed to the nodes in the top surface of the shell elements through this macro. “eposforxy.mac” was used to search the

element in which the wheel load located at any given position and “tri_area.mac” was used to calculate the area of any give triangular.

Figure 3.20 shows the formulas used to statically distribute the wheel loads. The flowcharts of the procedure for distributing the given point load are shown in Figures 3.21 and 3.22. After determining the truck position on the bridge, concentrated loads are linearly distributed to adjacent nodes based on the location of the load.



$$P1 = P \times \frac{(c-a)(d-b)}{c \cdot d}$$

$$P2 = P \times \frac{(c-a)(b)}{c \cdot d}$$

$$P3 = P \times \frac{(a)(b)}{c \cdot d}$$

$$P4 = P \times \frac{(a)(d-b)}{c \cdot d}$$

$$P1 = P \times \frac{A1}{A1 + A2 + A3}$$

$$P2 = P \times \frac{A2}{A1 + A2 + A3}$$

$$P3 = P \times \frac{A3}{A1 + A2 + A3}$$

Figure 3.20 Distributions of Concentrated Loads to Adjacent Nodes

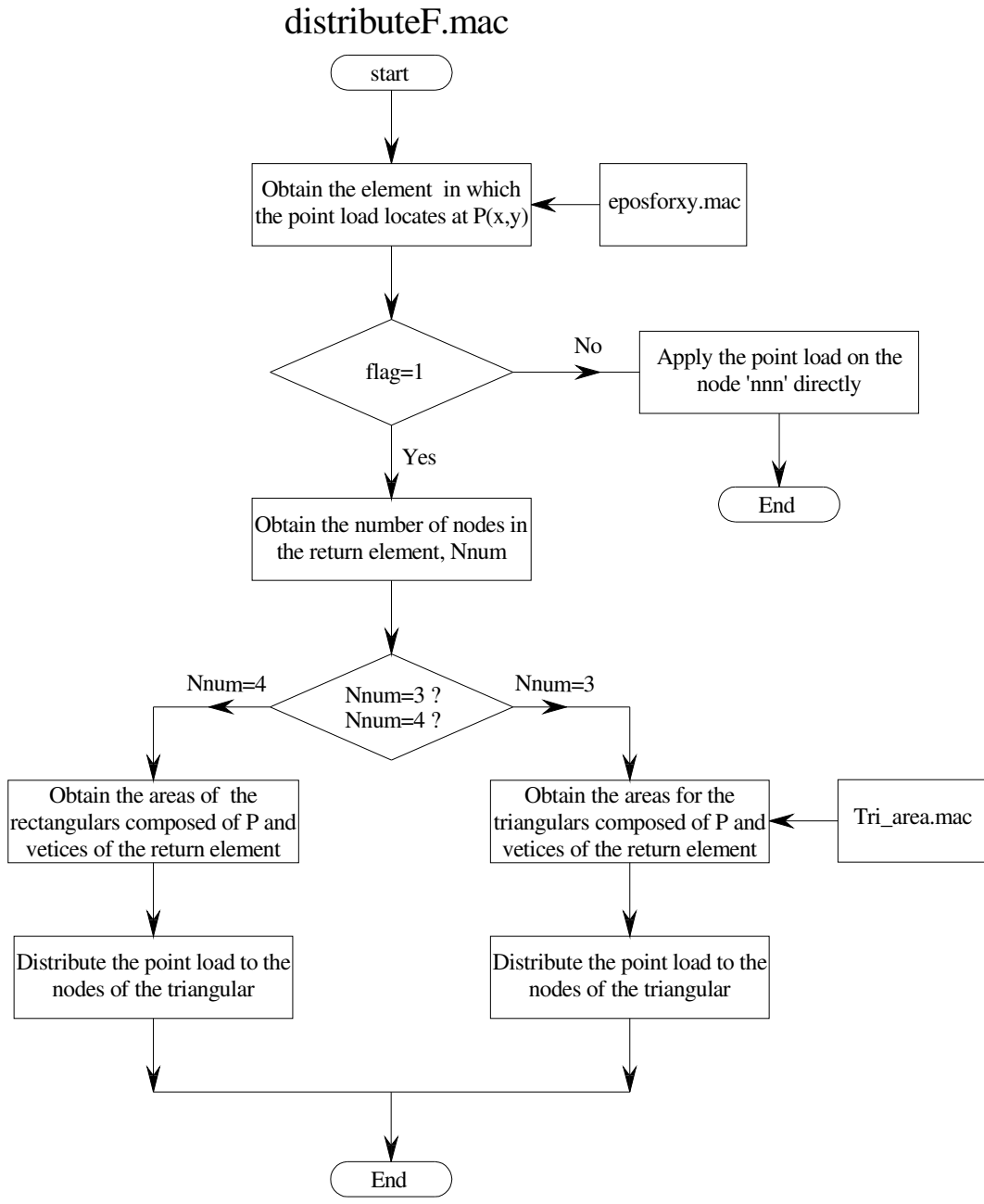


Figure 3.21 Flowchart-Distribute Concentrated Loads

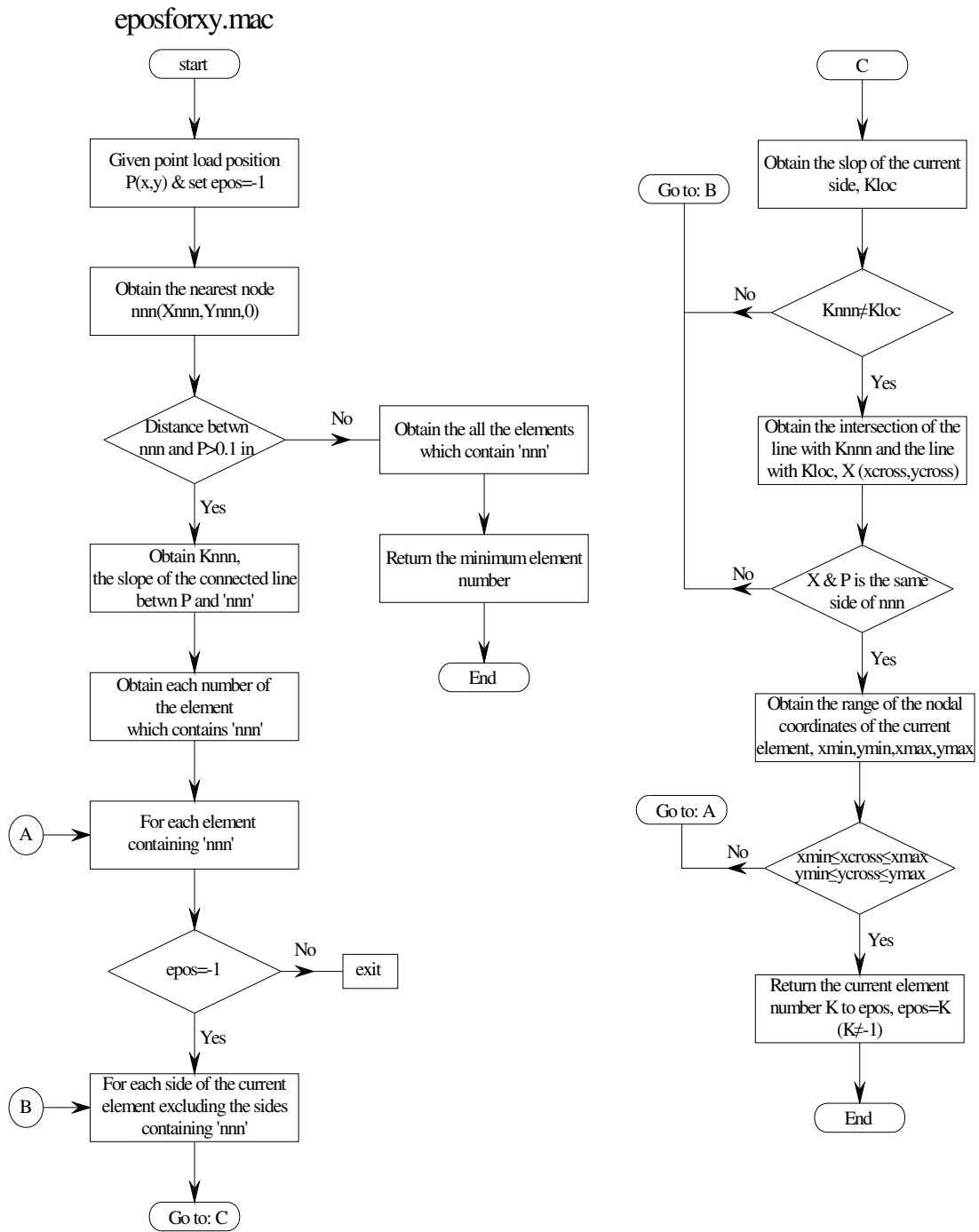


Figure 3.22 Flowchart-Obtain Element Position Based on Given Locations

CHAPTER 4

CONSTRUCTION OF BRIDGE DATABASE

4.1 Method to Construct Bridge Database

In order to eliminate the limitations on the ranges of applicability set in current skew correction factor equations in the AASHTO-LRFD and NCHRP12-62, the bridges with structural parameters beyond the applicable range were developed and analyzed to obtain the accurate maximum responses. At the same time, a certain number of regular bridges within the applicable ranges were also developed and analyzed for the purpose of investigating live load distribution factors for reactions. All the bridges were analyzed with the APDL program developed in Chapter 3.

There are no significant limitations on the Ontario method, i.e. α - θ method, which was introduced in the literature review, so all bridges were developed using this method to construct the bridge database. Figure 4.1 presents the five types of slab-on-girder bridges studied in this research. However, only the steel I-girder bridge was taken as an example to demonstrate the procedure for developing slab-on-girder bridges with the Ontario method.

The Ontario method is based upon the orthotropic plate theory. The slab-on-girder bridge can be described by two characterizing parameters, α and θ , that are in different ranges for various bridge types. These parameters in the equation are given by

$$\alpha = \frac{D_{xy} + D_{yx} + D_1 + D_2}{2(D_x D_y)^{0.5}} \quad (4-1)$$

$$\theta = \frac{W}{2L} \left(\frac{D_x}{D_y} \right)^{0.25} \quad (4-2)$$

In which

$$D_x = \frac{E_g I_{comp}}{S} = \frac{E_c \cdot n \cdot I_{comp}}{S} \quad (4-3)$$

$$D_y = \frac{E_c \cdot t_s^3}{12} \quad (4-4)$$

$$D_{xy} = D_{yx} = \frac{E_c}{2(1 + \nu_c)} \frac{t_s^3}{6} \quad (4-5)$$

$$D_1 = D_2 = \nu_c (\text{lesser of } D_x \text{ and } D_y) \quad (4-6)$$

$$n = \frac{E_g}{E_c} \quad (4-7)$$

The steps to develop bridges with the α - θ method were given by

1. The girder spacing was changed from 12 to 20 ft with an increment of 2 ft. Corresponding to the variation of girder spacing, the span length ranged from 100 to 400 ft with an increment of 50 ft (20-ft girder spacing and 400-ft span length were assumed to be the maximum limitations in practice for steel I-girder bridges, respectively).
2. For any combination of spacing and span length, the parameter, θ , varied from 0 to 2.5 with an increment of 0.1.
3. Bridge width was increased from 20 to 90 ft for each combination of Step 1 and Step 2, and the corresponding slab thickness can be obtained according to the relationship between girder spacing and recommended minimum slab thickness specified in the specification. Modulus of elasticity and Poisson's ratio for steel

and concrete were assumed to be commonly used in practice. Therefore, all parameters but D_x and α in Equations 4-1 and 4-2 can be obtained.

4. Since θ and D_y had already known, the moment of inertia of the composite cross section, I_{comp} , can be solved from Equations (4-2), (4-3), and (4-4):

$$I_{comp} = \frac{4 \cdot t^3 \cdot S \cdot L^4 \cdot \theta^4}{3 \cdot W^4 \cdot n}$$

5. After the moment of inertia for each bridge was calculated, α can be calculated and compared to the range of α for slab-on-girder bridges specified in OHBDC. The bridge, with α falling into the range of 0.05-0.2, was accepted for steel I-girder bridges.
6. Based on the AASHTO LRFD Specifications, the steel I-girder section dimensions can finally be confirmed since span length, girder spacing, number of girders, width of the deck, and overhang width have been known. Accordingly, the moment of inertia of the composite cross section, I_{bc} , can be obtained with the current specification.
7. If the moment of inertia of any candidate bridge (I_{comp}) from Step 3 equals (I_{bc}) from Step 5 while the α and θ of this bridge fall into the practical ranges, the bridge was considered to be developed finally.

4.2 Practical Limits for Various Structural Parameters

In practice, there exist many bridges with the structure parameters in excess of the limitations on the range of applicability set in the LRFD specification. When engineers

design these bridges, the simplified equations specified in the LRFD specifications are not applicable. Therefore, it is necessary to eliminate the limitations on the applicable ranges.

Skew angle, girder spacing and span length were the most crucial for the skew correction factors, which were considered in this research. It is necessary to know the practical limits of these structural parameters. Reasonable estimations of practical limits were conducted for various types of slab-on-girder bridges. The maximum values for span length, girder spacing, and skew angle are defined in Table 4.1.

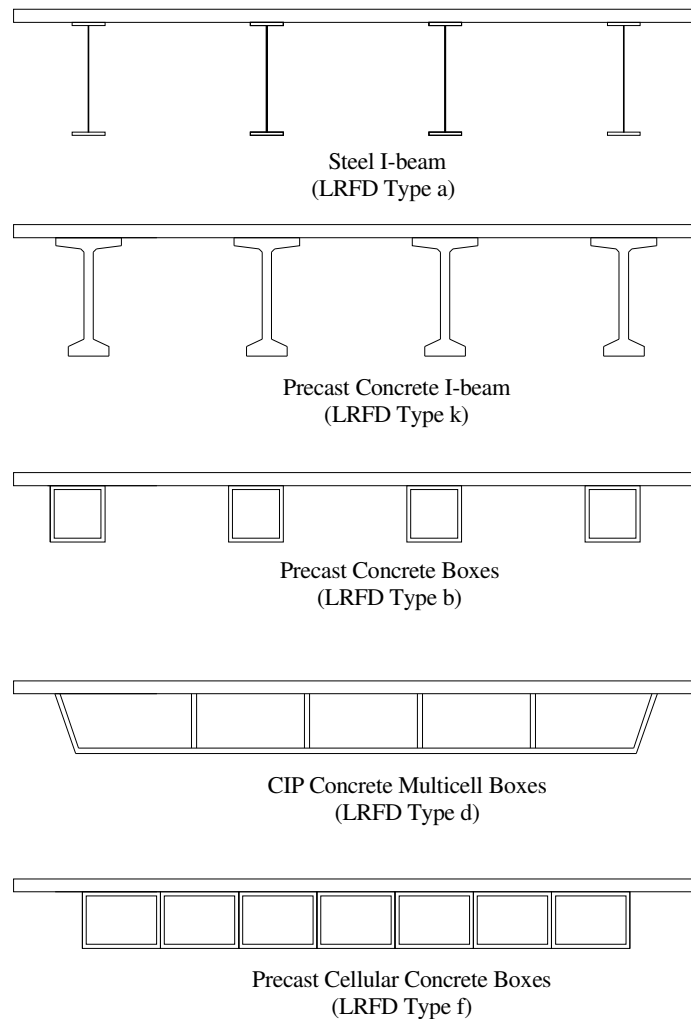


Figure 4.1 Typical Cross Section Studied

Table 4.1 Practical Limits of Structural Parameters for Slab-on-girder Bridges

Supporting components	Span Length L(ft)	Girder Spacing S (ft)	Skew Angle θ (deg)	Number of Bridges
Steel I(a)	100-400 (w/ 50 ft increment)	12-20 (w/ 2 ft increment)	30 45 60 65 70 75	210
Precast conc. I (k)	50-150 (w/ 50 ft increment)	12-20 (w/ 2 ft increment)		90
Precast conc. boxes (b)	50-150 (w/ 50 ft increment)	8-16 (w/ 2 ft increment)		90
Precast cellular conc. boxes (f)	40-160 (w/ 40 ft increment)	/		72
CIP conc. multicell boxes (d)	100-300 (w/ 50 ft increment)	10-16 (w/ 2 ft increment)		120

4.3 Selection of Bridges

The material properties for various types of slab-on-girder bridges selected for this research are listed in Table 4.2. The modulus of elasticity and Poisson ratio for steel were taken 29000 ksi and 0.3, respectively. The Poisson ratio for concrete was taken as 0.15. The bridge databases developed for LRFD Type a, k, b, f, and d are listed in Tables 4.3 through 4.7, respectively.

Table 4.2 Material Properties for Slab-on-girder Bridges Studied

Supporting components	Modulus of Elasticity of girder (ksi)	Poisson's ratio of girder	Modulus of Elasticity of deck (ksi)	Poisson's ratio of deck
Steel I(LRFD Type a)	29000	0.3	3830 ⁽¹⁾	0.15
Precast concrete I (LRFD Type k)	4890 ⁽²⁾	0.15	3830 ⁽²⁾	0.15
Precast concrete boxes (LRFD Type b)	5070 ⁽³⁾	0.15	3830 ⁽³⁾	0.15
Precast cellular concrete boxes (LRFD Type f)	5070 ⁽³⁾	0.15	3830 ⁽³⁾	0.15
CIP concrete multicell boxes (LRFD Type d)	3320 ⁽⁴⁾	0.15	3320 ⁽⁴⁾	0.15

Note:

- 1) From Ebeido T. and Kennedy J. B., 1996
- 2) From Yousif Z. and Hindi R., 2007
- 3) From NCHRP12-62, 2003-2006
- 4) From the drawings of two box-girder bridges (One is over Lick Creek at Greene County, Tennessee and the other is over Harpeth River at Williamson County, Tennessee.)

Table 4.3 Database for Steel I-girder Bridges Studied

ID	S (ft)	Θ (deg)	ts (in)	Ns	Span 1 (ft)	Span 2 (ft)	Span 3 (ft)	W (ft)	Ng	Wo (ft)	H (in)	d (in)	btf (in)	bbf (in)	tff (in)	tbf (in)	dw (in)	tw (in)
A-1	12	30 45 60 65 70 75	9	2	100	100		60	5	6	56	47	8	8	0.5	1	45.50	0.33
A-2	14		9.75	2	100	100		70	5	7	60	50.25	8.5	8.5	0.625	1	48.63	0.35
A-3	16		10.5	2	100	100		60	4	6	66.75	56.25	9.5	9.5	0.625	1.25	54.38	0.39
A-4	18		11.25	2	100	100		70	4	8	70.75	59.5	10	10	0.625	1.25	57.63	0.41
A-5	20		12	2	100	100		80	4	10	85.75	73.75	12.5	12.5	0.875	1.75	71.13	0.51
A-6	12		9	2	150	150		60	5	6	72	63	10.5	10.5	0.75	1.5	60.75	0.43
A-7	14		9.75	2	150	150		70	5	7	78.5	68.75	11.5	11.5	0.75	1.5	66.50	0.48
A-8	16		10.5	2	150	150		60	4	6	72	61.5	10.5	10.5	0.75	1.5	59.25	0.42
A-9	18		11.25	2	150	150		70	4	8	82	70.75	12	12	0.75	1.5	68.50	0.49
A-10	20		12	2	150	150		80	4	10	90	78	13	13	0.875	1.75	75.38	0.54
A-11	12		9	2	200	200		70	6	5	96	87	14.5	14.5	1	2	84.00	0.60
A-12	14		9.75	2	200	200		70	5	7	109.25	99.5	17	17	1.125	2.25	96.13	0.69
A-13	16		10.5	2	200	200		80	5	8	104.5	94	16	16	1	2	91.00	0.65
A-14	18		11.25	2	200	200		70	4	8	109.25	98	16.5	16.5	1.125	2.25	94.63	0.68
A-15	20		12	2	200	200		80	4	10	104.5	92.5	15.5	15.5	1	2	89.50	0.64
A-16	12		9	2	250	250		80	7	4	111.25	102.25	17.5	17.5	1.125	1.75	99.38	0.71
A-17	14		9.75	2	250	250		80	6	5	120	110.25	18.5	18.5	1.25	1.875	107.13	0.77
A-18	16		10.5	2	250	250		80	5	8	115.5	105	17.5	17.5	1.125	1.75	102.13	0.73
A-19	18		11.25	2	250	250		80	5	4	120	108.75	18.5	18.5	1.25	1.875	105.63	0.75
A-20	20		12	2	250	250		80	4	10	109.25	97.25	16.5	16.5	1.125	1.75	94.38	0.67

Table 4.3 Continued

A-21	12	30 45 60 65 70 75	9	2	300	300		70	6	5	112.5	103.5	17.5	17.5	1.125	1.75	100.63	0.72
A-22	14		9.75	2	300	300		70	5	7	120	110.25	18.5	18.5	1.25	1.875	107.13	0.77
A-23	16		10.5	2	300	300		60	4	6	120	109.5	18.5	18.5	1.25	1.875	106.38	0.76
A-24	18		11.25	2	300	300		70	4	8	144	132.75	22.5	22.5	1.5	2.25	129.00	0.92
A-25	20		12	2	300	300		80	4	10	133.5	121.5	20.5	20.5	1.375	2.125	118.00	0.84
A-26	12		9	2	350	350		60	5	6	86.75	77.75	13	13	0.875	1.375	75.50	0.54
A-27	14		9.75	2	350	350		60	4	9	100	90.25	15.5	15.5	1	1.5	87.75	0.63
A-28	16		10.5	2	350	350		60	4	6	106.5	96	16	16	1	1.5	93.50	0.76
A-29	18		11.25	2	350	350		70	4	8	131.25	120	20	20	1.25	1.875	116.88	0.83
A-30	20		12	2	350	350		80	4	10	123.75	111.75	19	19	1.25	1.875	108.63	0.78
A-31	12		9	2	400	400		60	5	6	102.25	93.25	16	16	1	1.5	90.75	0.65
A-32	14		9.75	2	400	400		80	6	5	111.75	102	17	17	1.125	1.75	99.13	0.71
A-33	16		10.5	2	400	400		80	5	8	120	109.5	18.5	18.5	1.25	1.875	106.38	0.76
A-34	18		11.25	2	400	400		90	5	9	150	138.75	23.5	23.5	1.5	2.25	135.00	0.96
A-35	20		12	2	400	400		80	4	10	141.25	129.25	22	22	1.375	2.125	125.75	0.90

Table 4.4 Database for Precast Concrete I-girder Bridges Studied

bridge ID	# of beams	Skew (deg)	Girder spacing (ft)	Deck thick. (in)	Deck width (ft)	Overhang width (ft)	# of spans	Span 1 (ft)	Span 2 (ft)	Span 3 (ft)	Sect. Type
	Ng	skew	Gspac	ts	Width		Nspan	span(i)			
K-1	5	30 45 60 65 70 75	12	9	56	4	2	50	50		III
K-2	5		14	9.75	64	4	2	50	50		III
K-3	5		16	10.5	74	5	2	50	50		IV
K-4	4		18	11.25	64	5	2	50	50		V
K-5	4		20	12	74	7	2	50	50		VI
K-6	4		12	9	44	4	2	100	100		III
K-7	5		14	9.75	64	4	2	100	100		III
K-8	5		16	10.5	74	5	2	100	100		IV
K-9	4		18	11.25	64	5	2	100	100		V
K-10	5		20	12	90	5	2	100	100		VI
K-11	6		12	9	64	2	2	150	150		VI
K-12	4		14	9.75	56	7	2	150	150		VI
K-13	5		16	10.5	74	5	2	150	150		VI
K-14	4		18	11.25	64	5	2	150	150		VI
K-15	4		20	12	74	7	2	150	150		VI

Table 4.5 Database for Precast Concrete Box-girder Bridges Studied

Type B precast concrete spread box girder bridge database										
bridge ID	# of beams	Skew (deg)	Girder spacing (ft)	Deck thick. (in)	Deck width (ft)	Overhang width (ft)	# of spans	Span 1 (ft)	Span 2 (ft)	Sect. Type
	Ng	skew	Gspac	ts	Width		Nspan	span(i)		
B-1	6	30 45 60 65 70 75	8	7.25	46	3	2	50	50	BII-36
B-2	5		10	8	46	3	2	50	50	BIII-36
B-3	4		12	9	46	5	2	50	50	BIV-36
B-4	5		14	9.75	62	3	2	50	50	BIII-48
B-5	4		16	10.5	62	7	2	50	50	BIII-48
B-6	6		8	7.25	46	3	2	100	100	BII-36
B-7	5		10	8	46	3	2	100	100	BIII-36
B-8	4		12	9	46	5	2	100	100	BII-48
B-9	5		14	9.75	62	3	2	100	100	BIV-36
B-10	4		16	10.5	62	7	2	100	100	BIII-48
B-11	6		8	7.25	46	3	2	150	150	BIV-48
B-12	5		10	8	46	3	2	150	150	BIV-48
B-13	4		12	9	46	5	2	150	150	BIV-48
B-14	5		14	9.75	62	3	2	150	150	BIV-48
B-15	4		16	10.5	62	7	2	150	150	BIV-48

Table 4.6 Database for Precast Cellular Concrete Box-bridges Studied

Type F Precast cellular concrete box bridge database										
bridge ID	# of beams	Skew (deg)	Girderspac. (ft)	Deck thick. (in)	Deck width (ft)	Overhang width(ft)	# of spans	Span 1 (ft)	Span 2 (ft)	Sect. Type
	Ng	skew	Gspac	ts	Width		Nspan	span(i)		
F-1	6	30 45 60 65 70 75	4	6	24	2	2	40	40	BI-48
F-2	6		4	6	24	2	2	80	80	BII-48
F-3	6		4	6	24	2	2	120	120	BIII-48
F-4	6		4	6	24	2	2	160	160	BIV-48
F-5	10		4	6	40	2	2	40	40	BI-48
F-6	10		4	6	40	2	2	80	80	BII-48
F-7	10		4	6	40	2	2	120	120	BIII-48
F-8	10		4	6	40	2	2	160	160	BIV-48
F-9	14		3	6	42	1.5	2	40	40	BI-36
F-10	14		3	6	42	1.5	2	80	80	BII-36
F-11	14		3	6	42	1.5	2	120	120	BIV-36
F-12	14		3	6	42	1.5	2	160	160	BIV-36

Table 4.7 Database for CIP Concrete Multi-cell Box-girder Bridges

Type D CIP concrete multicell box bridge database												
bridge ID	Skew (deg)	# of cells	Girder spac. (box width) (ft)	Overhang width (ft)	Deck width (ft)	Deck thick. (in)	Web thick. (in)	Bottom flange thick (in)	Total height (in)	# of spans	Span 1 (ft)	Span 2 (ft)
	skew	Ng	Gspac		Width	ts		tw	tf		h	Nspan
D-1	30 45 60 65 70 75	4	10	4	48	8	9	6	60	2	100	100
D-2		4	12	5	58	9	10	7	63	2	100	100
D-3		4	14	5	66	9.75	12	8	66	2	100	100
D-4		4	16	6	76	10.5	14	9	70	2	100	100
D-5		4	10	4	48	8	10	7	81	2	150	150
D-6		4	12	4	56	9	11	8	85	2	150	150
D-7		4	14	5	66	9.75	12	9	90	2	150	150
D-8		4	16	6	76	10.5	14	10	94	2	150	150
D-9		4	10	4	48	8	12	8	104	2	200	200
D-10		4	12	4	56	9	14	9	109	2	200	200
D-11		4	14	5	66	9.75	15	11	114	2	200	200
D-12		4	16	6	76	10.5	17	12	120	2	200	200
D-13		4	10	4	48	8	13	9	125	2	250	250
D-14		4	12	4	56	9	15	10	130	2	250	250
D-15		4	14	5	66	9.75	17	11	136	2	250	250
D-16		4	16	6	76	10.5	18	12	142	2	250	250
D-17		4	10	4	48	8	14	10	144	2	300	300
D-18		4	12	4	56	9	16	11	150	2	300	300
D-19		4	14	5	66	9.75	18	12	156	2	300	300
D-20		4	16	6	76	10.5	19	12	163	2	300	300

4.4 Loading Conditions

Truck loads were applied on various slab-on-girder bridges to search for the maximum responses. One design lane loaded and two or more design lanes loaded were considered in this research. The analyses were conducted within the elastic limits so that the principle of superposition can be applied. For example, the support reaction at a pier under two trucks can be considered as the superposition of the support reactions resulting from two separated single trucks. The principle of superposition can save much computation time especially dealing with a large number of bridges.

For one design lane loaded, the maximum shear at the ends of the spans and maximum reaction at the supports were obtained by running one truck in the longitudinal direction (foot by foot) until the maximum responses of interest were found. After acquiring the maximum responses in one longitudinal direction, the truck was moved by one foot in the transverse direction to conduct the same search for the maximum responses in the longitudinal direction. After all the possible positions in the transverse and longitudinal directions are checked, the maximum responses can easily be obtained from the results under one truck loading. For two or more lanes loaded, the maximum responses were obtained by superimposing the results calculated from one lane loaded. When applying the principle of superposition, at least four feet between vehicles was kept.

As mentioned above, the transverse position where the maximum response occurred was not clear. Therefore all the transverse and longitudinal positions should be checked to search for the maximum response of interest, which will require significant

computation time even with a very simple bridge model. The following section presents the summary of transverse positions where the maximum responses can easily be obtained without checking all the transverse positions.

4.4.1 Transverse Positions where Maximum Responses Occur

The maximum shear and support reaction can be obtained by running the truck in the longitudinal directions with the fixed transverse positions. Figure 4.2 shows one example of a steel I-girder bridge plan. The structural reference point ($x=0, y=0$) is at the intersection of the west edge of deck and north face of the south parapet. The reference point of the truck is the driver side front wheel. 'Xmove' and 'Ymove' represent the distances in the longitudinal and transverse directions between the structural reference point and truck reference point, respectively. The transverse truck positions (Ymove) where maximum responses occur for the interior and exterior girders were summarized in Table 4.8.

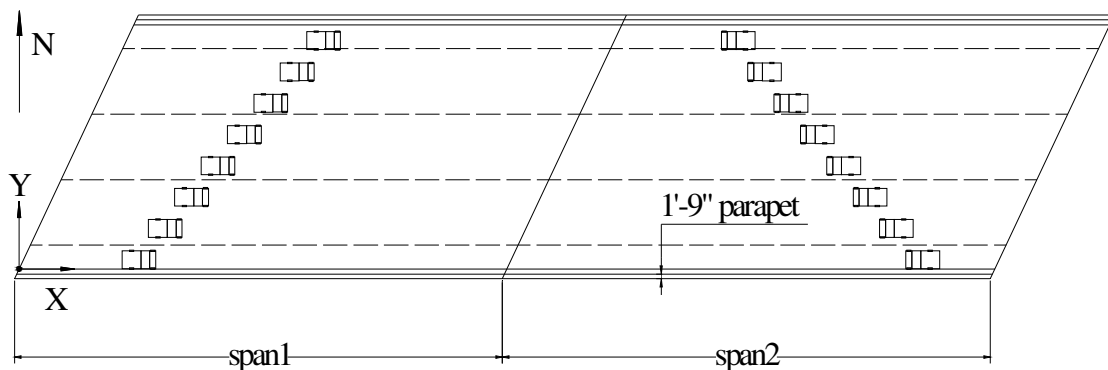


Figure 4.2 Truck Arrangements in the Transverse Direction

4.4.2 Verification of Estimated Transverse Positions for Maximum Responses

To validate the transverse position estimated in Table 4.8, some bridges were analyzed using the detailed analyses in which all the transverse positions were checked to search for the maximum response. Then, the responses obtained from the estimated transverse positions listed in Table 4.8 were compared to those from detailed analyses. About 5% of the bridges in the bridge database were checked with detailed analyses to verify that the maximum responses can correctly and easily be predicted with estimated transverse positions. Two steel I-girder bridges in the bridge database were selected to show the comparison results.

The first steel bridge is A-15 with a skew angle of 65°. The second steel bridge selected is A-19 with a skew angle of 60°. Figures 4.3 and 4.4 present the detailed analysis results for the interior girder and exterior girder for A-15 and A-19, respectively. Tables 4.9 and 4.11 list the maximum responses obtained from the estimated transverse positions for A-15 and A-19, respectively. For each bridge, the above maximum

Table 4.8 Transverse Positions for Maximum Responses

	1 lane	2 lanes	3 lanes	4 lanes
Exterior Girder	Ymove1	Ymove1+Ymove2	Ymove1+ Ymove2+ Ymove3	Ymove1+ Ymove2+ Ymove3+ Ymove4
Interior Girder	Ymove5	Ymove6+Ymove7 or Ymove5+Ymove8 or Ymove5+Ymove9	Ymove5+ Ymove8+ Ymove9	Ymove5+ Ymove5+ Ymove8+ or Ymove8+ Ymove9+ Ymove9+ Ymove10 Ymove11

Note:

1. Ymove1=0 ft, Ymove2=10 ft, Ymove3=20 ft, and Ymove4=30 ft;
2. Ymove5=S+d_c-3 ft, Ymove6= Ymove5-5 ft, Ymove7= Ymove5+5 ft, Ymove8= Ymove5-10 ft, Ymove9= Ymove5+10 ft, Ymove10=Ymove5-20 ft, Ymove11= Ymove5+20 ft;
3. S is the girder spacing of the studied bridge;
4. d_c =overhang width-parapet width-2 (ft).

responses obtained from the two methods were compared in Tables 4.10 and 4.12 to show if the estimated transverse positions are correct. The maximum errors between detailed analysis results and those from estimated transverse positions was 2.03% and 1.92 %for bridges A-15 and A-19, respectively. It is concluded that the maximum shears and reaction forces can be computed with the estimated transverse positions. Thus, the researchers can save much time searching for maximum responses with the estimated transverse positions for slab-on-girder bridges.

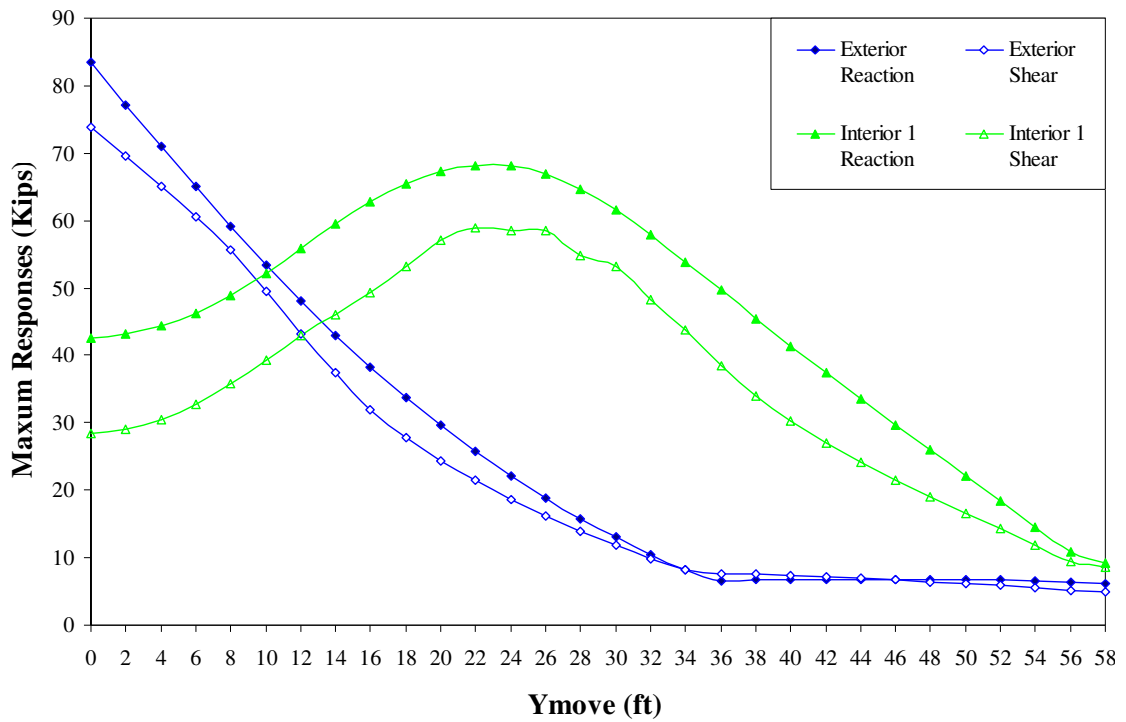


Figure 4.3 Maximum Responses from Detailed Analysis for A-15

Table 4.9 Maximum Responses from Estimated Transverse Positions for A-15

Truck Transverse Position	Exterior				Interior			
	Reaction	Shear	Reaction	Shear	Reaction	Shear	Reaction	Shear
Ymove1	83.45	73.81	1 lane(1.2):		42.45	28.30	1 lane(1.2):	
Ymove2	53.44	47.67	100.14	88.57	52.15	38.47	81.53	70.74
Ymove3	29.58	24.37	2 lanes(1.0)		67.38	57.04	2 lanes(1.0)	
Ymove4	12.92	11.80	136.89	121.48	61.31	50.06	129.58	103.82
Ymove5	23.43	19.59	3 lanes(0.85)		67.94	58.95	3 lanes(0.85)	
Ymove6	33.15	27.34	141.50	123.97	65.27	52.49	154.03	125.15
Ymove7	15.39	13.57			64.31	50.35		
Ymove8	44.87	38.93			57.96	43.41		
Ymove9	8.96	8.75			55.31	44.87		

Table 4.10 Comparison of Detail Analysis Results to Those from Estimated Transverse Positions for A-15

	1 lane loaded			2 lanes loaded			3 lanes loaded		
	Detail computed	Approx. computed	Error (%)	Detail computed	Approx. computed	Error (%)	Detail computed	Approx. computed	Error (%)
Ext. R	100.14	100.14	0.00	136.93	136.89	0.03	141.55	141.50	0.04
Ext. Q	88.56	88.57	-0.01	123.37	121.48	1.53	125.63	123.97	1.32
Int. 1 R	81.85	81.53	0.39	130.18	129.58	0.46	154.62	154.03	0.38
Int. 1 Q	70.74	70.74	0.00	105.90	103.82	1.96	127.74	125.15	2.03

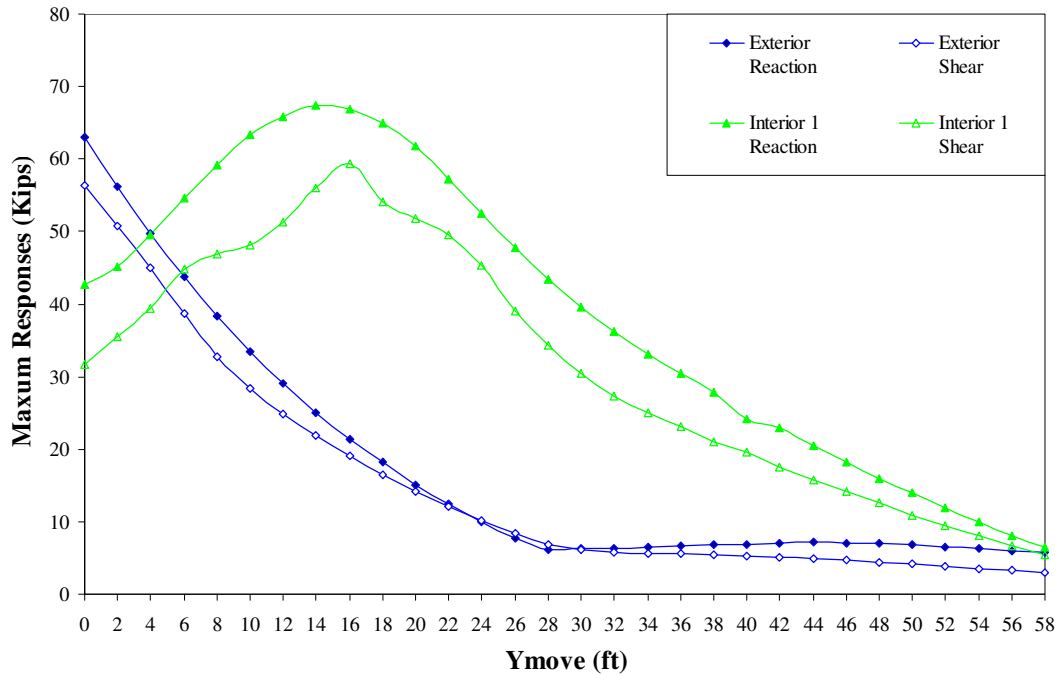


Figure 4.4 Maximum Responses from Detailed Analysis for A-19

Table 4.11 Maximum Responses from Estimated Transverse Position for A-19

Truck Transverse Position	Exterior				Interior			
	Reaction	Shear	Reaction	Shear	Reaction	Shear	Reaction	Shear
Ymove1	63.06	56.37	1 lane(1.2):		42.71	31.75	1 lane(1.2):	
Ymove2	33.48	28.43	75.67	67.64	63.44	48.10	80.70	69.86
Ymove3	15.10	14.23	2 lanes(1.0)		61.87	51.90	2 lanes(1.0)	
Ymove4	6.31	6.16	96.54	84.80	39.55	30.38	125.21	101.72
Ymove5	22.76	19.97	3 lanes(0.85)		67.25	58.22	3 lanes(0.85)	
Ymove6	32.87	27.91	94.89	84.18	63.93	48.12	143.90	122.19
Ymove7	14.76	13.96			61.28	51.71		
Ymove8	45.86	41.33			52.46	43.5		
Ymove9	8.49	9.08			49.58	42.03		

Table 4.12 Comparison of Detail Analysis Results to That from Estimated Transverse Positions for A-19

	1 lane loaded			2 lanes loaded			3 lanes loaded		
	Detail computed	Approx. computed	Error (%)	Detail computed	Approx. computed	Error (%)	Detail computed	Approx. computed	Error (%)
Ext. R	75.67	75.67	0.00	96.54	96.54	0.00	94.89	94.89	0.00
Ext. Q	67.64	67.64	0.00	84.80	84.80	0.00	84.18	84.18	0.00
Int. 1 R	80.77	80.70	0.09	125.31	125.21	0.08	144.02	143.90	0.08
Int. 1 Q	71.23	69.86	1.92	100.00	101.72	-1.72	121.72	122.19	-0.39

CHAPTER 5

COMPARISON OF DISTRIBUTION FACTOR OF LIVE LOAD REACTION WITH SHEAR AT PIERS OF CONTINUOUS SKEWED BRIDGES

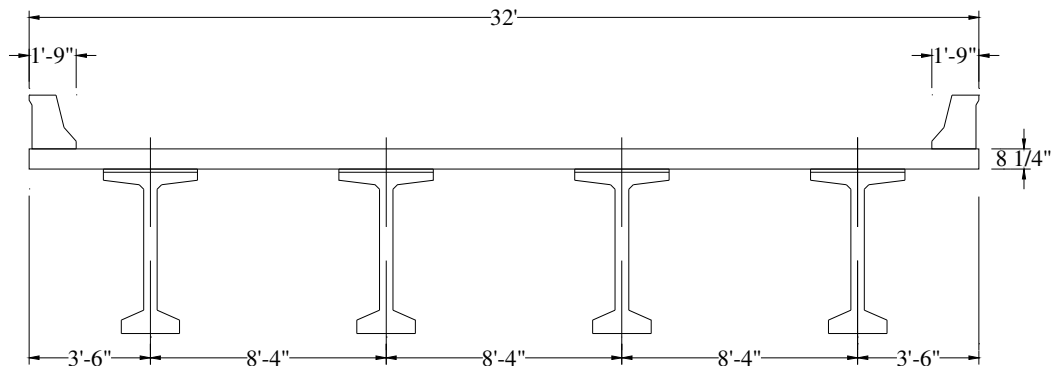
As mentioned earlier in the literature review, lateral distribution factors for live load moment and shear are determined using the AASHTO LRFD Specifications. The specifications do not provide skew correction factors for the reaction distribution when the line of bridge support is skewed even though the distribution of live load reaction at piers is affected by bridge skewness. It has been observed in previous studies that the reactions at piers in a skewed continuous bridge are amplified and the skew correction factors for reactions are unique from those for beam shear (Modjeski and Masters 2002, Huo and Zhang 2006).

Most of the modern bridges are continuous and skewed, so use of inaccurate estimation of live load reactions would lead to incorrect design for bridge substructures. Although extensive studies have been conducted for the skew effect on live load shear distribution, very little has been done regarding the skew effect on live load reactions of skewed continuous bridges. This chapter investigates the effect of bridge skewness on live load reactions at supports of continuous bridges. The bridge design community is interested in learning about the effect of bridge skewness on live load reactions and the difference between skew corrections for reaction and for shear.

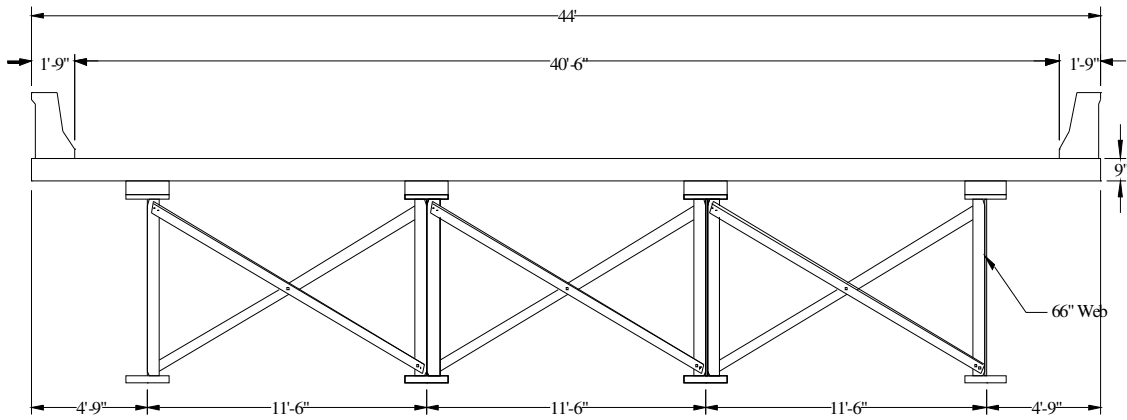
5.1 Bridges Analysis for Live Load Reaction Distribution

To avoid any possible errors resulting from the newly developed bridges, the bridges used in this chapter were originated from three actual continuous bridges in Tennessee. Bridge #1, a two-span, prestressed concrete, Bulb-Tee girder bridge, is Porter Road Bridge; Bridge #2, another two-span bridge, but with steel I-girders, is a bridge on state route 840; and Bridge #3, a four-span, prestressed concrete, Bulb-Tee girder bridge, is Rocky River Bridge. Figure 5.1 shows the typical cross sections of the three bridges. To study the effect of the skewness on live load reactions, the skew angle of the bridges was changed from 0° to 60° with a 15° increment. A total of fifteen bridges were analyzed for live load reaction and shear distribution factors. Figure 5.2 shows the plan view of the bridges with varied skew angles.

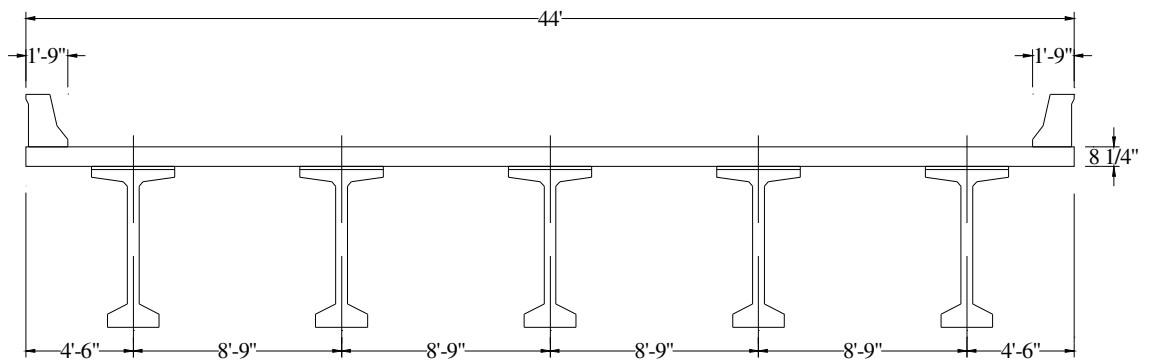
The bridge was loaded with a series of two-truck moving loads. The maximum responses of interior and exterior girders were determined by placing the trucks at various locations in the transverse directions until the maximum response was obtained. Figure 5.3 give the support designation for the studied bridges. An example of the transverse vehicle spacing is shown in Figure 5.4.



(a) Bridge #1 – Two-span, prestressed concrete bridge

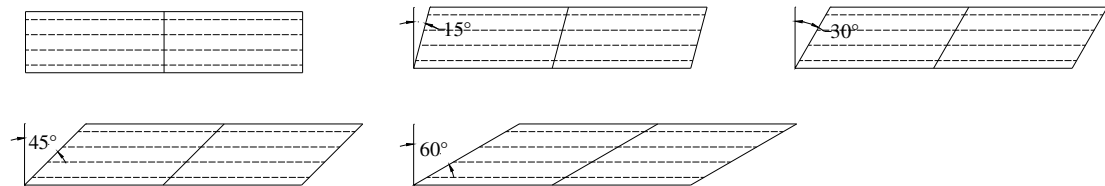


(b) Bridge #2 - Two-span, steel bridge

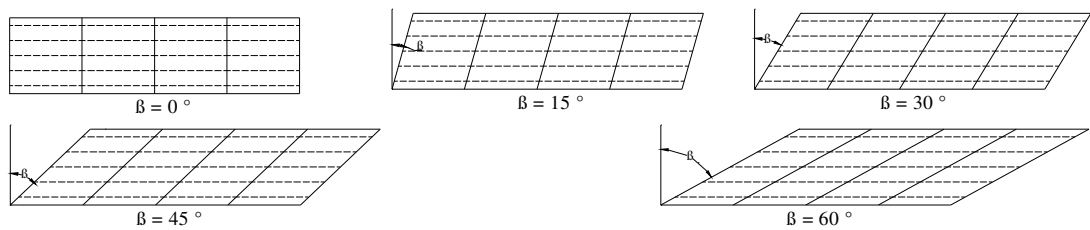


(c) Bridge #3 - Four-span, prestressed concrete bridge

Figure 5.1 Typical Cross Sections of Selected Bridges

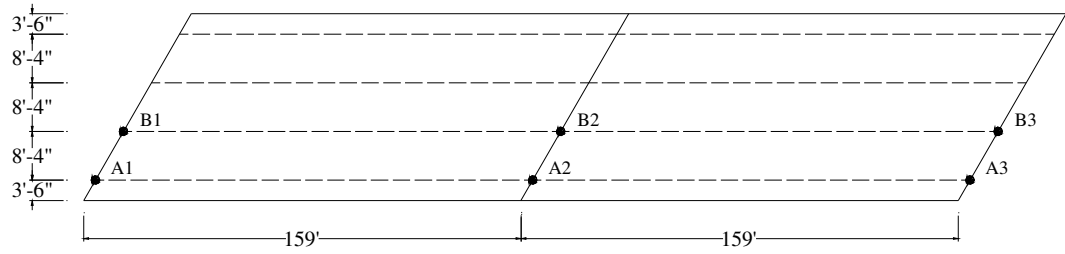


(a) Bridge #1 and #2 – two-span bridges

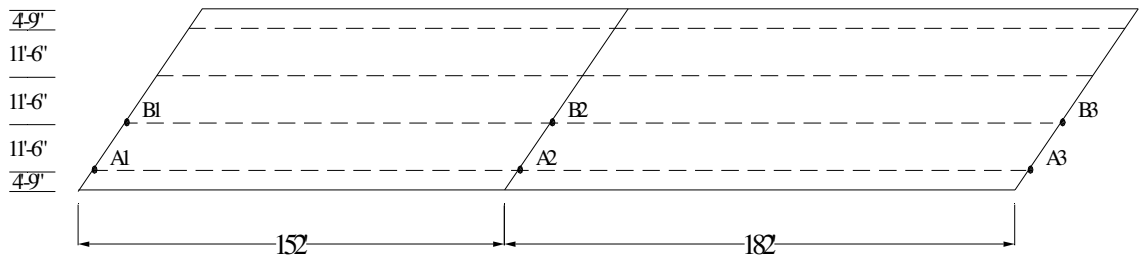


(b) Bridge #3– four-span bridge

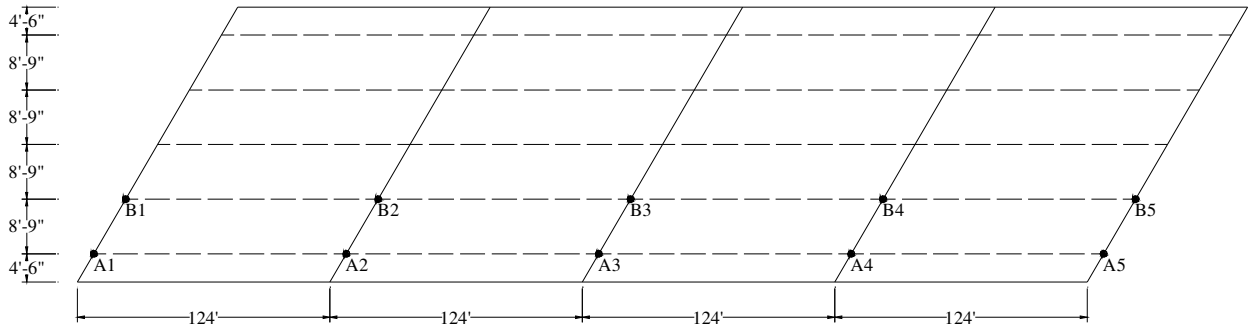
Figure 5.2 Plan View of Skewed Bridges Studied



(a) Bridge #1 – two-span, prestressed concrete bridge



(b) Bridge #2 – two-span, steel bridge



(c) Bridge #3 – four-span, prestressed concrete bridge

Figure 5.3 Support Designations of Selected Bridges

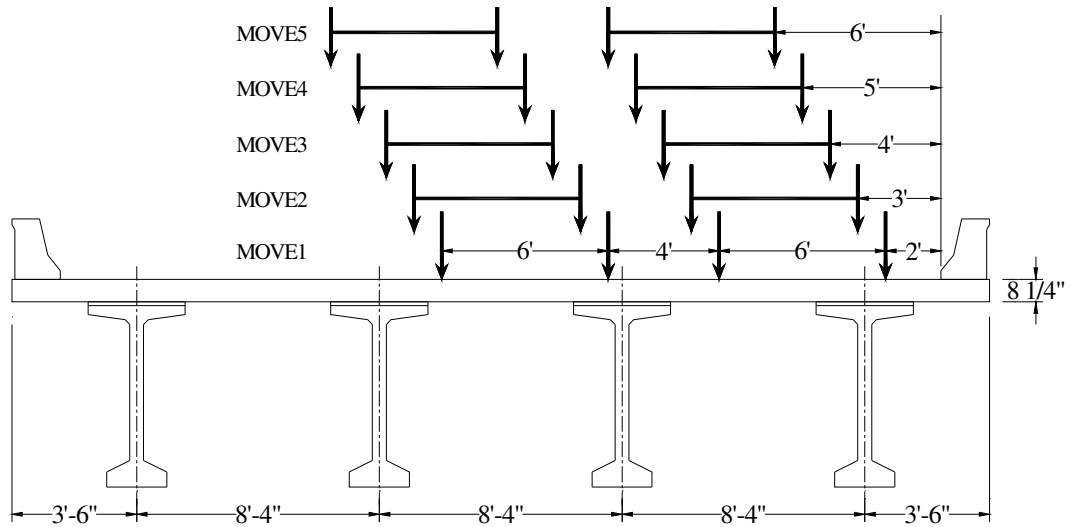


Figure 5.4 Sample Loading Positions for Two-lane Loads on Bridge #1

5.2 Results of Analysis and Comparison

5.2.1 Variation of Distribution Factor of Live Load Reaction at Supports

The obtained analytical results include the maximum live load reactions and shear forces at supports on the exterior beam line A and the interior beam line B in each bridge, as shown in Tables 5.1 to 5.3. Distribution factors of the reactions at supports were determined by dividing the maximum reaction responses from bridge analysis by the maximum reaction from a single beam line analysis at the corresponding location. Table 5.1 shows the distribution factors of live load reactions at the supports of Bridge #1. In the exterior beam line, the reaction distribution factor at acute corner A1 decreased as the bridge skew angle increased, varying from 0.680 to 0.565. At obtuse corner A3, the reaction distribution factor increased with the increase of the skew angle, varying from 0.680 to 0.824. At pier A2, the reaction steadily increased as the skew angle became

larger. A similar trend was observed for the reaction distribution factors at B1 through B3 in the interior beam line. The reaction distribution factor for Bridge #2, the two-span, steel bridge, exhibits the same variation in the interior and exterior beam lines as obtained in Bridge #1 (see Table 5.2). Table 5.3 shows the distribution factors of live load reaction at supports of Bridge #3, a four-span, concrete bulb-tee bridge. Although the reaction distribution factor increased consistently at all pier locations as the skew angle became larger, the magnitude of the amplification varied depending on the location of the piers. The maximum increase happened at exterior pier A2 and interior pier B2 with an increase of 17.6% and 25.2%, respectively, when skew angle varied from 0° to 60°.

The shear distribution factors at beam ends are also shown in Tables 5.1 through 5.3. As the skew angle increased, the shear distribution factor decreased at the acute corner and increased at the obtuse corner. For example, for Bridge #1, the shear distribution factor at A2_{left}, an obtuse corner, increased from 0.691 to 0.794 and the shear distribution factor at A2_{right}, an acute corner, decreased from 0.691 to 0.577 as the skew angle varied from 0° to 60°. The shear distribution factors at the interior beam ends followed similar trends as the ones in the exterior beam.

Table 5.1 Distribution Factors of Reaction and Shear at Support – Bridge #1

Skew angle (deg)	A1	A2		A3	B1	B2			B3	
	React./Shear	React.	Shear (left)	Shear (right)	React./Shear	React./Shear	React.	Shear (left)	Shear (right)	React./Shear
0	0.680	0.689	0.691	0.691	0.680	0.891	0.936	0.748	0.748	0.891
15	0.663	0.716	0.710	0.670	0.699	0.841	0.989	0.856	0.745	0.892
30	0.639	0.754	0.715	0.653	0.712	0.802	1.026	0.882	0.736	0.914
45	0.610	0.816	0.758	0.624	0.753	0.770	1.120	0.927	0.708	0.942
60	0.565	0.886	0.794	0.577	0.824	0.733	1.223	0.969	0.602	0.946

Table 5.2 Distribution Factors of Reaction and Shear at Support – Bridge #2

Skew angle (deg)	A1	A2			A3	B1	B2			B3
	React./Shear	React.	Shear (left)	Shear (right)	React./Shear	React./Shear	React.	Shear (left)	Shear (right)	React./Shear
0	0.959	0.969	0.950	0.977	0.982	1.035	1.123	0.964	0.968	1.032
15	0.941	0.978	0.969	0.970	0.997	0.988	1.131	1.016	0.939	1.062
30	0.910	0.995	0.992	0.935	1.026	0.942	1.183	1.051	0.912	1.101
45	0.875	1.024	1.018	0.896	1.063	0.890	1.247	1.083	0.837	1.118
60	0.839	1.085	1.048	0.852	1.112	0.840	1.338	1.138	0.809	1.131

Table 5.3 Distribution Factors of Reaction and Shear at Support – Bridge #3

Skew angle (deg)	B1	B2			B3			B4			B5
	React./Shear	React.	Shear (left)	Shear (right)	React.	Shear (left)	Shear (right)	React.	Shear (left)	Shear (right)	React./Shear
0	0.884	0.954	0.810	0.766	0.940	0.769	0.769	0.954	0.766	0.810	0.883
15	0.856	0.989	0.829	0.754	0.971	0.800	0.754	0.956	0.800	0.781	0.891
30	0.811	1.046	0.870	0.743	1.025	0.843	0.743	1.014	0.853	0.737	0.906
45	0.746	1.097	0.921	0.714	1.074	0.908	0.720	1.059	0.906	0.699	0.951
60	0.719	1.194	0.969	0.696	1.166	0.947	0.683	1.149	0.960	0.677	0.977

Skew angle (deg)	A1	A2			A3			A4			A5
	React./Shear	React.	Shear (left)	Shear (right)	React.	Shear (left)	Shear (right)	React.	Shear (left)	Shear (right)	React./Shear
0	0.802	0.820	0.769	0.735	0.793	0.740	0.740	0.820	0.735	0.769	0.803
15	0.778	0.836	0.783	0.714	0.802	0.768	0.709	0.827	0.755	0.745	0.817
30	0.749	0.860	0.816	0.686	0.819	0.793	0.691	0.843	0.777	0.720	0.825
45	0.721	0.899	0.853	0.669	0.850	0.822	0.677	0.854	0.819	0.705	0.867
60	0.678	0.964	0.934	0.634	0.903	0.862	0.674	0.880	0.842	0.684	0.916

5.2.2 Comparison of the Distribution Factors of Live Load Reaction and Shear

The distribution factors of shear and reaction at the same pier location were compared to identify the difference between these two values due to bridge skewness. For all three bridges, the reaction distribution factors at the piers in the exterior beam line were slightly higher than the shear distribution factors near the same pier. The difference between the reaction and shear distribution factors became larger when the skew angle

was greater than 30° . For the piers in the interior beam line, the reaction distribution factors were higher than the shear distribution factors. The difference between the two distribution factors increased quickly as the skew angle varied from 30° to 60° . Figures 5.5 through 5.7 show the ratio of the reaction distribution factor to the average shear distribution factor at the piers of Bridge #1, #2, and #3, respectively. For both piers A2 and B2, the ratio of reaction to shear distribution factors became larger when the skew angle varied from 30° to 60° . The results from the analysis revealed that the reactions at piers in a skewed continuous bridge were amplified as the skew angle increased, and the reaction distribution factors increased faster than the shear distribution factors when the skew angle was greater than 30° .

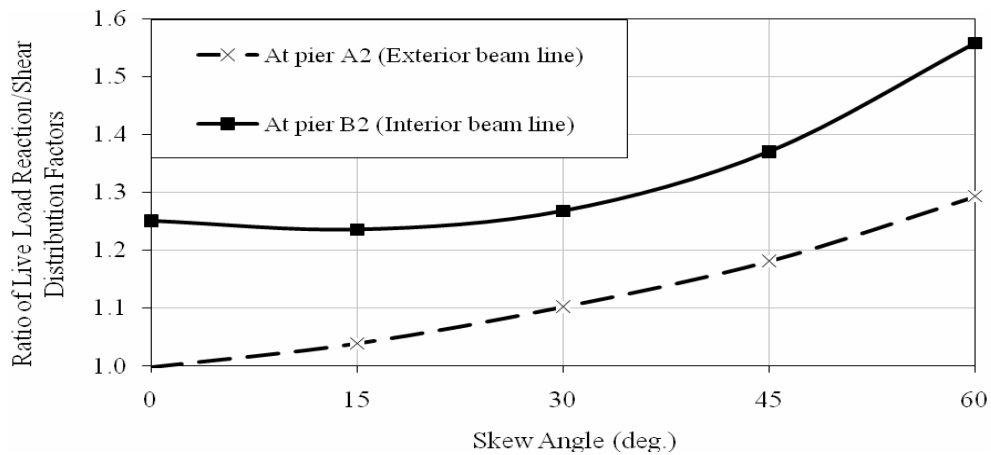


Figure 5.5 Ratio of LDF for Reaction to Shear– Bridge #1

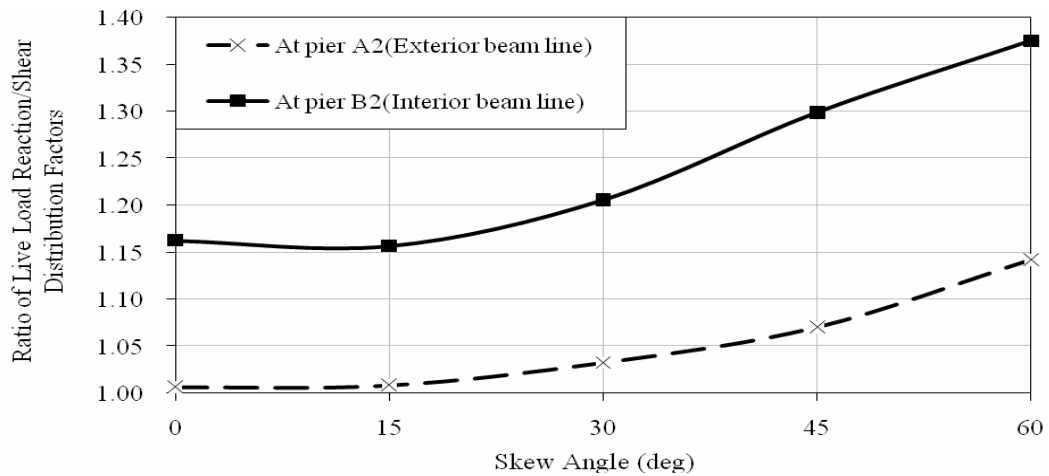


Figure 5.6 Ratio of LDF for Reaction to Shear– Bridge #2

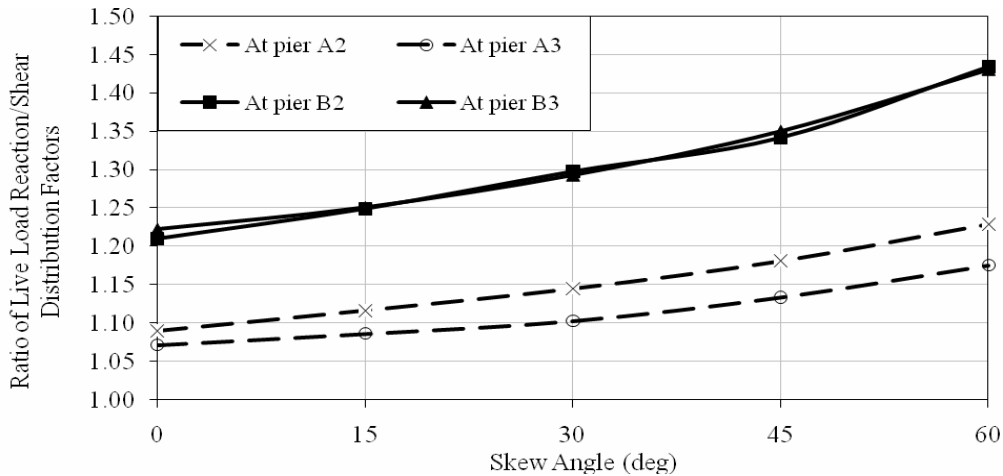
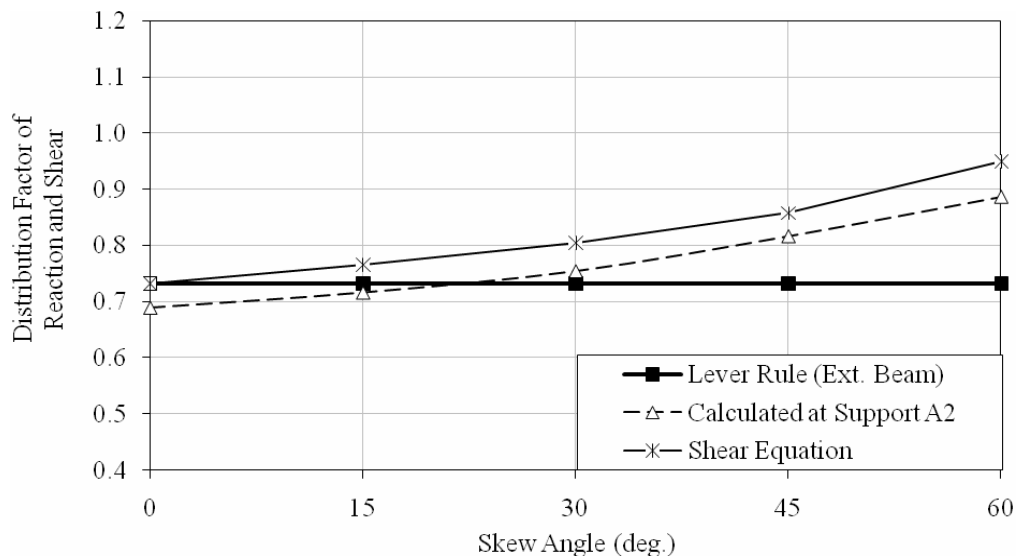


Figure 5.7 Ratio of LDF for Reaction to Shear– Bridge #3

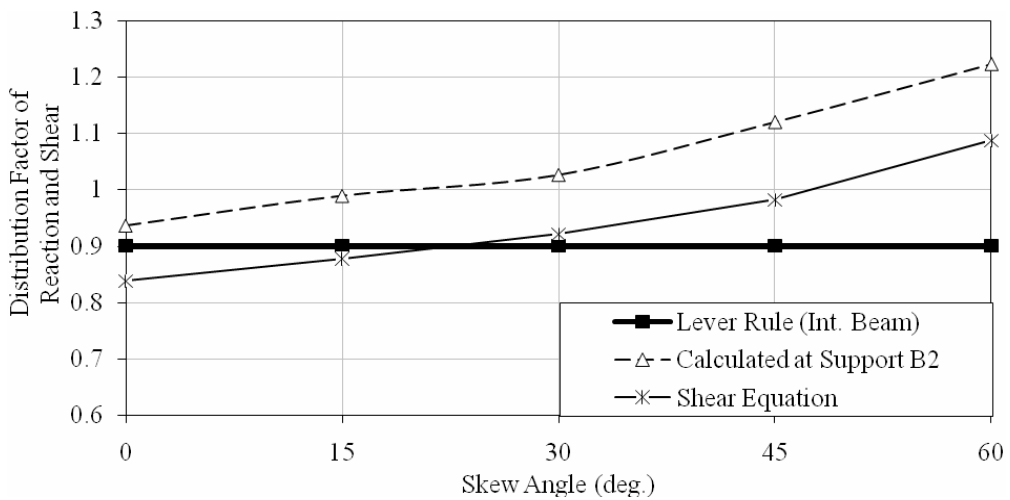
5.2.3 Comparison to the Current Procedures

Currently, the reaction distribution factors are determined by using either the lever rule method or the LRFD shear distribution equations with skew correction. To compare the analytical results to the current procedures, the distribution factors of the reaction were calculated using the two methods. As mentioned previously, the LRFD equation has a skew correction factor that accounts for the skew effect on shear distribution. The lever

rule method, on the other hand, is based on the static equilibrium of a simply supported member, so no skew effect is considered. The distribution factors of the reactions for Bridge #1 through #3 are presented in Figures 5.8 through 5.10, respectively. For each bridge, the reaction distribution factors were calculated with the finite element method, the lever rule method, and the shear equation specified in the AASHTO LRFD Specification.

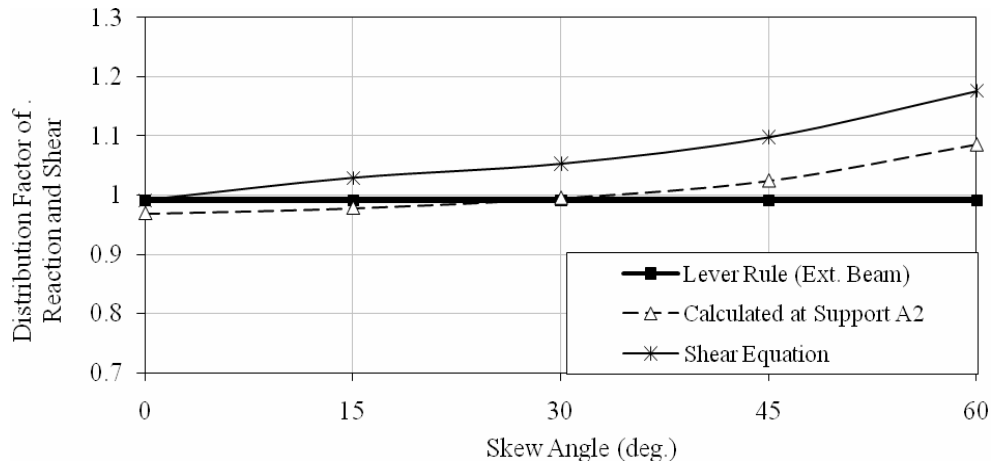


(a) Exterior piers

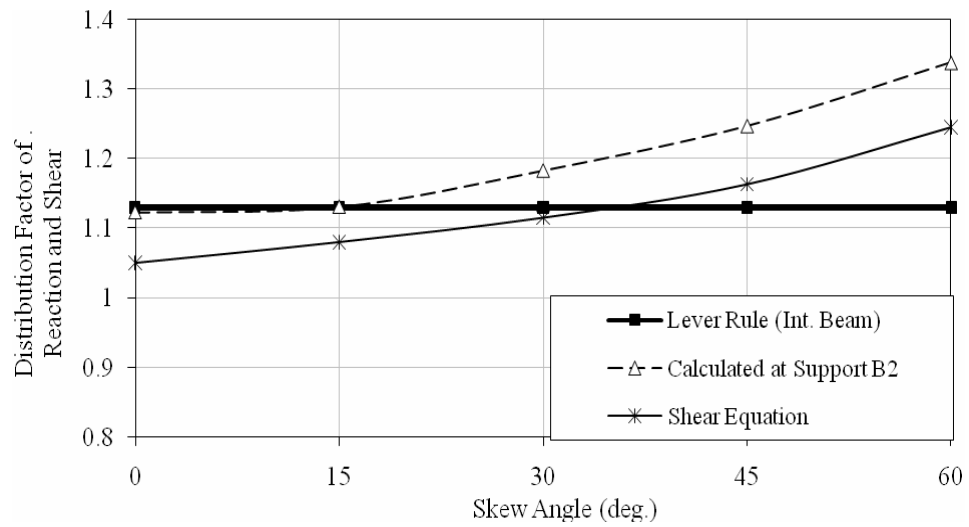


(b) Interior piers

Figure 5.8 Comparisons to the Current Procedures – Bridge #1

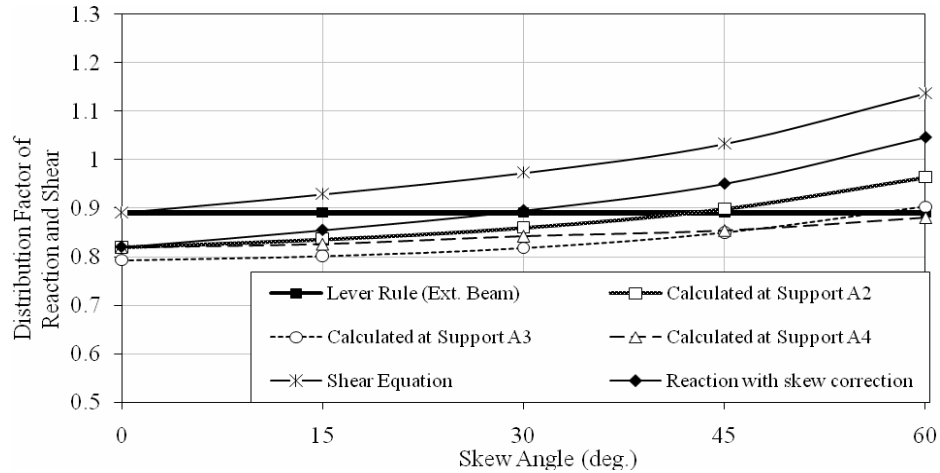


(a) Exterior piers

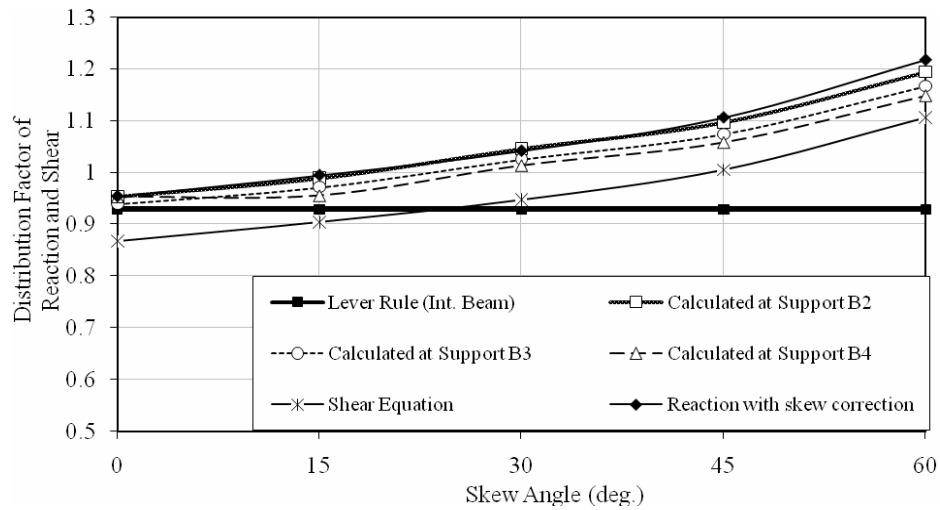


(b) Interior piers

Figure 5.9 Comparisons to the Current Procedures – Bridge #2



(a) Exterior piers



(b) Interior piers

Figure 5.10 Comparisons to the Current Procedures – Bridge #3

As shown in Figures 5.8 through 5.10, at piers in the exterior beam line, the LRFD equation for the shear distribution factor predicted higher values than the reaction distribution factors obtained from the analysis, although the equation can reasonably predict the variation trend of the reaction distribution factor as the skew angle changed. The lever rule method can give a reasonable prediction of the maximum reaction distribution factor for small skew angle scenarios but underestimated the reaction distribution factors when the skew angle became larger. For the piers in the interior beam

Table 5.4 Comparison of Distribution Factor of Reaction and Shear at Support with Different Methods– Bridge #3

Skew angle (deg)	A2					A3				
	AASHTO Guide Specs. 1994	Henry's method w/ skew correct.	AASHTO LRFD 2004	Lever rule	FEA results	AASHTO Guide Specs. 1994	Henry's method w/ skew correct.	AASHTO LRFD 2004	Lever rule	FEA results
0	0.798	0.695	0.891	0.891	0.820	0.798	0.695	0.891	0.891	0.793
15	0.814	0.709	0.929		0.836	0.814	0.709	0.929		0.802
30	0.833	0.726	0.973		0.860	0.833	0.726	0.973		0.819
45	0.858	0.748	1.033		0.899	0.858	0.748	1.033		0.850
60	0.902	0.786	1.137		0.964	0.902	0.786	1.137		0.903
Skew angle (deg)	B2					B3				
	AASHTO Guide Specs. 1994	Henry's method w/ skew correct.	AASHTO LRFD 2004	Lever rule	FEA results	AASHTO Guide Specs. 1994	Henry's method w/ skew correct.	AASHTO LRFD 2004	Lever rule	FEA results
0	0.912	0.695	0.867	0.929	0.954	0.912	0.695	0.867	0.929	0.940
15	0.930	0.709	0.904		0.989	0.930	0.709	0.904		0.971
30	0.952	0.726	0.947		1.046	0.952	0.726	0.947		1.025
45	0.981	0.748	1.005		1.097	0.981	0.748	1.005		1.074
60	1.031	0.786	1.106		1.194	1.031	0.786	1.106		1.166

line, both prediction methods underestimated the live load distribution of reaction for interior supports. Although the LRFD equation showed the trend of the reaction distribution varying with the skew angle, the predicted shear distribution factors were smaller than the obtained analytical results. Apparently, the lever rule method cannot account for the effect of skew.

As presented in Table 5.4, to search for possible methods which can correctly predict the distribution factors of live load reaction in the skewed bridges, several other procedures were also investigated such as the 1994 AASHTO Guide Specification and the Henry's method with skew correction factors from AASHTO LRFD Specifications. However, no current procedures can correctly predict the distribution factors of reaction, especially in the interior piers.

It is obvious that the bridge skewness is an important factor to live load reaction distribution and should not be ignored. Based on the results of the limited study in this chapter, the following conclusions have been made: (1) The reaction distribution factor at the piers of continuous skewed bridges increases with the increase of the skew angles. (2) The distribution factors of the reactions at the piers are higher than those of shear near the same piers. The increase in the reaction distribution factor at the piers is more significant than that in the shear distribution factor when skew angle is greater than 30° . (3) No current procedures could correctly predict live load reaction distribution in the skewed piers, which clearly underestimate live load reaction distribution at piers in the interior beam line. Therefore, it is necessary that more research be performed on the distribution factor of live load reaction to quantify the responses. In the following chapters, the distribution factors for live load reaction were separated from those for shear in the girders of skewed bridges and were predicted with the specific equations instead of using those for shear.

CHAPTER 6

PARAMETRIC STUDY ON SKEW CORRECTION FACTORS FOR SHEAR AND REACTION DISTRIBUTIONS

According to the comparison studies of distribution factors for live load reaction to those for shear in the skewed bridges presented in Chapter 5, it is necessary to develop specific distribution factors for live load reaction. The procedure to calculate the reaction distribution factor in the skewed bridge is to use the proposed skew correction factor for reaction to adjust the shear distribution factor for corresponding straight bridges calculated from NCHRP12-62 or AASHTO LRFD Specifications. Appendix C listed an example showing how to calculate the distribution factors in straight bridges in NCHRP12-62 for steel I girder bridges. In other words, the procedure to calculate the distribution factors for live load reaction were kept the same as that for live load shear while the difference between reaction and shear were taken into account with the different proposed skew correction factors.

The live load shear and reaction distribution factors were obtained using the FEM for various types of slab-on-girder bridges. The effects of various structural parameters on SCFs were investigated in detail to identify the parameters sensitive to the load distribution factors under live loads. The SCF herein was defined as the ratio of shear or reaction distribution factor for a given skewed bridge to that for a non-skewed bridge. The shear or reaction distribution factors for the skewed bridge were obtained using FEM and the distribution factors for non-skewed bridges were obtained from the unlimited equations proposed in NCHRP12-62. The following sections present the effects of span

length, girder spacing, and skew angle on skew correction factors for various types of bridges. One parameter at a time was considered, whereas the other parameters remained fixed.

6.1 Steel I-girder Bridges

6.1.1 Effect of Span Length on SCF

In order to investigate the effect of span length (L) on SCF for steel I-girder bridges, the finite element analyses of 210 steel I-girder bridges with span lengths ranging from 100 to 400 ft were performed. Figures 6.1 and 6.2 show the effect of span length on skew correction factors for live load reaction and shear distributions for exterior and interior girders, respectively. The bridge with a girder spacing of 20 ft was randomly selected to represent the typical results. The skew angle varied from 30° to 75° .

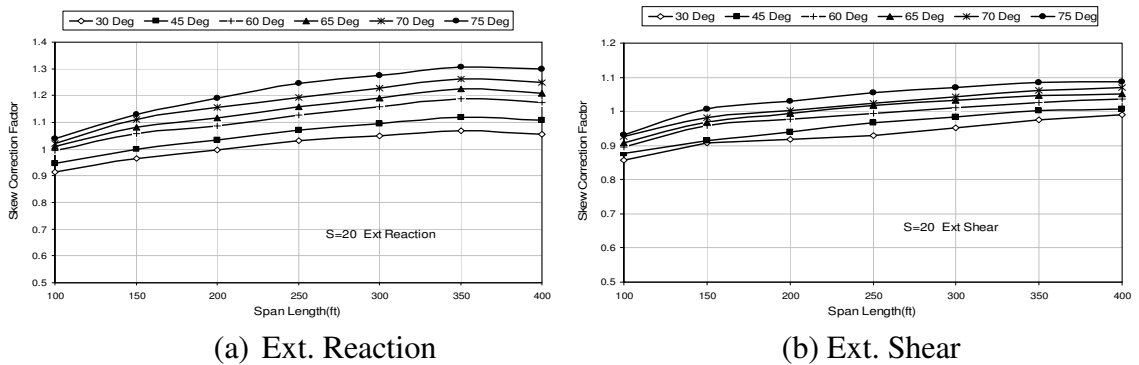
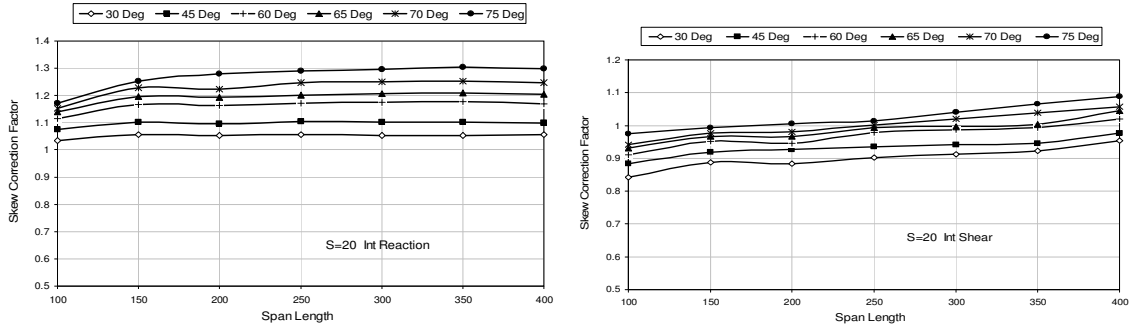


Figure 6.1 SCF on Exterior Girders with Spacing of 20ft



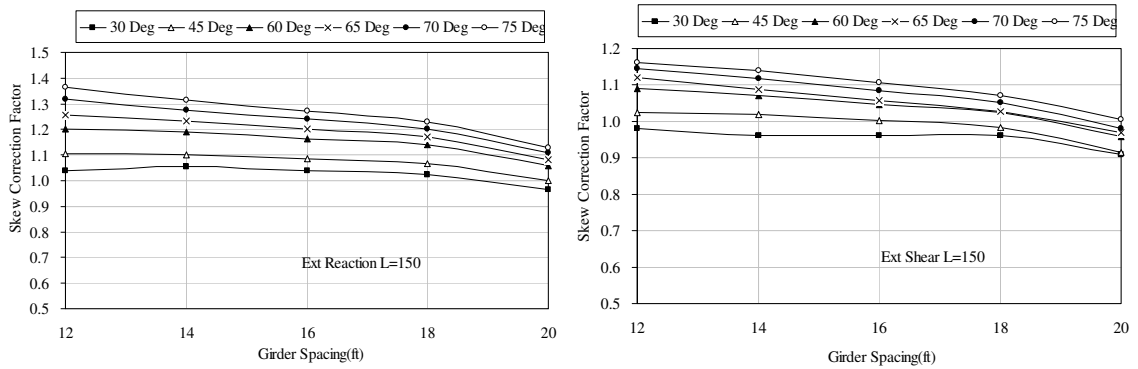
(a) Int. Reaction (b) Int. Shear
Figure 6.2 SCF on Interior Girders with Spacing of 20ft

In comparing the SCF for reaction and shear, it was found that the SCFs for reaction at piers were larger than those for shear in both exterior and interior girders, which validated that the reaction distribution factors should be considered with the specific SCF equations instead of those for shear distribution factors. For example, at a skew angle of 75°, the SCF for reaction is 1.3, which is larger than that of 1.09 for shear on the exterior girder presented in Figure 6.1. In addition, for the exterior girder shown in Figure 6.1 and the interior girder shown in Figure 6.2, as the skew angle increased, the skew correction factor increased.

For both exterior and interior girders, Figures 6.1 and 6.2 reveal that regardless of skew angle, the SCFs for live load shear and reaction increased as span length increased. For example, as shown in Figure 6.1, the SCFs for live load reaction and shear on exterior girders increased by 25.0 % and 17.2%, respectively, as span length varied from 100 to 400 ft at a skew angle of 75°. The similar trends were observed from the SCFs for shear and reaction distributions obtained from the finite element analysis results of the other steel I-girder bridges. When developing the formulas for SCFs for both reaction and shear distributions, the effect of span length, L , was significant and should be included.

6.1.2 Effect of Girder Spacing on SCF

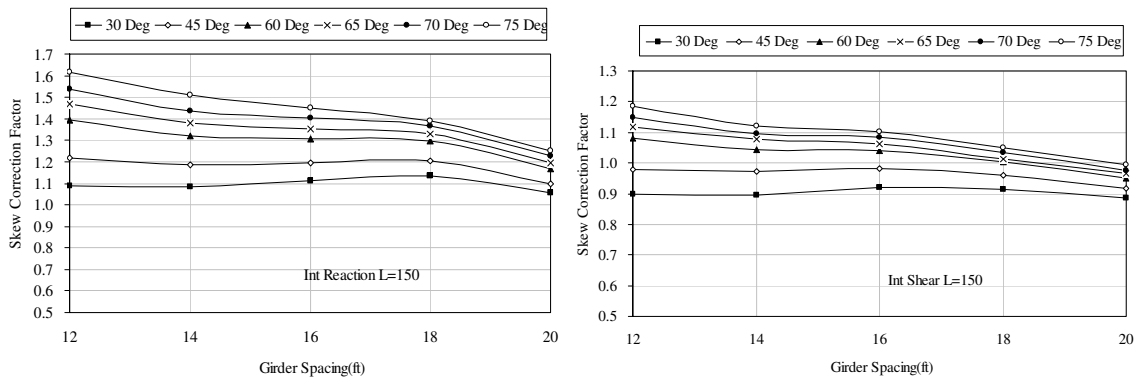
According to the procedures in the AASHTO-LRFD, the girder spacing (S) is one of the most important parameters that affects the distribution factor. Similar to span length, in order to investigate the influence of girder spacing on SCF for steel I-girder bridges, the finite element analyses of 210 bridges with girder spacing ranging from 12 to 20 ft were conducted. The typical results were illustrated through the bridge with the span length of 150 ft in Figures 6.3 and 6.4 for exterior girders and interior girders, respectively.



(a) Ext. Reaction

(b) Ext. Shear

Figure 6.3 SCF on Exterior Girders with Span Length of 400ft



(a) Int. Reaction

(b) Int. Shear

Figure 6.4 SCF on Interior Girders with Span Length of 150ft

In comparing the SCFs of reaction and shear distributions, as shown in Figures 6.3 and 6.4, the SCFs for reaction at skewed piers was amplified compared to those for shear. It is obvious that the SCF for reaction of 1.68 is higher than that of 1.24 for shear on the interior girder with the 12-ft girder spacing at the skew angle of 75°. Again, it verified that the SCFs for reaction at piers are larger than those for shear in both exterior and interior girders, which is consistent with the previous conclusion drawn in Chapter 5. Therefore, Skew correction factors for reaction distributions should be considered with specific equations instead of using those for shear distributions.

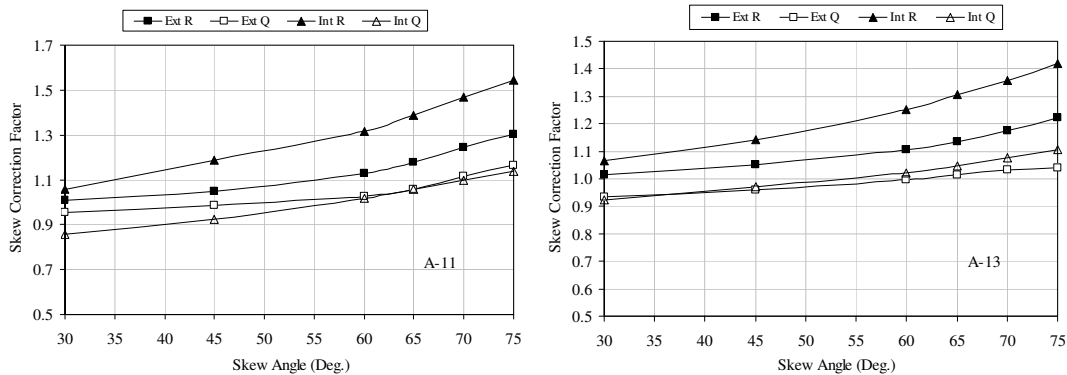
For both exterior and interior girders, as shown in Figures 6.3 and 6.4, in contrast to the effect of span length, the SCFs for live load shear and reaction decreased as girder spacing increased. For example, the SCF for live load reaction and shear on exterior girders decreased by 29.3% and 23.8%, respectively, when the girder spacing varied from 12 to 20ft at 75° (see Figure 6.3). Similarly, the reduction of SCFs for reaction and shear on interior girders was 22.6% and 12.1%, respectively, when subject to the same change of girder spacing (see Figure 6.4). The FEA results from the other steel I-girder bridges in the database showed the similar trend. Therefore, the girder spacing was treated as an important parameter in developing the formulas of SCFs because of its marked effect on SCFs.

6.1.3 Effect of Skew Angle on SCF

As discussed in the literature review, the skew angle is another important parameter that affects the live load distribution factors. The shear in the girder at the

obtuse corner was found to be higher than that at the acute corner in the girder of skewed bridges. Therefore, the effect of skew was investigated by performing finite element analyses on 210 steel I-girder bridges with skew angles ranging from 30° to 75°. Figure 6.5 presents the effect of skew angle on SCF for live load reaction and shear distributions with the skew angles ranging from 30° to 75°. The SCFs obtained from FEA for bridge Nos.11 and No.13 were randomly selected to represent the typical results.

Figure 6.5 shows that, on both exterior and interior girders, an increase in skew angle caused the corresponding increase in SCF. For example, for Bridge #A-11, the SCF for live load reaction and shear on exterior girders was increased by 19.0% and 9.5%, respectively, when skew angle varied from 30 to 75 ft. Similarly, the corresponding increase of skew correction factors for reaction and shear on interior girders were 17.9% and 12.9%, respectively. Similar trends were observed in the other steel I-girder bridges. Therefore, the skew angle was treated as another important parameter in the proposed formulas of SCFs.



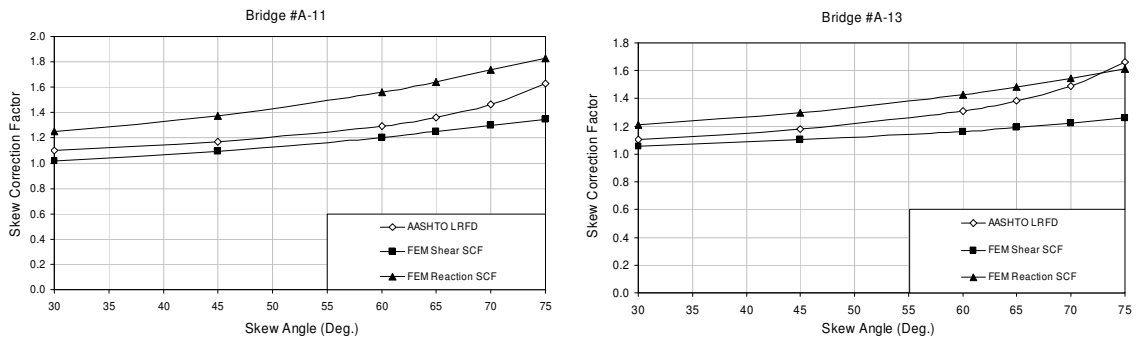
(a) Bridge#A-11

(b) Bridge#A-13

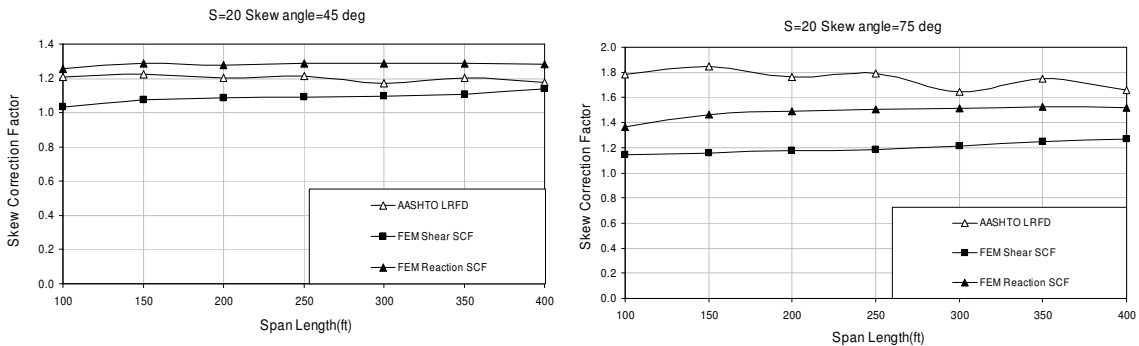
Figure 6.5 Effect of Skew Angle on SCF

6.1.4 Comparison of SCF from AASHTO LRFD to FEM SCF

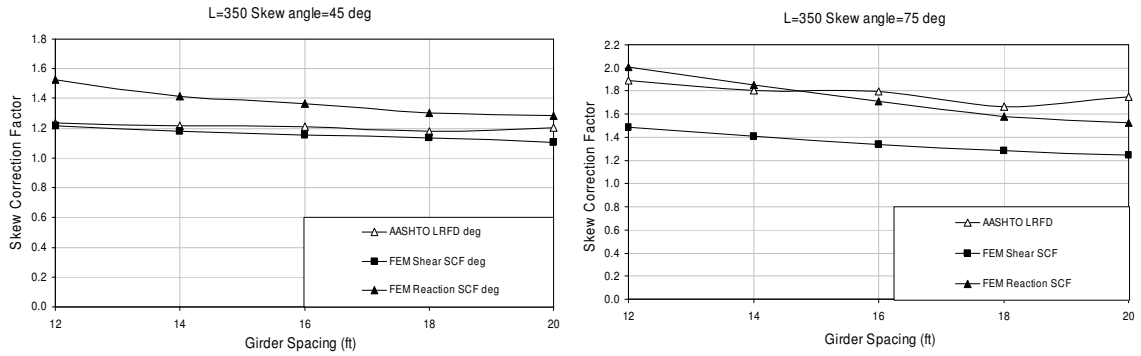
In order to verify the SCF equations in the LRFD specifications are not suitable for the bridges with the parameters outside the applicable ranges, the SCFs in this section were based on the LDF for straight bridges specified in the AASHTO LRFD Specifications instead of those proposed in NCHRP12-62. Herein, the current LRFD equations for non-skewed bridges were assumed to be unlimited in the range of applicability. FEM SCF in the following figures was calculated with finite element results and the LRFD equations for straight bridges. Then FEM SCFs were compared to those calculated with the codified skew correction factor in the current LRFD Specification.



(a) Bridge #A-11 (b) Bridge #A-13
Figure 6.6 Comparison of AASHTO LRFD Based SCF to FEM SCF- θ



(a) S=20, $\theta=45^\circ$ (b) S=20, $\theta=75^\circ$
Figure 6.7 Comparison of AASHTO LRFD Based SCF to FEM SCF-L



(a) $L=350, \theta=45^\circ$ (b) $L=350, \theta=75^\circ$
Figure 6.8 Comparison of AASHTO LRFD Based SCF to FEM SCF-S

All steel I-girder bridges were studied in detail to show the differences between the SCFs obtained from the current AASHTO LRFD Specifications and those using the finite element analyses. The steel I-girder bridges No.11 and No. 13 were randomly selected to illustrate the results as the variation of the skew angle in Figure 6.6. Regardless of shear or reaction, the SCF obtained from the LRFD specifications did not give comparable results to the finite element results, especially when skew angles are larger than 60° . Figures 6.7 and 6.8 presented the comparison of finite element results to SCF from AASHTO LRFD for various span lengths and girder spacings, respectively. All the comparisons shown in the figures demonstrated that the SCFs from the current LRFD Specifications cannot correctly predict the SCFs for the shear and reaction distributions in the skew steel I-girder bridges with structural parameters outside the range of applicability. Similar trends were observed in the other steel I-girder bridges. Therefore, it is necessary to develop the new skew correction equations for the bridges with structural parameters outside the limitations in the current specifications.

6.2 Precast Concrete I-girder Bridges

6.2.1 Effect of Span Length on SCF

To study the effect of span length on SCF for precast concrete I-girder bridges, finite element analyses of 90 precast concrete I-girder bridges with span lengths ranging from 50 to 150 ft were performed. Figures 6.9 and 6.10 present the effect of span length on live load reaction and shear skew correction factor with the skew angle ranging from 30° to 75° for both exterior and interior girders with the girder spacing of 18 ft.

Similar to what was shown for the steel I-girder bridge, the SCFs for live load shear and reaction increased as the span length was increased. As shown in Figure 6.9,

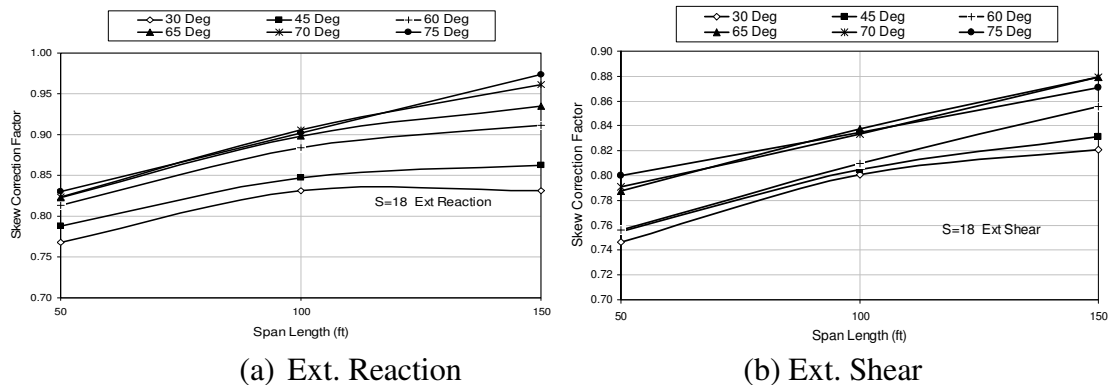


Figure 6.9 SCF on Exterior Girders with Spacing of 18ft

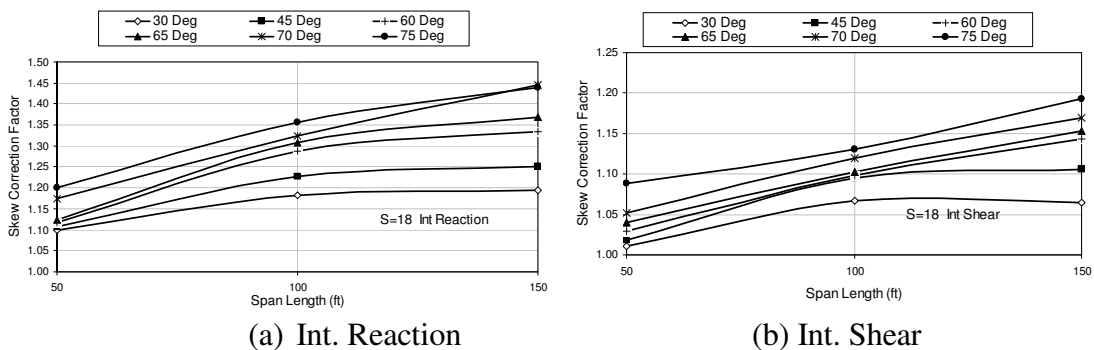


Figure 6.10 SCF on Interior Girders with Spacing of 18ft

the SCFs for live load reaction and shear on exterior girders increased by 27.6 % and 19.2%, respectively, as span length varied from 50 ft to 150 ft at 75°. Similarly, the increase of skew correction factors for reaction and shear on interior girders were 10.8 % and 9.2%, respectively, when subject to the same variation of span length (See Figure 6.10). The finite element analysis results from the other precast concrete I-girder bridges in the database also showed a similar trend. Therefore, the effect of span length on reaction and shear distribution factors is important and should be employed in the proposed formulas.

6.2.2 Effect of Girder Spacing on SCF

Similar to span length, the effect of girder spacing on SCF for precast concrete I-girder bridges was also investigated to determine whether this parameter should be included in the proposed formulas. The girder spacing varied from 12 to 20 ft with an increment of 2 ft. Figures 6.11 and 6.12 present the effect of girder spacing on skew correction factors for live load reaction and shear with the skew angle ranging from 30° to 75°, for both exterior and interior girders with the span length of 100 ft.

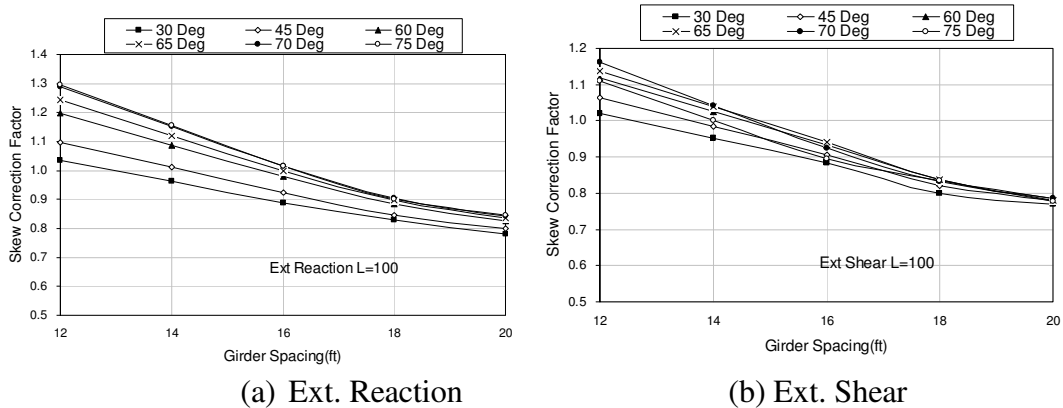


Figure 6.11 SCF on Exterior Girders with Span Length of 100ft

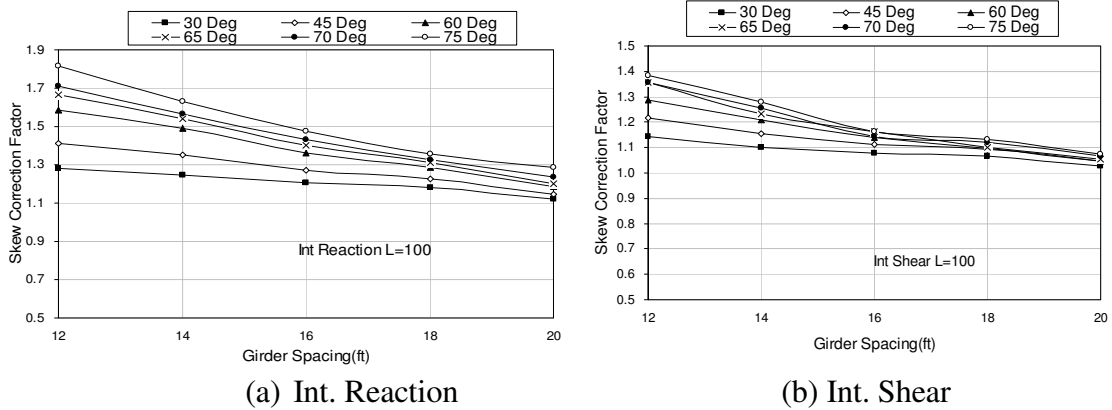
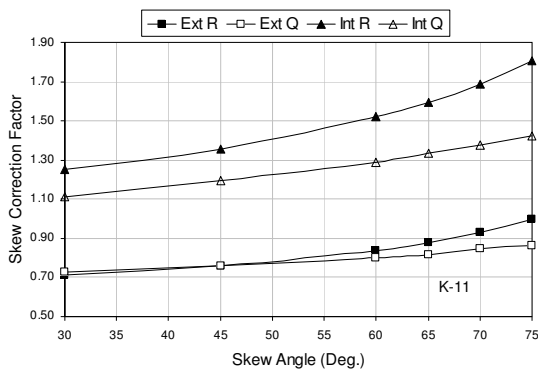


Figure 6.12 SCF on Interior Girders with Span Length of 100ft

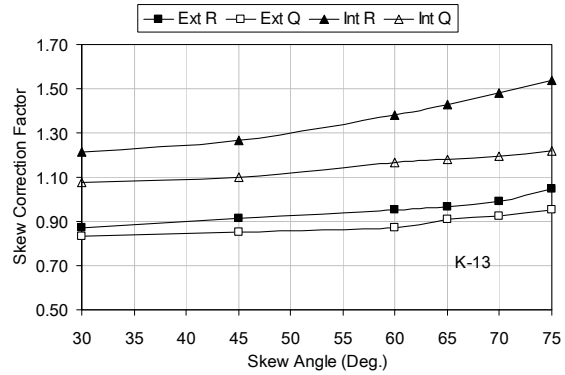
Figures 6.11 and 6.12 demonstrated that, on both exterior and interior girders, the SCFs for live load shear and reaction decreased as girder spacing increased, which was opposite to the effect of span length. The SCFs for live load reaction and shear on exterior girders were decreased by 35.4% and 29.7%, respectively, when girder spacing varied from 12 to 20 ft at 75° (See Figure 6.11). Similarly, the decrease of skew correction factors for reaction and shear on interior girders, were 29.6% and 22.5% respectively (See Figure 6.12). The FEA results from the other precast concrete I-girder bridges in the database also showed the similar trend. Therefore, the girder spacing was treated as an important parameter in developing the formulas for skew correction factors.

6.2.3 Effect of Skew Angle on SCF

Similar to span length and girder spacing, skew angle in precast concrete I-girder bridges is another important factor considered in the proposed SCF equations. Figure 6.13 presents the effect of skew angles on SCF for live load reaction and shear distributions with the skew angle ranging from 30° to 75°, for both exterior and interior



(a) Bridge #K-11



(b) Bridge #K-13

Figure 6.13 Effect of Skew Angle on SCF

girders with span length of 100 ft. The No.11 and No.13 precast concrete I-girder bridges were randomly chosen to represent the typical results.

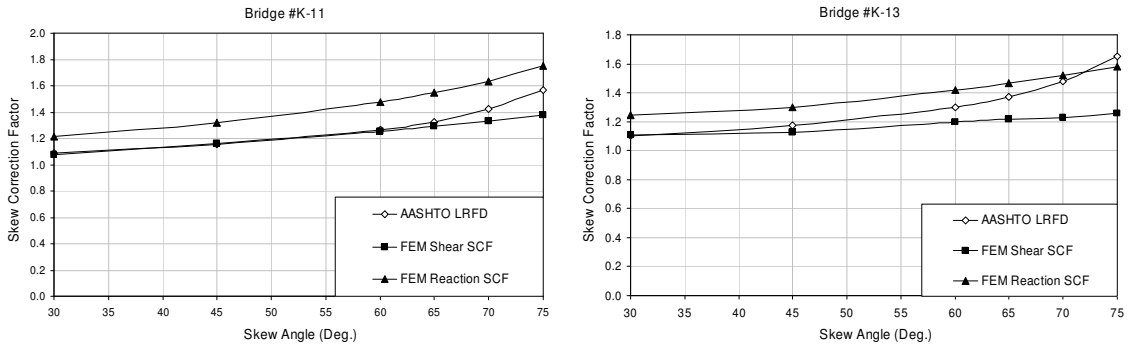
As shown in Figure 6.11, the SCFs for live load shear and reaction increased as skew angle increased on both interior and exterior girders. For example, as shown in Figures 6.13(a), the SCFs for live load reaction and shear on exterior girders increased by 25.0% and 8.8%, respectively, when the skew angle varied from 30° to 75°. Similarly, the corresponding increase of SCFs for reaction and shear on interior girders were 42.2% and 21.1%, respectively. Similar trends were observed in the other precast concrete I-girder bridges. Therefore, the skew angle was treated as another important parameter in the proposed formulas of SCFs.

6.2.4 Comparison of SCF from AASHTO LRFD to FEM SCF

In order to verify that the LRFD equations for SCFs are not applicable for the bridges with parameters outside the range of applicability, the SCFs obtained from finite

element analyses were compared to those calculated with the codified skew correction factors in the current LRFD Specification.

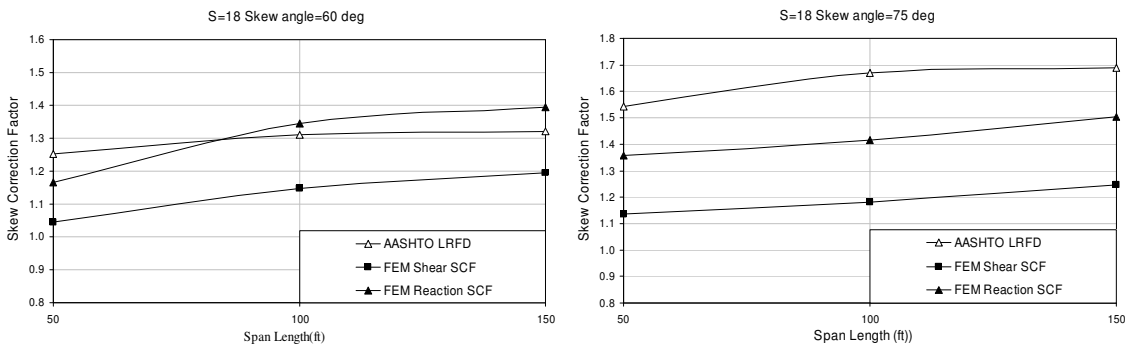
All precast concrete I-girder bridges in the database were analyzed to investigate the differences between the SCFs calculated from the current AASHTO LRFD Specification and those obtained from finite element analyses. For the SCFs for shear



(b) Bridge #K-11

(b) Bridge #K-13

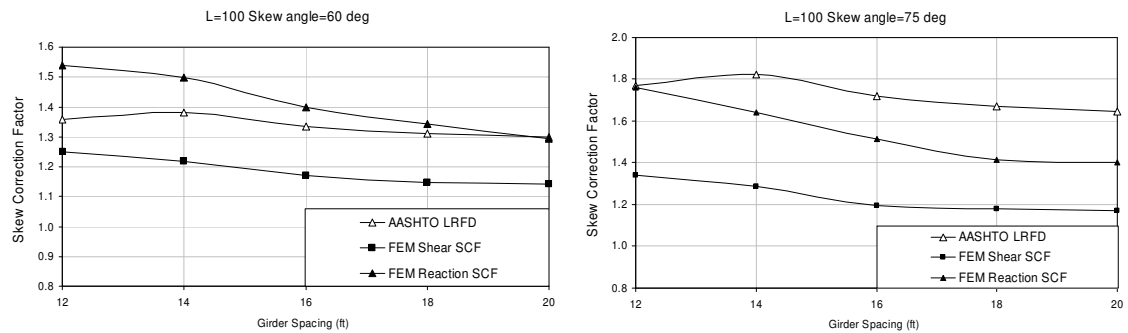
Figure 6.14 Comparison of AASHTO LRFD Based SCF to FEM SCF-θ



(a) S=18, θ=60°

(b) S=18, θ=75°

Figure 6.15 Comparison of AASHTO LRFD Based SCF to FEM SCF-L



(a) L=100, θ=60°

(b) L=100, θ=75°

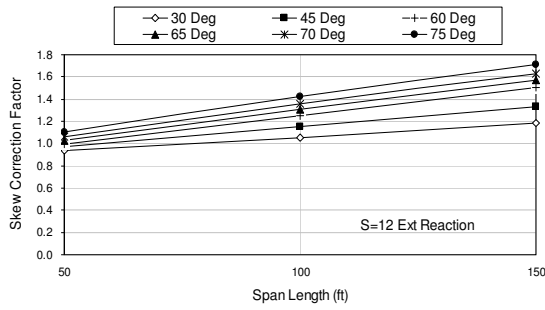
Figure 6.16 Comparison of AASHTO LRFD Based SCF to FEM SCF-S

and reaction distributions, the finite element results are different from those calculated using the current AASHTO LRFD Specifications, especially when skew angles are larger than 60° . Figures 6.15 and 6.16 present the comparison of finite element results to SCF obtained from AASHTO LRFD in different ways. Figure 6.15 compares the finite element results to those obtained from the LRFD equations in terms of span length (L) while Figure 6.16 was in terms of girder spacing (S). The comparisons demonstrated that the SCFs from the current LRFD Specifications did not correctly predict the SCFs for the shear and reaction distributions in the skew precast concrete I-girder bridges with structural parameters outside the range of applicability. Similar trends were observed in the other precast concrete I-girder bridges. Therefore, it is necessary to develop the new skew correction equations for shear and reactions for the bridges with structural parameters outside the limitations in the current specifications.

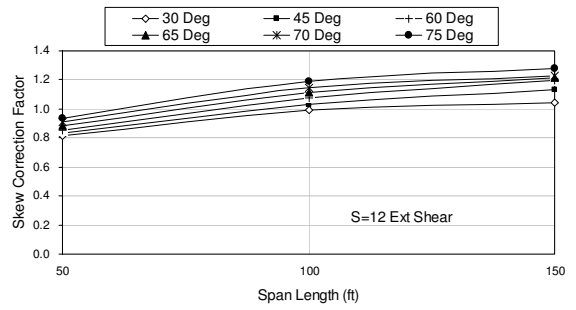
6.3 Precast Concrete Spread Box Girder Bridges

6.3.1 Effect of Span Length on SCF

To investigate the effect of span length on SCF for precast concrete spread box-girder bridges, 90 bridges were analyzed using FEM with span lengths ranging from 50 to 150 ft. Figures 6.17 and 6.18 present the effect of span length on skew correction factors for live load reaction and shear distributions, respectively. The bridge with the girder spacing of 12 ft was randomly chosen to show the results. The skew angle varied from 30° to 75° .

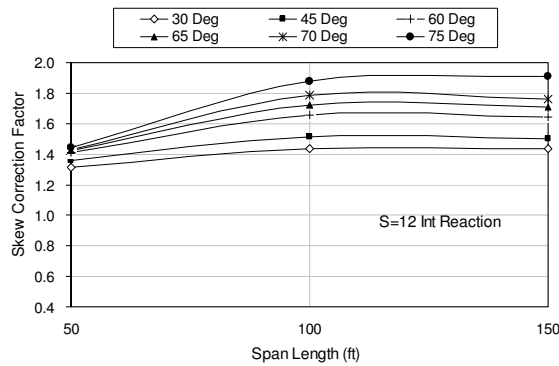


(a) Ext. Reaction

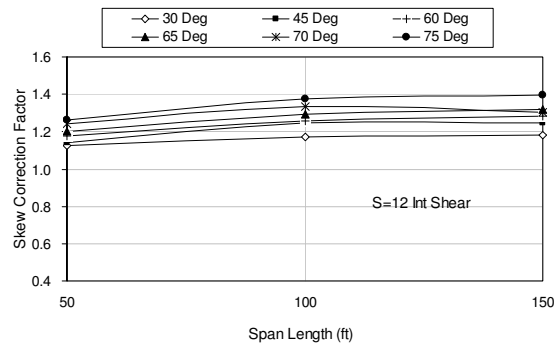


(b) Ext. Shear

Figure 6.17 SCF on Exterior Girders with Spacing of 12ft



(a) Int. Reaction



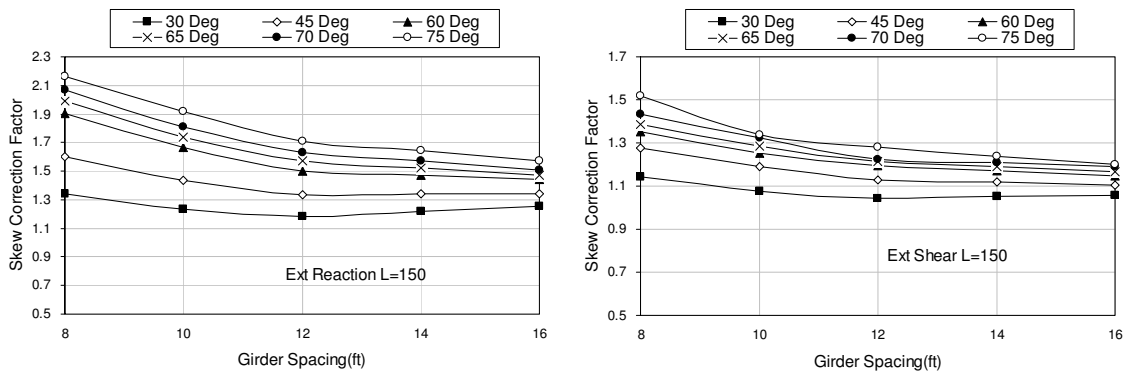
(b) Int. Shear

Figure 6.18 SCF on Interior Girders with Spacing of 12ft

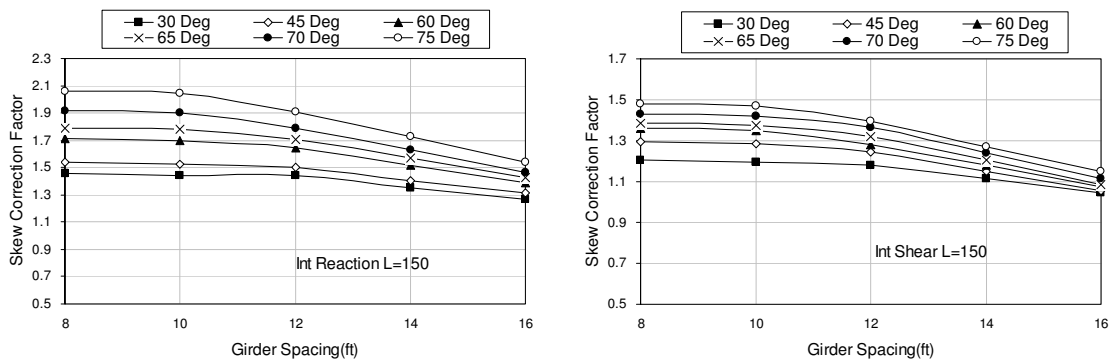
Similar to what was shown for the steel I-girder and precast concrete I-girder bridges, the SCFs for live load shear and reaction increased as the span length increased. For exterior girders as shown in Figure 6.17, the SCFs for live load reaction and shear increased by 35.7% and 26.6%, respectively, as span length varied from 50 ft to 150 ft at 75°. In addition, Figure 6.18 showed that the corresponding increases on interior girders were 24.6% and 9.35% for reaction and shear, respectively. The FEA results from the other precast concrete spread box-girder bridges in the database also revealed a similar trend. Therefore, the effect of span length on SCF for reaction and shear distributions was important and should be employed in the proposed formulas.

6.3.2 Effect of Girder Spacing on SCF

Similar to span length, the effect of the girder spacing (S) on SCFs for precast concrete spread box-girder bridges was also investigated to determine whether this parameter should be included in the proposed formulas. Finite element analyses of 90 precast concrete spread box-girders were performed. Figures 6.19 and 6.20 present the effect of the girder spacing on skew correction factors for live load reaction and shear with the skew angle ranging from 30° to 75° , for both exterior and interior girders with the span length of 150 ft.



(a) Ext. Reaction (b) Ext. Shear
Figure 6.19 SCF on Exterior Girders with Span Length of 150 ft



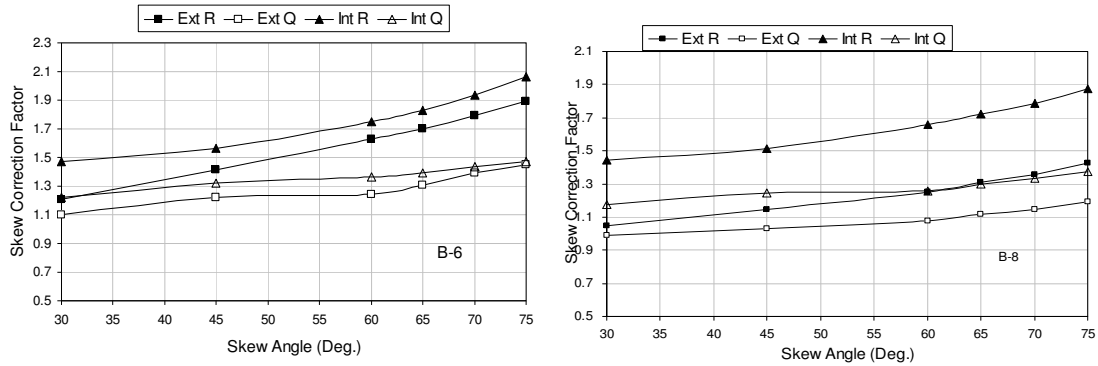
(a) Ext. Reaction (b) Ext. Shear
Figure 6.20 SCF on Interior Girders with Span Length of 150 ft

For both exterior and interior girders, as shown in Figures 6.19 and 6.20, the SCFs for live load shear and reaction decreased as girder spacing increased. The SCFs for live load reaction and shear on exterior girders were decreased by 26.9% and 21.1%, respectively, when girder spacing varied from 8 to 16 ft at 75° (See Figure 6.19). Similarly, the decrease of skew correction factors for reaction and shear on interior girders were 25.2% and 22.3% respectively (See Figure 6.20). The FEA results obtained from the other precast concrete spread box-girder bridges in the database also showed a similar trend. Therefore, the girder spacing was treated as an important parameter in developing the formulas for skew correction factors.

6.3.3 Effect of Skew Angle on SCF

Similar to span length and girder spacing, skew angle in precast concrete spread box-girder bridges is another important factor considered in the proposed skew correction factor equations. Figure 6.21 presents the effect of skew angles on SCF for live load reaction and shear distributions with the skew angle ranging from 30° to 75°, for both exterior and interior girders with span length of 100 ft. The No.6 and No.8 precast concrete spread box-girder bridges were randomly chosen to show the results.

As shown in Figure 6.21, the SCFs for live load shear and reaction increased as skew angle increased on both interior and exterior girders. For example, as shown in Figures 6.21 (a), the SCFs for live load reaction and shear on exterior girders increased by 36.1% and 24.3%, respectively, when the skew angle varied from 30° to 75°. Similarly, the corresponding increase of skew correction factors for reaction and shear on



(a) Bridge #B-6

(b) Bridge #B-8

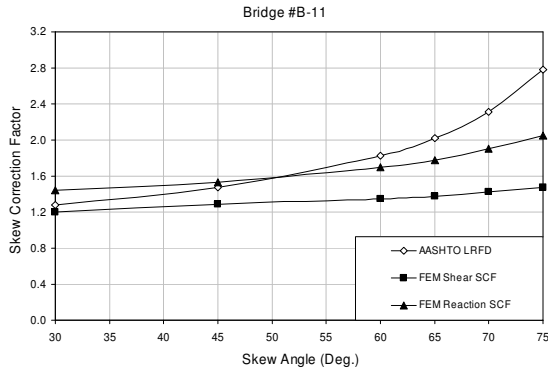
Figure 6.21 Effect of Skew Angle on SCF

interior girders were 28.6% and 16.9%, respectively. Similar trends were observed in the other precast concrete spread box-girder bridges. Therefore, the skew angle was treated as another important parameter in the proposed formulas of SCFs.

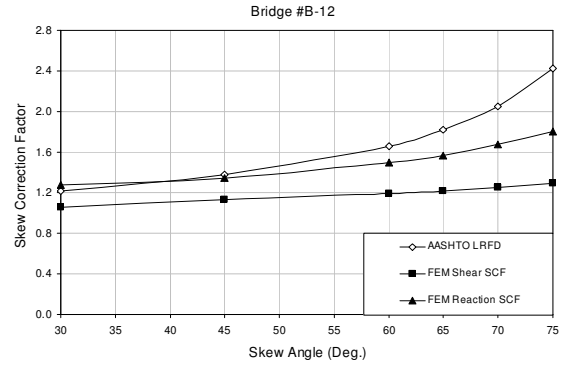
6.3.4 Comparison of SCF from AASHTO LRFD to FEM SCF

To help bridge engineers understand the difference between the skew correction factors specified in the AASHTO LRFD and those calculated with finite element analysis, the comparisons of SCF obtained from the AASHTO-LRFD to those from FEM were presented in term of skew angle (θ), span length (L), and girder spacing(S), which is shown in Figures 6.22 through 6.24. These comparisons were helpful in deciding if the new equations for SCF are necessary.

The precast concrete spread box girder bridges No.11 and No. 12 were randomly selected to illustrate the results in Figure 6.22. Regardless of shear or reaction, the finite element results are different from those calculated using the current AASHTO LRFD Specifications, especially for skew angles larger than 60° . Figures 6.23 and 6.24 present

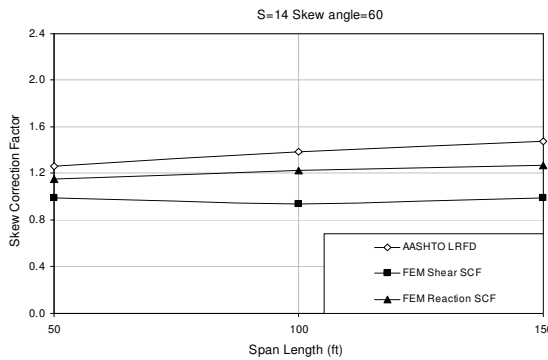


(a) Bridge #B-11

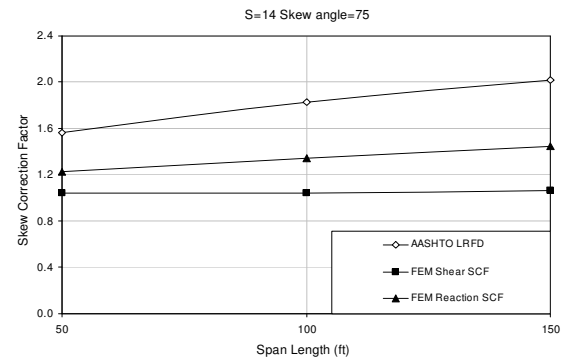


(b) Bridge #B-12

Figure 6.22 Comparison of AASHTO LRFD Based SCF to FEM SCF- θ

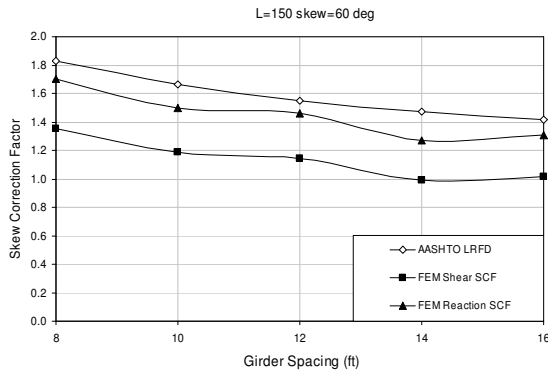


(a) $S=14, \theta=60^\circ$

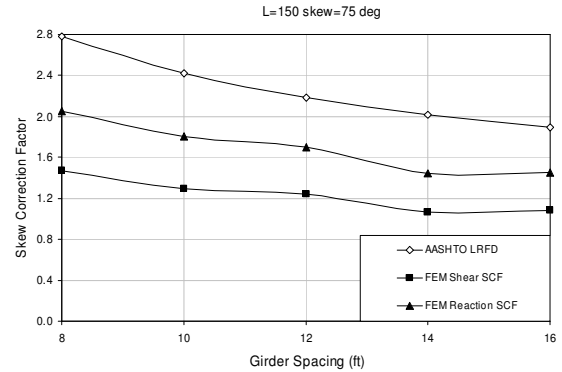


(b) $S=14, \theta=75^\circ$

Figure 6.23 Comparison of AASHTO LRFD Based SCF to FEM SCF-L



(a) $L=150, \theta=60^\circ$



(b) $L=150, \theta=75^\circ$

Figure 6.24 Comparison of AASHTO LRFD Based SCF to FEM SCF-S

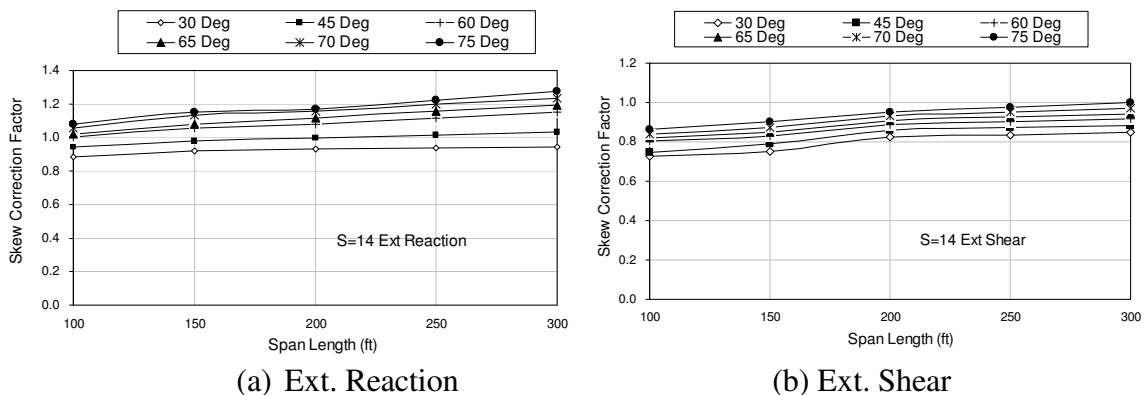
the comparison of finite element results to SCF from AASHTO LRFD in terms of span length (L) and girder spacing (S), respectively. All the comparisons shown in the figures demonstrated that the SCFs from the current LRFD Specifications did not correctly predict the SCFs for the shear and reaction distributions in the skew precast concrete

spread box-girder bridges with structural parameters outside the range of applicability. Similar trends were observed in the other precast concrete spread box girder bridges. Therefore, it is necessary to develop the new skew correction equations for the bridges with structural parameters outside the limitations in the current specifications.

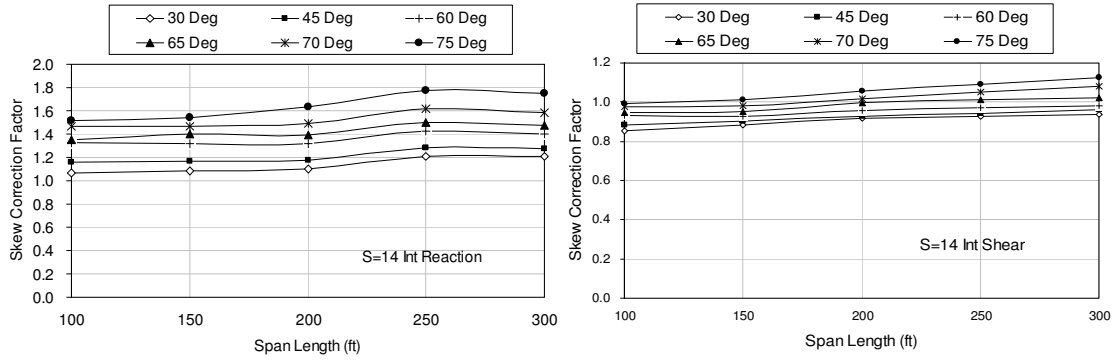
6.4 CIP Multi-cell Box Girder Bridges

6.4.1 Effect of Span Length on SCF

To investigate the effect of span length on SCF for CIP multicell box-girder bridges, the finite element analyses of 120 bridges with span length ranging from 100 to 300 ft were performed. Figures 6.25 and 6.26 present the effect of span length on skew correction factors for live load reaction and shear distributions respectively. The bridge with the girder spacing of 14 ft was randomly selected to show the results. The skew angle varied from 30 to 75 degrees.



(a) Ext. Reaction (b) Ext. Shear
Figure 6.25 SCF on Exterior Girders with Spacing of 14 ft

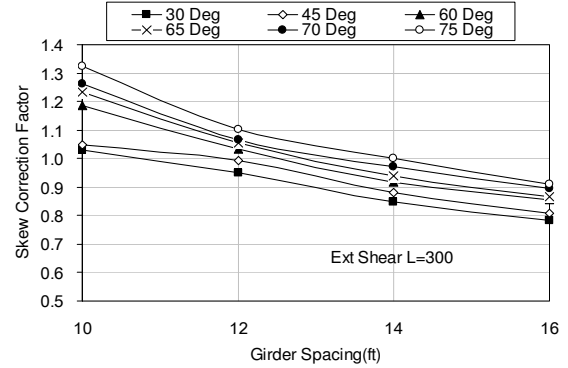
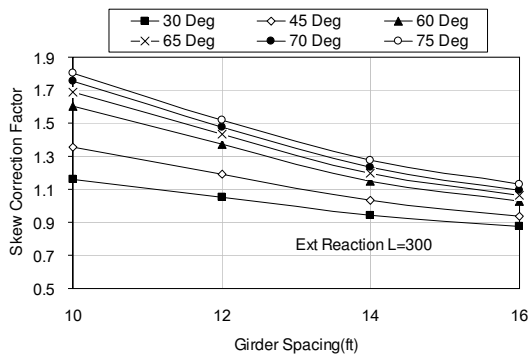


(a) Int. Reaction (b) Int. Shear
Figure 6.26 SCF on Interior Girders with Spacing of 14 ft

Similar to what was shown for the previous types of bridges, the SCFs for live load shear and reaction increased as the span length increased. As shown in Figure 6.25, the SCFs for live load reaction and shear on exterior girders increased by 18.5% and 10.0%, respectively, as span length varied from 100 to 300 ft at 75°. The corresponding increases on interior girders were 15.9% and 14.2% for reaction and shear, respectively (see Figure 6.26). The FEA results from the other CIP multi-cell box-girder bridges in the database also showed a similar trend. Therefore, the effect of span length on SCF for reaction and shear distributions is important and should be employed in the proposed formulas.

6.4.2 Effect of Girder Spacing on SCF

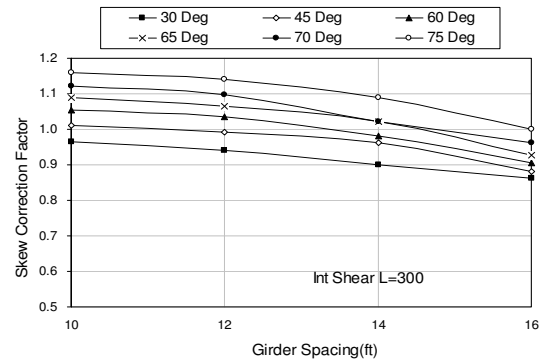
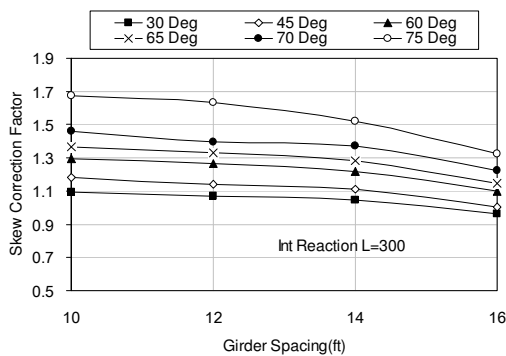
Similar to span length, the effect of the girder spacing for CIP multicell box-girder bridges was also investigated to determine whether this parameter should be included in the proposed formulas. Figures 6.27 and 6.28 present the effect of the girder spacing on skew correction factors for live load reaction and shear with the skew angle ranging from 30° to 75°, for both exterior and interior girders with a span length of 300 ft.



(a) Ext. Reaction

(b) Ext. Shear

Figure 6.27 SCF on Exterior Girders with Span Length of 300 ft



(a) Int. Reaction

(b) Int. Shear

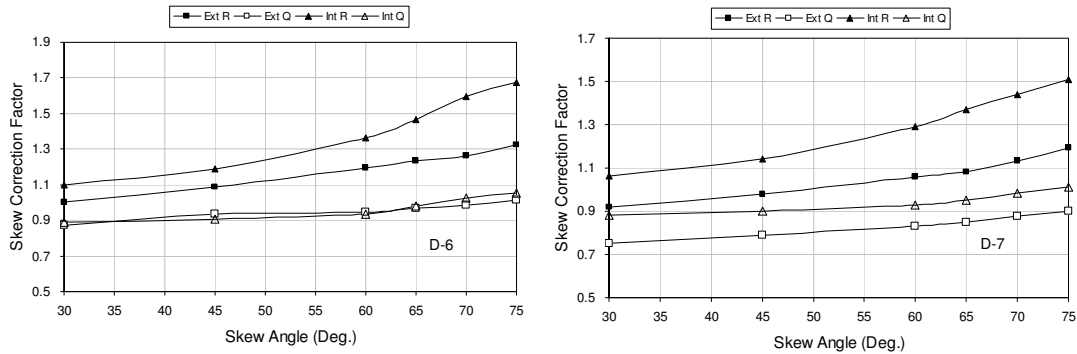
Figure 6.28 SCF on Interior Girders with Span Length of 300 ft

For both exterior and interior girders, as shown in Figures 6.27 and 6.28, the SCFs for live load shear and reaction decreased as girder spacing increased. The SCFs for live load reaction and shear on exterior girders were decreased by 31.1% and 20.8%, respectively, when girder spacing varied from 10 ft to 16 ft at 75° (See Figure 6.27). Similarly, the decrease of skew correction factors for reaction and shear on interior girders, presented in Figures 6.28, were 16.0% and 26.5%, respectively. The FEA results from the other CIP multicell box-girder bridges in the database also showed a similar trend. Therefore, the girder spacing was treated as an important parameter in developing the formulas of skew correction factors.

6.4.3 Effect of Skew Angle on SCF

Similar to span length and girder spacing, skew angle in CIP multicell box-girder bridges is another important factor considered in the proposed skew correction factor equations. Figure 6.29 presents the effect of skew angles on SCF for live load reaction and shear distributions with the skew angle ranging from 30° to 75°, for both exterior and interior girders. The No.6 and No.7 CIP multicell box-girder bridges were randomly selected to represent the results.

As shown in Figure 6.29, the SCFs for live load shear and reaction increased as skew angle increased on both interior and exterior girders. For example, as shown in Figures 6.29 (a) for Bridge No. 6, the SCFs for live load reaction and shear on exterior girders increased by 32.4% and 16.5%, respectively, when the skew angle varied from 30° to 75°. Similarly, the corresponding increase of skew correction factors for reaction and shear on interior girders were 34.5% and 18.7%, respectively. Similar trends were observed in the other CIP multicell box-girder bridges. Therefore, the skew angle was treated as another important parameter in the proposed formulas for skew correction factors.



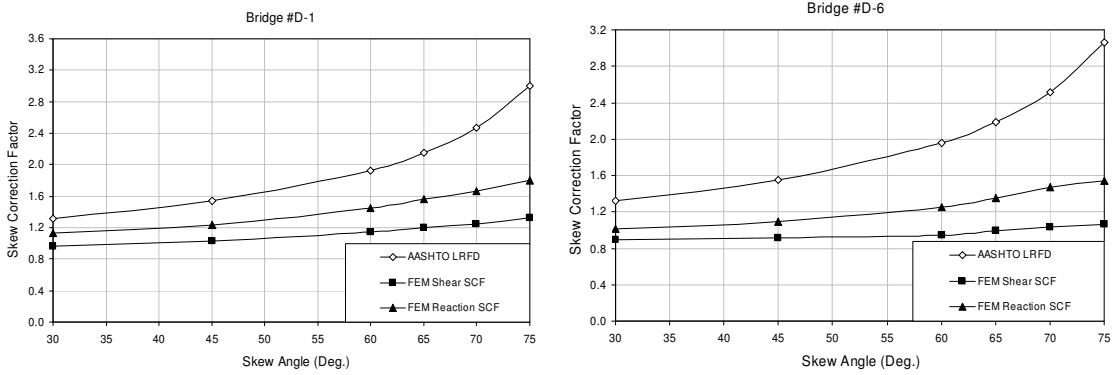
(a) Bridge #D-6

(b) Bridge #D-7

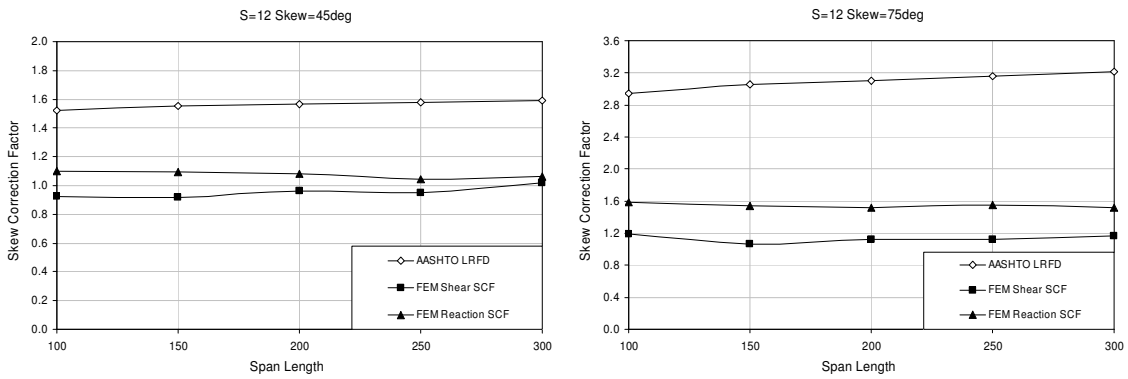
Figure 6.29 Precast Cellular Box Girder Bridges

6.4.4 Comparison of SCF from AASHTO LRFD to FEM SCF

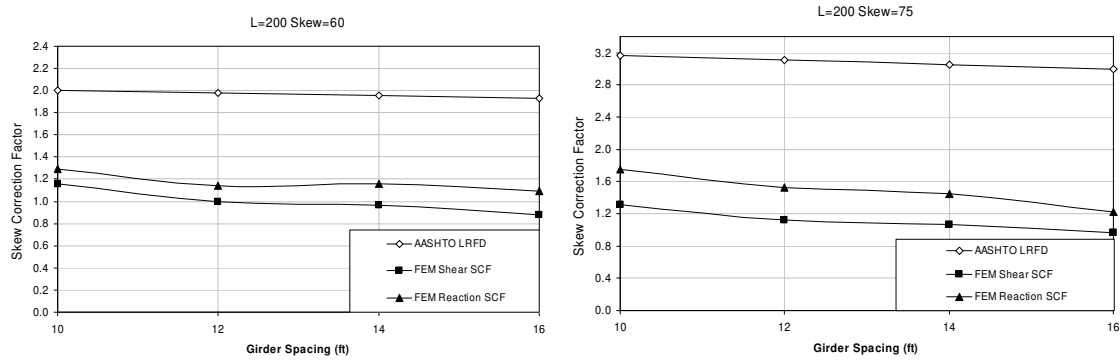
Similar to the previous types of bridges, the SCF equations specified in the AASHTO-LRFD were investigated to make sure that it is necessary to develop new SCF equations when the structural parameters are in excess of the range of applicability set in the AASHTO-LRFD SCF formulas. Skew correction factors calculated from finite element results were compared to those obtained from the LRFD equations.



(a) Bridge #D-1 (b) Bridge #D-6
Figure 6.30 Comparison of AASHTO LRFD Based SCF to FEM SCF- θ



(a) S=12, $\theta=45^\circ$ (b) S=12, $\theta=75^\circ$
Figure 6.31 Comparison of AASHTO LRFD Based SCF to FEM SCF-L



(a) $L=200$, $\theta=60^\circ$ (b) $L=200$, $\theta=75^\circ$
Figure 6.32 Comparison of AASHTO LRFD Based SCF to FEM SCF-S

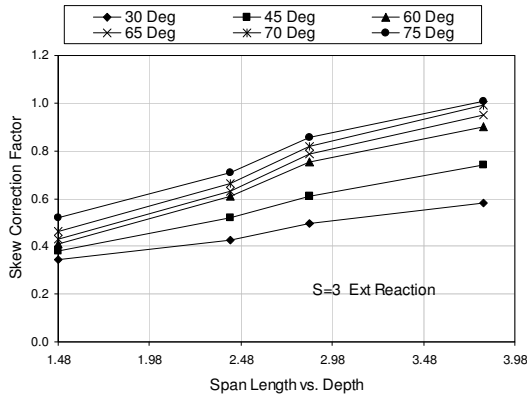
The precast concrete spread box girder bridges No.1 and No. 6 were randomly chosen to illustrate the results in Figure 6.30. Figures 6.31 and 6.32 present the comparison of finite element results to SCF obtained from AASHTO LRFD in term of span length (L) and girder spacing (S), respectively. Regardless of skew angle (θ), span length (L), or girder spacing (S), a large discrepancy existed between FEM results and SCF calculated from the AASHTO-LRFD. The comparisons shown in the figures demonstrated that the SCFs from the current LRFD Specifications did not correctly predict the SCFs for the shear and reaction distributions in the skew CIP multicell box-girder bridges with structural parameters outside the range of applicability. Similar trends were observed for the skew correction factor comparisons for shear and reaction distributions in the other CIP multicell box girder bridges. Therefore, it is necessary to develop the new skew correction equations for the bridges with structural parameters outside the limitations in the current specifications.

6.5 Precast Cellular Concrete Box Bridges

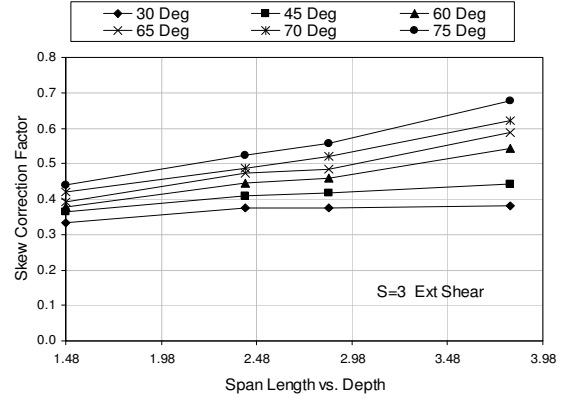
6.5.1 Effect of Span Length vs. Girder Height on SCF

Due to the SCF equation for precast cellular concrete box-girder bridges in the current AASHTO LRFD Specifications contains the term, L/d (Span length/girder depth). This term was kept in the proposed formulas. So the effect of L/d on SCF was investigated for this type of bridge. Figures 6.33 and 6.34 present the effect of span length vs. girder depth (L/d) on SCFs for live load reaction and shear distributions. The bridge with a width of 40 ft was randomly chosen to show the results. The skew angle varied from 30° to 75° .

The SCFs for live load shear and reaction increased as L/d increased. As shown in Figure 6.33, the SCFs for live load reaction and shear on exterior girders were increased by 48.5% and 35.3%, respectively, as L/d varied from 1.48 to 3.81 at the skew angle of 75° . The corresponding increases on interior girders were 22.4% and 23.9% for reaction and shear, respectively, which can be seen in Figure 6.34. The FEA results obtained from the other precast cellular concrete box-girder bridges in the database also showed the similar trend. Therefore, the effect of L/d on SCF for reaction and shear distributions is important and should be employed in the proposed formulas.

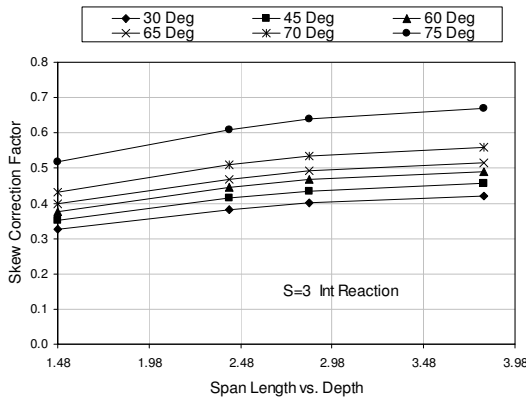


(a) Ext. Reaction

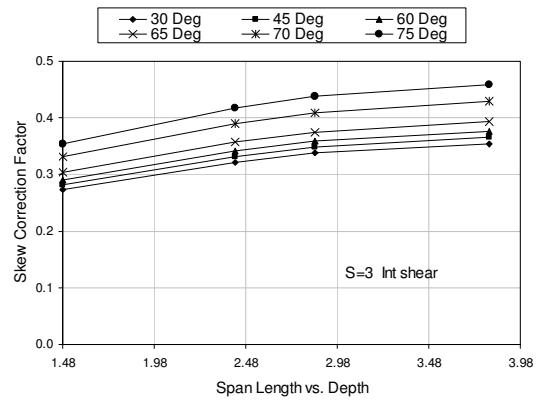


(b) Ext. Shear

Figure 6.33 SCF on Exterior Girders with Spacing of 3 ft



(a) Int. Reaction

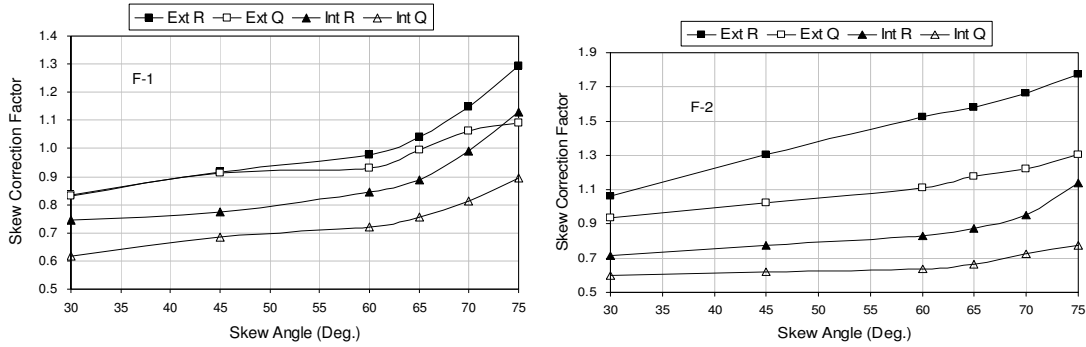


(b) Int. Shear

Figure 6.34 SCF on Interior Girders with Spacing of 3 ft

6.5.2 Effect of Skew Angle on SCF

The skew angle in precast cellular concrete box-girder bridges is another important factor considered in the proposed skew correction factor equations. Figure 6.35 presents the effect of skew angles on SCF for live load reaction and shear distributions with the skew angle ranging from 30° to 75° , for both exterior and interior girders. The No.1 and No.2 precast cellular concrete box-girder bridges were randomly chosen to show the results.



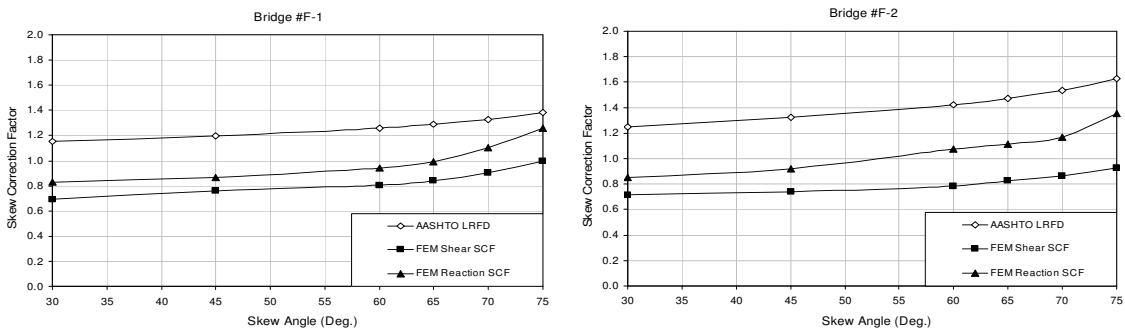
(a) Bridge #F-1

(b) Bridge #F-2

Figure 6.35 Effect of Skew Angle

As shown in Figure 6.35, the skew correction factors for live load shear and reaction increased as skew angle increased on both interior and exterior girders. For example, as shown in Figures 6.35 (a) for Bridge No.1, the skew correction factors for live load reaction and shear on exterior girders increased by 54.8% and 31.1%, respectively, when the skew angle varied from 30° to 75°. Similarly, the corresponding increases of skew correction factors for reaction and shear on interior girders were 51.7% and 44.6%, respectively. Similar trends were observed in the other precast cellular concrete box-girder bridges. Therefore, the skew angle was treated as another important parameter in the proposed formulas for skew correction factors.

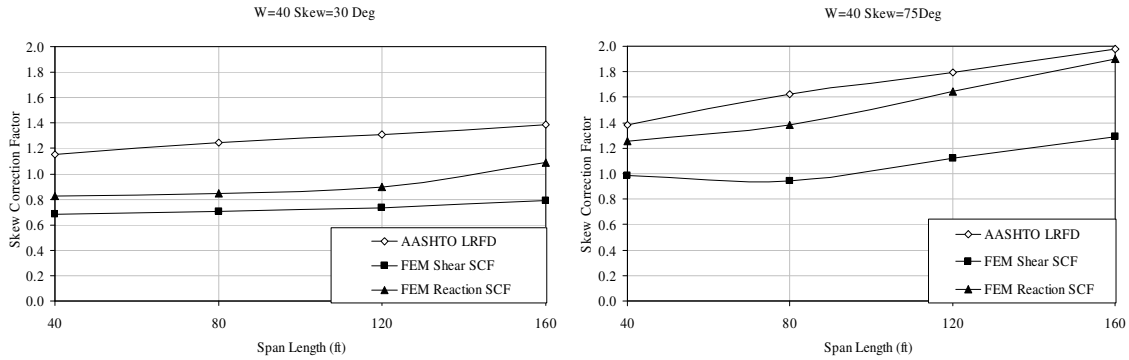
6.5.3 Comparison of SCF from AASHTO LRFD to FEM SCF



(a) Bridge #F-1

(b) Bridge #F-1

Figure 6.36 Comparison of AASHTO LRFD Based SCF to FEM SCF-0



(b) $W=40, \theta=30^\circ$

(b) $W=40, \theta=75^\circ$

Figure 6.37 Comparison of AASHTO LRFD Based SCF to FEM SCF-L

All precast cellular concrete box bridges in the database were investigated to show the differences between the SCFs resulting from the current AASHTO LRFD Specification and those from finite element analyses. The precast concrete spread box girder bridges No.1 and No. 2 were randomly selected to illustrate the results in Figure 6.36. For shear or reaction, the finite element results were different from those calculated using the current LRFD Specifications. Figures 6.37 present the comparison of finite element results to SCF from AASHTO LRFD in term of span length, L. All the comparisons shown in the figures demonstrated that the SCFs from the current LRFD Specifications cannot correctly predict the SCFs for the shear and reaction distributions in the skew precast cellular concrete box-girder bridges with structural parameters outside the range of applicability. Similar trends were observed for the skew correction factor comparisons for shear and reaction distributions in the other precast cellular concrete box bridges. Therefore, it is necessary to develop the new skew correction equations for the bridges with structural parameters outside the limitations in the current specifications.

CHAPTER 7

EQUATION DEVELOPMENT

7.1 Introduction

In 1993, the NCHRP developed new live load distribution factors in the NCHRP12-26 research based on the study by Zokaie et al. (1991). The first edition of the AASHTO LRFD Specifications (1994) was based on this study. The current AASHTO LRFD Specifications (2005) impose limitations in terms of range of applicability on its live load distribution factors of highway bridges. These limitations are specified in terms of bridge span, slab thickness, girder spacing, and longitudinal stiffness, which are also applied on the SCF equations. Even though NCHRP12-62 had already developed more simple unlimited distribution factor formulas for non-skewed bridges, the limitations on the SCF equations were kept fundamentally the same as the current LRFD specifications.

To eliminate the limitations on the range of applicability set in the current LRFD and NCHRP12-62, two sets of the unlimited equations for SCFs for shear distributions were developed, which were based on the finite element results and parametric studies for various types of bridges. One is based on NCHRP12-62, and the other is based on the AASHTO LRFD Specifications. In the meanwhile, the similar equations for SCFs for live load reaction distributions were also proposed to account for the differences between reaction and shear in the skewed bridges. Therefore, distribution factors for shear and reaction in the skewed bridges can be calculated with the proposed SCFs developed in

this dissertation in conjunction with the distribution factor equations for straight bridges specified in NCHRP12-62 or the AASHTO LRFD Specifications.

The SCFs for the shear distributions specified in the current AASHTO LRFD bridge design specifications were developed by a number of bridge analyses with different methods (i.e., grillage analysis, finite element analysis). These SCFs had already included the key structural parameters which affect the load distributions. Similarly, the proposed formulas in this dissertation contain the key parameters that affect the SCFs for both shears and reactions, according to the results of the parametric studies. The parameters for various types of bridges mainly include span length (L), girder space(S), girder height (d), and skew angle (θ).

For straight bridges, the process of calculating the reaction distribution factors follows the same procedure as that of obtaining the shear distribution factors in NCHRP12-62 or the AASHTO LRFD Specifications. After obtaining the distribution factors for straight bridges, the proposed SCFs for reaction distribution are used to account for the effect of the skew angle, which are unlimited on the ranges of applicability in practice. Therefore, the distribution factors for shear and reaction can be obtained without significant limitations on structural parameters by using the proposed SCF equations combined with the corresponding unlimited equations for straight bridges in NCHRP 12-62 or the AASHTO LRFD Specifications.

7.2 Methodology

To develop the formulas for SCFs for shear and reaction distributions in the skewed bridges, the key structural parameters were examined to investigate their effects on SCFs. The steps to develop the SCFs formulas for shear and reaction are as follows:

- It is assumed that the effect of each parameter can be modeled by an exponential function of the form ax^b , where 'x' is the value of the given parameter, and 'a' and 'b' are to be determined based on the variation of 'x'.
- It is assumed that the effects of different parameters are independent of each other, so that each parameter can be considered separately. The final skew correction factors are modeled by the polynomial formula of the following form:

$$SCF = 1 + (a)(L^{b_1})(S^{b_2})(d^{b_3})(\tan \theta)^{b_4}(\dots) \quad (7.1)$$

SCF is the skew correction factor, L, S, d, and θ are the parameters included in the formula, a is the scale factor, and b_1 , b_2 , b_3 , and b_4 are determined from the variation of L, S, d, and θ , respectively. Below is an example of how to develop the unknown scale factor and exponents in Equation 7.1. The distribution factor changes from SCF_1 to SCF_2 when S changes from S_1 to S_2 , but all the other bridge parameters remain unchanged:

$$SCF_1 = 1 + (a)(S_1^{b_1})(L^{b_2})(N_l^{b_3})(N_b^{b_4})(\dots) \quad (7.2)$$

$$SCF_2 = 1 + (a)(S_2^{b_1})(L^{b_2})(N_l^{b_3})(N_b^{b_4})(\dots) \quad (7.3)$$

Therefore:

$$\frac{SCF_1 - 1}{SCF_2 - 1} = \left(\frac{S_1}{S_2}\right)^{b_1} \quad (7.4)$$

Then:

$$b1 = \frac{\ln \frac{(SCF_1 - 1)}{(SCF_2 - 1)}}{\ln \frac{S_1}{S_2}} \quad (7.5)$$

If (n) different values of S are examined and successive pairs are used to determine the value of b1, then (n-1) different values for b1 can be obtained. If these b1 values are close to each other, an exponential curve may be used to accurately model the variation of the distribution factor with S. In that case the average of (n-1) values of b1 is used to achieve the best match. Once all the power factors are determined, the value of a can be obtained:

$$a = \frac{SCF_0 - 1}{[(L^{b1})(S^{b2})(d^{b3})(\tan(\theta)^{b4})(...)]} \quad (7.6)$$

In certain cases where an exponential function is not suitable to model the effect of a parameter, slight variation from this procedure is used to achieve the required accuracy. For example, the SCF for shear in Cast-in-Place, concrete, multi-cell, box bridges in AASHTO-LRFD is $1.0 + (0.25 + \frac{12.0L}{70d})\tan\theta$, so the proposed formulas for the SCFs for shear and reaction distributions employ the similar format.

7.3 Proposed Formulas for Skew Correction Factors

The SCFs for shear and reaction distributions in skewed bridges are developed and proposed in the following sections for various types of bridges. Evaluation of the proposed skew correction factor equations was achieved by statistical analyses.

The purpose of the statistical analyses was to determine the values of the parameters for a trend line that can best fit the set of plotted points. If the trend line is very close to the unity line, it indicates that the difference between the proposed skew correction factor and the rigorous analysis is reasonably small.

The ratios of the proposed skew correction factors to the rigorous finite element results were calculated and examined in order to assess the accuracy of the developed formula. The average, standard deviation, and coefficient of variation of the ratios were obtained for each formula.

- **Average, standard deviation, & coefficient of variation**

The average values (AVE.) of the ratios (formulas/rigorous) for SCFs always remain 1.0 or slightly higher than 1.0, which standing for the average proposed skew factors are almost equal to or slightly higher than the average rigorous skew correction factors.

The standard deviation (SD) is the most common measure of statistical dispersion, measuring how widely the values are spread in a data set. If many data points are close to the mean, the standard deviation is small; if many data points are far from the mean, the standard deviation is large. If all data values are equal, the standard deviation is zero. A useful property of standard deviation is that, unlike variance, it is expressed in the same units as the data.

The coefficient of variation (CoV) is a normalized measure of dispersion of a probability distribution. It is defined as the ratio of the standard deviation to the mean. The coefficient of variation is a dimensionless number.

- **Coefficient of determination**

The coefficient of determination, R^2 , was determined in the regression analysis. The R^2 factor gives the proportion of the variance (fluctuation) of one variable that is predictable from the other variable. It is a measure that can be used to determine how certain one can be in making predictions from a certain graph. The coefficient of determination represents the percent of the data that is the closest to the line of best fit. Thus, a high R^2 means a low variety of the data.

The procedures to obtain SCFs for reaction and shear distributions are listed below:

(1) To obtain the distribution factors for live load shear in the girders of straight bridges with the unlimited equations presented in NCHRP 12-62 or the assumed unlimited equations specified in the AASHTO LRFD Specifications;

(2) To adjust the values in step (1) with the proposed SCFs for shear distributions in order to account for the effect of skew. The values obtained are the distribution factors for shear in the girders of the skewed bridges.

(3) To calibrate the values calculated in step (1) with the proposed SCFs for reaction distributions in order to account for the difference between shear and reaction. The resulting values are the distribution factors for reaction in the skewed bridges.

As mentioned earlier, the SCF is defined as the ratio of the shear or reaction distribution factors for a given skewed bridge (DF_{skew}) to that for a non-skewed bridge (DF_{str}) (i.e., $SCF = DF_{skew}/DF_{str}$). The DF_{skew} herein is obtained using FEA. If DF_{str} is calculated from the unlimited formulas proposed in NCHRP12-62, the corresponding proposed SCF formulas are named as “NCHRP12-62 Based Equation.” Otherwise, if

DF_{str} is calculated from the assumed unlimited formulas specified in the current AASHTO-LRFD Specifications, the corresponding proposed SCF formulas are named as “AASHTO LRFD Based Equation.”

Based on the extensive data generated from the finite element analyses and the parametric studies, the SCFs equations for shear and reaction distributions were proposed for various types of skewed bridges, respectively. For each bridge type, the SCF equations for shear and reaction distributions based on NCHRP12-62 were presented, followed by those based on the AASHTO LRFD Specifications. The proposed formulas consist of the following key structural parameters: span length (L) in feet, girder space (S) in feet, girder height (d) in inches, and skew angle (θ) in degrees. After that, the statistical properties of the presented equations, such as AV, SD, CoV, and R^2 , were investigated. Finally, the comparisons of the proposed equations to the finite element results were used to validate the proposed equations.

7.3.1 Steel I Girder Bridges

7.3.1.1 NCHRP 12-62 based equations. Skew Correction Factors for Shear (SCF_V) and reaction (SCF_R) are given in Equations 7.7 and 7.8, respectively.

$$SCF_V = 1 + 0.2 \times (\tan \theta)^{0.7} \times \frac{12}{S^{1.05}} \times \frac{L}{400} \quad (7.7)$$

$$SCF_R = 1 + 2.4 \times \frac{\tan \theta}{S^{0.95}} \quad (7.8)$$

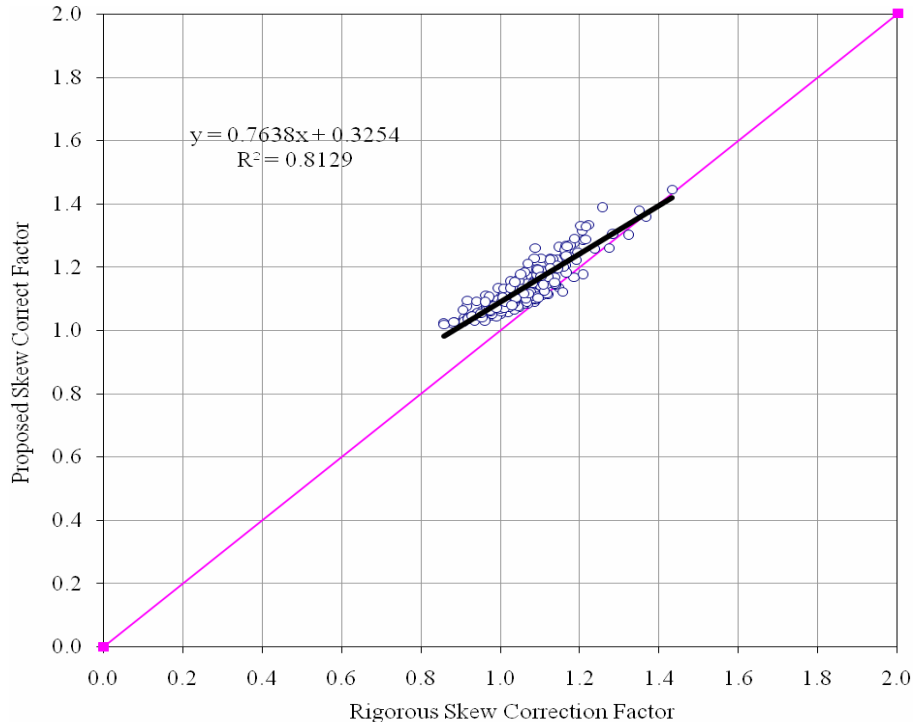


Figure 7.1 Proposed NCHRP 12-62 based SCF vs. Rigorous SCF for Shear in Steel I-girder Bridges

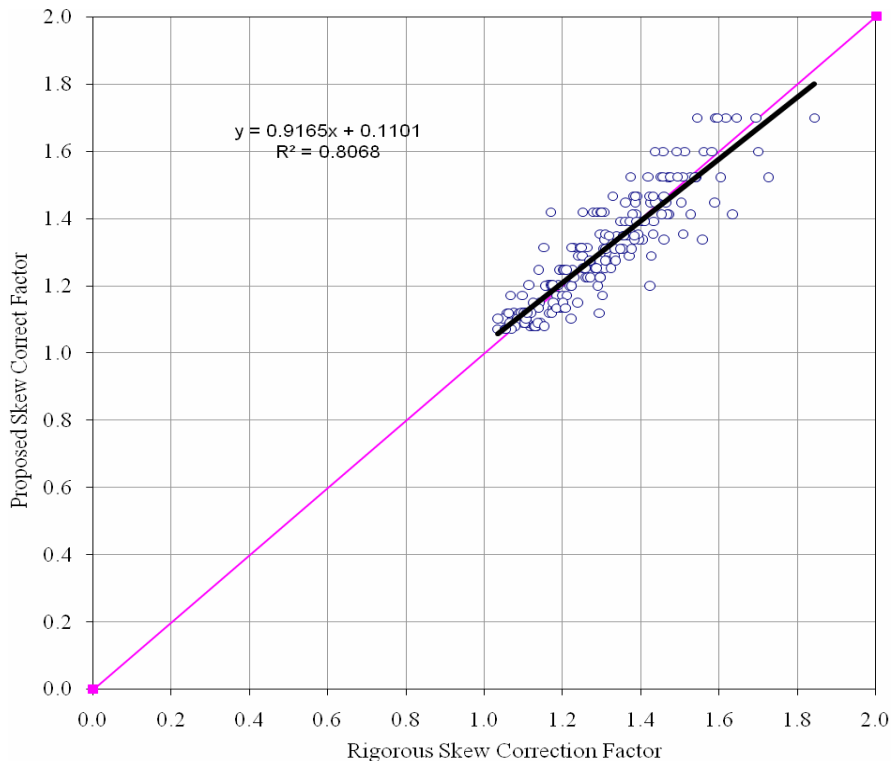


Figure 7.2 Proposed NCHRP 12-62 based SCF vs. Rigorous SCF for Reaction in Steel I-girder Bridges

7.3.1.2 AASHTO LRFD based equations. Skew Correction Factors for Shear

(SCF_V) and reaction (SCF_R) are given in Equations 7.9 and 7.10, respectively.

$$SCF_V = 1 + 0.2 \times (\tan \theta)^{0.8} \times \frac{12}{S^{0.9}} \times \left(\frac{L}{400}\right)^{0.8} \quad (7.9)$$

$$SCF_R = 1 + 0.16 \times (\tan \theta)^{0.4} \times \frac{12}{S^{0.5}} \times \left(\frac{L}{400}\right)^{0.1} \quad (7.10)$$

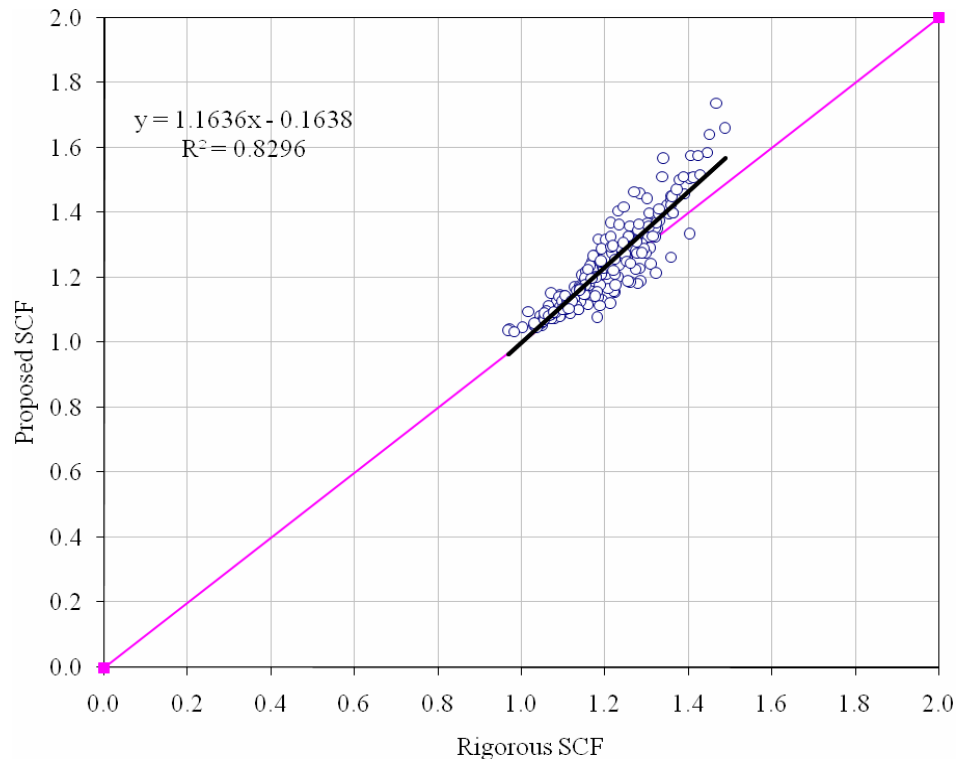


Figure 7.3 Proposed AASHTO LRFD Based SCF vs. Rigorous SCF for Shear in Steel I-girder Bridges

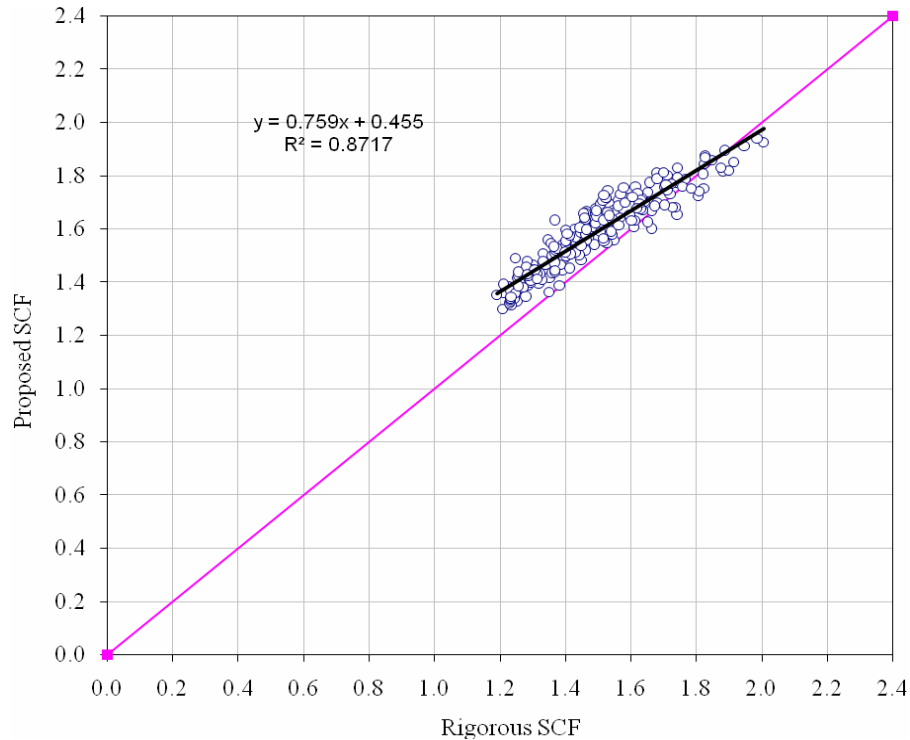


Figure 7.4 Proposed AASHTO LRFD Based SCF vs. Rigorous SCF for Reaction in Steel I-girder Bridges

As shown in Figures 7.1 through 7.4, the regression analyses were used to evaluate the formulas of SCFs for shear and reaction distributions presented in Equations 7.7 through 7.10, based on NCHRP12-62 or the AASHTO-LRFD Specifications. The thinner diagonal line on the graph indicates that the SCFs calculated from the proposed formulas are equal to those obtained from the rigorous analysis results. The plotted points on the graphs show the values from the proposed skew correction formulas versus their counterparts from the FEA results. The thicker line on the graph is the regression trend line of the plotted points obtained through regression analysis. The coefficients of determination, R^2 , range from 0.8068 to 0.8717 for the SCF equations for shear and reaction distributions based on NCHRP12-62 and the AASHTO LRFD Specifications, respectively. This range is acceptable.

Table 7.1 Comparative Statistics of SCFs for Steel I-girder Bridges

		AVE	SD	COV
NCHRP12-62	Shear	1.074	0.044	0.041
Based Equation	Reaction	1.003	0.054	0.054
AASHTO LRFD	Shear	1.026	0.047	0.045
Based Equation	Reaction	1.070	0.049	0.046

Table 7.1 summarizes the statistical results for AVE, SD, and COV. The AVEs show the slightly-greater-than unity averages, which means that the proposed expressions can yield slightly conservative SCFs for the design of skewed, steel I girder bridges. The values of the SDs and COVs for each proposed equations were considered low, which indicates that these proposed SCFs equations are good representations of FEM results without significant variance.

7.3.1.3 Proposed equations validation. Figures 7.5 and 7.6 present the comparison of SCFs obtained from the proposed formulas to SCFs from the finite element results for shear and reaction, respectively. The 23rd steel I girder bridge was randomly selected to represent the typical results. Thereafter, the conclusion can be drawn that the proposed SCF formulas are in fair to good agreement for all the finite element results with a reasonably small percentage of errors.

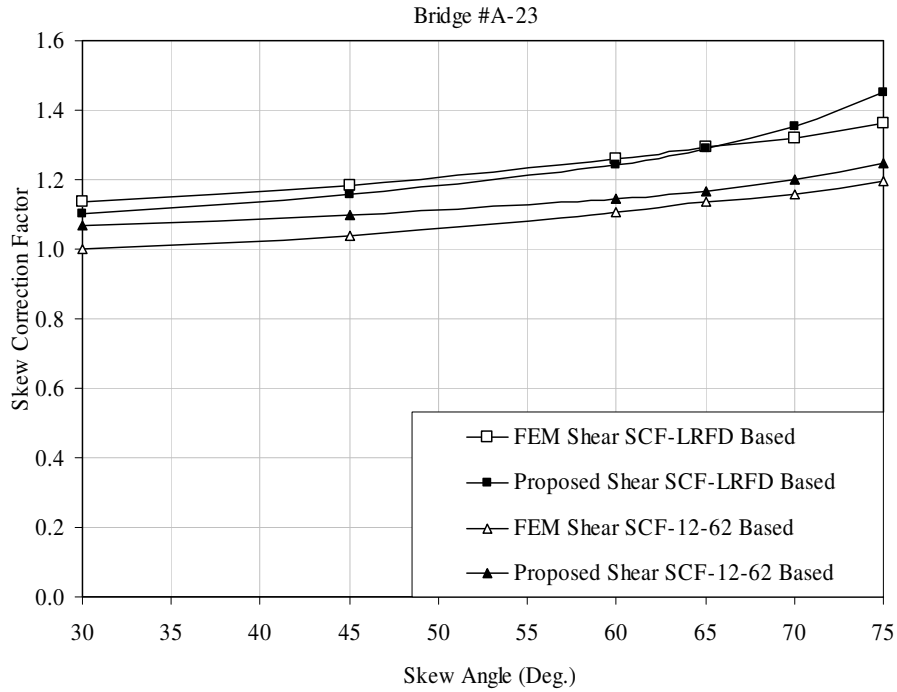


Figure 7.5 Proposed SCF vs. FEM SCF for Shear in Steel I-girder Bridges

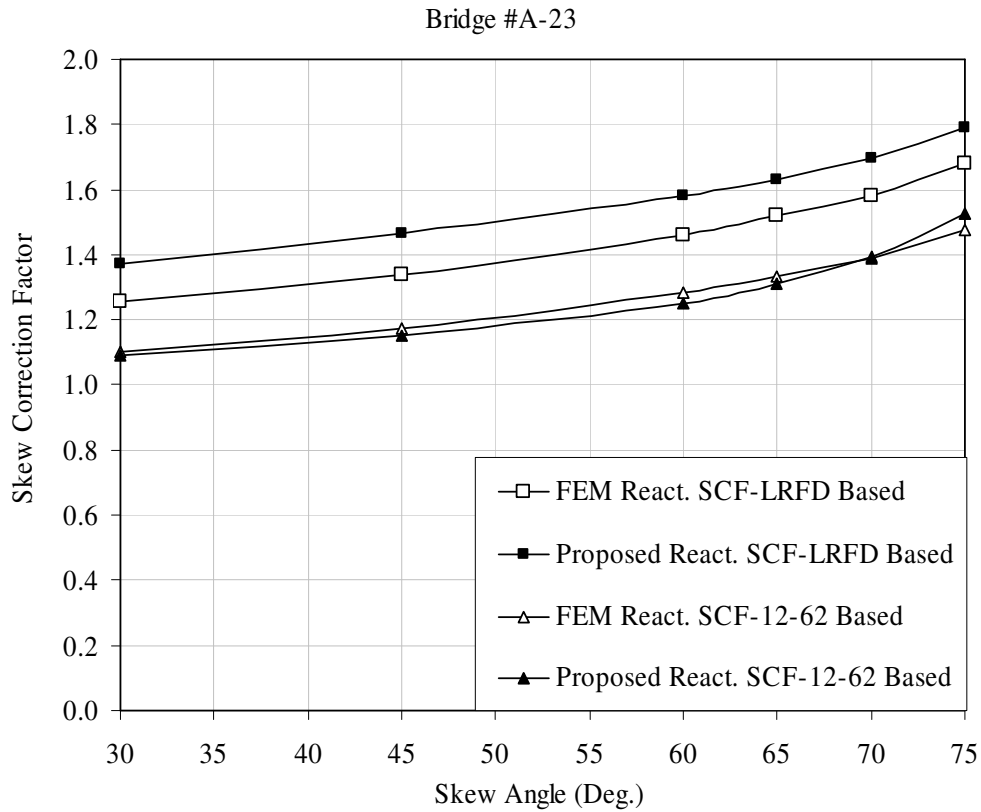


Figure 7.6 Proposed SCF vs. FEM SCF for Reaction in Steel I-girder Bridges

7.3.2 Precast Concrete I Girder Bridges

7.3.2.1 NCHRP 12-62 based equations. Skew Correction Factors for Shear

(SCF_V) and reaction (SCF_R) are given in Equations 7.11 and 7.12, respectively.

$$SCF_V = 1 + 0.15 \times (\tan \theta)^{0.5} \times \frac{12}{S} \times \left(\frac{L}{50}\right)^{0.5} \quad (7.11)$$

$$SCF_R = 1 + 0.2 \times (\tan \theta)^{0.5} \times \frac{12}{S} \times \left(\frac{L}{40}\right)^{0.7} \quad (7.12)$$

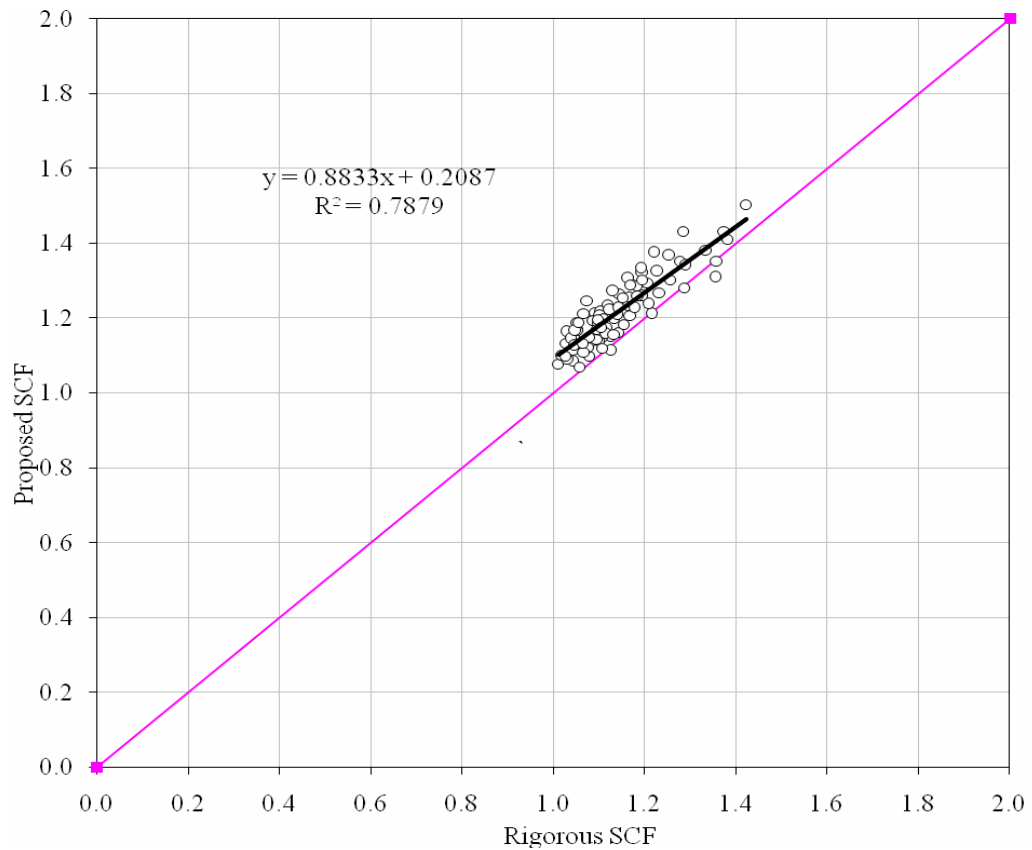


Figure 7.7 Proposed NCHRP 12-62 based SCF vs. Rigorous SCF for Shear in Precast Concrete I-girder Bridges

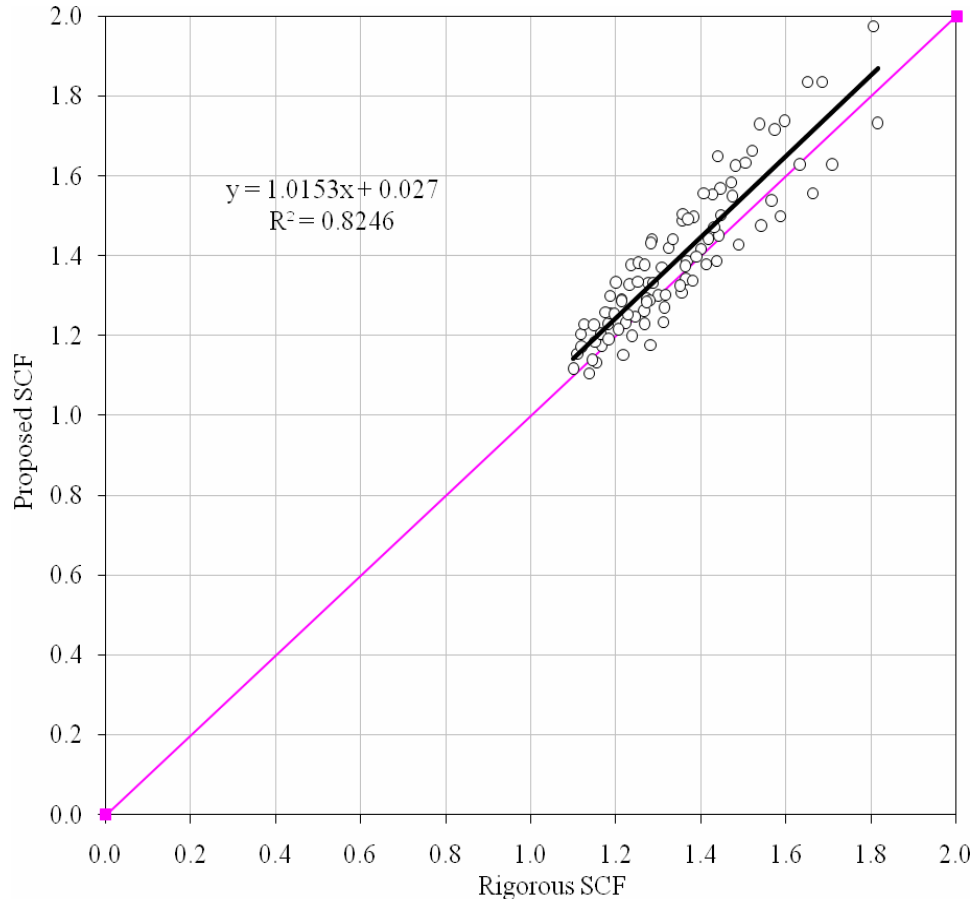


Figure 7.8 Proposed NCHRP 12-62 based SCF vs. Rigorous SCF for Reaction in Precast Concrete I-girder Bridges

7.3.2.2 AASHTO LRFD based equations. Skew Correction Factors for Shear

(SCF_V) and reaction (SCF_R) are given in Equations 7.13 and 7.14, respectively.

$$SCF_V = 1 + 0.1 \times (\tan \theta)^{0.5} \times \frac{12}{S} \times \left(\frac{L}{50}\right)^{0.75} \quad (7.13)$$

$$SCF_R = 1 + 0.25 \times (\tan \theta)^{0.5} \times \frac{12}{S} \times \left(\frac{L}{40}\right)^{0.5} \quad (7.14)$$

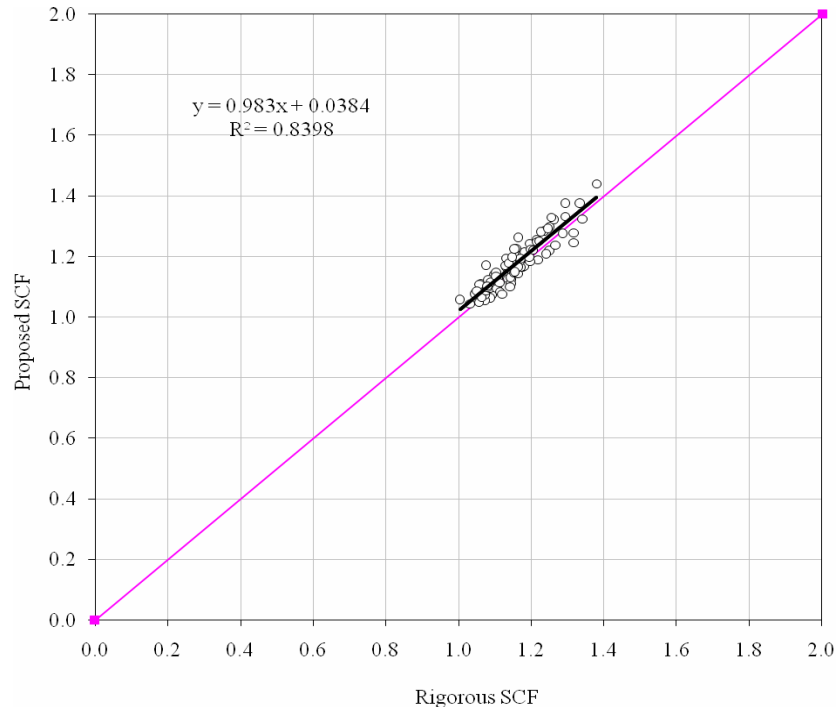


Figure 7.9 Proposed AASHTO LRFD SCF vs. Rigorous SCF for Shear in Precast Concrete I-girder Bridges

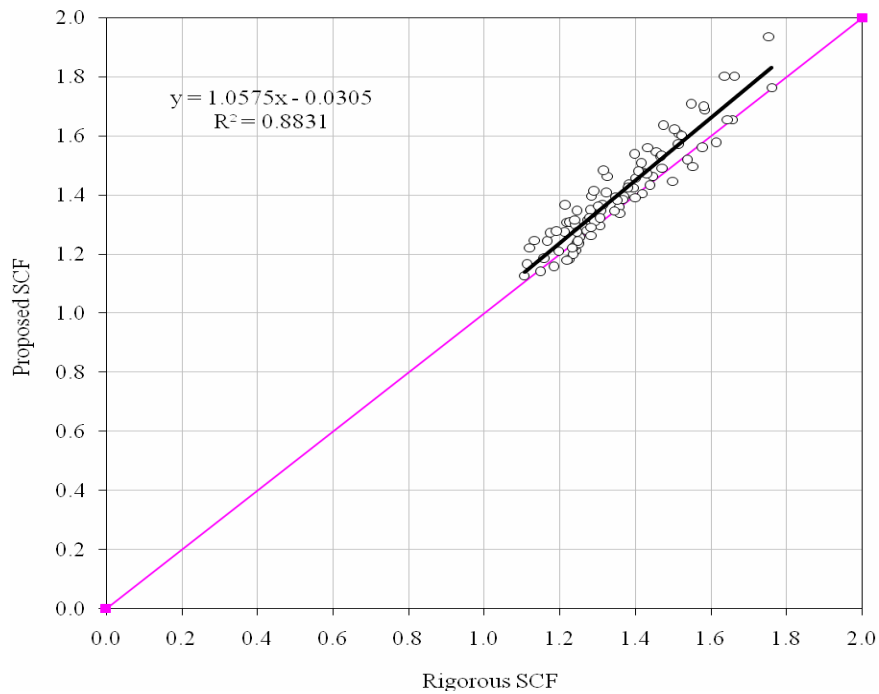


Figure 7.10 Proposed AASHTO LRFD SCF vs. Rigorous SCF for Reaction in Precast Concrete I-girder Bridges

Table 7.2 Comparative Statistics of SCFs for Precast Concrete I-girder Bridges

		Average	SD	COV
NCHRP12-62	Shear	1.067	0.039	0.036
Based Equation	Reaction	1.036	0.055	0.053
AASHTO LRFD	Shear	1.016	0.029	0.028
Based Equation	Reaction	1.035	0.042	0.041

The regression analyses presented in Figures 7.7 through 7.10 were used to evaluate the SCFs for shear and reaction distributions for precast concrete, I-girder bridges. The coefficients of determination in the figures, R^2 , range from 0.7879 to 0.8831, which means a low variety of the data and is acceptable.

Table 7.2 presents the statistical results for AVE, SD, and COV for precast concrete I-girder bridges. The slightly-greater-than unity average in the regression studies shows that the expressions in Equations 7.11 and 7.14 can be used conservatively in the prediction of SCFs for both shear and reaction in the precast concrete, I-girder bridges. For each proposed equation, the SDs and COVs listed in Table 7.2 were considered low enough to confirm that the proposed equations can be used to predict the SCFs with low variety.

7.3.2.3 Proposed equations validation. Figures 7.11 and 7.12 present the comparison of the SCFs calculated from the proposed formulas to those obtained from the FEA results. The 9th precast concrete, I girder bridge was randomly selected to represent the typical results. The figures show that the proposed equations match the finite element results very well.

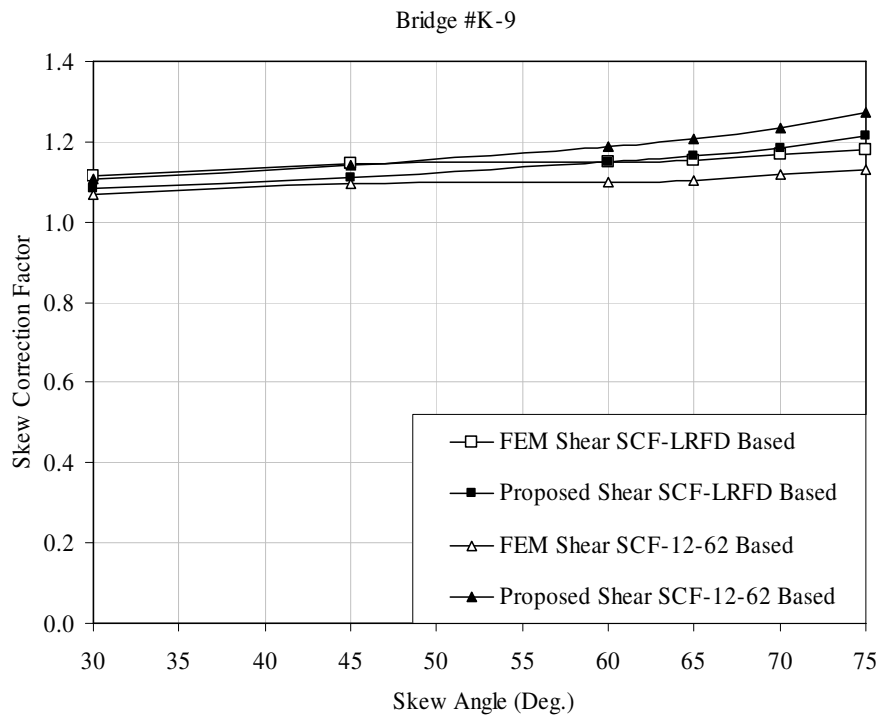


Figure 7.11 Proposed SCF vs. FEM SCF for Shear in Precast Concrete I-girder Bridges

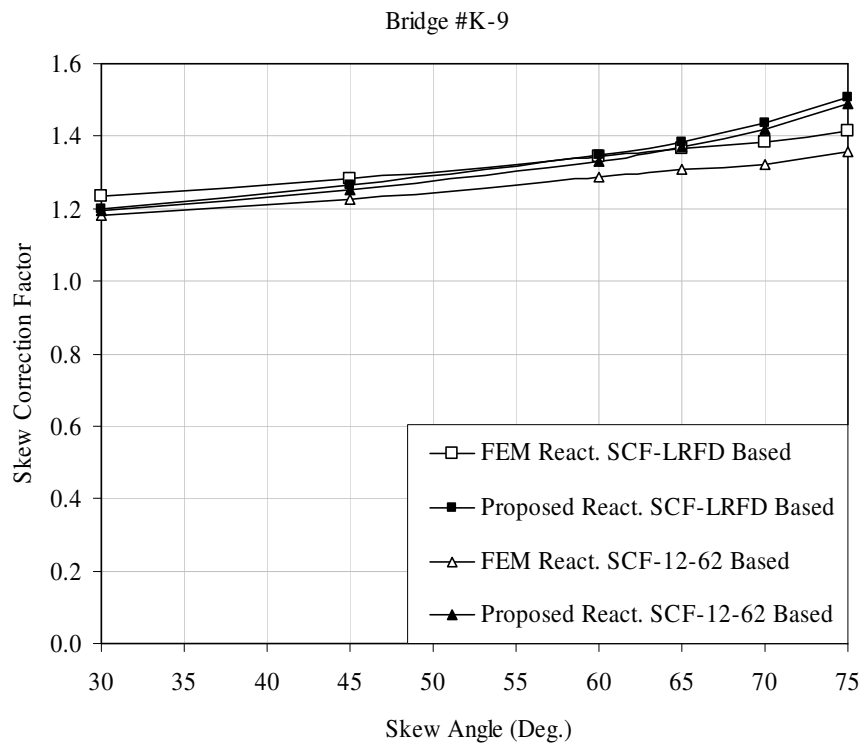


Figure 7.12 Proposed SCF vs. FEM SCF for Reaction in Precast Concrete I-girder Bridges

7.3.3 Precast Concrete Box Girder Bridges

7.3.3.1 NCHRP 12-62 based equations. Skew Correction Factors for Shear

(SCF_V) and reaction (SCF_R) are given in Equations 7.15 and 7.16, respectively.

$$SCF_V = 1 + \left(\frac{L}{4}\right)^{0.1} \times d^{0.65} \times \frac{1}{3.5 \cdot S^{1.1}} \times (\tan \theta)^{0.35} \quad (7.15)$$

$$SCF_R = 1 + \frac{1}{2.5} \cdot \sqrt{\frac{L \cdot d}{12}} \times \frac{1}{S^{1.05}} \times (\tan \theta)^{0.35} \quad (7.16)$$

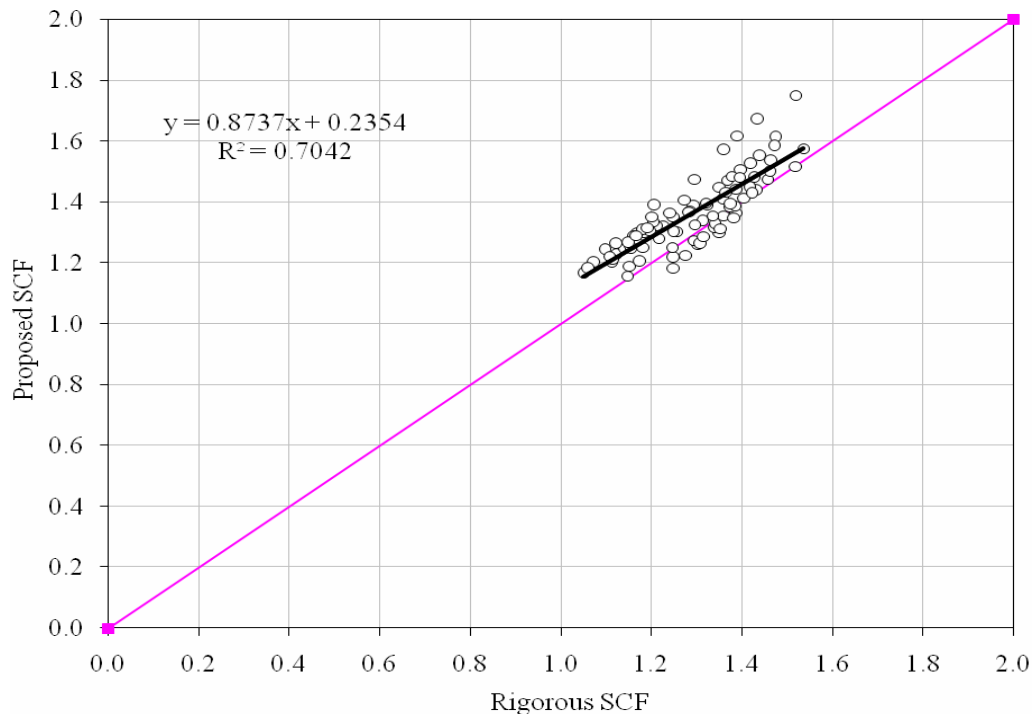


Figure 7.13 Proposed NCHRP 12-62 based SCF vs. Rigorous SCF for Shear in Precast Concrete Box-girder Bridges

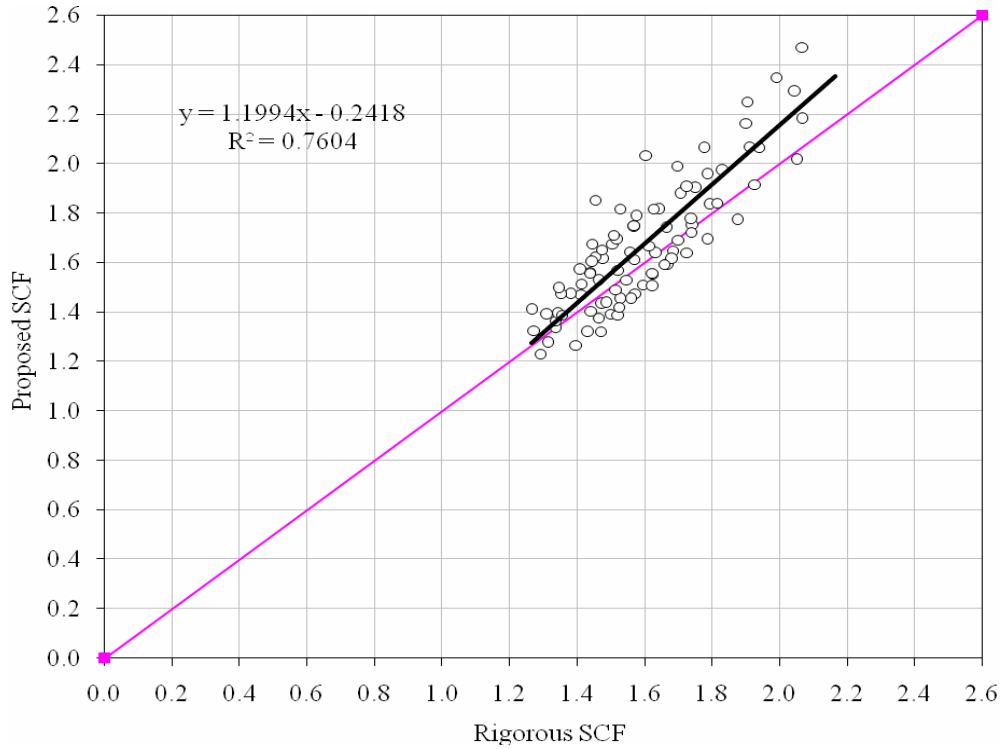


Figure 7.14 Proposed NCHRP 12-62 based SCF vs. Rigorous SCF for Reaction in Precast Concrete Box-girder Bridges

7.3.3.2 AASHTO LRFD based equations. Skew Correction Factors for Shear

(SCF_V) and reaction (SCF_R) are given in Equations 7.17 and 7.18, respectively.

$$SCF_V = 1 + \left(\frac{L}{12}\right)^{0.4} \times d^{0.6} \times \frac{1}{6 \cdot S^{1.2}} \times (\tan \theta)^{0.3} \quad (7.17)$$

$$SCF_R = 1 + \frac{1}{2.5} \cdot \sqrt{\frac{L \cdot d}{12}} \times \frac{1}{S^{1.15}} \times (\tan \theta)^{0.3} \quad (7.18)$$

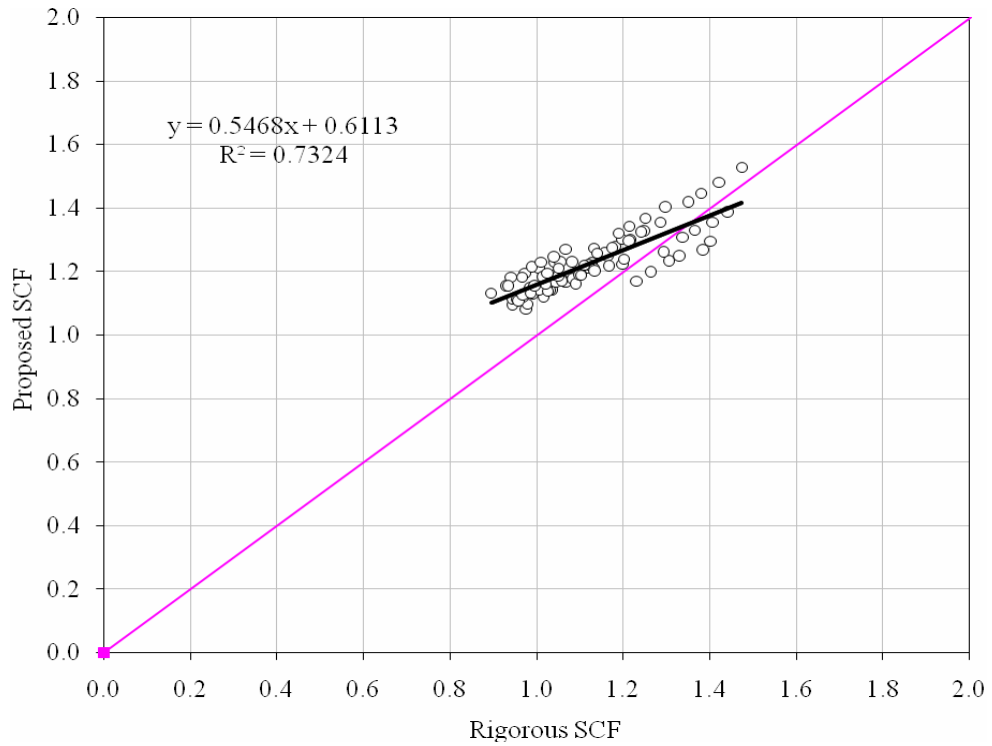


Figure 7.15 Proposed AASHTO LRFD SCF vs. Rigorous SCF for Shear in Precast Concrete Box-girder Bridges

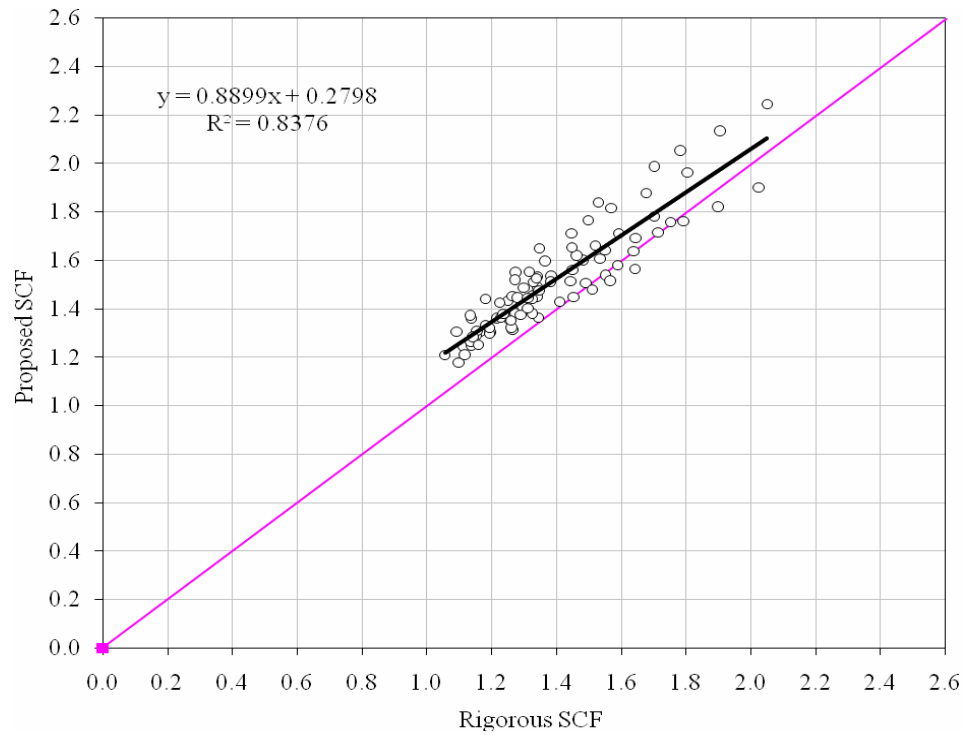


Figure 7.16 Proposed AASHTO LRFD SCF vs. Rigorous SCF for Reaction in Precast Concrete Box-girder Bridges

Table 7.3 Comparative Statistics of SCFs for Precast Concrete Box-girder Bridges

		Average	SD	COV
NCHRP12-62	Shear	1.058	0.054	0.051
Based Equation	Reaction	1.046	0.086	0.083
AASHTO LRFD	Shear	1.101	0.077	0.070
Based Equation	Reaction	1.096	0.065	0.060

For shear and reaction distributions, Equations 7.15 through 7.18 present the SCFs for precast concrete, box girder bridges based on NCHRP12-62 or the AASHTO-LRFD Specifications, respectively, which were validated by the regression analyses shown in Figures 7.13 through 7.16. The coefficient of determination, R^2 , ranges from 0.7042 to 0.8376, which indicates a lower variety of data.

Table 7.3 lists the statistical results for AVE, SD, and COV for precast concrete, box girder bridges. The slightly-greater-than unity averages show that the above equations can be used conservatively in the prediction of SCFs for both shear and reaction in the precast concrete, box girder bridges. The low COV of the proposed SCF to the rigorous analysis data for the skew correction factor for shear and reaction varied from 0.051 to 0.083, which means a low variety and is acceptable.

7.3.3.3 Proposed equations validation. Figures 7.17 and 7.18 present the comparison of SCFs calculated from the proposed formulas to those obtained from the finite element results. The 6th precast concrete box-girder bridge was randomly selected to represent the typical results. As shown in the figures, the proposed equations produce a SCF comparable to the FEM.

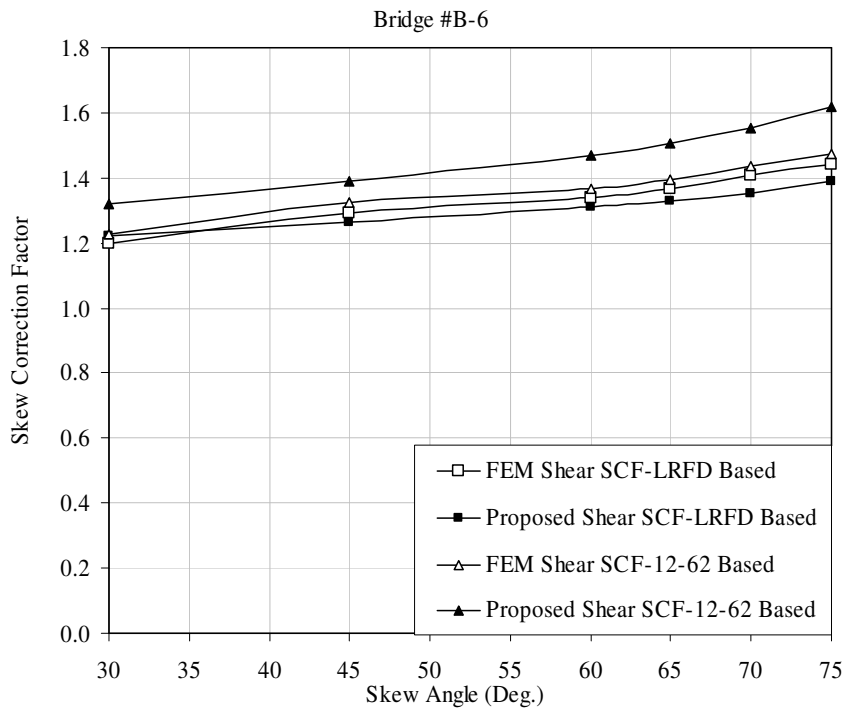


Figure 7.17 Proposed SCF vs. FEM SCF for Shear in Precast Concrete Box-girder Bridges

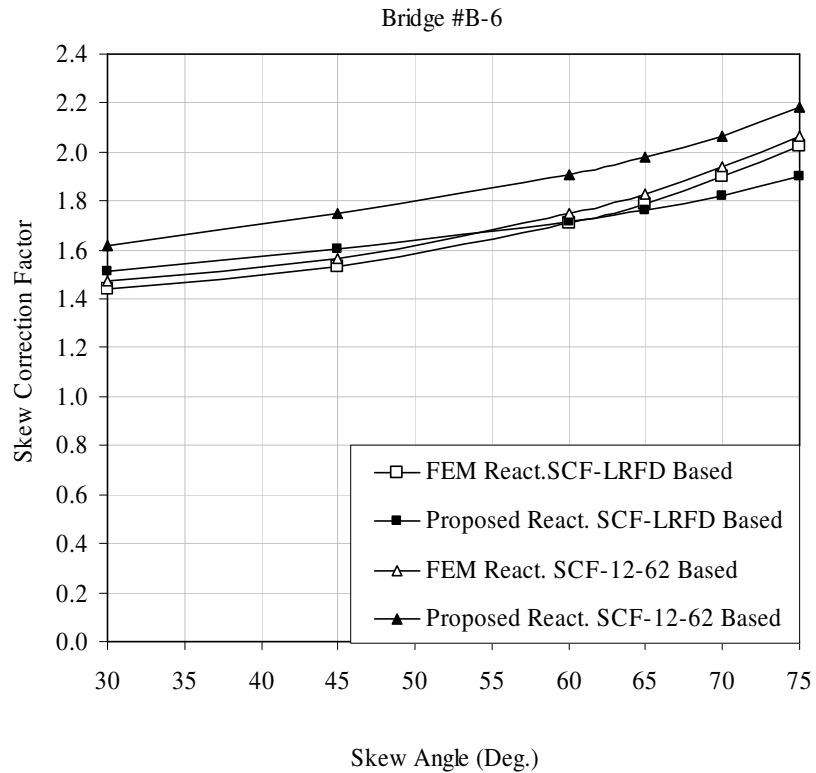


Figure 7.18 Proposed SCF vs. FEM SCF for Shear in Precast Concrete Box-girder Bridges

7.3.4 CIP Concrete Multicell Box Girder Bridges

7.3.4.1 NCHRP 12-62 based equations. Skew Correction Factors for Shear

(SCF_V) and reaction (SCF_R) are given in Equations 7.19 and 7.20, respectively.

$$SCF_V = 1 + \left(0.25 + \frac{12 \cdot L^3}{50 \cdot d^3}\right) \times (\tan \theta)^{1.0} \times \frac{1}{S^{1.2}} \quad (7.19)$$

$$SCF_R = 1 + \left(0.15 + \frac{12 \cdot L}{50 \cdot d}\right) \times (\tan \theta) \times \frac{1}{S^{0.4}} \quad (7.20)$$

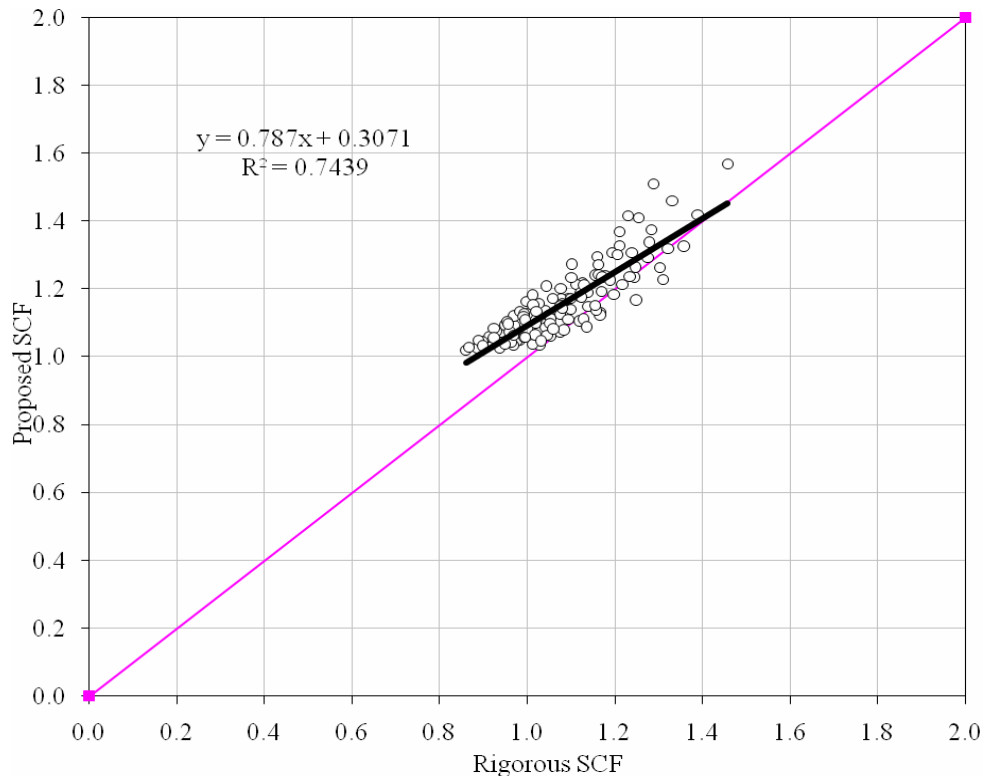


Figure 7.19 Proposed NCHRP 12-62 based SCF vs. Rigorous SCF for Shear in CIP Concrete Multi-cell Box-girder Bridges

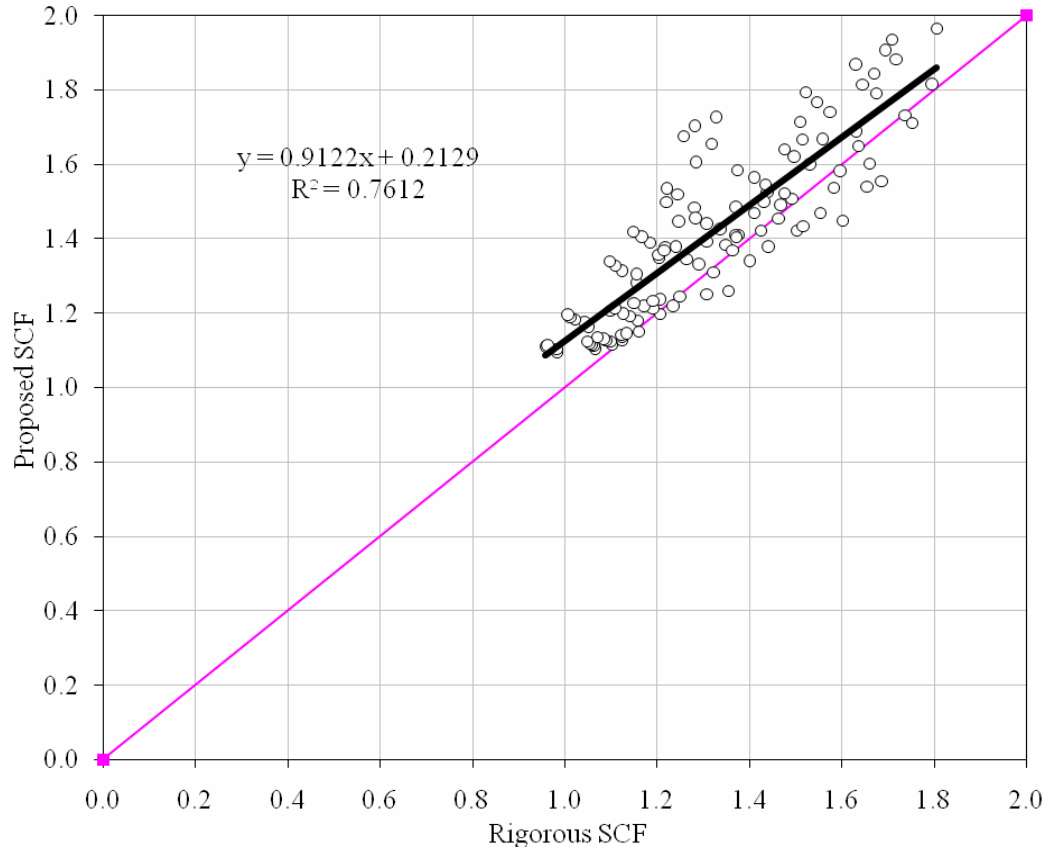


Figure 7.20 Proposed NCHRP 12-62 based SCF vs. Rigorous SCF for Reaction in CIP Concrete Multi-cell Box-girder Bridges

7.3.4.2 AASHTO LRFD based equations. Skew Correction Factors for Shear

(SCF_V) and reaction (SCF_R) are given in Equations 7.21 and 7.22, respectively.

$$SCF_V = 1 + \left(0.15 + \frac{12 \cdot L^2}{140 \cdot d^2}\right) \times (\tan \theta)^{0.6} \times \frac{1}{S^{0.6}} \quad (7.21)$$

$$SCF_R = 1 + \left(0.15 + \frac{12 \cdot L}{30 \cdot d}\right) \times (\tan \theta)^{0.6} \times \frac{1}{S^{0.4}} \quad (7.22)$$

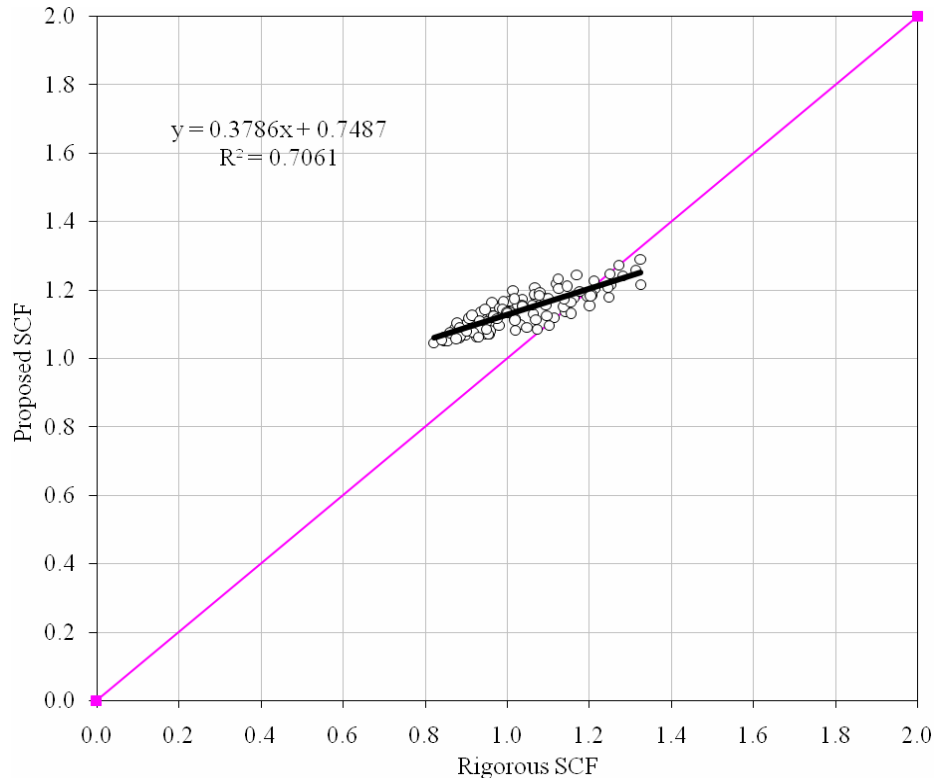


Figure 7.21 Proposed AASHTO LRFD SCF vs. Rigorous SCF for Shear in CIP Concrete Multi-cell Box-girder Bridges

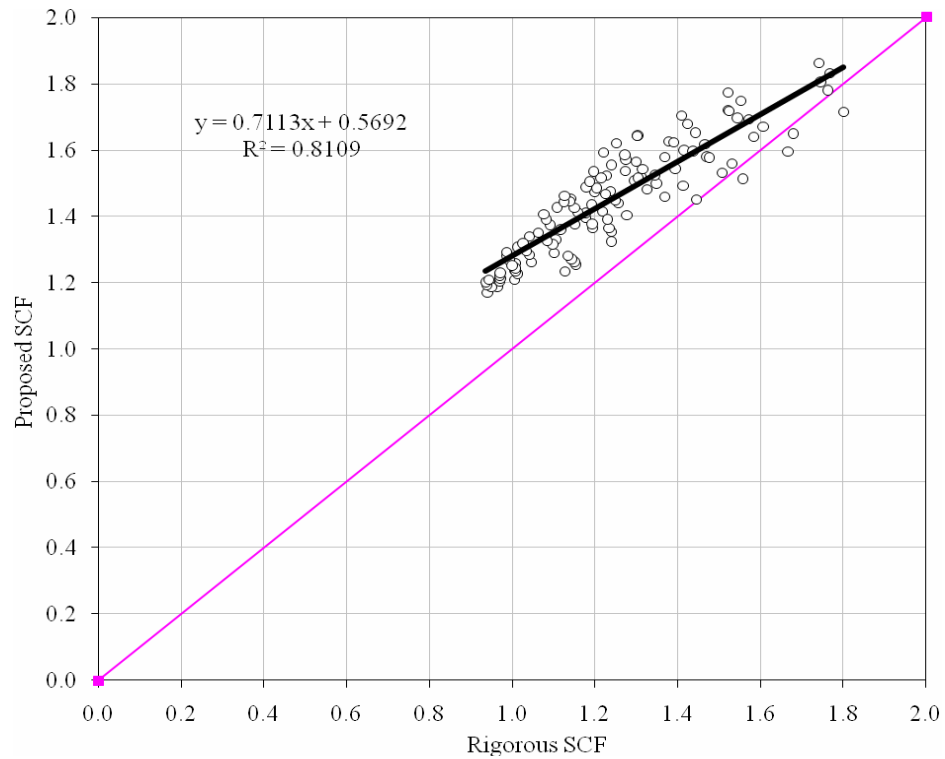


Figure 7.22 Proposed AASHTO LRFD SCF vs. Rigorous SCF for Reaction in CIP Concrete Multi-cell Box-girder Bridges

Table 7.4 Comparative Statistics of SCFs for CIP Concrete Multi-Cell Box Girder Bridges

		Average	SD	COV
NCHRP12-62 Based Equation	Shear	1.074	0.061	0.057
	Reaction	1.078	0.088	0.081
AASHTO LRFD Based Equation	Shear	1.121	0.087	0.078
	Reaction	1.180	0.089	0.076

The regression analyses for CIP concrete, multi-cell, box girder bridges were used to evaluate the SCFs for shear and reaction, respectively, proposed in Equations 7.19 through 7.22. The coefficient of determination, R^2 , ranges from 0.7061 to 0.8109, which means lower variety of the data.

Table 7.4 presents the statistical results for AVE, SD, and COV for CIP concrete multi-cell box-girder bridges. The slightly-greater-than unity average shows that the above formulas can be used conservatively in the prediction of the skew correction factors for both shear and reaction in the CIP concrete, multi-cell, box girder bridges. The SD, ranging from 0.061 to 0.089, and the COV, ranging from 0.057 to 0.081, are excellent and indicate that the proposed equations can be used conservatively and economically in the design of skewed CIP concrete, multi-cell, box-girder bridges.

7.3.4.3 Proposed equations validation. Figures 7.23 and 7.24 present the comparison of the SCFs obtained from the proposed formulas to those from the FEA results. The 19th CIP concrete, multi-cell, box-girder bridge was randomly selected to represent the typical results. The figures show that the proposed equations fairly match the finite element results.

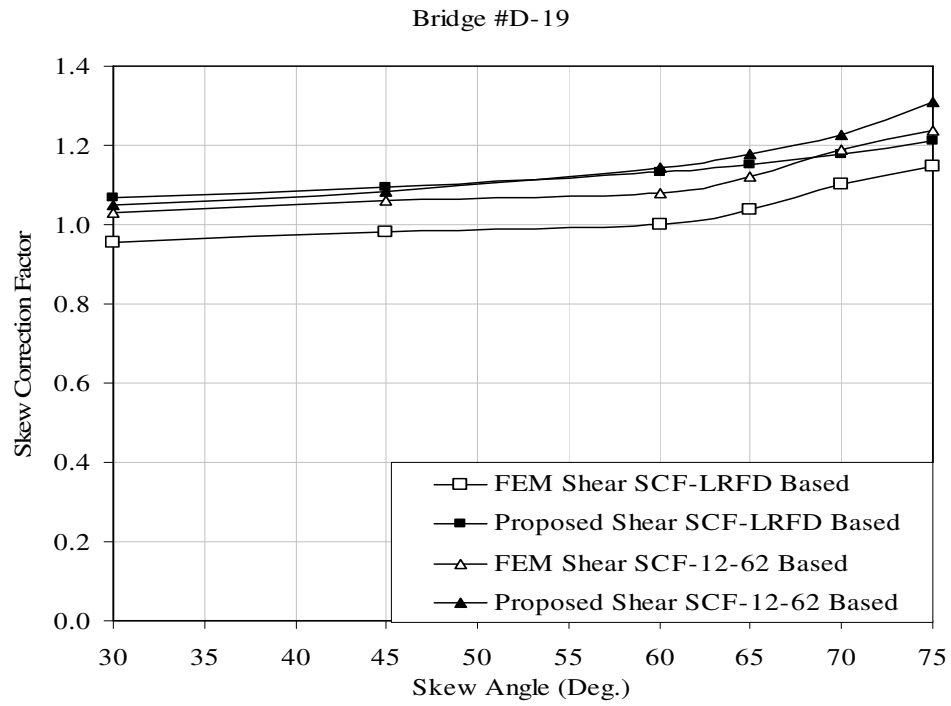


Figure 7.23 Proposed SCF vs. FEM SCF for Shear in CIP Concrete Multi-cell Box-girder Bridges

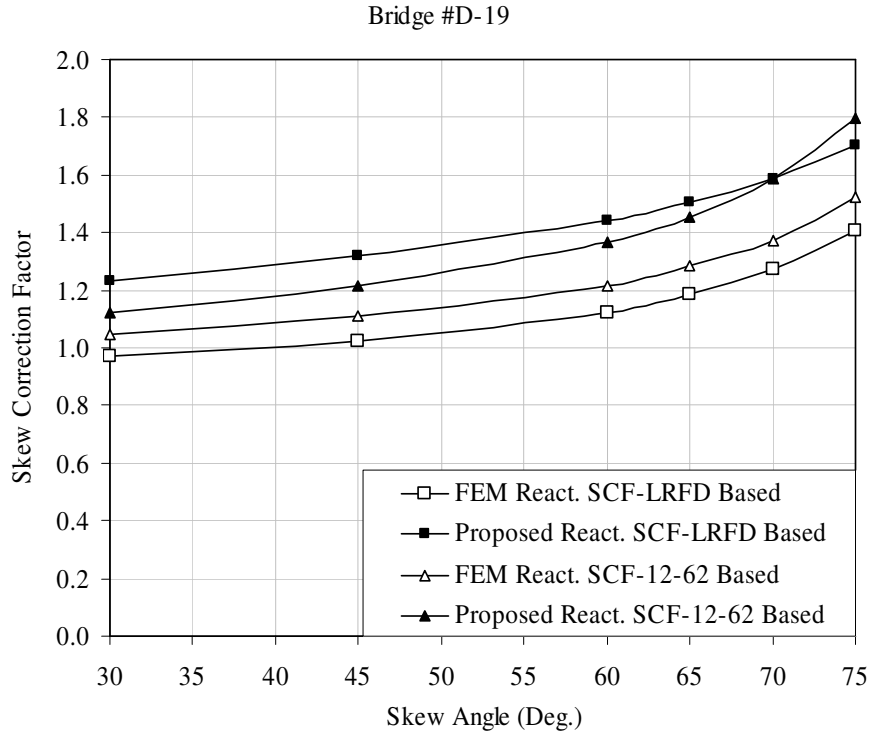


Figure 7.24 Proposed SCF vs. FEM SCF for Reaction in CIP Concrete Multi-cell Box-girder Bridges

7.3.5 Precast Cellular Concrete Box Girder Bridges

7.3.5.1 NCHRP 12-62 based equations. Skew Correction Factors for Shear (SCF_V)

and reaction (SCF_R) are given in Equations 7.23 and 7.24, respectively.

$$SCF_V = 1 + \left(\frac{12 \cdot L}{250 \cdot d}\right) \times (\tan \theta)^{1.3} \quad (7.23)$$

$$SCF_R = 1 + \left(\frac{12}{90} \cdot \left(\frac{L}{d}\right)^{1.2}\right) \cdot \tan \theta \quad (7.24)$$

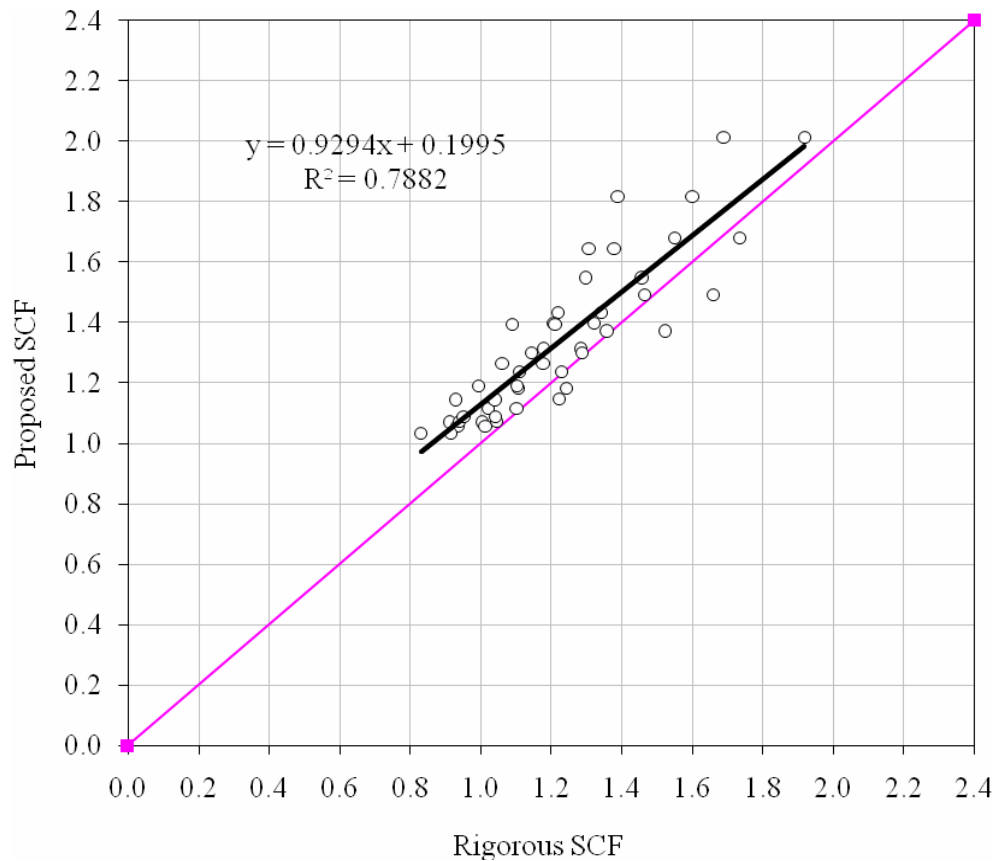


Figure 7.25 Proposed NCHRP 12-62 based SCF vs. Rigorous SCF for Shear in Precast Cellular Concrete Box-girder Bridges

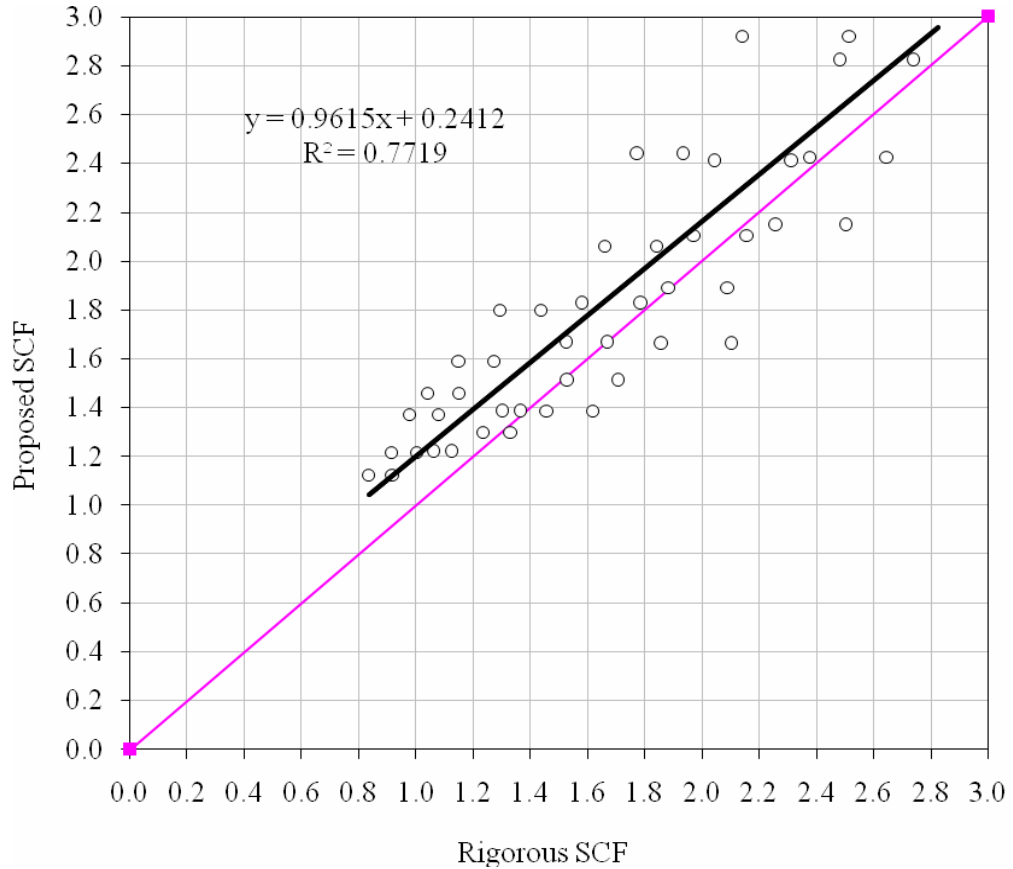


Figure 7.26 Proposed NCHRP 12-62 based SCF vs. Rigorous SCF for Reaction in Precast Cellular Concrete Box-girder Bridges

7.3.5.2 AASHTO LRFD based equations. Skew Correction Factors for Shear

(SCF_V) and reaction (SCF_R) are given in Equations 7.25 and 7.26, respectively.

$$SCF_V = 1 + \frac{12}{500} \times \left(\frac{L}{d}\right)^{0.6} \times (\tan \theta)^{1.2} \quad (7.25)$$

$$SCF_R = 1 + \left(\frac{12}{250} \times \left(\frac{L}{d}\right)^{1.4} \times (\tan \theta)^{1.0}\right) \quad (7.26)$$

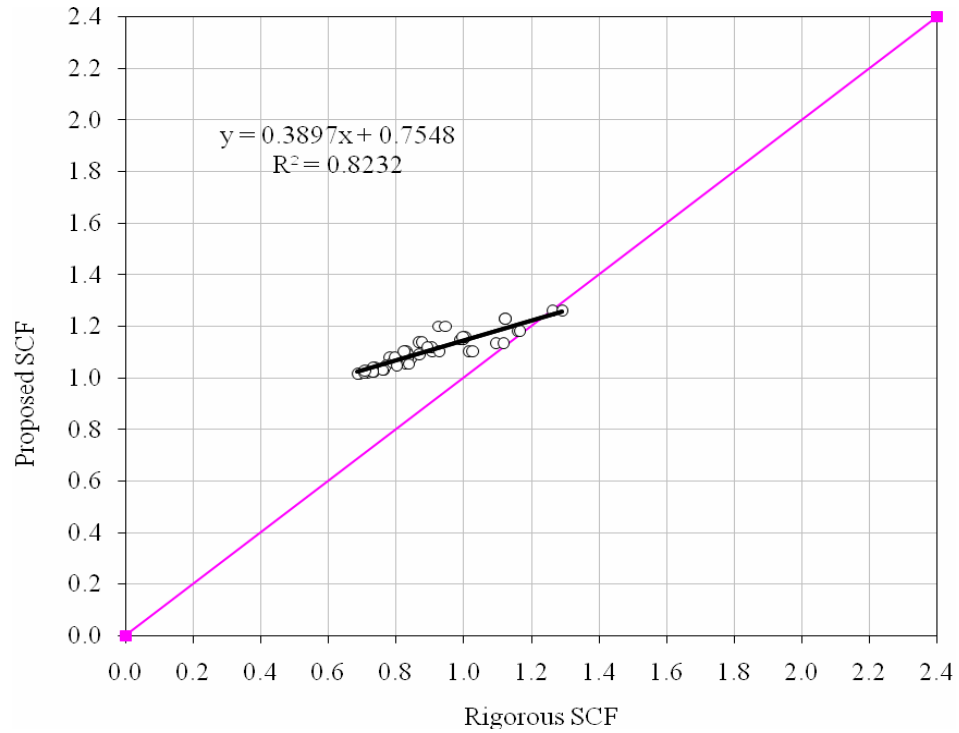


Figure 7.27 Proposed AASHTO LRFD SCF vs. Rigorous SCF for Shear in Precast Cellular Concrete Box-girder Bridges

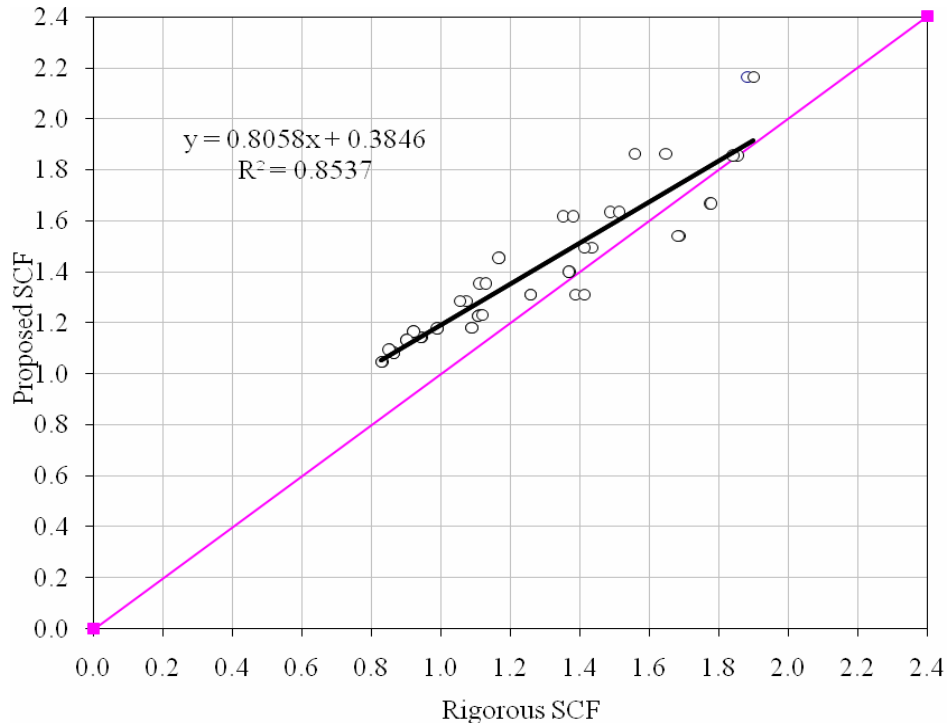


Figure 7.28 Proposed AASHTO LRFD SCF vs. Rigorous SCF for Reaction in Precast Cellular Concrete Box-girder Bridges

To validate Equations 7.23 through 7.26, the regression analyses for the precast cellular concrete, box girder bridges were performed. The coefficients of determination, R^2 , are 0.7882 and 0.7719 for shear and reaction, respectively, which indicates a low variety of the data.

Table 7.5 presents the statistical results for AVE, SD, and COV for precast cellular concrete, box-girder bridges. The slightly-greater-than unity averages show that the above expressions can be used conservatively in the prediction of SCFs for both shear and reaction in the precast concrete cellular, box girder bridges. The SDs, ranging from 0.095 to 0.171, and the COVs, ranging from 0.086 to 0.152, are a bit higher compared to those for the aforementioned types of girder bridges. The LDFs for straight bridges from NCHRP12-62 or AASHTO-LRFD are conservative for precast cellular concrete, box girder bridges, so the corresponding SCFs obtained from the FEM and these conservative LDFs for straight bridges are sometimes lower than 1. However, the SCF equation employed in this dissertation is definitely larger than 1. Therefore, this discrepancy resulted in the deviation of the proposed SCFs from those from the FEM and a bit higher SD or COV. However, these statistical results were still considered acceptable in this dissertation.

Table 7.5 Comparative Statistics of SCFs for Precast Concrete Cellular Box Girder Bridges

		Average	SD	COV
NCHRP12-62 Based Equation	Shear	1.099	0.095	0.086
	Reaction	1.123	0.171	0.152
AASHTO LRFD Based Equation	Shear	1.262	0.142	0.112
	Reaction	1.134	0.114	0.100

7.3.5.3 Proposed equations validation. Figures 7.29 and 7.30 present the comparison of the SCFs obtained from the proposed formulas to those from the finite element results. The 7th precast cellular concrete, box-girder bridge was randomly selected to represent the typical results. The figures show that the proposed equations can conservatively predict the finite element results very well.

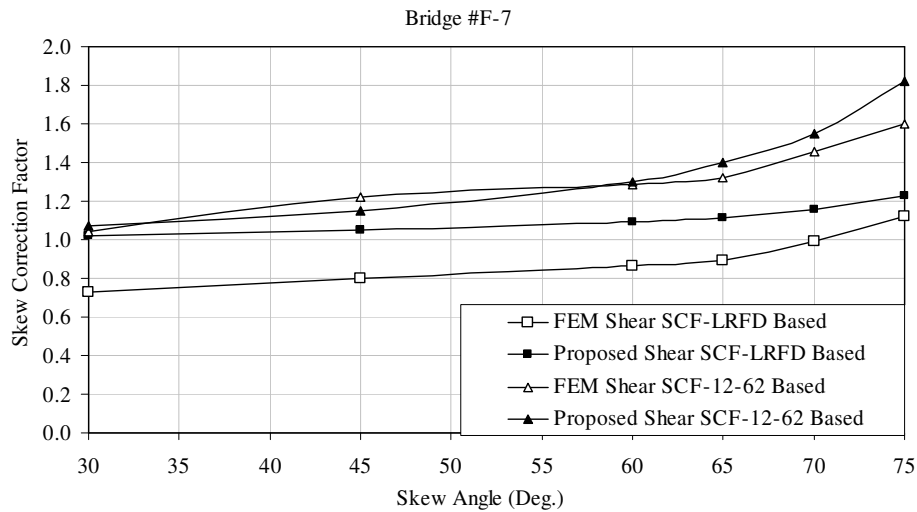


Figure 7.29 Proposed SCF vs. FEM SCF for Shear in Precast Cellular Concrete Box-girder Bridges

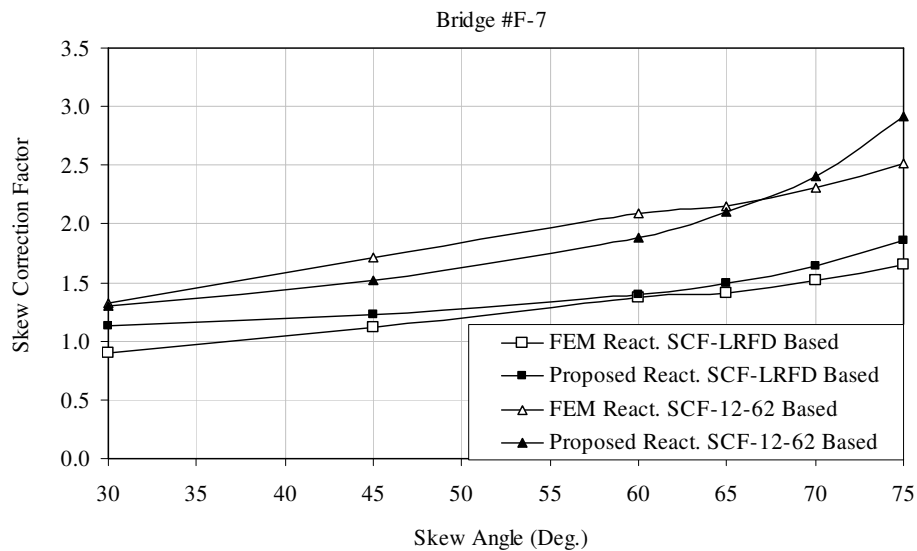


Figure 7.30 Proposed SCF vs. FEM SCF for Reaction in Precast Cellular Concrete Box-girder Bridges

CHAPTER 8

SUMMARY, CONCLUSIONS, AND RECOMMENDATIONS

8.1 Summary

The current AASHTO LRFD Specifications (2005) impose limitations on the range of applicability for live load distribution factors of for highway bridges. These limitations are specified in terms of bridge span, slab thickness, girder spacing and longitudinal stiffness, which are also imposed on the SCF equations. However, since the adoption into the LRFD Specifications, many engineers have expressed that the complexity of the new equations is troubling. The new equations are also not applicable to the bridges when the structural parameters are in excess of the limitations. The LRFD Specifications mandate that when these ranges of applicability are exceeded, a rigorous analysis is required. But the rigorous analysis usually requires special skill and software, which is time-consuming, costly, and inconvenient in most cases. Even though research NCHRP12-62 had already developed more simple unlimited distribution factor formulas for non-skewed bridges, the limitations on the SCF equations were kept fundamentally the same as the current LRFD specifications. Therefore, one of the objectives of this research was to develop the unlimited formulas for the SCFs for live load shear distribution for various types of skewed bridges. In conjunction with the LDF equations for non-skewed bridges presented in NCHRP12-62 or the AASHTO LRFD Specifications, the proposed unlimited formulas for SCFs can be used by bridge

engineers to predict the maximum shear in the girders to design and evaluate skewed slab-on-girder bridges without limitations on the range of applicability.

Based on the studies on comparing distribution factors for live load reaction with those for shear at piers of continuous skewed bridges in the actual skewed bridges, it was found that the distribution factors for live load reaction are different from those for shear in the skewed piers. Therefore, it is necessary to develop the specific distribution factors for live load reaction instead of those for shear in order to obtain the maximum reactions. This was the second objective of this dissertation.

The two objectives have been accomplished through several steps. The first step was to use the α - θ method to develop the bridge database and analyze the developed bridges with the improved finite element models in order to obtain the maximum responses such as shear and reaction. APDL was used to develop the program to accomplish the preprocessing, solution, and post-processing automatically and to expedite the entire finite element analysis process. After that, the SCFs for shear and reaction distribution in skewed bridges were calculated based on NCHRP 12-62 or AASHTO-LRFD. After obtaining the SCFs for various types of bridges, parametric studies were performed to identify the key parameters that are sensitive to the SCFs for shear and reaction, respectively. As mentioned in previous chapters, $SCF = DF_{skew} / DF_{str}$, and the DF_{skew} was obtained using FEA. If DF_{str} was calculated from the unlimited formulas proposed in NCHRP12-62, the corresponding proposed SCF formulas were named “NCHRP12-62 Based Equation.” Otherwise if DF_{str} was calculated from the assumed unlimited formulas specified in the current AASHTO-LRFD, the corresponding proposed SCF formulas were named “AASHTO LRFD Based Equation.” Thus, two sets

of SCF equations for shear and reaction were finally developed, respectively, and validated through the regression analyses for various types of bridges.

8.2 Conclusions

Based on the results of the research documented in this dissertation the following conclusions can be drawn:

1. The good agreement of the structural responses between the 2-D improved concentric beam model and detailed 3-D finite element results or experimental results verified that the selected 2-D finite element model can reliably predict the responses of slab-on-girder bridges.
2. APDL was used to automate the analysis process for searching for the maximum responses including preprocessing, solution, and post-processing, which saved significant computation time and avoided the possible mistakes made through the typical GUI.
3. The perfect match of the maximum shears and support reactions obtained from the estimated truck transverse positions with the detailed analysis results indicated the estimated transverse positions can be used to correctly predict the maximum responses for slab-on-girder bridges and save much computation time.
4. Through the comparison of the support reactions to shear forces at the beam ends for actual skewed bridges, it was concluded that the distribution factors of reactions at piers are higher than those of shear near the same piers and the

increase in reaction distribution factor at piers is more significant than that in the shear distribution factor when the skew angle is greater than 30°. It is necessary to develop the specific SCF equations for reaction distributions to predict the reaction distributions for skewed bridges combined with LDF for shear forces in the girders of straight bridges specified in NCHRP12-62 or the AASHTO LRFD Specifications.

5. For skew correction factors for both reaction and shear distributions, the discrepancy between finite element results and those calculated using the codified LRFD equations indicated that the LRFD specifications are not suitable to predict the skew correction factors for both reaction and shear distributions for the bridges with the parameters exceeding the limitations on the range of applicability. Therefore, it is necessary to develop the new SCF equations for both shear and reaction for the bridges with the parameters in excess of the applicable ranges.
6. Based on the results of the parametric study for various types of bridges, span length (L), girder spacing (S), and skew angle (θ) were identified as the sensitive parameters to affect skew correction factors for shear and reaction distributions. The SCFs for both reaction and shear distributions increase with the increase of span length and skew angle, but decrease with the increase of girder spacing.
7. Two sets of simplified equations were developed for SCFs for both shear and reaction distributions for the LRFD types a, k, b, d, and f, respectively. One was based on the AASHTO LRFD Specifications and the other based on

NCHRP project 12-62. The slightly-greater-than unity average and low standard deviation and coefficient of variation for each proposed equation indicate high reliabilities for these proposed equations in predicting the SCFs for shear and reaction distributions for various types of bridges.

8. The comparison of SCFs obtained from the proposed formulas to those calculated from finite element analyses validated that the proposed equations of SCFs for slab-on-girder bridges can correctly predict the maximum responses without limitations in conjunction with the codified LDF equations for straight bridges specified in the current LRFD Specifications or NCHRP 12-62.
9. Figure 8.1 is the flowchart for obtaining the distribution factors for shear and reaction in the skewed bridges.

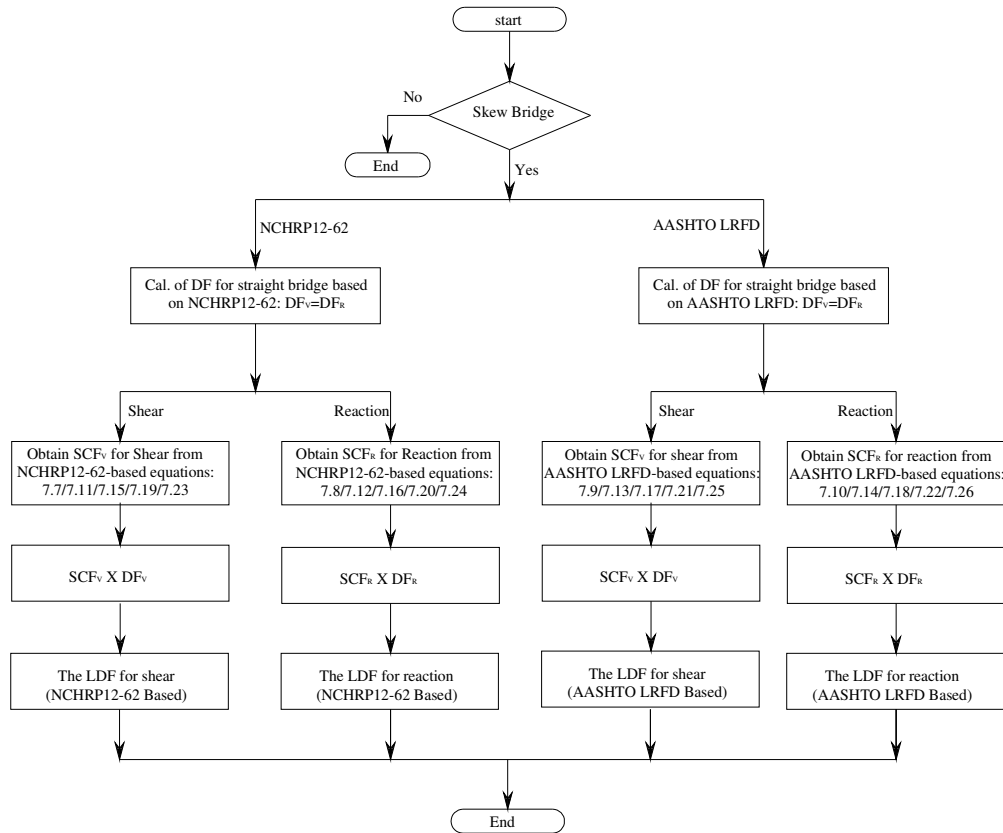


Figure 8.1 Flowchart to obtain distribution factors in skewed bridges

8.3 Recommendations

Based on the results of the research documented in this dissertation, the following recommendations are made:

1. Both NCHRP12-62-based equations and LRFD-based equations were proposed to predict SCFs for various types of bridges. However the NCHRP12-62 based equations are preferred. Thus the maximum responses can be obtained with the proposed SCF equations in conjunction with the unlimited LDF for straight bridges presented in NCHRP12-62 without any restriction on the range of applicability.

2. Research similar to this study on other types of bridges should be conducted.
3. Effects of secondary elements such as bracing, parapets, etc., on the skew correction factors should be investigated and, if necessary, considered in the proposed equations.

DEFINITION

AASHTO: American Association of State Highway and Transportation Officials

APDL: ANSYS Parametric Design Language

AVE: Average Value

CHBDC: Canadian Highway Bridge Design Code

CIP: Cast In Place

COV: Coefficient of Variation

DOF: Degree of Freedom

EDF: Equal Distribution Factor

ENF: Equivalent Nodal Force

FE: Finite Element

FEA: Finite Element Analysis

FEM: Finite Element Method

GUI: Graphical User Interface

LDF: Load Distribution Factor

LRFD: Load and Resistance Factor Design

MDF: Moment Distribution Factor

NCHRP: National Cooperative Highway Research Program

OHBDC: Ontario Highway Bridge Design Code

SCF: Skew Correction Factor

SD: Standard Deviation

2-D: Two Dimensional

3-D: Three Dimensional

NOTATION

L: Span Length

S: Girder Spacing

θ : Skew Angle

d: Girder depth

W: Bridge Width

R^2 : Coefficients of Determination

t_s : Thickness of Slab

N_b : Number of Beam

E_g : Modulus of Elasticity for Girder

E_c : Modulus of Elasticity for Concrete

REFERENCES

Abendroth R., Fanous F., and Andrawes B., "Steel Diaphragms in Prestressed Concrete Girder Bridges." Report No.: TR-424, Center for Transportation Research and Education, Iowa State University, IA.

American Association of State Highway and Transportation Officials. AASHTO Standard Specifications for Highway Bridges, 16th Edition, Washington, D.C. (1996).

American Association of State Highway and Transportation Officials. AASHTO LRFD Bridge Design Specifications, 3rd Edition, Washington, D.C. (2005).

ANSYS 11.0, ANSYS Inc., 2008.

Bakht, B. and Jaeger, L.G., Bridge Analysis Simplified, McGraw-Hill Book Company, New York (1985).

Barr, P.J., Eberhard, M.O., and Stanton, J.F., "Live-Load Distribution Factors in Prestressed Concrete Girder Bridges," Journal of Bridge Engineering, Vol. 6, No. 5 (September/October 2001), pp. 298-306.

Barr P. J. and Amin MD. N., "Shear Live-Load Distribution Factors for I-Girder Bridges" Journal of Structural Engineering, Vol. 11, No. 2 (March 2006), pp. 197-204.

Berglund E. M. and Schultz A. E., "Girder Differential Deflection and Distortion-included Fatigue in Skewed Steel Bridges," Journal of Bridge Engineering, Vol. 11, No. 2 (March 2006), pp. 169-177.

Bishara, A.G., and Soegiarso, R., "Load Distribution in Multibeam Precast Pretopped Prestressed Bridges," Journal of Structural Engineering, Vol. 119, No. 3 (March 1993), pp. 920-937.

Brockenbrough, R. L., "Distribution factors for curved I-girder bridges." Journal of Structural Engineering, 112(10), (1986).

Cai.C.S., P.E. and Asce.M., "Discussion on AASHTO LRFD Load Distribution Factors for Slab-on-Girder Bridges," Practice Periodical on Structural Design and Construction, Vol. 10, No.3. (2005).

Chan, T.H.T. and Chan, J.H.F., "The Use of Eccentric Beam Elements in the Analysis of Slab-on-Girder Bridges." Structural Engineering and Mechanics, Vol. 8, No.1, pp 85-102, (1999).

Chen, Y., "Distribution of vehicular loads on bridge girders by the FEA using ADINA: modeling, simulation, and comparison." Computers & Structures, Vol. 72, pp 127-139, (1999).

Chen, Y., and Aswad, A., "Stretching Span Capability of Prestressed Concrete Bridges Under AASHTO LRFD," *Journal of Bridge Engineering*, Vol. 1, No. 3 (August 1996), pp. 112-120.

Choo T., Linzell D., Lee J., and Swanson J., "Response of a continuous, skewed, steel bridge during deck placement," *Journal of Constructional Steel Research*, 61(2005), pp. 567-586.

Cross B., Panahshahi N., Vaughn B., Petermeier D., Siow Y. "Investigation of select LRFD design factors through instrumentation of bridge bearings," Report No.: FHWA/IL/HRC.2006-2/152, Southern Illinois Univ. Edwardsville Edwardsville, IL.

Dennis Mertz, etc., "Simplified Live Load Distribution Factor Equations," NCHRP12-62 Report No. 592, BridgeTech, Inc., Laramie, WY in association with Tennessee Technological University, Cookeville, TN. Transportation Research Board, Washington, D.C., 2007.

Ebeido, T., and Kennedy, J.B., "Shear Distribution in Simply Supported Skew Composite Bridges," *Canadian Journal of Civil Engineering*, Vol. 22, No. 6 (December 1995), pp. 1143-1154.

Ebeido, T., and Kennedy, J. B., "Girder moments in continuous skew composite bridges," *Journal of Bridge Engineering*, 1(1), 37-45, (1996a).

Ebeido, T., and Kennedy, J. B., "Shear and reaction distributions in continuous skew composite bridges," *Journal of Bridge Engineering*, 1(4), 155-165, (1996b).

Eom, J. and Nowak, A.S., "Live Load Distribution for Steel Girder Bridges," *Journal of Bridge Engineering*, Vol. 6, No. 6, November/December, pp 489-497, (2001).

Hays, C., Sessions, L., and Berry, A., "Further Studies on Lateral Load Distribution Using a Finite Element Method," *Transportation Research Record No. 1072*, Transportation Research Board, Washington, D.C. (1986), pp. 6-14.

Huang H., Shenton H., and Chajes M., "Load Distribution for a Highly Skewed Bridge: Testing and Analysis," *Journal of Bridge Engineering*, Vol. 9, No. 6 (November 2004), pp. 558-562.

Huo, X.S., Conner, S.O., and Iqbal, R., "Re-examination of the Simplified Method (Henry's Method) of Distribution Factors for Live Load Moment and Shear," Final Report, Tennessee DOT Project No. TNSPR-RES 1218, Tennessee Technological University, Cookeville, TN (June 2003).

Huo, X.S., Zhang, Q. (2006), "The effect of Skewness on Live Load Reactions at Piers of Continuous Bridges," *Proceedings, ASCE structures congress*, St. Louis, Missouri, May 17-20.

Huo, X.S., Zhang, Q. (2008) "Effect of Skewness on the Distribution of Live Load Reaction at Piers of Continuous Skewed Bridges," *Journal of Bridge Engineering*, Vol. 13, No. 1, pp. 110-114.

Imbsen, R.A., and Nutt, R.V., "Load Distribution Study on Highway Bridges Using STRUDL Finite Element Analysis Capabilities," *Conference On Computing in Civil Engineering: Proceedings (1978)*, pp. 639-655.

Khaleel, A.K. and Itani, R.Y., "Live-Load Moments for Continuous Skew Bridges." *Journal of Structural Engineering*, Vol. 116, No. 9, September, pp 2361-2373, (1990).

Mabsout, M.E., Tarhini, K.M., Frederick, G.R., and Tayar, C., "Finite-Element Analysis of Steel Girder Highway Bridges," *Journal of Bridge Engineering*, Vol. 2, No. 3 (August 1997), pp. 83-87.

Marx, H.J., "Development of Design Criteria for Simply Supported Skew Slab-and-Girder Bridges." Ph.D. Dissertation, Department of Civil Engineering, University of Illinois, Urbana-Champaign,(1985).

Ministry of Transportation and Communications, Ontario Highway Bridge Design Code (OHBDC), 2nd Ed., Downsview, Ontario, Canada, (1983).

Ministry of Transportation and Communications, Ontario Highway Bridge Design Code (OHBDC), 2nd Ed., Commentary, Downsview, Ontario, Canada, (1983).

Modjeski and Masters, Inc. (2002) "Shear in Skewed Multi-Beam Bridges," National Cooperative Highway Research Project 20-7/Task 107.

Nicola Greco, " Cross-Sectional Compactness and Bracing Requirements for Hybrid HPS Girders," Master thesis, University of Pittsburgh,(2002).

Nowak A. S., Eom J., and Ferrand D. " Verification of Girder Distribution of Factors for Continuous Steel Girder Bridges," University of Michigan 2340 G.G. Brown Bldg. Ann Arbor, MI,(2003).

Patrick M., Huo X., Puckett J. et al, "Sensitivity of Live Load Distribution Factors to Vehicle Spacing," *Journal of Bridge Engineering*, Vol. 11, No. 1, January(2006), pp. 131-134.

Schwarz, M. and Laman, J., "Response of Prestressed Concrete I-Girder Bridges to Live Load." *Journal of Bridge Engineering*, Vol. 6, No. 1, January/February, pp 1-8, (2001).

Shahawy, M. and Huang, D., "Analytical and Field Investigation of Lateral Load Distribution in Concrete Slab-On-Girder Bridges." *ACI Structural Journal*, Vol. 98, No. 4, July-August, pp 590-599, (2001).

Sotelino E., Liu Judy, Chung W. and Phuvoravan K., "Simplified Load Distribution Factor for Use in LRFD Design," Final Report, FHWA/IN/JTRP-2004/20, Indiana DOT, Joint Transportation Research Program, Purdue University. West Lafayette, IN (2004).

Tabsh, S.W. and Tabatabai, M. "Live Load Distribution in Girder Bridges Subject to Oversized Trucks." *Journal of Bridge Engineering*, Vol. 6, No. January/February, pp 9-16, (2001).

Tarhini, K.M., and Frederick, G.R., "Wheel Load Distribution in I-Girder Highway Bridges," *Journal of Structural Engineering*, Vol. 118, No. 5 (May 1992), pp. 1285-1295.

The Canadian Standards Association. *Canadian Highway Bridge Design Code*, 2000 Edition, Toronto, Ontario, Canada (2000).

Tobias, D.H., Anderson, R.E., Khayyat, S.K., Uzman, Z.B., and Riechers, K.L., "Simplified AASHTO LRFD Girder Live Load Distribution in Illinois," *Journal of Bridge Engineering*, (2004).

Yousif, Z., "Live load distribution for highway bridges based on AASHTO LRFD and finite element analysis." Master's thesis, Dept. of Civil Engineering and Construction, Bradley Univ., Peoria, Ill, (2005).

Yousif, Z. and Hindi R., "AASHTO-LRFD Live Load Distribution for Beam-and-Slab Bridges: Limitations and Applicability," *Journal of Bridge Engineering*, Vol. 12, No. 6 (November 2007), pp. 765-773.

Zokaie, T., Mish, K., and Imbsen, R.A., "Distribution of Wheel Loads on Highway Bridges," NCHRP 12-26 Project Final Report, Vol. 3, Transportation Research Board, National Research Council, Washington, D.C. (1993).

Zokaie, T., Mish, K., and Imbsen, R.A., "Distribution of Wheel Loads on Highway Bridges," NCHRP 12-26 Project Final Report, Vol. 1, Transportation Research Board, National Research Council, Washington, D.C. (1991).

Zokaie, T., Mish, K., and Imbsen, R.A., "Distribution of Wheel Loads on Highway Bridges," NCHRP 12-26 Project Final Report, Vol. 2, Transportation Research Board, National Research Council, Washington, D.C. (1991).

Zokaie, T., Mish, K., and Imbsen, R.A., "Distribution of Wheel Loads on Highway Bridges," NCHRP 12-26 Project Final Report, Vol. 3, Transportation Research Board, National Research Council, Washington, D.C. (1993).

Zokaie, T., "AASHTO-LRFD live load distribution specifications." *Journal of Bridge Engineering*, 5(2), pp. 131-138, (2000).

APPENDICES

Appendix A APDL for Slab-on-girder Bridges

```

!-----Under one lane loaded-----
!Unit: kip-inch Longitudinal: X Transverse Y Vertical Z

!*****Create Girder Section plus Haunch*****

Finish
/clear,START
/prep7
et,3,plane82

bh=(0)      !width of haunch in.
th=(0)      !thickness of haunch in.

bf1=(8)     !top flange width in.
tf1=(0.5)   !top flange thickness in.
bf2=(8)     !bottom flange width in.
tf2=(1)     !bottom flange thickness in.

tw=(0.33)   !web thickness in.
hw=(45.5)   !web height in.

meshsize=2.0 ! the size of girder elements in.
!-----
BLC4,-bh/2,0,bh,-th
BLC4,-bf1/2,-th,bf1,-tf1
BLC5,0,-(th+tf1+hw/2),tw,hw
BLC5,0,-(th+tf1+hw+tf2/2),bf2,tf2
wpave,-tw/2,-(th+tf1)
wpro,,90.0
asbw,all
wpave,tw/2,-(th+tf1)
asbw,all
allsel,all
asel,s,loc,y,-th,0
aatt,1,,3
asel,inve
aatt,2,,3
allsel,all
aplot
nummrg,all
numcmp,all
lsl,s,length,,0,1
LESIZE,all,,1,,,,,1
lsl,inve
LESIZE,all,meshsize,,,,,1
allsel,all
mshape,0,2d
mshkey,1
amesh,all
alls

secwrite,A-1,sect !name should be changed with various bridges
!*****Girder Section Creation End*****

```

```
!*****: Eposforxy Macro *****
```

```
! Objective: To judge in which element any given point (arg1, arg2, 0) locates  
! Return value is element number the given point associate with: epos
```

```
*Dim,ELocArray,Array,10 !maximum related elements:10  
*Dim,S_elm,,10 !record areas of triangle related to given pt  
*Dim,NNX,,4  
*Dim,NNY,,4
```

```
*create,eposforxy,mac
```

```
xx =arg1
```

```
yy =arg2
```

```
nnn = node(xx,yy,0) !Obtain the nearest node nnn
```

```
ePos=-1 !Assign the impossible value to the unknown elem
```

```
Xnnn=Nx(nnn)
```

```
Ynnn=Ny(nnn)
```

```
!the distante Dist bwtm the input pt and the nearest node
```

```
Dist=SQRT((xx-Xnnn)*(xx-Xnnn)+(yy-Ynnn)*(yy-Ynnn))
```

```
!if Dist can be neglected,return any element nnn belong
```

```
DistTolerance=1e-1
```

```
*If,Dist,LT,DistTolerance,Then
```

```
AllSel,All
```

```
Nsel,S,Node,,nnn !select the nearest node
```

```
Esln,S,0,All
```

```
esel,r,type,,1
```

```
eplot
```

```
*Get, Eloc, Elem, , Num, Min
```

```
ePos=eLoc
```

```
npos=nnn
```

```
flag=0 ! flag=0 means the point is exactly on the node
```

```
*Else !if Dist is big
```

```
flag=1
```

```
Lx=(xx-Xnnn)/Dist
```

```
Ly=(yy-Ynnn)/Dist
```

```
*If,Lx,NE,0,Then
```

```
Knnn=Ly/Lx
```

```
*Else
```

```
Knnn=1e+20
```

```
*EndIf !connect two pts and obtain the slope of the original line
```

```
AllSel,All
```

```
Nsel,S,Node,,nnn !select the nearest pt of given pt
```

```
Esln,S,0 !select all elements containing this node
```

```
Esel,r,type,,1
```

```
Enum = ElmIqr(0,13) !Obtain total num of selected elements
```

```
!Obtain the minimum elem number and save all elem numbers
```

```
*Get, Eloc, Elem, , Num, Min
```

```

*Do,Ar20,1,ENum
  ElocArray(Ar20)=ELoc
  Eloc=ElNext(Eloc)
*EndDo
!Judge the element number in which the node is in

*Do,Ar20,1,enum  !selected element loop
  Eloc=ElocArray(Ar20)
  Esel,s,,eloc  !select elemen based on element number
  Nsle,S,All
  Nnum=NdInqr(0,13) !return the sum of selected nodes
*Do,Ar21,1,Nnum  !node loop, delete two sides containing nnn
  *If,Ar21,LT,NNum,Then
    Ar22=Ar21+1
  *Else
    Ar22=1
  *EndIf
*If,NElem(ELoc,Ar21),NE,nnn,And,NElem(ELoc,Ar22),NE,nnn,Then
  xLoc1 =Nx(NElem(ELoc,Ar21))
  yLoc1 =Ny(NElem(ELoc,Ar21))
  xLoc2 =Nx(NElem(ELoc,Ar22))
  yLoc2 =Ny(NElem(ELoc,Ar22)) !Obtain two pts coodinates
  Dist=DistND(NElem(ELoc,Ar21),NElem(ELoc,Ar22))
  LxLoc=(xLoc1-xLoc2)/Dist
  LyLoc=(yLoc1-yLoc2)/Dist!slop of this line with two pts
  *If,LxLoc,NE,0,Then
    KLoc=LyLoc/LxLoc
  *Else
    KLoc=1e+20
  *EndIf
  *If,Knnn,NE,KLoc,Then !see if this line // orignal line
    xCross=(yLoc1-yy+knnn*xx-KLoc*xLoc1)/(knnn-kLoc)
    yCross=knnn*(xCross-xx)+yy !obtain intersection pt
!see if intersection pt is same side of nnn with given pts
    LxLoc=xCross-Nx(nnn)
    IP=0
    *If,Lx,NE,0,Then
      *If,LxLoc*Lx,GT,0,Then
        IP=1
      *EndIf
    *Else
      LyLoc=yCross-Ny(nnn)
      *If,LyLoc*Ly,GT,0,Then
        IP=1
      *Endif
    *Endif
!judge if intersection is on the line
    *If,IP,EQ,1,Then
      xMin=Min(xLoc1,xLoc2,Xnnn)  ! Obtain max/min x/y coordinates
      xMax=Max(xLoc1,xLoc2,Xnnn)
      yMin=Min(yLoc1,yLoc2,Ynnn)
      yMax=Max(yLoc1,yLoc2,Ynnn)
      *If,xCross,GE,xMin,And,xCross,LE,xMax,Then
        *If,yCross,GE,yMin,And,yCross,LE,yMax,Then
          ePos=eLoc !obtain unknown element number
          *Exit  !Got results, exit from loop

```

```

        *Endif
        *EndIf !judge if intersection on the line
        *EndIf !judge if cos() same
        *EndIF !judge if two lines are parallel
        *Endif !judge if one of selected nodes same as nnn
        *EndDo !end node loop
        *IF,ePos,NE,-1,Then
        *Exit
        *EndIF
        *Enddo !end element loop
        *EndIF !judge if Dist is neglected, ie given pts same as nnn

*End
!*****eposforxy macro end*****

!*****Tri_area Macro *****
! Objective: to calculate area of the triangle (Tri_area.MAC)
! Input three vertices of the triangle (x1,y1;x2,y2;x3,y3)
*create,Tri_area,mac
x1=Arg1
y1=Arg2
x2=Arg3
y2=Arg4
x3=Arg5
y3=Arg6
Dist1=Sqrt((x1-x2)**2+(y1-y2)**2)
Dist2=Sqrt((x2-x3)**2+(y2-y3)**2)
Dist3=Sqrt((x3-x1)**2+(y3-y1)**2) !length of sides of triangle
Dc=(Dist1+Dist2+Dist3)/2.0 !half of the primeter of triangle
S_Tri=Sqrt((ABS(Dc*(Dc-Dist1)*(Dc-Dist2)*(Dc-Dist3)))) !area
*END
!*****Tri_area macro end*****

!*****DistributeF Macro *****
! Objective: To distribute the concentrated load to the nodes contained in the return element
*create,distributeF,mac
/solu

alls
xPos = arg1
yPos = arg2
P=arg3
esel,s,type,,1
nsle,s
eposforxy,xPos,yPos !Obtain element #,ePos,into which given pt fall

*if,flag,eq,0,then
*get,NodeFZnnn,NODE,npos,F,FZ
F,npos,FZ,P+NodeFZnnn
*endif

*if,flag,eq,1,then
AllSel,All
Esel,s,,ePos
Nsle,s,All
Nnum=NdInqr(0,13) !the total numbers of nodes in the selected elem

```



```

*if,Nnum,EQ,3,THEN
  Se_Total=0 !total area of the element
  *Do,Ar20,1,Nnum
    !Calculate area of all possible triangles
    *If,Ar20,LT,Nnum,Then
      ie=Ar20+1
    *Else
      ie=1
    *EndIf
    xTr1=Nx(NElem(ePos,Ar20))
    yTr1=Ny(NElem(ePos,Ar20))
    xTr2=xPos
    yTr2=yPos
    xTr3=Nx(NElem(ePos,ie))
    yTr3=Ny(NElem(ePos,ie))
    Tri_area,xTr1,yTr1,xTr2,yTr2,xTr3,yTr3 !ara of the triangle S_tri
    S_Elm(Ar20)=S_Tri
    SE_Total=Se_Total+S_Tri !total area of the element
  *EndDo
  ! apply the force on the pts of triangle
  *Do,Ar20,1,Nnum
    !Calculate area of all possible triangles
    *If,Ar20,LT,Nnum,Then
      ie=Ar20+1
      thirdpt=Ar20+2
      *If,thirdpt,GT,Nnum,Then
        thirdpt=Ar20-1
      *Endif
    *Else
      ie=1
      thirdpt=Ar20-1
    *EndIf
    nsel,s,loc,z,0,0
    *get,NodeFZ1,NODE,NElem(ePos,thirdpt),F,FZ
    F,NElem(ePos,thirdpt),FZ,P*(S_Elm(Ar20)/SE_Total)+NodeFZ1
  *EndDo

*ElseIf,Nnum,EQ,4

*GET,Xmax, NODE, 0, MXLOC, X
*GET,Ymax, NODE, 0, MXLOC, Y
*GET,Xmin, NODE, 0, MNLOC, X
*GET,Ymin, NODE, 0, MNLOC, Y

NNX(1)=Xmax
NNY(1)=Ymax
NNX(2)=Xmax
NNY(2)=Ymin
NNX(3)=Xmin
NNY(3)=Ymin
NNX(4)=Xmin
NNY(4)=Ymax

  xa=ABS(NNX(2)-NNX(3))
  yb=ABS(NNY(1)-NNY(2))

```

```

xc=ABS(xPos-NNX(1))
yd=ABS(yPos-NNY(1))

SE_Total=xa*yb
nsel,s,loc,z,0,0
*get,NodeFZ1,NODE,NODE(NNX(1),NNY(1),0),F,FZ
*get,NodeFZ2,NODE,NODE(NNX(2),NNY(2),0),F,FZ
*get,NodeFZ3,NODE,NODE(NNX(3),NNY(3),0),F,FZ
*get,NodeFZ4,NODE,NODE(NNX(4),NNY(4),0),F,FZ

F,NODE(NNX(1),NNY(1),0),FZ,P*((xa-xc)*(yb-yd)/SE_Total)+NodeFZ1
F,NODE(NNX(2),NNY(2),0),FZ,P*((xa-xc)*(yd)/SE_Total)+NodeFZ2
F,NODE(NNX(3),NNY(3),0),FZ,P*((xc)*(yd)/SE_Total)+NodeFZ3
F,NODE(NNX(4),NNY(4),0),FZ,P*((xc)*(yb-yd)/SE_Total)+NodeFZ4
*Endif
alls
Finish
*endif
*END
!*****DistributeF macro end *****

!***** SolnforMQ Macro *****
!Objective: to obtain the maximum moment and shear force

*create,SolnforMQ,mac      ! apply by: SolnforMQ,X,Y,WIDTH
x0=arg1
y0=arg2
Gspac=arg3 ! should be equal to girder spacing
Edgewidth=arg4
flagintext=arg5 !1 interior girders 0 exterior girder
alls
nsel,s,loc,z,0,0
nsel,r,loc,x,x0,x0
nsel,r,loc,y,y0,y0
nplot
esln,s
esel,r,type,,2

nsle,s
nplot
*GET,Xmax, NODE, 0, MXLOC, X
*GET,Xmin, NODE, 0, MNLOC, X

ALLS
nsel,s,loc,z,0,0
NSEL,r,LOC,x,Xmin-1,x0+1
*if,flagintext,eq,1,then
nsel,r,loc,y,y0-Gspac/2-1,y0+Gspac/2+1 ! 1 interior
*else
nsel,r,loc,y,y0-Edgewidth-1,y0+Gspac/2+1 ! 0: exterior
*endif
nplot
esln,s,1
esel,r,type,,1
nsel,r,loc,x,x0,x0

```

```

nplot
SPOINT,Node(x0,y0,0)
FSUM,0,ALL
*GET,FZdeckleft,FSUM,0,ITEM,FZ
*GET,MYdeckleft,FSUM,0,ITEM,MY

ALLS
nsl,s,loc,z,0,0
NSEL,r,LOC,x,x0-1,Xmax+1
*if,flagintext,eq,1,then
nsl,r,loc,y,y0-Gspac/2-1,y0+Gspac/2+1 ! 1: interior
*else
nsl,r,loc,y,y0-Edgewidth-1,y0+Gspac/2+1 ! 0: exterior
*endif
nplot
esln,s,1
esel,r,type,,1
nsl,r,loc,x,x0,x0
nplot
SPOINT,Node(x0,y0,0)
FSUM,0,ALL
*GET,FZdeckright,FSUM,0,ITEM,FZ
*GET,MYdeckright,FSUM,0,ITEM,MY

alls
ESEL,S,type,,2
nsl,s,node,,node(x0,y0,0),node(x0,y0,0)
esln,r
*GET,NumbeamMIN, ELEM, 0, NUM, MIN
*GET,NumbeamMAX, ELEM, 0, NUM, MAX
esel,r,elem,,NumbeamMIN,NumbeamMIN
nsle,s
nsl,u,loc,x,x0,x0
*GET,NumNode, NODE, 0, NUM, MIN

*If,NX(NumNode),LT,x0,Then
    Ebeamleft=NumbeamMIN
    Ebeamright=NumbeamMAX
*Else
    Ebeamleft= NumbeamMAX
    Ebeamright=NumbeamMIN
*EndIf

alls
ESEL,S,type,,2
ESEL,R,ELEM,,Ebeamleft,Ebeamleft
Nsle,s
nsl,r,loc,x,x0,x0
nplot
SPOINT,Node(x0,y0,0)
FSUM,0,ALL
*GET,FZbeamleft,FSUM,0,ITEM,FZ
*GET,MYbeamleft,FSUM,0,ITEM,MY

alls
ESEL,S,type,,2
nsl,s,node,,node(x0,y0,0),node(x0,y0,0)

```

```

esln,r
*GET,NumbeamMIN, ELEM, 0, NUM, MIN
*GET,NumbeamMAX, ELEM, 0, NUM, MAX
esel,r,elem,,NumbeamMIN,NumbeamMIN
nsle,s
nse1,u,loc,x,x0,x0
*GET,NumNode, NODE, 0, NUM, MIN

*If,NX(NumNode),LT,x0,Then
    Ebeamleft=NumbeamMIN
    Ebeamright=NumbeamMAX
*Else
    Ebeamleft= NumbeamMAX
    Ebeamright=NumbeamMIN
*EndIf
alls
ESEL,S,type,,2
ESEL,R,ELEM,,Ebeamright,Ebeamright
Nsle,s
nse1,r,loc,x,x0,x0
nplot
SPOINT,Node(x0,y0,0)
FSUM,0,ALL
*GET,FZbeamright,FSUM,0,ITEM,FZ
*GET,MYbeamright,FSUM,0,ITEM,MY

!for any point (x,y), the rusultant force and memoment
FZleft=FZdeckleft+FZbeamleft    !for the left part of the point
FZright=FZdeckright+FZbeamright !for the right part of the point
MYleft=MYdeckleft+MYbeamleft    !for the left part of the point
MYright=MYdeckright+MYbeamright !for the right part of the point
ALLS
*END
!***** SolnforMQ macro end*****

! *****Main Program*****
!-----Under one lane loaded-----
!Unit: kip-inch  Longitudinal: X Transverse Y Vertical Z

Finish
/clear,start
/prep7
/title,A-15-65          !A-1-skew angle

!-----Geometry input information-----
*AFUN,DEG
skew=(65)              !skew angle deg.
ts=(12)                !slab thickness in.
Ng=(4)                 !number of girders
Gspac=(20)*12          !girder spacing in.
Width=(80)*12          !bridge width in.
PPwidth=(1.75)*12     !Parapet width in.

Nspan=(2)              !span numbers

*DIM,span,ARRAY,Nspan,1,1  !span length in.

```

```

span(1)=(200)*12
span(2)=(200)*12
totallength=span(1)+span(2) !total length in.

Xmesh=(2)*12 !mesh the slab @Xmesh in X direction in.
Ymesh=(2)*12 !mesh the slab @Ymesh in Y direction in.

Xmove=(2)*12 !Truck move @ Xmove in X direction in.
Ymove=(38)*12 !Truck move @ Ymove in Y direction in.

!*****geometry calculation based on the above input*****
Edgewidth=(Width-(Ng-1)*Gspac)/2 !edge width in.
skewlength=Width*tan(skew) !skew angle opposite side in.
!-----Truck transverse position (Y)-----
OutmostTK_Y=PPwidth+2*12 !The outmost truck wheel postion in
TKY1=OutmostTK_Y+Ymove !The first wheel Y coordinate in.
TKY2=TKY1+72 !The second wheel Y coordinate in.
!-----span coordinate (in.)-----
*DIM,L,ARRAY,Nspan,1,1
L(1)=span(1)
L(2)=span(1)+span(2)
!-----
NL=Ng+2 ! NL: number of lines
*DIM,GLY,ARRAY,NL,1,1,,
*DIM,GLX,ARRAY,NL,1,1,,
GLX(1)=0
GLY(1)=0
GLY(NL)=Edgewidth*2+Gspac*(Ng-1)
GLX(NL)=GLY(NL)*tan(skew)
*do,i,2,NL-1
GLY(i)=Edgewidth+Gspac*(i-2)
GLX(i)=GLY(i)*tan(skew)
*enddo

!-----concrete properties-----
Ec=3625 !ksi(modulus for deck concrete)
vconc=0.15
!-----Steel properties-----
Es=29000 !ksi ( will change if concrete girder)
vsteel=0.3

!*****input over*****
!-----
Num_int=NINT(Ng/2)-1 !For postprocess results

*dim,Ext_X,,(Nspan+1)
*dim,Ext_Y,,(Nspan+1)

*DIM,INT_X,array,Num_int,Nspan+1
*DIM,INT_Y,array,Num_int,Nspan+1
!-----

*dim,Ext_MID_X,,Nspan !middle span nodes for moments
*dim,Ext_MID_Y,,Nspan

*DIM,INT_MID_X,array,Num_int,Nspan

```

```

*DIM,INT_MID_Y,array,Num_int,Nspan

  Ext_X(1,1)=GLX(2)      !Ext_X(1,i),Ext_Y(1,i) for support node
  *do,i,2,Nspan+1
  Ext_X(1,i)=GLX(2)+L(i-1)
  *enddo
  *do,i,1,Nspan+1
  Ext_Y(1,i)=GLY(2)
  *enddo

  *do,j,1,Num_int      !Int_X(j,jj),Int_Y(j,jj) for support node
  INT_X(j,1)=GLX(j+2)
  INT_Y(j,1)=GLY(j+2)
  *do,jj,2,Nspan+1
  INT_X(j,jj)=GLX(j+2)+L(jj-1)
  INT_Y(j,jj)=GLY(j+2)
  *enddo
  *enddo
!-----
  *do,i,1,Nspan
  Ext_MID_X(1,i)=(Ext_X(1,i)+Ext_X(1,(i+1)))/2
  Ext_MID_Y(1,i)=Ext_Y(1,1)
  *enddo

  *do,j,1,Num_int
  *do,jj,1,Nspan
  Int_MID_X(j,jj)=(Int_X(j,jj)+Int_X(j,(jj+1)))/2
  Int_MID_Y(j,jj)=Int_Y(j,1)
  *enddo
  *enddo

!-----Input real const. and material properties to ANSYS-----
Et,1, shell181      !concrete deck
Mp,ex,1, Ec
Mp,prxy,1, vconc
R,1,ts

KEYOPT,1,3,2      !keyopt(3)=2
KEYOPT,1,8,2      !keyopt(8)=2

Et,2, beam188      !steel or concrete girder
Mp,ex,2,Es
Mp,prxy,2,vsteel
R,2,

sect,1,shell,,
secdata,ts,1,0,0,3
secoffset,MID      !offset shell element
seccontrol,,,, , , ,

SECTYPE,2,BEAM,MESH
SECOFFSET,User,,ts/2,
SECREAD,'A-15','SECT',' ',MESH !be changed with various bridges*****

!-----Beam188 Property-----
KEYOPT, 2, 1, 1

```

```

KEYOPT, 2, 4, 2
KEYOPT, 2, 6, 3
!-----
*do,i,1,NL
  k,i,GLX(i),GLY(i),0
*enddo
KSEL,ALL

*do,i,1,Nspan      !Create all kpts on girder lines
  KGEN,2,1,NL,1,L(i),0,0,,1
*enddo

!Create the area
*do,j,0,Nspan-1
*do,i,0,NL-2
  A,(1+i+NL*j),(2+i+NL*j),(NL+2+i+NL*j),(NL+1+i+NL*j)
*enddo
*enddo
Allsel,all
!-----Cut the area along X transverse direction -----
WPCSYS,-1,0
WPSTYLE,,,,,,,,,1
wpro,-90.0,
allsel,all

iii=nint(Edgewidth/Ymesh)
*do,j,1,iii-1,1
  wpoff,,Edgewidth/iii
  asbw,all,,dele
*enddo

*do,i,2,NL-2,1
  KWPAVE,kp(GLX(i),GLY(i),0)
  wpoff,,Gspac/2
  asbw,all,,dele
*enddo

ii=nint(Gspac/(2*Ymesh))
*do,i,2,NL-2,1
  KWPAVE,kp(GLX(i),GLY(i),0)
  *do,j,1,ii-1,1
    wpoff,,Gspac/(2*ii)
    asbw,all,,dele
  *enddo
*enddo

ii=nint(Gspac/(2*Ymesh))
*do,i,3,NL-1,1
  KWPAVE,kp(GLX(i),GLY(i),0)
  *do,j,1,ii-1,1
    wpoff,,-Gspac/(2*ii)
    asbw,all,,dele
  *enddo
*enddo

KWPAVE,kp(GLX(NL-1),GLY(NL-1),0)

```

```

*do,i,1,iii-1,1
  wpoff,,Edgewidth/iii
  asbw,all,,dele
*enddo

! PICK all keypoints and attribute them to array kpnum1
*get,kpcount1,kp,,count
*dim,kpnum1,array,kpcount1
*get,kpnum1(1),kp,,num,min
*do,i,2,kpcount1,1
  kpnum1(i)=kpnext(kpnum1(i-1))
*enddo
!cut the area along Y direction
wpro,,,-90
*do,i,1,kpcount1,1
  KWPAVE,kpnum1(i)
  asbw,all,,dele
*enddo
!-----lesize the lines-----
alls
lsel,s,loc,x,0,skewlength
*do,i,1,Nspan,1
  lsel,a,loc,x,L(i),L(i)+skewlength
*enddo
lplot
lesize,all,,1

lsel,inve
lesize,all,Xmesh
alls
Nummrg,all
Numcmp,all
Lplot
!-----

!copy kps as the orientation points for the beam188 line
*do,i,1,Ng,1
  ALLS
  Ksel,s,loc,x,GLX(i+1),GLX(i+1)
  Ksel,r,loc,Y,GLY(i+1),GLY(i+1)
  KGEN,2,all, , , ,200, ,0
  ALLS
*enddo
! attribute the Ng beam lines with the mat, sec.
*do,i,1,Ng,1
  Alls
  Lsel,s,loc,y,GLY(i+1),GLY(i+1)
  LATT,2,2,2, , kp(GLX(i+1),GLY(i+1),200), ,2
  Lmesh,all
  Allsel
*enddo
ALLS
!choose the triangluar elements as components
CSYS,0
wpave,,0
WPCSYS,-1,0

```



```

wpro,90-skew,,
wpro,,90,

csys,4
lsel,s,loc,z,0,0
*do,i,1,Nspan,1
  CSYS,0
  KWPAVE,kp(L(i),0,0)
  csys,4
  lsel,a,loc,z,0,0
*enddo
asll,s
cm,triangle,area

aatt,1,1,1,0,1
mshape,1,2d
mshkey,0
amesh,all

asel,inve
aplot
aatt,1,1,1,0,1
mshape,0,2d
mshkey,1
amesh,all

csys,0
alls
eplot
!-----meshing is over-----
!applying the restraints on the nodes
/solu
Alls
*do,i,1,Ng,1
  ALLS
  nsel,s,loc,x,GLX(i+1),GLX(i+1)
  nsel,r,loc,Y,GLY(i+1),GLY(i+1)
  nsel,r,loc,z,0,0
  D,node(GLX(i+1),GLY(i+1),0), , , , , UX,UY,UZ, , ,
  ALLS
*enddo

*do,j,1,Nspan,1
*do,i,1,Ng,1
  ALLS
  nsel,s,loc,x,GLX(i+1)+L(j),GLX(i+1)+L(j)
  nsel,r,loc,Y,GLY(i+1),GLY(i+1)
  nsel,r,loc,z,0,0
  D,node((GLX(i+1)+L(j)),GLY(i+1),0), , , , , UY,UZ, , ,
  ALLS
*enddo
*enddo

/COLOR,U,RED
Alls
eplot

```

Finish
WPSTYLE,,,,,,,,,0

!NEXT: must run the macro 'ENF' to distribute the concentrated load
!NEXT: must run the macro 'SolnforMQ' to obtain M&Q in the postprocess

!start a new calculation from here after 'Ymove' is changed*****

!-----
*del,PRM_ !del user-defined PARAMETERS named with trailing underbar
!-----

*DIM,Q_EXT_,,(Nspan*2) !the exterior shear at beam ends
*DIM,Q_INT_,array,Num_int,Nspan*2 !the interior shear at beam ends
*DIM,R_EXT_,,(Nspan+1) !the exterior reaction at supports
*DIM,R_INT_,array,Num_int,Nspan+1 !the interior reaction at supports

*DIM,M_EXT_,,(Nspan) !the exterior moment at middle spans
*DIM,M_INT_,array,Num_int,Nspan !the interior moment at middle spans

*DIM,Qmax_EXT_,,(Nspan*2) !max. exterior shear at beam ends
*DIM,Qmax_INT_,array,Num_int,Nspan*2 !max. interior shear at beam ends
*DIM,Rmax_EXT_,,(Nspan+1) !max. exterior reaction at supports
*DIM,Rmax_INT_,array,Num_int,Nspan+1 !max. interior reaction at supports

*DIM,Qmax_EXT__Pos_,,(Nspan*2) !max.exterior shear TK pos.
*DIM,Qmax_INT__Pos_,array,Num_int,Nspan*2 !max.interior shear TK pos.
*DIM,Rmax_EXT__Pos_,,(Nspan+1) !max.exterior reaction TK pos.
*DIM,Rmax_INT__Pos_,array,Num_int,Nspan+1 !max.interior reaction TK pos.

*DIM,Mmax_EXT_,,(Nspan) !max.exterior moment at middle spans
*DIM,Mmax_INT_,array,Num_int,Nspan !max.interior moment at middle spans

! Moving the truck in LEFT direction 4 16 16

allsel

eplot

runtime=0

! Truck will run @Xmove and @Ymove

trucklength=2*14*12

totalruntime=nint((totallength-trucklength-72*tan(skew))/Xmove)

*do,kk,0,totalruntime,1

runtime=runtime+1

/uis,msgpop,3 !2:only warning/errors display !3:only error display

/solu

antype,static

esel,all

fdelete,all,all !delete all loads on nodes

xcood1=TKY2*tan(skew)+kk*Xmove

xcood2=xcood1+168

xcood3=xcood1+168*2

ycood1=TKY1

ycood2=TKY2

TKload1=-4 !TKload1=-16 !change the direction of trucks

TKload2=-16

TKload3=-16 !TKload3=-4 !change the direction of trucks

distributeF,xcood1,ycood1,TKload1

```

distributeF,xcood2,ycood1,TKload2
distributeF,xcood3,ycood1,TKload3
distributeF,xcood1,ycood2,TKload1
distributeF,xcood2,ycood2,TKload2
distributeF,xcood3,ycood2,TKload3
alls
epplot
/solu
  SOLVE
  finish

/post1

!Ext_X(1,i),Ext_Y(1,i) Int_X(j,j),Int_Y(j,j) are supports coordinates

!*****To obtain the shear force Q for beam ends*****

! For exterior girders
alls
SolnforMQ,Ext_X(1,1),Ext_Y(1,1),Gspac,Edgewidth,0      !0: ext.
Q_EXT_(1,1)=FZright
SolnforMQ,Ext_X(1,Nspan+1),Ext_Y(1,Nspan+1),Gspac,Edgewidth,0 !0: ext.
Q_EXT_(1,Nspan*2)=FZleft
  *do,i,2,Nspan,1
    SolnforMQ,Ext_X(1,i),Ext_Y(1,i),Gspac,Edgewidth,0      !0: ext.
    Q_EXT_(1,2*i-2)=FZleft
    Q_EXT_(1,2*i-1)=FZright
  *enddo
! For interior girders
alls
*do,i,1,Num_int
  SolnforMQ,Int_X(i,1),Int_Y(i,1),Gspac,Edgewidth,1      !1: int.
  Q_INT_(i,1)=FZright
  SolnforMQ,Int_X(i,Nspan+1),Int_Y(i,Nspan+1),Gspac,Edgewidth,1 !1: int.
  Q_INT_(i,Nspan*2)=FZleft
  *do,j,2,Nspan,1
    SolnforMQ,Int_X(i,j),Int_Y(i,j),Gspac,Edgewidth,1      !1: int.
    Q_INT_(i,2*j-2)=FZleft
    Q_INT_(i,2*j-1)=FZright
  *enddo
*enddo
alls
epplot
!*****the shear force Q for beam ends over*****

!*****To obtain the reaction R for supports*****

*do,i,1,Nspan+1
  alls
  *get,R_EXT_(1,i),NODE,NODE(EXT_X(1,i),EXT_Y(1,i),0),RF,FZ
*enddo

*do,i,1,Num_int
  *do,j,1,Nspan+1
    alls

```

```

*get,R_INT_(i,j),NODE,NODE(INT_X(i,j),INT_Y(i,j),0),RF,FZ
*enddo
*enddo
!*****the reaction R for supports over*****

!save the maximum value and Corresponding postions of TK for :M,Q,R----
*do,i,1,Nspan*2
*If,ABS(Q_EXT_(1,i)),GT,ABS(Qmax_EXT_(1,i)),Then
Qmax_EXT_(1,i)=0
Qmax_EXT_(1,i)= Q_EXT_(1,i)
Qmax_EXT__Pos_(1,i)=xcood1
*EndIf
*enddo

*do,i,1,Nspan+1
*If,ABS(R_EXT_(1,i)),GT,ABS(Rmax_EXT_(1,i)),Then
Rmax_EXT_(1,i)=0
Rmax_EXT_(1,i)= R_EXT_(1,i)
Rmax_EXT__Pos_(1,i)=xcood1
*EndIf
*enddo

*do,i,1,Num_int
*do,j,1,Nspan*2
*If,ABS(Q_INT_(i,j)),GT,ABS(Qmax_INT_(i,j)),Then
Qmax_INT_(i,j)=0
Qmax_INT_(i,j)= Q_INT_(i,j)
Qmax_INT__Pos_(i,j)=xcood1
*EndIf
*enddo
*enddo

*do,i,1,Num_int
*do,j,1,Nspan+1
*If,ABS(R_INT_(i,j)),GT,ABS(Rmax_INT_(i,j)),Then
Rmax_INT_(i,j)=0
Rmax_INT_(i,j)= R_INT_(i,j)
Rmax_INT__Pos_(i,j)=xcood1
*EndIf
*enddo
*enddo

*enddo ! corresponding to the kk do loop
!-----OUTPUT THE RESULTS FOR M,Q,R-----

*CREATE,OUTPUT
*CFOPEN,A-15-65-TK38-6 results,dat,f:\
*VWRITE
(10X, 'A-15-65-TK38-6 results(Ymove=38)') !be changed with various bridges
*VWRITE
(/-----Exterior Girder Reaction & Shear-----')
*VWRITE
(/*** (REACT. for EXT supports) *** (start position of load) ***)
*do,i,1,Nspan+1
*VWRITE,ABS(Rmax_EXT_(1,i)),Rmax_EXT__Pos_(1,i)

```

```

(F10.2,20X,F10.2)
*enddo

*VWRITE
(/***(SHEAR for EXT girders)***(start position of load)*****)
  *do,i,1,Nspan*2
  *VWRITE,ABS(Qmax_EXT_(1,i)),Qmax_EXT__Pos_(1,i)
  (F10.2,20X,F10.2)
  *enddo

*VWRITE
(/-----Interior Girder Reaction & Shear-----')
*VWRITE
(/***(REACT. for outmost INT supports)***(start position of load)***')
  *do,i,1,Num_int
  *If,i,GT,1,Then
  *VWRITE
  (/-----REACT. for next adjacent INT supports-----')
  *EndIf
  *do,j,1,Nspan+1
  Rmax=Rmax_INT_(i,j)
  Rmaxpos=Rmax_INT__Pos_(i,j)
  *VWRITE,ABS(Rmax),Rmaxpos
  (F10.2,20X,F10.2)
  *enddo
*enddo

*VWRITE
(/***(SHEAR for outmost INT girder)***(start position of load)*****)
  *do,i,1,Num_int
  *If,i,GT,1,Then
  *VWRITE
  (/-----SHEAR for next adjacent INT girder-----')
  *EndIf
  *do,j,1,Nspan*2
  Qmax=Qmax_INT_(i,j)
  Qmaxpos=Qmax_INT__Pos_(i,j)
  *VWRITE,ABS(Qmax),Qmaxpos
  (F10.2,20X,F10.2)
  *enddo
*enddo
*CFCLOSE
*END
/INPUT,OUTPUT
!*****

```

Appendix B Example of calculation of α and θ

(bridge analysis simplified by Bakht. B and Jaeger L. G.)

Girder type: W690x152

Span: $L=12.27\text{m}$

Width: $W=10.81\text{m}$

Girder spacing: $S=1830\text{ mm}$

Moment of inertia of a girder: $I_g=1.51 \times 10^9\text{ mm}^4$

Area of a girder: $A_g=19354.8\text{ mm}^2$

Girder depth: $d=690\text{mm}$

Flange width of a girder: $bf=254\text{ mm}$

Modular ratio $\frac{E_g}{E_c}$: $n=9.0$

Poisson's ratio: $\nu_c=0.15$

Slab thickness: $t=150\text{ mm}$

Effective width of deck: $B_{\text{effect}} = \min \left\{ \frac{L}{4}, \frac{S}{1000}, 12 \cdot t + \frac{bf}{2 \cdot 1000} \right\} \text{ m}$

$$B_{\text{effect}} = 1.83\text{ m}$$

Transformed deck width: $B_{\text{trans}} = \frac{B_{\text{effect}} \cdot 1000}{n} \text{ mm}$

$$B_{\text{trans}} = 203.333\text{ mm}$$

Transformed deck area: $A_{\text{deck}} = B_{\text{trans}} \cdot t$

$$A_{\text{deck}} = 3.05 \times 10^4\text{ mm}^2$$

Solution:

$$y_b = \frac{[A_{deck} \cdot (d + \frac{t}{2}) + A_g \cdot \frac{d}{2}]}{(A_{deck} + A_g)} \quad y_b = 601.946 \text{ mm}$$

$$I_{comp} = I_g + A_g \cdot (y_b - \frac{d}{2})^2 + B_{trans} \cdot \frac{t^3}{12} + A_{deck} \cdot (d - y_b + \frac{t}{2})^2$$

$$I_{comp} = 3.656 \times 10^9 \text{ mm}^4 \quad \text{which is in terms of girder materials}$$

$$D_x = \frac{I_{comp}}{S} \cdot E_g = \frac{I_{comp}}{S} \cdot n \cdot E_c \quad D_x = 1.798 \times 10^7 E_c$$

$$D_y = \frac{t^3}{12} \cdot E_c \quad D_y = 2.813 \times 10^5 \cdot E_c$$

$$D_{xy} = \frac{\frac{t^3}{6}}{2 \cdot (1 + \nu_c)} \cdot E_c \quad D_{xy} = 2.446 \times 10^5 \cdot E_c$$

$$D_{yx} = D_{xy} \quad D_{yx} = 2.446 \times 10^5 \cdot E_c$$

$$D_1 = \nu_c \times \{\min(D_x, D_y)\} \quad D_1 = 4.219 \times 10^4 \cdot E_c$$

$$D_2 = D_1 \quad D_2 = 4.219 \times 10^4 \cdot E_c$$

$$\alpha = \frac{(D_{xy} + D_{yx} + D_1 + D_2)}{2 \cdot (D_x \cdot D_y)^{0.5}} \quad \alpha = 0.128$$

$$\theta = \frac{W \cdot (\frac{D_x}{D_y})^{0.25}}{2 \cdot L} \quad \theta = 1.246$$

Appendix C LDF for Straight Bridges in NCHRP12-62

Given:

Girder spacing: $S=14$ ft

Span length: $L_1=200$ ft; $L_2=200$ ft

Slab thickness: $t_s=10$ in.

Number of girders: $N_g=4$

Distance from center of the exterior girder to the location of the outer most wheel load:

$d_e=1$ ft

Clear roadway width: $W_c=48$ ft

Skew angle: $\theta=0^\circ$

$$N_L = \text{Int}\left(\frac{W_c}{12}\right) = 4$$

Interior Girder:

Shear:

One lane loaded:

$$a_v=1.04$$

$$b_v=-0.12$$

$$m_1=1.2$$

$$\gamma_{a_{sli}}=1.05$$

$$g_{sli}=\gamma_{a_{sli}} \times [a_v \times (1-3/S) + b_v] = 0.732$$

$$m_1 \times g_{sli} = 0.878$$

Lower Bound Distribution Factor:

$$g_{sli,lb} = \frac{N_L}{N_g} = 1.000$$

$$m_1 \times g_{si_lb} = 1.200$$

Two or more lanes loaded:

One lane loaded:

$$a_v = 0.99$$

$$b_v = 0.01$$

$$m_2 = 1.0$$

$$\gamma_{a_si} = 1.10$$

$$g_{si} = \gamma_{a_si} \times [a_v \times (2 - 10/S) + b_v] = 1.411$$

$$m_2 \times g_{si} = 1.411$$

Lower Bound Distribution Factor:

$$g_{si_lb} = \frac{N_L}{N_g} = 1.000$$

$$m_2 \times g_{si_lb} = 1.000$$

Controlling Distribution Factor:

$$mg_{si_max} = \max (m_1 \times g_{si}, m_1 \times g_{si_lb}, m_2 \times g_{si}, m_2 \times g_{si_lb}) = 1.411$$

Skew Correction Factor (SCF):

$$SCF = 1 + 0.2 \times \tan(\theta) = 1.000$$

$$Mg_{si} = mg_{si_max} \times SCF = 1.411$$

Exterior Girder:

Shear:

One lane loaded:

$$a_v = 0.70$$

$$b_v = 0.13$$

$$m_1 = 1.2$$

$$\gamma_{a_{s1e}}=1.05$$

$$g_{s1e}=\gamma_{a_{s1e}} \times [a_v \times (1+d_e/S-3/S) + b_v] = 0.766$$

$$m_1 \times g_{s1e} = 0.920$$

Lower Bound Distribution Factor:

$$g_{s1e_lb} = \frac{N_L}{N_g} = 1.000$$

$$m_1 \times g_{s1e_lb} = 1.200$$

Two or more lanes loaded:

One lane loaded:

$$a_v = 0.83$$

$$b_v = 0.11$$

$$m_2 = 1.0$$

$$\gamma_{a_{se}} = 1.05$$

$$g_{se} = \gamma_{a_{se}} \times [a_v \times (3/2 + 3d_e/2S - 8/S) + b_v] = 0.793$$

$$m_2 \times g_{se} = 1.018$$

Lower Bound Distribution Factor:

$$g_{se_lb} = \frac{N_L}{N_g} = 1.000$$

$$m_2 \times g_{se_lb} = 1.000$$

Controlling Distribution Factor:

$$mg_{se_max} = \max (m_1 \times g_{s1e}, m_1 \times g_{s1e_lb}, m_2 \times g_{se}, m_2 \times g_{se_lb}) = 1.200$$

Skew Correction Factor (SCF):

$$SCF = 1 + 0.2 \times \tan(\theta) = 1.000$$

$$Mg_{se} = mg_{se_max} \times SCF = 1.200$$

Summary for Shear LDF:

Interior Girder: $m_{g_{si}} = 1.411$

Exterior Girder: $m_{g_{se}} = 1.200$

Vita

Qinghe Zhang was born in Fu Xin, Liao Ning Province, P.R.China on March 28, 1977. He graduated from Northeast Dianli (Power) University, China, in 2000. He received his Master of Engineering Degree in harbor, ocean, and offshore engineering from Dalian University of Technology in 2003. After that, as a structural engineer, he worked at Central Research Institute of Building and Construction, MCC, Beijing, China.

He left China to enter the doctoral program at Tennessee Technological University in August, 2005. In September 2007, he is a candidate for the Doctor of Philosophy Degree in Engineering. Upon graduation, he will work in American Bureau of Shipping, Houston, Texas, U.S.A.